Instabilités et formation de motifs dans les systèmes mécaniquement contraints

Mohktar Adda-Bedia

Université Pierre et Marie-Curie
Laboratoire de Physique Statistique
Ecole Normale Supérieure
24 rue Lhomond, 75231 Paris Cedex 05, France.

Instabilités et formation de motifs dans les systèmes mécaniquement contraints

Habilitation à diriger les recherches présentée par

Mokhtar Adda-Bedia

Soutenue le 2 juin 2006

devant le jury composé de :

Martine Ben Amar (Invitée)
Sergio Ciliberto (Examinateur)
Jean-Baptiste Leblond (Président)
Raúl Madariaga (Rapporteur)
Itamar Procaccia (Rapporteur)
James R. Rice (Examinateur)
Stéphane Roux (Rapporteur)

Remerciements

Je tiens à remercier Martine Ben Amar pour m'avoir accepté comme collaborateur, pour avoir toujours été disponible et pour son aide inestimable.
Je remercie également les rapporteurs Raúl Madariaga, Itamar Procaccia et Stéphane Roux et les membres du jury Sergio Ciliberto, Jean-Baptiste Leblond et Jim Rice d'avoir accepté de juger cette habilitation.
Durant ces années, le LPS a été pour moi un environnement scientifique exceptionnel. Il l'est toujours par ailleurs. Je remercie tous les membres d'avoir contribué à rendre cet endroit plein d'émulation. Particulièrement je remercie tous les directeurs qui se sont succédé durant la période que j'ai passée au LPS.
Je remercie également José Da-Silva-Quintas, Zaïre Dissi, Marie Gefflot, Carole Philippe, Annie Ribaudeau et Nora Sadaoui, pour leur disponibilité et leur aide précieuse.
Je remercie particulièrement et pour différents aspects de la vie d'un chercheur (amitié, collaborations, discussions, ...) :
Au LPS : Steffen Bohn, Daniel Bonn, Arezki Boudaoud, Laurent Boué, Marc-Etienne Brachet, Didier Chatenay, Francis Corson, Yves Couder, Georges Debrégeas, Stéphane Douady, Compte Fictif, Vincent Hakim, Eytan Katzav, Xavier Leyronas, Jacques Meunier, Yves Pomeau, Alexis Prevost, Sergio Rica et Julien Scheibert.
Ailleurs : Catherine Allain, Yacine Amarouchène, Bruno Andreotti, Rodrigo Arias, Basile Audoly, Belgoumène Berrezoug, José Bico, Hervé Henry, Christophe Josserand, Hamid Kellay, Fernando Lund, L. Mahadevan, Sébastien Neukirch, Caroline Nore, Pedro Partìcio, Ludovic Pauchard, Laurent Quartier, La Rivière, Benoît Roman, Chaïeb Sahraoui, Stefan Lewellyn Smith et Denis Vallet.
Et biensûr tous les étudiants qui sont passés par le LPS ou qui y sont encore. Car sans eux, le laboratoire serait presque mort.
Finalement, je dédie ce manuscrit à ma famille.

Table des matières

CURRICULUM VITAE **i**

Préambule **1**

1 Mécanique de la rupture fragile **5**
1.1 Propagation quasi-statique d'une pointe de fissure 6
1.2 Plusieurs fissures en interaction 7
1.3 Propagation quasi-statique d'un front de fissure 8
1.3.1 Instabilité d'un front de décollement 9
1.3.2 Equation de mouvement d'un front de fissure dans un milieu hétérogène 9
1.3.3 Rugosité d'un front de fissure dans un milieu hétérogène 10
1.4 Propagation dynamique des fissures 11
1.4.1 Equations de mouvement 11
1.4.2 Instabilité de branchement 12

2 Impact et friction **15**
2.1 Ondes de glissement 15
2.2 Rayonnement sismique de failles hétérogènes 16
2.3 Dynamique de l'impact 16

3 Autres Problèmes **19**
3.1 Instabilités d'une arche 19
3.2 Formes d'équilibre des gouttes superposées 19

4 Projets **21**
4.1 Morphogénèse induite par la mécanique 21
4.1.1 Filaments élastiques confinés 22
4.1.2 La géométrie des feuilles minces pliées 22
4.1.3 Nervures des feuilles 23
4.2 Modélisation de la croissance du crâne de l'enfant 24
4.3 Projets expérimentaux 25
4.3.1 Croissance et compaction 25
4.3.2 fracture des objets minces 27
4.3.3 Friction sur une membrane tendue 27

LISTE DES PUBLICATIONS **29**

SELECTION DE PUBLICATIONS **33**

CURRICULUM VITAE

ADDA-BEDIA Mokhtar
Fonction : Chargé de recherches au CNRS
Date de prise de fonction : 01/10/1996 (CR2) ; 01/10/2000 (CR1)
Etablissement : Laboratoire de Physique Statistique,
Ecole Normale Supérieure, UMR 8550.
24 rue Lhomond 75005 Paris.
Tél : 01-44-32-25-26
Fax : 01-44-32-34-33
e-mail : `adda@lps.ens.fr`
site web : http ://www.lps.ens.fr/∼adda

Titre universitaire :

Docteur de l'Université Pierre et Marie Curie en Physique, 4 Février 1994.
Titre de la thèse : Sur quelques problèmes de croissance cristalline : Formes et dynamique.
Directeur de thèse : Martine BEN AMAR

Formation et diplômes :

02/2002–01/2003 : Mis à disposition au Department of Applied Mathematics and Theoretical Physics, University of Cambridge.
1994–1996 : Post-Doc au Laboratoire de Physique Statistique de l'ENS Paris.
02/1994 : Doctorat de Physique de l'Université Pierre et Marie Curie, Paris VI. Mention Très Honorable avec Félicitations du Jury.
06/1989 : D.E.A de Physique Théorique de l'Université Paris VI, mention Assez Bien.
06/1988 : Diplôme d'Etudes Supérieures de Physique Théorique à l'Université d'Oran (Algérie). Mention Bien.

Enseignement et encadrement :

1997 : Encadrement du stage théorique de Y. Amarouchène (Maîtrise).
2003 : Encadrement du stage expérimental de T. Machado (L3).
2004 : Encadrement du stage théorique de D. Elmasri (M2).
2004–2006 : Tutorats de Mécanique à l'ESPCI.
2005 : Encadrement des stages expérimentaux de D. Cassani (M2), E. Couturier (M2), A. Eddi (L3) et du stage théorique de L. Boué (M2).
2005– : Encadrement de la thèse de F. Corson.
2005– : Encadrement de la thèse de L. Boué.
09/2005–01/2008 : Encadrement de la recherche post-doctorale de E. Katzav.
2006 : Encadrement du stage expérimental de M. Trejo (M2).

Financements :

1994–1995 : Contrat avec l'Institut de l'Ecole Normale Supérieure pour l'élaboration du rapport "Croissance Cristalline : Formes et Dynamique".
10/1995–09/1996 : Bourse post-doctorale DRET.

1997–1998, 2000–2001, 2001–2002, 2004–2005 : Financements d'une coopération avec Rodrigo Arias du département de physique de l'Université Santiago du Chili dans le cadre de l'accord CNRS–CONICYT.
09/2004–08/2007 : Participant à l'ACI Jeunes Chercheurs Structures élastiques minces : géométrie, rigidité, instabilités.
06/2005–05/2008 : Participant au contrat européen "MechPlant" : The role of mechanical instabilities in leaf development. Nature du contrat : Specific Targeted Research Project (STREP). Programme : New and Emerging Science and Technology (NEST).
02/2006–01/2007 : Responsable de la Bourse Marie Curie "PatForm" : Pattern formation induced by elastic stresses and geometrical constraints. Bénéficiaire : E. Katzav.
04/2006–03/2009 : Participant au contrat européen "MONAT" : Measurement of naturalness. Nature du contrat : STREP. Programme : NEST.

Conférences et workshops invité :

3–6 Janvier 1996 : Dynamics Days à Houston, Texas.
29 Juin–3 Juillet 1997 : McNU 97, Northwestern University. Organisateur : American Association of Mechanical Engineering.
14 Juillet–26 Juillet 1997 : "Elasticity and viscoelasticity in solids and liquids", Cargèse.
Juillet 1998 : "Flow, Friction and Fracture", Beyrouth (Liban).
Juillet 1999 : MRS meeting, Strasbourg. Organisateur ; European Materials Research Society.
25–27 Octobre 1999 : Symposium en l'honneur de G. I. Barenblatt : "Similarity, Singularity and Scaling in Mechanics". Organisateur : Society of Engineering Science.
Novembre 1999 : "Models of Fracture", Workshop au Isaac Newton Institute, Cambridge.
Décembre 1999 : Instabilities and Nonequilibrium Structures VIII, Viña del Mar, Chili.
Décembre 2001 : Instabilities and Nonequilibrium Structures IX, Viña del Mar, Chili.
15–20 Décembre 2003 : Instabilities and Nonequilibrium Structures X, Viña del Mar, Chili.

Séjours à l'étranger :

11/1997, 11/2000, 11/2001 : Séjours au département de physique de l'Université Santiago du Chili, dans le cadre d'une coopération CNRS–CONICYT.
03/1998 : Visite au James Franck Institute, Université de Chicago.
04/1998 : Invitation par J. Rice au Division of Engineering and Applied Sciences, Harvard University et par L. Mahadevan au Department of Mechanical Engineering, M.I.T.
11/1999 : Séjour au Isaac Newton Institute dans le cadre du Workshop : "Models of Fracture".
12/1999 : Séjour au département de physique de l'Université du Chili, dans le cadre d'une coopération ECOS.
02/2002–01/2003 : Mis à disposition au Department of Applied Mathematics and Theoretical Physics, University of Cambridge.

Autres activités :

2000–2002 : Co–organisateur du séminaire du Laboratoire de Physique Statistique.
15–17 Septembre 2004 : Organisateur des journées du Laboratoire de Physique Statistique à l'IHP.
2004 : Rédaction du rapport d'activité à quatre ans du Laboratoire de Physique Statistique.
15–17 Juin 2005 : Organisateur du meeting pour le lancement du projet MechPlant à l'IHP.

Préambule

Cette notice décrit mes travaux de recherche effectués au Laboratoire de Physique Statistique de l'Ecole Normale Supérieure. Ce préambule précise un peu l'historique de ces recherches.

J'ai préparé ma thèse de Doctorat sous la direction de Martine Ben Amar et de Vincent Hakim au LPS, et je l'ai soutenue le 4 Février 1994. Ces premiers travaux ont porté sur l'étude des phénomènes de croissance limités par la diffusion. J'ai ainsi travaillé sur les phénomènes non linéaires associés aux instabilités diffusives des interfaces que l'on rencontre en solidification. Plus particulièrement, ces études ont abordé les problèmes suivants :

– *Croissance limitée par la diffusion :*

Les recherches sur la croissance cristalline s'étaient souvent focalisées sur l'étude de prototypes simples de croissance qui sont modélisés par le problème dit de Saffman-Taylor, ou par celui de la croissance dendritique rugueuse d'un cristal en aiguille dans un espace illimité. Or, d'autres aspects du problème de solidification ont été mis en évidence par des observations expérimentales. Ces expériences ont montré que l'interface liquide-solide ne peut pas toujours être ramenée à l'un de ces deux cas académiques, mais que sa forme dépend étroitement du choix des paramètres physiques de contrôle, des échantillons de matériaux à étudier ainsi que de la géométrie de l'expérience. Le travail de ma thèse a donc consisté à étudier quelques problèmes liés à ces manifestations expérimentales. J'ai particulièrement abordé les trois problèmes suivants.

– *Croissance dendritique à tension de surface nulle :*

Dans tout problème de pénétration d'une substance dans une autre par le biais de la diffusion, il est très utile de connaître les solutions exactes à l'approximation de tension de surface nulle. De ce fait, nous avons analysé le degré de généralité des familles de solutions stationnaires d'Ivantsov et d'Horvay-Cahn (les seules solutions connues exactement). Nous avons montré que ces solutions sont uniques dans l'espace où le champ de diffusion peut être ramené à un champ décrit par une seule variable d'espace. Nous avons aussi discuté du cadre où de nouvelles familles de solutions, correspondant aux différentes formes observées expérimentalement, pourraient être déterminées.

– *Croissance cristalline facettée :*

C'est le problème de la croissance des cristaux qui présentent des formes facettées dans certaines directions privilégiées. Notre étude a consisté à étendre la théorie de la croissance limitée par la diffusion au régime de la croissance des cristaux qui présentent des

formes facettées dans certaines directions privilégiées. En rajoutant un minimum d'hypothèses supplémentaires, qui consistent à introduire des lois d'interfaces caractérisant le facettage, nous avons étudié, analytiquement et numériquement, ce phénomène dans le cas de la croissance dendritique libre pour les modèles unilatéral et symétrique ainsi qu'en solidification dirigée. Le traitement numérique comporte quelques subtilités liées à la présence simultanée de portions rugueuses et facettées dans l'interface du liquide-solide. En effet, pour le cas "classique" des cristaux complètement rugueux, c'est la loi, dite de Gibbs-Thomsom, sur tout le profil, qui fournit la relation nécessaire entre le champ de diffusion et la forme de l'interface, or dans le cas des facettes la forme du cristal est, par définition, déjà connue.

– *Croissance Laplacienne de pointes*

Nous nous sommes intéressé à un modèle dynamique décrivant la croissance Laplacienne de n aiguilles de différentes longueurs. Ce modèle théorique permet de connaître la nature de la dynamique de croissance des interfaces et de plus, se prête à des études analytiques de l'amas de branches qui peuvent être assimilées à des structures physiques en compétition. En effet, la description détaillée donnée par les équations de mouvement déterministes des interfaces ne peut être entreprise que numériquement et ne permet généralement pas une étude statistique satisfaisante. Nous avons présenté une étude analytique et numérique de ce modèle dans le cas d'une croissance d'aiguilles parallèles.

Juste après ma thèse, j'ai changé de thématique pour l'étude des instabilités associées à la propagation des fissures. En 1996, je suis rentré comme CR2 au CNRS, affecté au LPS. J'ai continué ma collaboration avec Y. Pomeau et M. Ben Amar. J'ai aussi collaboré avec Rodrigo Arias et Fernando Lund par le biais de projets CNRS-Conicyt. En Février 2002, j'ai été mis à disposition pour passer une année au Department of Applied Mathematics and Theoretical Physics, Cambridge University, afin de collaborer avec L. Mahadevan.

La dynamique de la propagation des fissures s'est imposée comme un sujet important en physique. L'approche que j'ai suivie dans ce domaine tourne autour de la formation de motifs (pattern formation) dans des systèmes en présence d'une ou de plusieurs fissures. Voici quelques questions qui sont posées autour de ce phénomène générique. Une fois qu'une fissure est formée et qu'elle commence à se propager quelle est sa trajectoire ? quelle sera sa dynamique ? est-ce que les instabilités dynamiques et morphologiques observées expérimentalement ont la même origine ? comment sont-elles corrélées ? lorsque plusieurs fissures sont présentes, comment interagissent-elles et quelle est la morphologie résultante ? peut-on contrôler le motif final en contrôlant seulement les conditions d'application des contraintes ou la géométrie globale ?

Dans ce cadre, j'ai effectué des travaux essentiellement théoriques dont les points forts sont énumérés ci-dessous.

– Stabilité d'une fissure en propagation quasi-statique : détermination de l'équation de mouvement de la fissure et des mécanismes provoquant la déstabilisation de sa trajectoire.

– Interaction entre plusieurs fissures : quelle est la part d'ordre et la part du désordre dans la prédiction des formes résultantes.

– Fissure dynamique : détermination d'une équation vectorielle de mouvement et des in-

stabilités dynamiques observées expérimentalement.
– Propagation quasi-statique d'un front de fissure : étude des mécanismes de déstabilisation du front. Détermination d'une équation de mouvement non linéaire d'un front de fissure dans un milieu hétérogène et de l'exposant de rugosité du front de fissure résultant.

La propagation des fissures est un phénomène irréversible hors-équilibre qui présente des instabilités quasi-statiques et dynamiques qui produisent des motifs d'une classe différente de celles induites par des champs "classiques". Cette observation m'a conduit à étudier la physique sous-jacente et à trouver d'autres archétypes de cette morphogenèse. En effet, le mécanisme de rupture peut se manifester dans d'autres phénomènes, par exemple dans les problèmes d'adhésion ou de friction. Une analogie a été mise en évidence avec la botanique et la morphogenèse des nervures des feuilles et qui fait l'objet d'un sujet de thèse que j'encadre.

Dernièrement, j'ai commencé à m'intéresser à de nouveaux problèmes autour de la morphogénèse induite par la mécanique (détaillés dans le chapitre projets). Une partie de ces travaux est reliée à une ACI Jeunes chercheurs et à un projet européen où nous proposons d'appliquer la mécanique des structures élastiques à des problèmes issus de la biologie. Le principal objectif de ces projets est d'apporter une meilleure compréhension du comportement mécanique de certaines structures biologiques, et de leur morphogenèse. L'autre direction concerne une collaboration avec la société TCI (Télé-Crâne-Innovation) afin de construire un modèle de la croissance du crâne de l'enfant et d'identifier des mécanismes physiques qui influencent la croissance de la sphère crânienne. Ce problème intéresse les professionnels de santé dont le domaine d'action est la sphère crânienne, en particulier les orthodontistes pour une meilleure conception des traitements de dysharmonies cranio-faciales et les anthropologues pour une meilleure analyse de la croissance des fossiles.

Nous avons aussi commencé à développer une activité expérimentale axée autour des instabilités et de la morphogenèse dans les systèmes mécaniques soumis à des contraintes induites par la croissance, une pression externe, des phénomènes interfaciaux ou un écoulement. Plus précisément, les principales directions de cette activité concernent la compression et le repliement d'objets élastiques, les instabilités d'interfaces comme la fracture et la friction, les vibrations des plaques en présence de singularités ou de structures organisées.

Finalement, mes directions de recherche dans le passé et dans le futur se rattachent à différentes problématiques générales, mais ont cependant un même fil directeur ; celui de l'étude des instabilités mécaniques et les formes qui en résultent. D'un point de vue théorique, les méthodes mathématiques associées à ces problèmes requièrent souvent des formulations assez élaborées. Ces types de problèmes requièrent en effet diffférentes techniques allant de la résolution d'équations intégrales singulières (utilisant des méthodes associées aux transformées de Hilbert, à la méthode de décomposition de Wiener-Hopf, aux transformations conformes, ...), aux techniques rencontrées en physique statistique (intégrale de chemin, équation de Fokker-Planck, fonctions de distributions de probabilité, ...).

Collaborations :
M. Ben Amar, A. Boudaoud, Y. Pomeau (LPS, ENS), R. Madariaga (Géophysique, ENS), S. Bohn, Y. Couder, S. Douady (MSC, Paris VII), B. Andreotti (PMMH, ESPCI), C. Allain, L. Pauchard (FAST, Orsay), H. Henry (PMC, Polytechnique), R. Arias, F. Lund (Université du Chili), L. Mahadevan (DEAS, Harvard), S. Lewellyn Smith (Mechanical and Aerospace Engineering, UCSD).

Chapitre 1

Mécanique de la rupture fragile

L'intérêt porté à la compréhension du processus de rupture d'objets solides est né dès que notre ancêtre *Homo habilis* a commencé à tailler la pierre. La fabrication d'outils taillés en silex remonte à plus de 1.75 millions d'années et son perfectionnement a duré des centaines de milliers d'années. La caractérisation des outils est une méthode de datation utilisée par les archéologues et paléontologues. Néanmoins, ce n'est qu'au début des années soixante qu'une approche mécanique de la rupture du silex a été développée pour caractériser les formes et quantifier l'efficacité de la fabrication des éclats. Ce type de formes se retrouve aussi dans les éclats coniques de roches produits par l'impact des météorites et dont l'étude peut indiquer la vitesse de l'impact et son orientation.

Néanmoins, on peut considérer que les fondements historiques de la mécanique de la rupture en tant que science remontent à 1638, date à laquelle Galilée publie son œuvre majeure *"Discours concernant deux sciences nouvelles"*. En effet, la première de ces sciences nouvelles (avant la science du mouvement) traîte de la résistance des matériaux à la rupture.

C'est au cours du vingtième siècle, et surtout à partir de la deuxième guerre mondiale, que la mécanique de la rupture est devenue une des branches les plus développées de la mécanique des milieux continus. En effet, la multiplication des procédures de détection des fissures, engendrée par le caractère de plus en plus exigeant des normes de sécurité et leur perfectionnement constant, ont entraîné la détection de fissures dans un très grand nombre de structures industrielles et à différentes échelles. Comme il est matériellement impossible de réparer toutes ces fissures ou de prévenir de leur apparition, on cherche maintenant à les "justifier", c'est-à-dire à montrer qu'elles ne présentent pas de danger ; d'où le développement de la mécanique de la rupture dont l'objet est d'étudier les conditions de propagation des fissures dans les matériaux solides.

L'étude de la dynamique de la propagation des fissures est un sujet à part entière en en géophysique. Bien qu'elle est actuellement implicitement admise, la connexion entre les mécanismes de rupture et les tremblements de terre n'a trouvé son essor que pendant la deuxième moitié du vingtième siècle. D'autre part, depuis une vingtaine d'années, la rupture est devenue un domaine en plein développement en physique. Ce phénomène irréversible hors-équilibre présente des instabilités quasi-statiques et dynamiques non

génériques qui sont dues à la singularité spécifique du champ des contraintes au voisinage du front de fissure. Ce comportement produit des motifs différents de ceux induits par des champs "classiques" tels que le champ de diffusion en croissance cristalline. Ma recherche dans ce domaine a consisté à étudier la physique sous-jascente de cette morphogenèse et à identifier les mécanismes d'instabilités morphologiques et dynamiques durant la rupture des matériaux fragiles.

1.1 Propagation quasi-statique d'une pointe de fissure

La propagation d'une fissure dans une plaque de verre soumise à un champ de température non uniforme donne lieu à différentes instabilités de formes. Des expériences simples et parfaitement reproductibles ont permis de définir un diagramme de phase d'instabilités des fractures en propagation quasi-statique, où les paramètres d'ordre sont reliés simplement aux paramètres de contrôle. En variant ces paramètres, on peut aussi bien ne pas casser la plaque de verre, que créer une fracture rectiligne qui elle-même peut devenir instable pour donner lieu à une fracture oscillante. En relation avec ces expériences, nous avons étudié ces deux cas de propagation quasi-statique. La condition de propagation rectiligne de la fracture en fonction des paramètres expérimentaux a été déterminée et les lois d'échelles correspondantes ont été déduites. Nous avons développé une analyse de stabilité linéaire basée sur un critère de propagation de la pointe de la fissure. Nous avons déduit qu'à partir d'un certain seuil, la fracture rectiligne devient instable et donne lieu à une fracture oscillante. Les résultats du seuil d'instabilité et de la valeur de la longueur d'onde sélectionnée ont été calculés et la comparaison avec les résultats expérimentaux a été concluante.

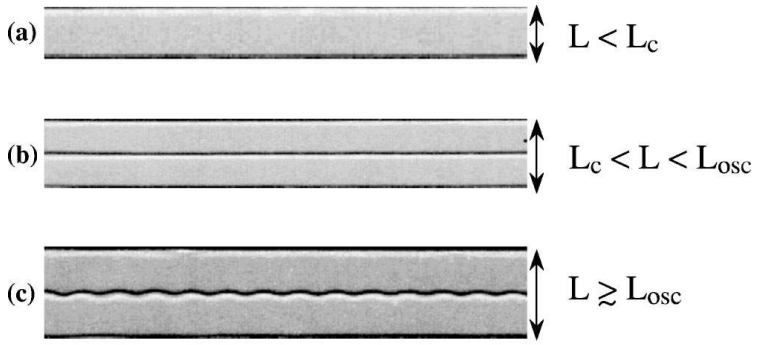

FIG. 1.1 – En variant les paramètres de contrôle, une plaque de verre soumise à un champ de température non uniforme peut : (a) ne pas se casser, (b) produire une fissure droite, (c) produire une fissure oscillante. (*O. Ronsin et al., Phys. Rev. Lett. (1995)*)

L'analyse de stabilité qui a permis de montrer l'existence de solutions oscillantes pour la forme de la fissure ne se restreint pas au cas thermo-élastique précédent. En effet, nous

avons montré que cette approche est applicable à toute fracture rectiligne en propagation quasi-statique et soumise à des contraintes uniaxiales. Par ailleurs, nous avons établi un critère de stabilité de la propagation rectiligne, et les résultats qui en découlent sont en accord avec les expériences qui mettent en jeu aussi bien des contraintes thermiques que mécaniques.

M. Adda-Bedia et Y. Pomeau : Crack instabilities of a heated glass strip, Phys. Rev. E 52 (1995) 4105-4113.
M. Adda-Bedia et M. Ben Amar : Stability of quasi-equilibrium cracks under Mode I loading, Phys. Rev. Lett. 76 (1996) 1497-1500.

1.2 Plusieurs fissures en interaction

Une continuation de ce travail a constitué à caractériser les différentes morphologies des fractures induites par le séchage des suspensions colloïdales. Dans ces systèmes, on observe que suivant les conditions expérimentales imposées, on peut engendrer des figures de fractures allant de simples fractures rectilignes, à des fractures en forme de paraboles et jusqu'à des fractures enchevêtrées avec des formes reproductibles. D'autre part, ce système expérimental a été à l'origine d'expériences analogiques qui montrent que la nervation des feuilles est régie par l'existence d'un champ tensoriel, qui de plus a été identifié au champ de contraintes induit lors de la croissance des feuilles.

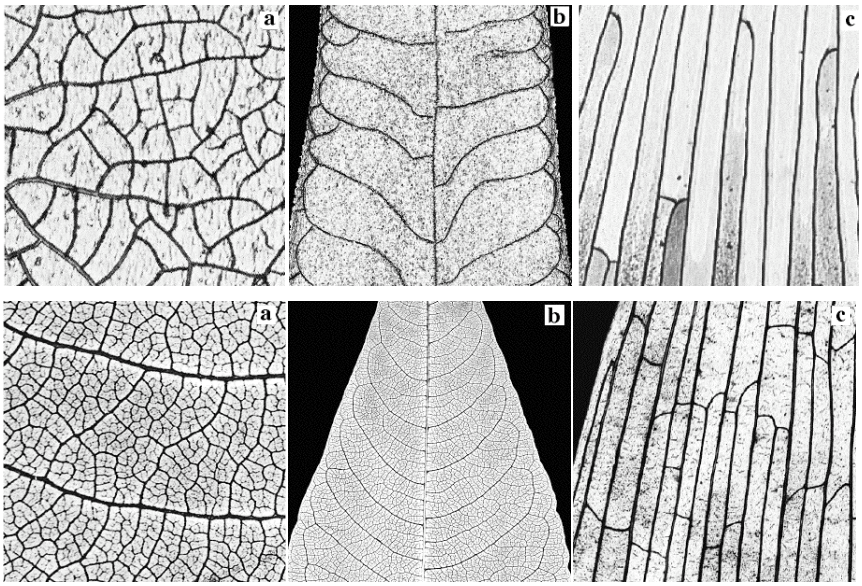

FIG. 1.2 – Analogie entre la nervation des feuilles et les figures induites par la propagation de fissures sous différentes conditions expérimentales. (*Y. Couder et al., EPJB (2003)*)

Nous nous sommes aussi intéressés à un problème d'un réseau de fractures parallèles.

Cette situation est celle que l'on rencontre dans les milieux stratifiés, car la présence d'interfaces entre les couches bloque la croissance des fractures. Lorsque la tension augmente, elle ne peut qu'entraîner l'apparition de nouvelles fractures, la longueur d'onde du réseau se trouvant divisée par deux. On peut se demander quelle limite sera atteinte lorsque la tension tend vers l'infini, le pas du réseau devant tendre alors vers zéro, suivant ce scénario. Il n'en est rien, comme le montre les observations et les simulations. Lorsque le pas du réseau atteint la longueur commune des fractures, la fracturation s'arrête et fait place à la compression de la zone fracturée. Nous avons proposé un modèle pour justifier le fait que la zone entre deux fractures passe de l'état de tension à un état de compression interdisant ainsi une nouvelle nucléation. Ce modèle résolu exactement prouve que lorsque les couches ont les mêmes coefficients élastiques, le pas minimal du réseau de fracture est donné par l'épaisseur de la couche considérée. Il est important de bien comprendre ce phénomène à cause des nombreuses applications en géophysique et dans l'industrie. En effet c'est le mécanisme phare de fracturation des milieux stratifiés.

D'autres projets en cours dans ce domaine concernent l'étude des raisons pour lesquelles les pointes des fissures s'évitent pendant leurs propagations et aussi l'étude des statistiques de distribution de l'apparition des fissures dans un milieu hétérogène soumis à des contraintes mécaniques.

M. Adda-Bedia et M. Ben Amar : Fracture spacing in layered materials, Phys. Rev. Lett. 86 (2001) 5703-5706.
L. Pauchard, M. Adda-Bedia, C. Allain et Y. Couder : Morphologies resulting from the directional propagation of fractures, Phys. Rev. E 67 (2003) 027103.
S. Bohn, J. Platkiewicz, B. Andreotti, M. Adda-Bedia et Y. Couder : Hierarchical crack pattern as formed by successive domain divisions. II. From disordered to deterministic behavior, Phys. Rev. E 71 (2005) 046215.

1.3 Propagation quasi-statique d'un front de fissure

La propagation d'un front de fissure dans un matériau fragile est le terrain d'un certain nombre de phénomènes physiques. La théorie existante de la mécanique de la rupture fragile a réussi à expliquer un certain nombre d'instabilités, néanmoins la propagation d'un front de fissure dans un milieu hétérogène est un problème théorique non résolu, bien qu'expérimentalement le comportement auto-affine universel du front de fissure a été observé et caractérisé. Ce phénomène est d'une importance fondamentale, parce que le mouillage d'un substrat désordonné est un autre exemple de systèmes avec une structure similaire. Nous avons approché ce problème en différentes étapes qui sont détaillées ci-dessous.

1.3.1 Instabilité d'un front de décollement

Le phénomène de décollement d'une plaque mince en contact avec un film d'adhésif se rencontre dans un bon nombre d'applications technologiques (bandes adhésives) et biologiques (pattes de lézards). Dans ce cadre, nous avons étudié l'instabilité oscillante d'un front de décollement initialement droit produit en décollant une plaque élastique flexible d'un film mince d'élastomère collé à un substrat rigide. Nous avons développé une analyse de stabilité linéaire qui a permis de prouver l'existence d'un seuil d'instabilité qui dépend du rapport des deux échelles de longueur qui surgissent naturellement dans ce problème ; l'épaisseur du film d'élastomère et une longueur élastique définie par la rigidité de la plaque et celle du film. Nous avons aussi montré que la longueur d'onde de l'instabilité est proportionnelle à l'épaisseur du film. Nos résultats sont qualitativement et quantitativement en accord avec les expériences récentes. Plus généralement, ils montrent comment les fronts de fissures peuvent être déstabilisés par la compétition entre des effets de volume et de surface.

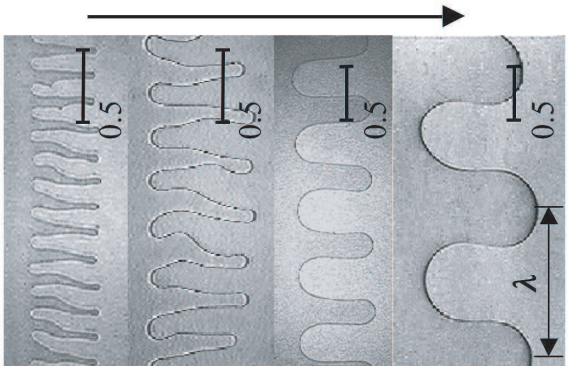

FIG. 1.3 – Fronts oscillants induits par le décollement d'une plaque en contact avec un film adhésif. (*A. Ghatak et M.K. Chaudhury, Langmuir (2003)*)

M. Adda-Bedia et L. Mahadevan : Peeling-induced crack-front instability in a confined elastic film, Proc. R. Soc. A (2006) à paraître.

1.3.2 Equation de mouvement d'un front de fissure dans un milieu hétérogène

Dans le cadre de la dynamique de propagation d'une fissure dans un milieu hétérogène, une quantité généralement étudiée est l'exposant de rugosité α qui décrit le caractère auto-affine du front de fissure. L'exposant caractérisant cette rugosité a été mesuré dans différents matériaux, et il s'est avéré que sa valeur se situe toujours autour de 0.5–0.6. En dépit de nombreux efforts depuis au moins une décennie, il n'y a malheureusement aucune théorie satisfaisante qui prévoit la valeur de cet exposant.

Dans une première approche, nous avons développé au second ordre le facteur d'intensité des contraintes d'un front de fissure courbe, autour de sa solution pour un front droit. La perturbation a été rendue possible grâce à l'introduction d'une nouvelle méthode qui a été utilisée pour l'étude de l'instabilité d'un front de décollement. Nous avons ainsi pu proposer une équation stochastique du mouvement d'un front de fissure qui se propage dans un milieu hétérogène et qui contient deux ingrédients principaux ; L'irréversibilité de la propagation du front et les effets non linéaires.

M. Adda-Bedia, E. Katzav et D. Vandembroucq : Second order variation in elastic fields of a tensile crack with a curved front, Phys. Rev. E 73 (2006) 035106(R).

1.3.3 Rugosité d'un front de fissure dans un milieu hétérogène

En utilisant l'équation stochastique proposée pour le mouvement du front de fissure, nous avons étudié la dynamique de propagation d'un front de fissure dans un milieu hétérogène dans le régime quasi-statique. L'approche consiste à utiliser une expansion auto-consistante (self consistent expansion) introduite par Schwartz et Edwards. Nous avons découvert une transition de phase dynamique continue entre une phase lisse (à grandes échelles) et une phase rugueuse, avec un exposant de rugosité $\alpha = 1/2$. La phase rugueuse devient possible à cause de la déstabilisation des modes linéaires par les termes non linéaires. En tenant compte de l'irréversibilité de la propagation de la fissure, nous avons déduit que l'exposant de rugosité mesuré expérimentalement pourrait devenir dépendant de la manière dont le front est amené à se propager. Ainsi, notre résultat peut être considéré comme une limite inférieure pour cet exposant, ce qui est en très bon accord avec les mesures expérimentales.

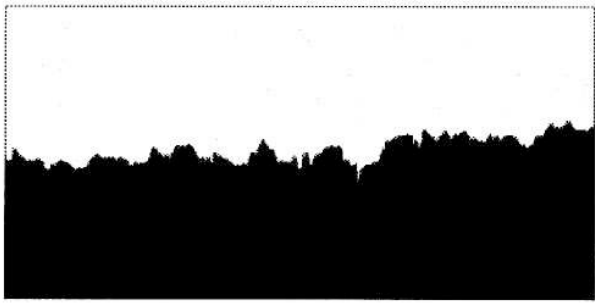

FIG. 1.4 – Front de fissure en mode I se propageant à travers un matériau hétérogène. (*A. Delaplace et al., Phys. Rev. E (1999)*)

Un autre problème auxquels ces calculs pourraient s'appliquer concerne les propriétés auto-affines des surfaces créées après le passage d'une fissure dans un milieu hétérogène. En effet, les études post-mortem des surfaces fissurées dans beaucoup de matériaux fragiles ont montré l'existence d'un autre exposant universel de rugosité (autour de 0.8). Ce travail est en cours.

E. Katzav et M. Adda-Bedia : Roughness of tensile crack fronts in heterogenous materials, soumis à Phys. Rev. Lett. (2005).

1.4 Propagation dynamique des fissures

Un deuxième champ d'investigation théorique en mécanique de la rupture concerne la propagation dynamique des fissures. Pour ce cas, les expériences ont montré qu'une fracture dynamique qui se propage à grande vitesse donne lieu à une variété de phénomènes dus à différents effets : contraintes appliquées, vitesse de propagation et conditions de préparation de la fissure. Les expériences sur la propagation rapide des fissures dans les matériaux fragiles montrent une instabilité dynamique qui se produit au dessus d'une vitesse critique de la pointe de la fissure. Cette instabilité induit un phénomène de branchement d'une fracture initialement droite. La surface créée par la fracture est initialement lisse, mais quand la vitesse atteint une valeur critique indépendante des conditions expérimentales, cette surface devient rugueuse à cause de l'apparition quasi-périodique de micro-fissures secondaires. Cette instabilité est accompagnée d'une oscillation de la vitesse de la fissure et d'une augmentation des émissions acoustiques.

1.4.1 Equations de mouvement

Partant de l'observation que ces différentes instabilités apparaissent indépendamment des conditions expérimentales et du matériau étudié, on a émis l'hypothèse qu'elles pouvaient être décrites par des modèles minimaux. La théorie de la mécanique de la rupture fragile, avec sa description élastique des contraintes et des déformations internes, complétée par des critères sur le processus de séparation de la matière, a réussi à décrire la progression des fissures dans le régime quasi-statique. Nous avons donc entrepris d'étudier la dynamique de la rupture fragile dans ce cadre du modèle purement élastique. Dans une première approche, on a étudié le comportement du champ des contraintes au voisinage de la pointe de la fracture en fonction de sa vitesse instantanée. On a introduit la notion de direction préférentielle de propagation qui est régie par le tenseur des contraintes diagonalisé. Le comportement de ce dernier nous a conduit à définir les instabilités morphologiques de la propagation dynamique de la fracture et à introduire des critères déterminant les transitions fracture lisse-fracture rugueuse-fracture branchée.

Concernant l'instabilité dynamique conduisant à la création des micro-fissures, nous avons entrepris une étude détaillée pour déterminer une équation de "mouvement" dynamique de la pointe d'une fissure. Nous avons ainsi généralisé l'approche classique pour une propagation de fracture non nécessairement rectiligne. Ceci nous a conduit à déterminer une équation *vectorielle* du mouvement de la pointe de la fracture, à l'opposé des modèles existants qui utilisent indépendamment deux critères de propagation de la fracture, l'un déterminant sa vitesse et le deuxième sa direction. Notre approche a permis d'unifier ces deux critères dans un seul formalisme. D'un point de vue formel, nous avons justifié le principe dit de symétrie locale que tout mécanicien utilise et nous l'avons étendu à toute

vitesse. Cette équation s'est avérée pouvoir produire, sous certaines conditions, une instabilité dynamique à une vitesse critique indépendante de la configuration expérimentale.

M. Adda-Bedia, M. Ben Amar et Y. Pomeau : Morphological instabilities of dynamic fractures in brittle solids, Phys. Rev. E 54 (1996) 5774-5779.
M. Adda-Bedia and M. Ben Amar : Crack dynamics in elastic media, Phil. Mag. B 78 (1998) 97-102.
M. Adda-Bedia, R. Arias, M. Ben Amar and F. Lund : Dynamic instability of brittle fracture, Phys. Rev. Lett. 82 (1999) 2314-2317.
M. Adda-Bedia, R. Arias, M. Ben Amar et F. Lund : Generalized Griffith criterion for dynamic fracture and the stability of crack motion at high velocities', Phys. Rev. E 60 (1999) 2366-2376.

1.4.2 Instabilité de branchement

Néanmoins, ces études ont été consacrées à la caractérisation du mouvement d'une fracture sans discontinuité dans sa vitesse, sans bifurcation brusque dans sa direction de propagation ni de branchement en deux ou plusieurs fissures. Ce sujet de la dynamique de la rupture fragile a été encore mal exploré, bien qu'expérimentalement, on observe ce type de comportement quand la vitesse de la fracture atteint des vitesses comparables à celles des ondes élastiques du milieu considéré. Les problèmes de radiation engendrée par une propagation "singulière" de la fracture sont sûrement responsables de l'instabilité dite de branchement, et sont aussi importantes dans l'étude des effets sismiques quand on considère la propagation d'une fissure sous cisaillement. Il s'est avéré donc nécessaire d'étudier quantitativement le comportement des contraintes au voisinage de la fissure quand celle-ci change brusquement de direction de propagation ou quand la fracture initiale bifurque en produisant deux fractures symétriques. La résolution analytique de ce problème difficile a constitué une grande partie de mes recherches menées durant ces dernières années.

Dans une première étape, nous avons réussi à élaborer une méthode analytique pour déterminer la distribution, spatiale et temporelle, des contraintes au voisinage de la pointe d'une fracture en mode anti-plan qui, initialement était en mouvement quelconque, et qui instantanément change sa direction et sa vitesse de propagation. Ce calcul n'était connu auparavant que pour le cas d'une propagation quasi-statique. Avec cette méthode en main, nous avons calculé une grandeur importante en mécanique de la rupture fragile : le facteur d'intensité des contraintes qui, pour cette configuration, dépend de la vitesse instantanée de la fracture et de l'angle de bifurcation. En outre, en utilisant une approche analogue, nous avons décrit d'une manière exacte le mécanisme de branchement des fissures en mode anti-plan.

Dans une seconde approche et pour le mode plan, nous avons utilisé une approximation quasi-statique qui néanmoins tient en compte la causalité induite par la propagation des ondes élastiques. Nous avons réussi à comparer la configuration d'une propagation d'une fracture unique avec celle d'une fracture branchée. En étudiant le bilan énergétique de ces

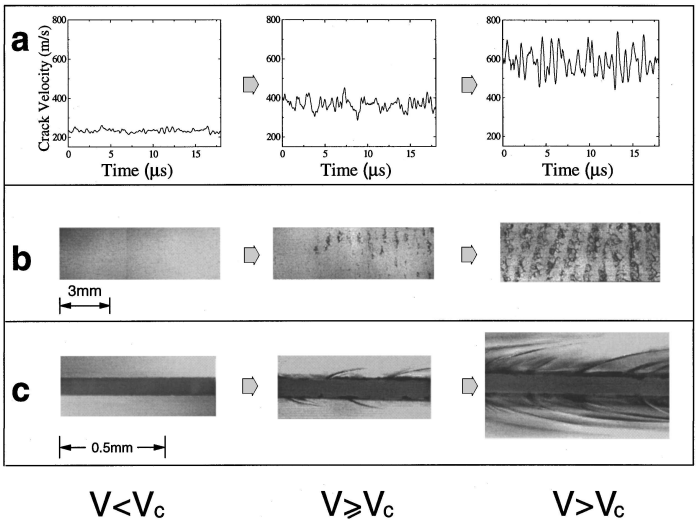

FIG. 1.5 – Instabilité dynamique de branchement. $V < V_c$, surface fissurée lisse. $V \simeq V_c$, apparition de micro-fissures. $V > V_c$, surface fissurée rugueuse. (*E. Sharon et J. Fineberg, Nature (1999)*)

deux configurations, on aboutit au résultat qu'une fracture peut se brancher si sa vitesse de propagation est supérieure à une vitesse critique indépendante de la géométrie de l'expérience et des contraintes appliquées. Comme ce modèle n'utilise que les paramètres élastiques du matériau, il a permis une comparaison systématique des prédictions du modèle avec les expériences sur différents matériaux.

A ce stade, nous avons montré que l'approche utilisant la théorie continue de la rupture fragile explique correctement certains aspects de l'instabilité dynamique de branchement associée à la propagation d'une fracture en mode hors-équilibre. De plus, le comportement de la trajectoire ultérieure des branches a été prédit. Afin de déterminer plus quantitativement cette trajectoire, nous avons entrepris dans le cadre d'une nouvelle collaboration Cnrs-Conicyt une étude du champ des contraintes associé à une géométrie branchée. L'analyse théorique consiste à évaluer le champ des contraintes asymptotiques au voisinage de chaque branche et à déterminer leurs effets sur les trajectoires ultérieures des branches. La trajectoire suivie par chaque branche étant obtenue en appliquant les équations de mouvement que nous avons établies précédemment

L'intérêt de cette étude consiste à valider la théorie continue de la mécanique de la rupture fragile en montrant que tous les aspects de l'instabilité dynamique de la fissure en propagation rapide sont reproduits par cette approche. La comparaison quantitative avec les résultats expérimentaux permettrait d'expliquer les différentes trajectoires des branches en fonction des différents types de chargements appliqués.

M. Adda-Bedia et R. Arias : Brittle fracture dynamics with arbitrary paths : I. Dynamic crack kinking under general antiplane loading, J. Mech. Phys. Solids 51 (2003) 1287-1304.

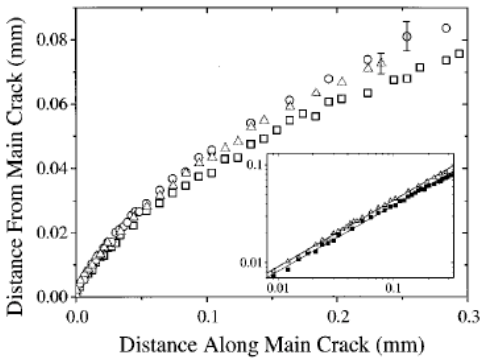

FIG. 1.6 – Forme "universelle" des micro-fissures après branchement. (*E. Sharon et J. Fineberg, Nature (1999)*)

M. Adda-Bedia : Brittle fracture dynamics with arbitrary paths : II. Dynamic crack branching under general antiplane loading, J. Mech. Phys. Solids 52 (2004) 1407-1420.
M. Adda-Bedia : Path prediction of kinked and branched cracks in plane situations, Phys. Rev. Lett. 93 (2004) 185502.
M. Adda-Bedia : Brittle fracture dynamics with arbitrary paths : III. The branching instability under general loading, J. Mech. Phys. Solids 53 (2005) 227-248.

Chapitre 2

Impact et friction

Comme continuation naturelle des travaux sur la rupture, je me suis intéressé aux problèmes de singularités à l'interface entre deux solides en contact. Ce domaine englobe des phénomènes tels que la friction, le contact dynamique ou la rupture entre les failles. Il est aussi le terreau d'instabilités dynamiques et de complexités générées par les hétérogénéités.

2.1 Ondes de glissement

Nous nous sommes intéressés à un problème simple, mais néanmoins fondamental, concernant l'existence de solutions stationnaires d'un pulse de taille finie qui se propage à vitesse constante entre deux matériaux différents. On montre qu'en utilisant la simple loi de friction de Coulomb, il existe un continuum de solutions pour toute vitesse de propagation et pour toute taille du pulse. Cependant, ces solutions ne sont pas physiques car elles exhibent une singularité du champ des contraintes et des vitesses à l'une des extrémités du pulse. Pour essayer de régulariser ces solutions, on introduit une loi de friction modifiée qui découle d'observations expérimentales, et qui consiste à introduire dans la loi de Coulomb un temps de relaxation caractéristique dans la réponse de la contrainte de cisaillement à une variation instantanée de la contrainte normale. On montre que même en utilisant des temps caractéristiques qui dépendent localement de la vitesse de glissement, la dégénérescence des solutions n'est pas levée puisque aucune solution physique n'est sélectionnée. Cette étude analytique montre que des modèles élastiques, même compliqués, ne peuvent pas être pertinents dans le cadre du comportement des failles et il faudrait sûrement rajouter des ingrédients tels que l'hétérogénéité locale des failles.

M. Adda-Bedia et M. Ben Amar : Self-sustained slip pulses of finite size between dissimilar materials, J. Mech. Phys. Solids 51 (2003) 1849-1861.

2.2 Rayonnement sismique de failles hétérogènes

Plusieurs observations fondamentales sur le comportement des failles et des tremblements de terre ne sont pas bien décrites en terme de rupture le long d'une faille homogène. En effet, il a été observé que la propagation d'une fissure le long d'une faille préexistante ne génère pas nécessairement d'énergie sismique. Dans certains modèles numériques, il a été démontré que la transition vers des vitesses de propagation de rupture supérieures aux ondes de cisaillement est intimement liée à la génération d'énergie sismique et à la dissipation d'énergie dues aux changements de la vitesse de rupture sur la faille. Ainsi, la rupture sur les failles lisses tend à être supersonique et ne produit pas beaucoup de rayonnement, alors que les failles géométriquement complexes se propagent à des vitesses inférieures aux ondes de cisaillement et génèrent du rayonnement. Une approche possible, que je poursuis avec R. Madariaga, pour carcactériser le bilan énergétique pendant les ruptures sismiques est de déterminer en détail la partition de l'énergie pendant la propagation d'une fissure en tenant compte de la complexité géométrique de la faille. Nous utiliserons les résultats exacts déjà obtenus sur la propagation d'une fissure en mode anti-plan initialement droite qui change instantanément sa direction et sa vitesse de propagation pour l'analyse des conséquences de la complexité géométrique de la faille sur l'énergie sismique rayonnée.

Notre projet est d'utiliser notre connaissance sur le coin élémentaire pour étudier de façon statistique le cas d'une faille qui, comme dans la nature, possède une complexité géométrique. Dans ce cas la rupture va interagir avec la géométrie afin de développer un champ de contraintes hétérogène qui, à son tour, conduira à une sismicité complexe. Plusieurs études sur le problème d'une faille plane montrent que dans ce cas la complexité qui apparaît n'est pas assez forte pour expliquer la distribution des magnitudes sismiques observées. Nous souhaitons explorer la nature de la sismicité qui apparaîtra dans un modèle de faille plus complexe possédant une distribution aléatoire de coins.

M. Adda-Bedia et R. Madariaga : Radiation from a kink on an antiplane fault, soumis à BSSA (2006).

2.3 Dynamique de l'impact

Quand deux sphères rentrent en contact, elles dissipent une partie de leurs énergies par divers processus. Cette observation a conduit Newton à définir le concept de restitution d'énergie, qui a survécu depuis et qui reste la seule représentation théorique de l'impact. Nous avons étudié la dynamique de propagation des ondes élastiques d'un disque entrant en contact avec une surface rigide. Cette étude étant restreinte aux temps très courts après l'impact, elle se situe dans un régime qui n'est pas exploré par la théorie quasi-statique due à Hertz. Dans ce régime, on a prouvé que la surface de contact croissait plus rapidement que la vitesse de propagation des ondes élastiques. D'autre part, nous avons étudié pour ce système modèle le comportement du champ des contraintes durant le passage de ce régime supersonique vers le régime subsonique. Nous avons prouvé l'existence d'une singularité faible du champ des contraintes au point transonique qui pourrait être responsable de la

détérioration systématique des matériaux lorsqu'ils sont soumis à des chocs, ainsi que des effets dissipatifs correspondants.

M. Adda-Bedia et S. G. Llewellyn Smith : Supersonic and subsonic stages of dynamic contact between bodies, Proc. R. Soc. A (2006) à paraître.

Chapitre 3

Autres Problèmes

3.1 Instabilités d'une arche

On a étudié le problème typique de l'*elastica*. Cette étude numérique est consacrée à une expérience faite par Born et reprise plus tard par Pippard. Elle consiste à soumettre une arche, aux extrémités fixées, à une force croissante appliquée à son milieu. Cette expérience simple donne un diagramme de phase très riche, déterminé expérimentalement par Pippard, et qui correspondant aux différentes formes prise par l'arche. Nous avons retrouvé théoriquement toutes les phases décrites par Pippard. Pour cela, l'étude statique et l'étude de la stabilité dynamique de ce système ont été nécessaires pour compléter le diagramme de phase expérimental.

P. Patricio, M. Adda-Bedia et M. Ben Amar : An elastica problem : instabilities of an elastic arch, Physica D 124 (1998) 285-295.

3.2 Formes d'équilibre des gouttes superposées

La thermodynamique nous indique que deux phases, comme un liquide et une vapeur à la même température, pression et potentiels chimiques, peuvent coexister sur une surface bidimensionnelle. Ceci est naturel, puisque génériquement l'intersection de deux volumes est donné par une surface. De même, quand on considère trois phases, comme une goutte, sa vapeur et une surface solide, l'intersection se fait sur une ligne. Ceci est aussi naturel, puisque cette ligne est l'intersection de trois phases volumiques. Il est connu depuis longtemps que la forme d'équilibre d'une goutte sur un substrat solide, en négligeant la gravité, est une hémisphère qui coupe le solide sur un cercle, la ligne de contact d'équilibre. L'étape suivante apparaît évidente : l'intersection entre quatre phases, dans ce cas deux fluides non miscibles, une vapeur et un solide, doivent-elles toujours se rencontrer en un point ? On a montré que dans certains cas, ceci n'est pas vrai. En fait, la rencontre de ces quatre phases se fait aussi sur une ligne. Ceci provient d'une particularité des conditions d'équilibre de Young-Laplace qui n'a pas été notée auparavant.

L. Mahadevan, M. Adda-Bedia et Y. Pomeau : Four-phase merging in sessile compound drops, J. Fluid Mech. 451 (2002) 411-420.

Chapitre 4

Projets

Les projets qui résultent de la continuation des travaux présentés ci-dessus ont été mentionnés dans leurs contextes. Cette partie expose des projets concernant de nouvelles directions de recherche. Parmi ces projets, il y en a qui sont dans leurs stades préliminaires et d'autres qui ont déjà commencé à produire des résultats.

4.1 Morphogénèse induite par la mécanique

Ce projet est en partie relié à une ACI Jeunes chercheurs et à un contrat européen. Dans ce cadre, nous proposons d'appliquer la mécanique des structures élastiques à des problèmes issus de la biologie. En effet, si les équations fondamentales gouvernant les structures élastiques sont bien établies (équations des tiges, plaques et coques), elles se trouvent souvent couplées, pour les applications aux systèmes vivants, à des champs autres qu'élastiques ou à des contraintes géométriques, ce qui leur confère une complexité spécifique. Les applications de la mécanique à la biologie suscitent un fort intérêt de la communauté scientifique depuis quelques années. Les recherches effectuées jusqu'ici favorisent le plus souvent une approche descriptive des phénomènes. Nous proposons d'aborder ces problèmes en identifiant un nombre minimal d'ingrédients essentiels (notion de systèmes modèles) afin de permettre une démarche prédictive.

Le principal objectif de notre projet est d'apporter une meilleure compréhension du comportement mécanique de certaines structures biologiques, et de leur morphogenèse. Les structures biologiques minces sont présentes sous des formes variées (feuilles, fleurs, peau, cheveux et autres fibres, ADN). Leur formes, parfois très complexes (fronces de fleurs et feuilles, arborescences végétales ou des poumons, circonvolutions du cerveau) soulève la question fondamentale de l'origine de ces géométries. Comment ces structures sont-elles générées du point de vue mécanique ? Nous aborderons cette question en étudiant des systèmes minces inertes qualitativement similaires : une tige confinée pour l'ADN d'un virus ou la compression d'un matériau cellulaire pour les nervures des feuilles, par exemple. Les formes biologiques sont souvent obtenues par un processus de croissance : c'est la croissance différentielle des tissus qui induit des contraintes mécaniques et, par flambage, des formes spécifiques. Les notions de métrique et de variétés mathématiques y

sont liées.

4.1.1 Filaments élastiques confinés

Collaboration avec A. Boudaoud (LPS), E. Katzav (Postdoc), L. Boué (Thésard).

Les propriétés mécaniques de la molécule d'ADN jouent un rôle important lors des phases de transcription des gènes en protéines. Nous nous intéressons aux régimes où elle est fortement confinée ou fortement contrainte. Dans ces régimes, les contributions entropiques à l'énergie libre sont petites devant l'énergie interne ; on peut alors étudier les propriétés mécaniques de l'ADN dans la cadre de l'élasticité des tiges. Par exemple, les virus bactériophages (virus attaquant des bactéries) ont la grande particularité que leur matériel génétique est fortement compacté dans l'enveloppe (appelée capside). Par exemple, le bactériophage T4 possède une molécule d'ADN de longueur 54 μm alors que la capside a un rayon de 50 nm (de l'ordre de la longueur de persistance de l'ADN), ce qui correspond à un taux de compression de l'ordre de 103. D'autres mesures ont montré que la pression effective provenant de ce confinement est énorme, de l'ordre de 50 atmosphères. Notre approche consistera à étudier les formes d'équilibre d'une tige élastique confinée dans un disque (2D) ou dans une boule (3D), par minimisation de l'énergie élastique et par étude statistique des configurations admissibles. En parallèle, de nouvelles expériences macroscopiques (injection contrôlée d'une tige dans une sphère transparente, et, pour une version 2D, d'une feuille à travers un anneau) permettront de mesurer simultanément le confinement et les forces correspondantes.

Dans une première étude nous avons proposé une approche statistique pour étudier le confinement d'une tige élastique dans une sphère. La méthode développée est basée sur une approche inroduite par Edwards qui a été appliquée avec succès à la physique des polymères et aux matériaux granulaires. Nous avous montré que le confinement induit une transition de phase entre une configuration désordonnée (isotrope) et une configuration ordonnée (nématique). Dans chaque phase, nous avons dérivé la pression exercée par la tige sur le récipient et la force nécessaire pour injecter la tige dans le récipient. Concernant l'ADN confiné dans les capsides virales, ces résultats établissent l'existence des configurations ordonnées, une hypothèse sur laquelle les études précédents ont été basées. Ils prouvent également qu'un tel ordre peut résulter seulement de contraintes mécaniques.

E. Katzav, M. Adda-Bedia et A. Boudaoud : A statistical approach to close packing of elastic rods and to DNA packaging in viral capsids, soumis à PNAS (2005).

4.1.2 La géométrie des feuilles minces pliées

Collaboration avec A. Boudaoud (LPS), L. Boué (Thésard).

Les feuilles de la plupart des plantes sont enroulées ou pliées quand elles sont encore à l'intérieur du bourgeon, et l'organisation de leurs veines primaires semble être fortement

corrélée avec la géométrie du confinement. Le déploiement des feuilles pendant leur croissance en dehors du bourgeon pose des questions géométriques complexes : comment est-il rendu possible ? Quels sont les géometries possibles des structures pliées pour la feuille à l'intérieur du bourgeon et du réseau correspondant des veines ? Nous développerons une méthodologie générale pour étudier le pliage et le déploiement des feuilles minces afin de répondre à ces questions. Du côté expérimental, nous concevrons un procédé systématique pour plier et déplier les feuilles élastiques minces d'une façon reproductible. Nous étudierons également le confinement d'une feuille dans un récipient afin de mesurer la pression en fonction du volume. Les simulations numériques directes de ce type de problèmes sont très difficiles en raison des différences d'échelles et des conditions de non interpénétration. Ceci exige de nouveaux outils théoriques mélangeant la mécanique (les équations de plaques minces) et la géométrie différentielle (l'origami).

4.1.3 Nervures des feuilles

Collaboration avec H. Henry (PMM, Polytechnique), F. Corson (Thésard).

Récemment, la mécanique des couches minces a pu être appliquée à la morphogenèse en biologie, au niveau cellulaire (parois cellulaires prises comme des coques élastiques ou élasto-plastiques) ou au niveau des organes (le tissu cellulaire étant alors pris comme matériau élastique). l'idée étant d'expliquer l'apparition de formes par des instabilités élastiques. Nous souhaitons étendre cette approche mécanique de la morphogénèse aux nervures des feuilles végétales.

Une famille de structures naturelles qui a été largement étudiée résulte de la croissance de formes induite par des champs scalaires, laplaciens ou diffusifs. Cette classe englobe, entre autres, la digitation visqueuse de fluides newtoniens, la croissance cristalline, la croissance de colonies de bactéries ou la croissance limitée par la diffusion. Bien que les formes résultantes aient chacune leurs spécificités, elles partagent toutes une même caractéristique topologique : une forme arborescente hiérarchisée. Il existe une autre classe de structures caractérisée par une forme en réseaux reconnectés. Cette famille encore mal étudiée englobe entre autres les nervures des feuilles, les figures de fractures induites par séchage (boue, céramiques,...) ou digitations visqueuses dans les fluides complexes. Contrairement aux structures arborescentes, ces formes sont dues à une croissance induite par des champs tensoriels, dont l'évolution peut souvent être réduite à une dynamique bi-laplacienne. Récemment, les réseaux de vénation d'une feuille de plante ont été expliqués par analogie avec les réseaux de fracture d'une boue qui sèche : les veines permettraient de relaxer un champ tensoriel, tout comme les fractures classiques relaxent le tenseur des contraintes. Cette analogie n'est cependant pas complète, car la croissance des feuilles à l'intérieur du bourgeon engendre des contraintes de compression, alors qu'une fracture classique est produite par des efforts d'extension. Par cet aspect, la croissance des feuilles ressemble plus à la compression des matériaux cellulaires qu'aux fissures classiques. La compression de ces matériaux cellulaires engendre d'ailleurs une focalisation inhomogène des contraintes, phénomène étudié notamment pour ses applications aux

matériaux nouveaux. Nous nous proposons d'approcher la croissance végétale en incluant les ingrédients suivants : croissance, existence de contraintes de compression bi-axiales (alors que les matériaux cellulaires sont généralement étudiés sous contrainte uni-axiale), géométrie (extension limitée de la feuille et confinement). Ces ingrédients réunis devraient permettre d'expliquer la complexité des motifs de vénation observés dans les plantes, et de les classifier sur une base mécanique rigoureuse.

Y. Couder, L. Pauchard, C. Allain, M. Adda-Bedia et S. Douady : The leaf venation as formed in a tensorial field, Eur. Phys. J. B 28 (2002) 135-138.

4.2 Modélisation de la croissance du crâne de l'enfant

Collaboration avec A. Boudaoud (LPS), B. Audoly (LMM, Paris 6), M.-J. Deshayes (TCI).

Les trajectoires de croissance de la sphère crânienne résultent de la compétition entre les différents os-moteurs qui forment la base du crâne. Ces os sont initialisés dès les premiers stades du développement neurologique fœtal et se poursuivent au cours de l'ontogenèse lors de l'expansion du système cérébral. Ces moteurs ont une action fondamentale sur le remodelage des os de la sphère crânienne au cours de la croissance (jusque vers l'âge de 6 ans). Comprendre les mécanismes physiques dynamiques qui sont responsables de la croissance du crâne intéresse tous les professionnels de santé dont le domaine d'action est la sphère crânienne, en particulier les orthodontistes pour une meilleure conception des traitements des dysharmonies cranio-faciales et les anthropologues pour une meilleure analyse de la croissance des fossiles.

D'autre part, la morphogenèse et l'interaction entre contraintes et croissance sont des domaines en plein essor en physique et en mécanique. Etant donné que la croissance du crâne est bien caractérisée et que ses propriétés mécaniques sont relativement simples, ce projet permettra de tester les idées physiques et les modèles qui en découlent en comparant les résultats de simulations numériques avec les données morphométriques sur la croissance du crâne. En particulier, le changement de forme des os crâniens devra être reproduit par les processus physiques implémentés dans le modèle. Ainsi un modèle de crâne virtuel sera développé et cet outil numérique permettra de simuler plusieurs trajectoires de croissance du crâne. A plus long terme, les résultats de cette étude devraient apporter une aide à la compréhension de la croissance crânienne, mais surtout un outil numérique totalement "contrôlable", absolument non invasif, d'observation de la croissance crânienne.

Les objectifs premiers de ce projet sont d'identifier les mécanismes physiques intervenant dans la croissance du crâne humain et de développer un modèle numérique fondé sur ces mécanismes afin de reproduire et prédire la croissance du crâne. Les objectifs à long terme concernent des applications à l'orthodontie – contraintes mécaniques à exercer pour corriger des dysharmonies cranio-faciales – et à la phylogénie – explication de l'évolution des morphologies crâniennes.

Ce projet est en collaboration avec le Docteur M.-J. Deshayes qui a étudié d'une

manière approfondie la croissance crânienne chez l'enfant et a établi un protocole de mesures morphométriques qui permet de distinguer différentes dynamiques de croissance et de quantifier les dysharmonies cranio-faciales qui peuvent y être associées. Nous nous baserons sur ses connaissances pour déterminer les mécanismes physiques à modéliser. Une fois le modèle physique développé, nous utiliserons sa base de données d'indices crâniens, issue de l'observation (instantanée ou répétée dans le temps) de cas cliniques, afin d'ajuster et/ou valider le modèle.

4.3 Projets expérimentaux

Collaboration avec A. Boudaoud (LPS), Y. Couder (MSC, Paris 7).

Nous désirons développer une activité expérimentale axée autour des instabilités et de la morphogenèse dans les systèmes mécaniques soumis à des contraintes induites par la croissance, une pression externe, des phénomènes interfaciaux ou un écoulement. Plus précisément, les principales directions de notre projet concernent la compression et le repliement d'objets élastiques, les instabilités d'interfaces comme la fracture et la friction, les vibrations des plaques en présence de singularités ou de structures organisées, et les déformations d'objets flexibles placés dans un écoulement. Ces directions se rattachent à différentes problématiques générales que nous présentons ci-dessous, mais elles ont un même fil directeur qui est l'étude des instabilités et des formes qui en résultent. Nous avons déjà travaillé sur certaines des expériences reliées à la première direction, croissance et compaction, nous comptons approfondir ces études et en commencer de nouvelles. Dans ce qui suit, nous présentons les différents thèmes et expériences que nous voulons développer dans le futur proche.

4.3.1 Croissance et compaction

La croissance d'un objet élastique génère des contraintes internes – par croissance différentielle comme un tissu vivant formé de deux couches (e.g. la peau) – ou externes – par la croissance dans un milieu confiné (feuille dans un bourgeon). Nous nous intéressons à la morphogenèse induite par ces contraintes et aux propriétés géométriques et mécaniques des structures résultantes. Voici les études expérimentales que nous avons entamées

Compaction d'objets flexibles–Nous comptons étudier les formes d'équilibre d'une tige ou d'une feuille élastique confinée dans un espace bidimensionnel ou tridimensionnel, ainsi que leurs propriétés statistiques et mécaniques (mesure des forces appliquées en fonction du taux de confinement). Les contraintes géométriques étant fortement dépendantes de la dimensionnalité de l'objet et du container, nous envisageons des expériences adaptées à chaque cas. Comme il est difficile d'introduire une tige dans un cercle sans artefacts expérimentaux et encore plus difficile de mesurer la pression exercée sur le cercle, nous avons conçu le dispositif du "rond de serviette", une feuille tirée à travers un trou circulaire et dont une section équivaut au confinement d'une tige dans un cercle. Les premières expériences (Antonin Eddi, stage de L3 et Davide Cassani, stage de M2) ont montré que

les configurations résultent d'une succession de changements de forme élémentaires associés à des minima de pression. L'étude systématique est en cours. En ce qui concerne la compaction d'une feuille (2D dans 3D), il est a priori difficile de visualiser les configurations. Couper les "boulettes de papier" permet de contourner cette difficulté et d'accéder à l'étude statistique des propriétés géométriques : les longueurs, les aires (Etienne Couturier, stage de M2).

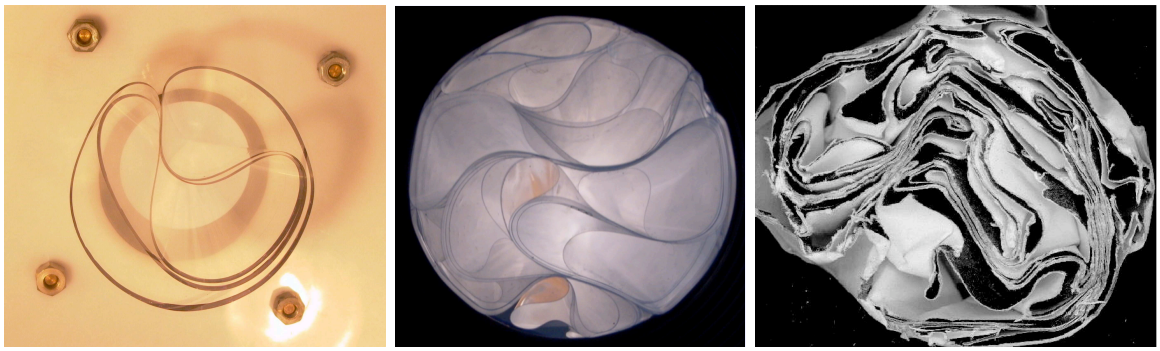

FIG. 4.1 – Formes de différents objets flexibles confinés.

Pliages réguliers, flambage d'un secteur angulaire–Les feuilles de nombreux arbres présentent dans les premières étapes de leur croissance une structure pliée au sein du bourgeon. C'est le cas par exemple du charme où la feuille même une fois dépliée conserve une structure ondulée. Afin de mimer la croissance d'une feuille dans un bourgeon, nous étudions les structures obtenues par la compression de feuilles de Mylar. Cette modélisation se justifie par l'analogie suivante : lors de la croissance de la feuille la nervure principale croît plus lentement que les nervures secondaires, il en résulte une différence de vitesse de croissance entre la direction de la veine principale et la direction perpendiculaire. On peut alors modéliser cette différence de vitesse de croissance par l'application d'une contrainte de compression suivant la nervure principale (Tristan Machado, stage de L3). Notre but est de déterminer l'influence de la géométrie de la feuille sur la distribution des nervures secondaires

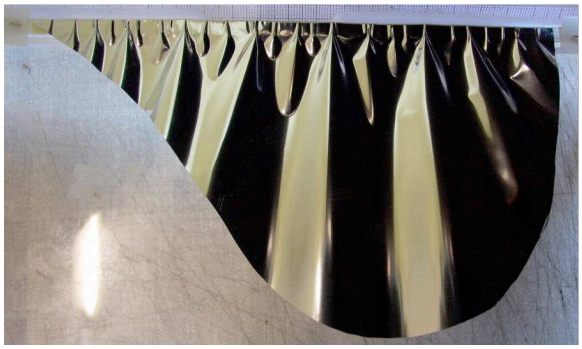

FIG. 4.2 – Flambage induit par la compression d'une feuille de Mylar de géométrie prédeterminée.

4.3.2 fracture des objets minces

Lorsque l'on veut arracher du papier peint, il est impossible de le détacher en entier, car il se forme des lambeaux. En d'autres termes, les deux pointes des fissures engendrées semblent toujours s'attirer. De façon générale, le cheminement d'une fissure dans une plaque mince est un phénomène mal compris. Nous reproduirons ce phénomène dans un dispositif expérimental simple et contrôlé (en construction). Nous étudierons la stabilité de la propagation rectiligne de la fissure et le profil selon l'épaisseur de la feuille. Malgré sa simplicité apparente, cette expérience devrait contribuer à éclaircir le problème général du mouvement des fissures. Elle peut également être modifiée pour étudier l'interaction entre plusieurs fissures parallèles.

4.3.3 Friction sur une membrane tendue

Nous comptons simplifier une expérience de Valette et Gollub (PRE, 1993) sur la friction d'un objet sur une membrane tendue dans la largeur. Nous imposerons le déplacement d'un indenteur isolé et sphérique sur une membrane tendue de manière isotrope. Notre but est d'étudier les ondes de surface générées par le déplacement de l'indenteur. La configuration de cette expérience est assez simple pour pouvoir étudier le rôle des ondes dans la dissipation par friction. Elle peut être étendue à d'autres géométries (plusieurs indenteurs ou substrat épais).

LISTE DES PUBLICATIONS [1]

Articles soumis :

– M. Adda-Bedia and R. Madariaga : "Radiaton from a kink on an antiplane fault", submitted to *BSSA* (2006).

– E. Katzav and M. Adda-Bedia : "Roughness of tensile crack fronts in heterogenous materials", submitted to *Phys. Rev. Lett.* (2005).

– E. Katzav, M. Adda-Bedia and A. Boudaoud : "A statistical approach to close packing of elastic rods and to DNA packaging in viral capsids", submitted to *PNAS* (2005).

Articles dans des revues à comité de lecture :

– M. Adda-Bedia, E. Katzav and D. Vandembroucq : "Second order variation in elastic fields of a tensile crack with a curved front", *Phys. Rev.* E **73** (2006) 035106(R).

– M. Adda-Bedia and S. G. Llewellyn Smith : "Supersonic and subsonic stages of dynamic contact between bodies", *Proc. R. Soc.* A (2006) to be published.

– M. Adda-Bedia and L. Mahadevan : "Peeling-induced crack-front instability in a confined elastic film", *Proc. R. Soc.* A (2006) to be published.

– S. Bohn, J. Platkiewicz, B. Andreotti, M. Adda-Bedia and Y. Couder : "Hierarchical crack pattern as formed by successive domain divisions. II. From disordered to deterministic behavior", *Phys. Rev.* E **71** (2005) 046215.

– M. Adda-Bedia : "Brittle fracture dynamics with arbitrary paths : III. The branching instability under general loading", *J. Mech. Phys. Solids* **53** (2005) 227-248.

– M. Adda-Bedia : "Path prediction of kinked and branched cracks in plane situations", *Phys. Rev. Lett.* **93** (2004) 185502.

– M. Adda-Bedia : "Brittle fracture dynamics with arbitrary paths : II. Dynamic crack branching under general antiplane loading", *J. Mech. Phys. Solids* **52** (2004) 1407-1420.

– M. Adda-Bedia and M. Ben Amar : "Self-sustained slip pulses of finite size between dissimilar materials", *J. Mech. Phys. Solids* **51** (2003) 1849-1861.

– M. Adda-Bedia and R. Arias : "Brittle fracture dynamics with arbitrary paths : I. Dynamic crack kinking under general antiplane loading", *J. Mech. Phys. Solids* **51** (2003) 1287-1304.

– L. Pauchard, M. Adda-Bedia, C. Allain and Y. Couder : "Morphologies resulting from the directional propagation of fractures", *Phys. Rev.* E **67** (2003) 027103.

– Y. Couder, L. Pauchard, C. Allain, M. Adda-Bedia and S. Douady : "The leaf venation as formed in a tensorial field", *Eur. Phys. J.* B **28** (2002) 135-138.

– L. Mahadevan, M. Adda-Bedia and Y. Pomeau : "Four-phase merging in sessile compound drops", *J. Fluid Mech.* **451** (2002) 411-420.

– M. Adda-Bedia and M. Ben Amar : "Fracture spacing in layered materials", *Phys. Rev. Lett.* **86** (2001) 5703-5706.

– M. Adda-Bedia, R. Arias, M. Ben Amar and F. Lund : "Generalized Griffith criterion for dynamic fracture and the stability of crack motion at high velocities", *Phys. Rev.* E **60** (1999) 2366-2376.

[1] La plupart des articles peuvent être téléchargées à partir du site : www.lps.ens.fr/∼adda/publis.html

– M. Adda-Bedia, R. Arias, M. Ben Amar and F. Lund : "Dynamic instability of brittle fracture", *Phys. Rev. Lett.* **82** (1999) 2314-2317.
– M. Adda-Bedia and M. Ben Amar : "Crack dynamics in elastic media", *Phil. Mag.* B **78** (1998) 97-102.
– P. Patricio, M. Adda-Bedia and M. Ben Amar : "An elastica problem : instabilities of an elastic arch", *Physica* D **124** (1998) 285-295.
– M. Adda-Bedia, M. Ben Amar and Y. Pomeau : "Morphological instabilities of dynamic fractures in brittle solids", *Phys. Rev.* E **54** (1996) 5774-5779.
– M. Adda-Bedia and M. Ben Amar : "Stability of quasi-equilibrium cracks under Mode I loading", *Phys. Rev. Lett.* **76** (1996) 1497-1500.
– M. Adda-Bedia and Y. Pomeau : "Crack instabilities of a heated glass strip", *Phys. Rev.* E **52** (1995) 4105-4113.
– M. Adda-Bedia and M. Ben Amar : "Faceting in free dendritic growth", *Phys. Rev.* E **51** (1995) 1268-1275.
– M. Adda-Bedia and V. Hakim : "Faceted needle crystals : an analytical approach", *J. Phys. I France* **4** (1994) 383-391.
– M. Adda-Bedia and M. Ben Amar : "Investigations on the dendrite problem at zero surface tension in 2D and 3D geometries", *Nonlinearity* **7** (1994) 765-776.
– M. Adda-Bedia and M. Ben Amar : "Faceting morphological instabilities", *Ann. Chim.-Sci. Mat.* **16** (1991) 275-283.
– M. Adda-Bedia and M. Ben Amar : "Faceting in directional solidification", *Phys. Rev.* A **43** (1991) 5702-5705.

Articles dans des proceedings :
– F. Corson, M. Adda-Bedia H. Henry : "A model for hierarchical patterns under mechanical stresses", in 5^{th} Plant Biomechanics Conference, Stockholm (2006).
– L. Boué, M. Adda-Bedia and A. Boudaoud : "Confinement isotrope d'un cylindre élastique", in Rencontres du non-linéaire. Ed. R. Ribotta (Paris Onze Editions, 2006).
– E. Katzav and M. Adda-Bedia : "Nonlinear equation of motion for propagating crack fronts in heterogenous materials", in Rencontres du non-linéaire. Ed. R. Ribotta (Paris Onze Editions, 2006).
– M. Adda-Bedia : "Branching instability of brittle fracture", in ICTAM Proceedings (Kluwer Academic Publishers, 2004).
– M. Adda-Bedia and M. Ben Amar : "Branching dynamics of brittle fracture", in Configurational Mechanics. Ed. V.K. Kalpakides and G.A. Maugin (A.A. Balkema Publishers, Rotterdam, 2004) p. 119-138.
– L. Pauchard, C. Allain, M. Adda-Bedia and Y. Couder : "Une nouvelle morphologie : fractures paraboliques induites par séchage", in Rencontres du non-linéaire. Ed. R. Ribotta (Paris Onze Editions, 2001).
– Y. Couder, L. Pauchard, C. Allain, M. Adda-Bedia and S. Douady : "Sur la similitude des morphologies des nervations des feuilles et de celles des fractures", in Rencontres du non-linéaire. Ed. R. Ribotta (Paris Onze Editions, 2000) p. 23-28.
– M. Adda-Bedia and M. Ben Amar : "Faceting of weakly anisotropic materials", in

Growth and forms, nonlinear aspects. Ed. M. Ben Amar, P. Pelcé and P. Tabeling (Plenum Press, New York, 1991).

Autres travaux

– D. Bonn, M. Adda-Bedia et T. Baumberger : "Au coeur de la fracture et du frottement", Contribution la brochure du département de Physique de l'Ecole Normale Supérieure, 1999.

– M. Adda-Bedia : "Croissance Cristalline : Formes et Dynamique", Rapport commandé par l'Institut de l'Ecole Normale Supérieure, Mars 1995.

– M. Adda-Bedia : "Sur quelques problèmes de croissance cristalline : Formes et Dynamique", Thèse de Doctorat (Université Paris 6, Février 1994).

SELECTION DE PUBLICATIONS

Crack instabilities of a heated glass strip

Mokhtar Adda-Bedia[1] and Yves Pomeau[1,2]
[1]*Laboratoire de Physique Statistique, Ecole Normale Supérieure, 24 rue Lhomond, F-75231 Paris Cedex 05, France*
[2]*Department of Mathematics, University of Arizona, Tucson, Arizona 85721*
(Received 9 March 1995)

Recently, Yuse and Sano [Nature (London) **362**, 329 (1993)] have observed that a crack traveling in a glass strip submitted to a nonuniform thermal diffusion field undergoes numerous instabilities. We study two cases of quasistatic crack propagation. The crack extension condition in straight propagation is determined. An asymptotic analysis of the elastic free energy is introduced and scaling laws are derived. A linear stability analysis of the straight propagation is performed, based on the assumption that the crack tip propagation deviates from the centered straight one as soon as it is submitted to a "physical" singular shear stress. It is shown that a straight propagation can become unstable after which a wavy instability appears. The condition for instability as well as the selected wavelength is calculated quantitatively. The results are compared with experiments and the agreement is favorable.

PACS number(s): 62.20.Mk, 46.30.Nz, 81.40.Np

I. INTRODUCTION

The study of crack propagation often follows two approaches. The first is for dynamical fracture formation, where the cracked surfaces are created at a velocity of the order of the Rayleigh wave speed [1]. The second one is for slow or quasiequilibrium cracks. For the second case, the work of Griffith in 1921 [2] is often seen as the beginning of equilibrium fracture mechanics as a quantitative science of material behavior. However, from that time on the progress was mainly made in the fields of engineering. Recently, a renewal of interest has been caused by the work of Yuse and Sano [3]. They have carried out an experiment making reproducible sequences of crack patterns. This is an important step in the understanding of crack instabilities because well-controlled experiments in this field are uncommon.

As shown in Fig. 1, the experiment [3] is performed by pulling a thin glass strip from a hot region (heater) to a cold one (water bath) at a slow and constant velocity V. The control parameters are [3,4] the pulling velocity V, the strip width $2b$, and the temperature variation ΔT between the heater and the cold bath. When these parameters are small enough the strip does not break. By increasing essentially b or ΔT, a centered straight crack appears and extends at a velocity $-V$ in the frame of the strip. By further increasing these parameters, the straight crack becomes unstable and the fracture follows an oscillating path.

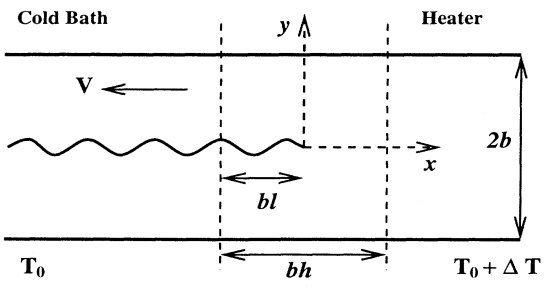

FIG. 1. Schematic representation of the experiment of Yuse and Sano [3].

The experiment has been simulated numerically with spring models [5] and by doing a complete numerical resolution of the corresponding thermoelastic problem but with discontinuous incrementation of the crack path [6]. On the other hand, theoretical treatments [7,8] have been undertaken to explain the bifurcation from the straight crack propagation to the wavy one. Although the noncracked-cracked plate transition was not studied quantitatively in [3], the results [6–8] of this bifurcation analysis are quite unanimous and agree with the qualitative measurements in [3]. In fact, the condition of existence of stably advancing straight cracks is based on a criterion of energy minimization [2] that is well understood. On the contrary, the physical origin of the instability straight-undulating crack remains unclear. Even in the asymptotic regions, results of Refs. [6–8] do not agree with each other, although they use the same criterion to explain this transition. Moreover, a comparison of these results with experiment [3] cannot be done rigorously because of the uncertainty in the value of the so-called *fracture energy* [9]. The quantitative experimental study of the no crack–straight crack transition could solve this problem [4].

Much effort has been devoted to the study of the oscillatory instability by using the "*criterion of local symmetry*" [10]. It states that the path taken by a crack in brittle homogeneous isotropic material is the one for which the local stress field at the tip is of mode I type. Let us recall that mode I loading causes an opening of the fracture while mode II loading causes a shearing off. The local analysis in the neighborhood of a crack tip shows that the asymptotic stress tensor field $\overline{\overline{\Sigma}}$, in the polar coordinate system (r,ϕ), takes the universal form [1]

$$\Sigma_{ij}(r,\phi) = \frac{K_{\rm I}}{\sqrt{2\pi r}} f_{ij}^{\rm I}(\phi) + \frac{K_{\rm II}}{\sqrt{2\pi r}} f_{ij}^{\rm II}(\phi), \tag{1}$$

where $f_{ij}^{\rm I}(\phi)$ and $f_{ij}^{\rm II}(\phi)$ are universal functions common to all configurations and loading conditions. The influence of configuration and loading are included in the asymptotic description of stress only through the scalar multipliers $K_{\rm I}$ and $K_{\rm II}$, which are the elastic stress intensity factors of mode I and mode II loadings, respectively. The criterion of local symmetry features that, if a shear loading exists at the crack tip, $K_{\rm II} \neq 0$ and the crack will move by changing the orientation of the tangent to the path.

Consider a straight crack subjected to mode I loading. Nominally, $K_{\rm II} = 0$, but due to the imperfections in the system and, consequently, in crack alignment, $K_{\rm II}$ will differ slightly from zero. The existence of such shear loading implies automatically that the crack deviates from a straight line [10,11]. Moreover, for this finite plate problem, there exists a "geometrical" shear loading that appears as soon as the crack deviates from the center of the strip. The combining of these two loadings leads to the appearance of the oscillatory instability [12]. The undulating crack may be due to an instability of the straight crack, which creates a mode II loading, and the geometry of the problem, which amplifies this shear loading and leads to the oscillatory instability of the crack tip.

These general considerations lead us to investigate the problem in a different manner than [6–8]. To define the wavy instability of the crack, we did not analyze it at the level of the criterion $K_{\rm II} = 0$, but before it. That is when a slight deviation from the straight crack will create a "physical" shear loading.

II. INSTABILITIES OF A CRACK IN A HEATED STRIP

The experimental configuration we will analyze is illustrated in Fig. 1. The coordinate system (x, y) is defined on an infinitely long strip of thin glass whose boundaries are located at $y = \pm b$. A semi-infinite crack, whose tip is taken as the origin of the coordinate system, is placed on the strip. In the following, we will take the half-width of the strip b as the unit length. Since we focus on quasistatic fractures, the advancing velocity V of the crack comes into the problem only through the temperature field, assumed to be constant in the cold bath $(x \leq -l)$ and independent of the transverse direction y. Here l denotes the crack tip position in the temperature gradient.

Under plane stress conditions, the strain tensor of a thin plate in the temperature field $T_l(x)$ is related to the stress tensor by [13]

$$\Sigma_{ij} = \frac{1}{1-\nu^2}\left\{(1-\nu)E_{ij} + \nu E_{kk}\delta ij - (1+\nu)T_l(x)\delta_{ij}\right\}, \tag{2}$$

where $\overline{\overline{\Sigma}}(x,y)$ $[\overline{\overline{E}}(x,y)]$ is the two-dimensional stress (strain) tensor and ν the Poisson ratio. For convenience, all the quantities in Eq. (2) are dimensionless: $\overline{\overline{\Sigma}}$ is scaled by $E\alpha_T\Delta T$, $\overline{\overline{E}}$ by $\alpha_T\Delta T$, and $T_l(x)$ by ΔT, where E is the Young modulus and α_T the coefficient of thermal expansion. Note that $\overline{\overline{\Sigma}}(x,y)$ $[\overline{\overline{E}}(x,y)$ and $T_l(x)]$ must be understood as the average of $\overline{\overline{\Sigma}}(x,y,z)$ $[\overline{\overline{E}}(x,y,z)$ and $T_l(x,z)]$ across the thickness of the strip [13]. Inversely, the strain tensor is given, in terms of the stress tensor, by

$$E_{ij} = \frac{1}{2}\left\{\frac{\partial U_i}{\partial x_j} + \frac{\partial U_j}{\partial x_i}\right\} = \{(1+\nu)\Sigma_{ij} - \nu\Sigma_{kk}\delta ij\} + T_l(x)\delta_{ij}, \tag{3}$$

where $\vec{U}$ is the displacement vector. For this problem, the temperature field $T_l(x)$ is usually approximated by

$$T_l(x) = \left(1 - e^{-P(x+l)}\right)\theta(x+l), \tag{4}$$

where $\theta(\,)$ is the Heaviside function. The parameter $P = bV/D$ is the ratio of the geometrical length b to the thermal diffusion length $d_{\rm th} = D/V$, where D is the diffusion constant. The temperature field given by Eq. (4) satisfies the stationary diffusion equation without a heat loss term $\Delta T_l + P\partial T_l/\partial x = 0$, but it does not take into account other effects corresponding mainly to the existence of other lengths in experiment [3]: the nonzero thickness e of the plate and the distance h between the cold bath and the heater. In fact, Eq. (4) assumes that the temperature is constant through the thickness (i.e., $eP \ll 1$) and that there is no heat exchange between the strip and its surroundings, which becomes important for low velocities [4].

The problem of a crack of unknown shape in a strip subjected to a temperature field consists in solving the equilibrium equations [7]

$$\frac{\partial \Sigma_{ij}}{\partial x_j} = 0, \quad \nabla^2\Sigma_{ii} = -\nabla^2 T_l(x), \tag{5}$$

with the boundary conditions

$$\Sigma_{yy}(x,\pm 1) = \Sigma_{xy}(x,\pm 1) = 0, \tag{6}$$

$$\Sigma_{ij}n_j = 0 \text{ on the crack}, \tag{7}$$

$$\overline{\overline{\Sigma}} = 0 \text{ for } x = \pm\infty, \tag{8}$$

where $\vec{n}$ is the unit vector normal to the crack edges. Under equilibrium conditions, the crack shape depends essentially on the stress, which is in this case related to the temperature field. The mathematics of this problem are, given the boundary conditions on a crack whose shape is *a priori* unknown, the solution of the whole problem will determine the correct shape of the crack [14].

Formally, there might exist more than one solution to the global problem and one has to select the crack shape that satisfies certain stability criteria. First, the solution must be in accordance with the criterion of local symmetry [10], which imposes that the crack path $s(x,y)$ is one for which $K_{\rm II} = 0$ at the tip. Also, the chosen crack path must satisfy another condition related to the energy criterion introduced by Griffith [2]. This criterion states

that the crack is at a *critical value of incipient growth* if the reduction in the stored elastic energy W_{el} associated with a small virtual crack advance ds from that state is equal to the fracture energy Γ

$$-\frac{\partial W_{el}}{\partial s} = \Gamma \quad \text{with} \quad -\frac{\partial^2 W_{el}}{\partial s^2} \leq 0, \tag{9}$$

Γ being a material constant independent of the crack shape. The second condition in Eq. (9) means that the system must be stable in the sense of mechanical equilibrium.

The total thermoelastic free energy per unit thickness W_{el} of a thin plate is given by [14]

$$W_{el} = Eb^2\alpha_T^2(\Delta T)^2\widetilde{W}, \tag{10}$$

where $\widetilde{W}$ is the dimensionless free energy given by

$$\widetilde{W} = \frac{1}{2}\int_{\text{surface}} dS \left[\Sigma_{ij}E_{ij} - \Sigma_{ii}(x,y)T_l(x) - \frac{3}{1-2\nu}T_l^2(x)\right]. \tag{11}$$

Note that in this writing, an integration across the thickness of the strip has already been done. Equation (11) can be simplified without specifying the crack shape. The first term of this equation can be calculated by using successively the equilibrium equations (5), the divergence theorem, and the boundary conditions (6–8)

$$\int_{\text{surface}} dS\,\Sigma_{ij}E_{ij} = \int_{\text{surface}} dS\,\frac{\partial(\Sigma_{ij}U_i)}{\partial x_j} = \oint_\Omega d\Omega\,\Sigma_{ij}U_i n'_j = 0, \tag{12}$$

where $\vec{n}'$ is the unit vector perpendicular to the contour Ω limiting the strip, including the edges of the crack and the boundaries of the plate. This term always vanishes, regardless of the shape of the crack. The third term of Eq. (11) is infinite in the configuration of an infinite strip, which is evidently not the case experimentally. Nevertheless, since this term depends on the temperature distribution only and not on the crack location, one can omit it by a convenient choice of the zero free energy. Finally, $\widetilde{W}$ is simply given by

$$\widetilde{W} = -\frac{1}{2}\int_{-\infty}^{\infty} dx\,T_l(x)\int_{-1}^{+1} dy\,\Sigma_{ii}(x,y). \tag{13}$$

Now we outline the analysis to be done and connect its relation to earlier works [6–8]. In the following, we will discuss first the problem of existence of a stably advancing straight crack. The transition between a non-cracked strip and a straight crack is studied. It consists in solving the problem of a centered straight crack and calculating the stress intensity factor $K_I(P,l)$. By using Eq. (9) and the well-known correspondence relation established by Irwin [15]

$$-\frac{\partial\widetilde{W}}{\partial l} = K_I^2, \tag{14}$$

one defines the region of existence of stably extending straight cracks (see Fig. 2). This problem has been solved numerically [6–8] and the results are in agreement with the experimental measurements [3,4]. Nevertheless, in addition to the previous studies, we will introduce a simple analysis that yields the scaling laws governing the transition from a receding to a moving crack. That also leads to the confirmation [8] and to extension of the invalidity of the hypothesis, which consists in taking, in certain limits, the approximation of an infinite strip.

In Sec. IV we investigate the straight-oscillating crack transition. We perform a linear stability analysis of a straight crack submitted to a small perturbation of its shape. In the vicinity of the bifurcation, we introduce a small smooth deviation $y(x)$ to the shape of the centered straight crack in the form

$$y(x) \approx Af(x) + O(A^3) \approx A\sin\omega x \quad \text{with} \quad |A| \ll 1, \tag{15}$$

where A is a constant small amplitude and ω the wave vector of the oscillation. By small deviations from the centered straight crack, it must be understood that $|y(x)| \ll 1$ and $|y'(x)| \ll 1$ ($|A\omega| \ll 1$) because the length "difference" between the two paths must also be small. From this observation, one can already expect that the sought after transition will derive from a low wave vector (high wavelength $\lambda = 2\pi/\omega$) stability analysis. We develop the stress and deformation fields as

$$\Sigma_{ij} = \sigma_{ij} + As_{ij} + A^2t_{ij} + O(A^3), \tag{16}$$

$$U_i = u_i + Av_i + A^2w_i + O(A^3). \tag{17}$$

Because of the symmetry $A \to -A$, the even perturbation

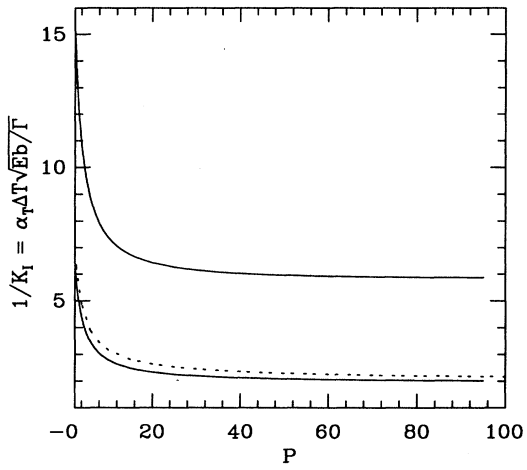

FIG. 2. Phase diagram in the P-K_I^{-1} plane. A crack can move in the region above the lower solid line. The transition to an oscillating propagation occurs at the upper solid curve. For comparison, the results obtained in [7] for the transition straight-oscillating morphology are also shown (dashed curve).

orders are of pure mode I type, while the odd ones are of pure mode II type. Therefore, using the tangential $U_t(x, y(x))$ and the normal $U_n(x, y(x))$ deformations [10]

$$U_t(x, y(x)) = \frac{1}{\sqrt{1 + y'^2(x)}} \times \{U_x(x, y(x)) + y'(x)\, U_y(x, y(x))\}, \quad (18)$$

$$U_n(x, y(x)) = \frac{1}{\sqrt{1 + y'^2(x)}} \times \{U_y(x, y(x)) - y'(x)\, U_x(x, y(x))\}, \quad (19)$$

one calculates $K_{\rm I}^{\rm tot}(P, l, \omega)$ and $K_{\rm II}^{\rm tot}(P, l, \omega)$, the stress intensity factors of mode I and mode II loadings, respectively. They are given by

$$K_{\rm I}^{\rm tot}(P, l, \omega) = \frac{1}{8} \lim_{x \to 0^-} \sqrt{\frac{2\pi}{-x}} \times \left\{U_n(x, y^+(x)) - U_n(x, y^-(x))\right\}, \quad (20)$$

$$K_{\rm II}^{\rm tot}(P, l, \omega) = \frac{1}{8} \lim_{x \to 0^-} \sqrt{\frac{2\pi}{-x}} \times \left\{U_t(x, y^+(x)) - U_t(x, y^-(x))\right\}, \quad (21)$$

where the superscripts + and − denote the upward and downward limits, respectively. At leading order, one finds that

$$K_{\rm I}^{\rm tot}(P, l, \omega) = K_{\rm I}(P, l) + O(A^2), \quad (22)$$

$$\frac{1}{A} K_{\rm II}^{\rm tot}(P, l, \omega) = \frac{1}{A} K_{\rm II}(P, l, \omega) + \frac{\omega}{2} K_{\rm I}(P, l) + O(A^2). \quad (23)$$

It is shown that at leading order, $K_{\rm I}^{\rm tot}$ is still given by $K_{\rm I}(P, l)$, the stress intensity factor of the centered straight crack. The stress intensity factor $K_{\rm II}(P, l, \omega)$ is the shear effect introduced by the first-order perturbation in loadings. It is given by the resolution of a pure mode II problem of a centered straight crack

$$K_{\rm II}(P, l, \omega) = \frac{A}{8} \lim_{x \to 0^-} \sqrt{\frac{2\pi}{-x}} \left\{v_x(x, 0^+) - v_x(x, 0^-)\right\}. \quad (24)$$

Our linear stability analysis is based on the following physical arguments. If $K_{\rm II}^{\rm tot}/A$ is found to be positive, this means that the stress intensity factor $K_{\rm II}^{\rm tot}$ and the orientation of the crack tip $y'(0)$ have the same sign. Therefore, according to the criterion of local symmetry, the crack tip tends to follow a path that decreases $|y'(0)|$ and consequently the amplitude of the perturbation will decrease. On the other hand, when $K_{\rm II}^{\rm tot}/A < 0$, the slope $|y'(0)|$ will increase in order to restore a pure mode I local stress field at the tip. So, under a small perturbation of its shape, the straight crack will be stable if $K_{\rm II}^{\rm tot}/A$ is found to be positive and unstable elsewhere. The oscillating crack configuration will then occur when $K_{\rm II}^{\rm tot}/A < 0$ is satisfied.

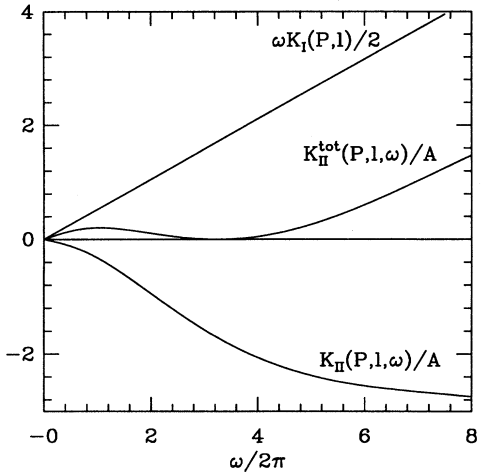

FIG. 3. Example of the variation of $K_{\rm II}/A$, $\omega K_{\rm I}/2$, and $K_{\rm II}^{\rm tot}/A = K_{\rm II}/A + \omega K_{\rm I}/2$ with respect to $\omega/2\pi$ for fixed values of l and P.

According to Eq. (23), Fig. 3 shows that $K_{\rm II}^{\rm tot}/A$ is the sum of two competitive terms: the first one $K_{\rm II}/A$, which is almost always negative, tends to amplify the instability of the straight crack. This destabilizing field effect is due to the variation of the stress field $\overline{\overline{\Sigma}}$ with respect to $\overline{\overline{\sigma}}$. The second term of Eq. (23), $\omega K_{\rm I}/2$, is a geometrical stabilizing effect. This quantity is always positive in the range of parameters where a straight crack can exist, so it tends to favor the straight configuration by damping the perturbation given by Eq. (15). It is foreseeable that the straight-undulating crack transition will occur when these two effects cancel each other. In Fig. 4 we plotted

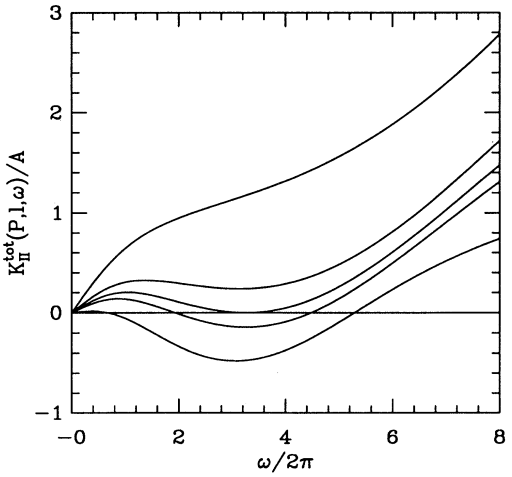

FIG. 4. $K_{\rm II}^{\rm tot}/A$ versus $\omega/2\pi$ for fixed P ($P = 50$) and for different values of l (from the upper to the lower curve, $l =$ 0.08, 0.11, 0.121, 0.13, and 0.16). By increasing l, $K_{\rm II}^{\rm tot}/A$ decreases. When $K_{\rm II}^{\rm tot}/A > 0$, the problem of a wavy crack has no physical solutions. For a certain $l_u(P)$, the minimum of $K_{\rm II}^{\rm tot}/A$ vanishes at $\omega = \omega_c$ and by increasing l further, any small perturbation of the straight crack in a well-defined range of wavelengths will cause a physical shear loading $K_{\rm II}^{\rm tot}/A < 0$.

K_{II}^{tot}/A with respect to ω at constant P and for different values of l. It is shown that there exist critical values of the parameters for which a small deviation from the centered straight crack begins to introduce a physical shear loading at the crack tip. At this point, the straight crack becomes unstable and an undulating crack path appears. From Fig. 4, one concludes that the straight-oscillating crack transition will occur when

$$K_{II}^{tot}(P,l,\omega)=0, \quad \frac{\partial K_{II}^{tot}}{\partial \omega}(P,l,\omega)=0. \tag{25}$$

Equations (25) are satisfied for $l = l_u(P)$ and $\omega = \omega_u(P)$, functions that can be computed from (25). The value of $l = l_u(P)$ is the critical position of the crack tip in the temperature gradient where a straight and an oscillating crack coexist (see Fig. 5). If $l \leq l_u$ ($l \geq l_u$), the straight (oscillating) crack is the most stable configuration. The critical wavelength of the oscillation near the transition region (see Fig. 6) is simply determined by $\lambda(P) = 2\pi/\omega_u(P)$. In order to complete the phase diagram and to quantify the straight-oscillating crack transition, one has to calculate according to Eq. (22) the stress intensity factor of the straight crack $K_I^{(u)}$ at the critical points $l_u(P)$. This is done by using the results of Sec. III (see Fig. 2).

This stability analysis is not in contradiction with the criterion of local symmetry. Our process consists in searching for when a small perturbation of the linear crack can create a shear loading able to lead to an oscillatory instability. Of course, once this instability is reached, the undulating crack will choose a path satisfying $K_{II} = 0$. Clearly, this condition cannot be satisfied by the simple shape given by (15). The reason is that the chosen shape must be an exact solution of the problem to satisfy completely the criterion of local symmetry.

In order to see the effect of the crack oscillation on the free energy, we have calculated W_u, the elastic free energy of a weakly oscillating crack. This energy is expanded for

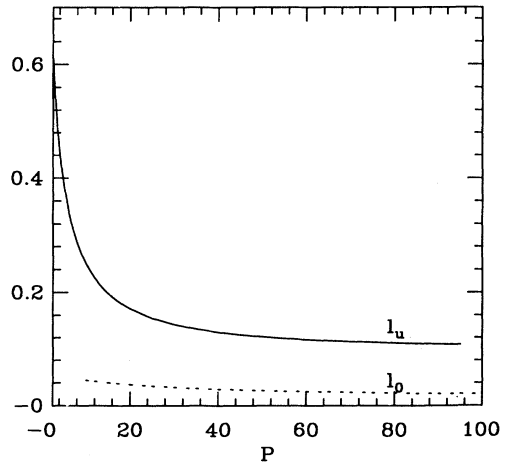

FIG. 5. $l_u(P)$ when $K_{II}^{tot}/A = 0$ (solid line) and the critical position $l_0(P)$ for which W_u becomes unstable at $\omega = 0$ (dashed line).

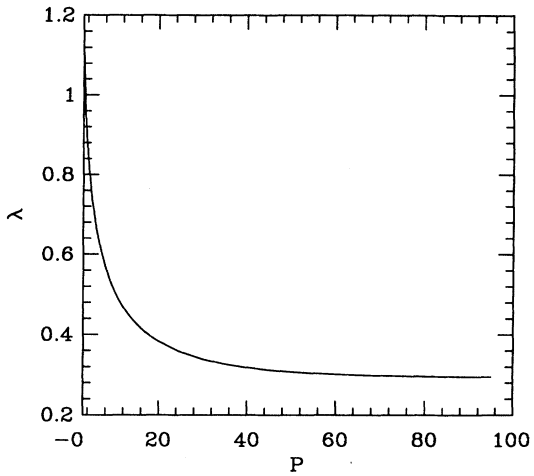

FIG. 6. Selected wavelength λ versus P at the transition from a straight to a wavy fracture.

A small under the form

$$W_u = W_s + A^2\delta W + O(A^4) \tag{26}$$

so that one has to solve the second-order perturbation problem to compute δW; W_s is the elastic free energy of a centered straight crack for the same tip position in the temperature gradient as the undulating crack. When the bifurcation to the wavy instability occurs, the deviation of the energy δW is always found to have an unstable maximum at $\omega = 0$. This serves as a consistency test for our approach (see Fig. 5).

III. THE STRAIGHT CRACK

This configuration has been studied previously [6–8] by numerical methods. Nevertheless, since we shall need some results for Sec. IV, we will discuss briefly the solution method (see [7] for details). The crack is assumed to be centered because of the constraint $K_{II} = 0$. The equilibrium equations (5) are rewritten as

$$\frac{\partial \sigma_{ij}}{\partial x_j}=0, \quad \nabla^2\sigma_{ii} = -\nabla^2 T_l(x) \tag{27}$$

and the boundary conditions (6) and (7) become

$$\sigma_{yy}(x,1)=\sigma_{xy}(x,1)=\sigma_{xy}(x,0)=0, \tag{28}$$

$$\sigma_{yy}(x,0)=0 \text{ for } x\leq 0, \quad u_y(x,0)=0 \text{ for } x\geq 0, \tag{29}$$

where some boundary conditions have been added because of the symmetry of the problem. By working in the interval $0 \leq y \leq 1$ and in the Fourier space of the x direction, one obtains [7]

$$\hat{\sigma}_{yy}(k,0) = -F(k)\hat{u}_y(k,0) + D_l(k), \tag{30}$$

$$\hat{\sigma}_{xx}(k,0) = H(k)\hat{\sigma}_{yy}(k,0) + S_l(k), \tag{31}$$

with

$$F(k) = k\frac{\sinh^2 k - k^2}{\sinh 2k + 2k},$$

$$D_l(k) = 2\widehat{T}_l(k)\frac{(1-\cosh k)(\sinh k - k)}{\sinh 2k + 2k},$$

$$H(k) = \frac{\sinh^2 k + k^2}{\sinh^2 k - k^2},$$

$$S_l(k) = \widehat{T}_l(k)\frac{\sinh k - k}{\sinh k + k}. \tag{32}$$

Once Eq. (30) is solved, the solution is complete. In order to satisfy the boundary conditions given by Eq. (29), one uses the Wiener-Hopf method [7,16], which consists of decomposing $F(k)$ as $F^-(k)/F^+(k)$, where $F^-(k)$ has neither poles nor zeros for $\mathrm{Im}(k) < 0$ and $F^+(k)$ has none for $\mathrm{Im}(k) > 0$. Then, one finds

$$\hat{u}_y(k,0) = \frac{1}{F^-(k)}\int_{-\infty}^{0} dx\, g_{\mathrm{I}}(x+l)e^{ikx}, \tag{33}$$

where

$$g_{\mathrm{I}}(x) = \int_{-\infty}^{+\infty}\frac{dk}{2\pi} D_0(k)F^+(k)e^{-ikx}. \tag{34}$$

In our calculations, we chose the large k behavior of $F^+(k)$ to be $\sqrt{2/(\delta - ik)}$, with δ infinitesimal. The stress intensity factor of this mode I propagation is then $K_{\mathrm{I}} = g_{\mathrm{I}}(l)$.

The dimensionless free energy W_s for a straight crack is given by

$$W_s = \widetilde{W}_0(P) - \int_{-\infty}^{l} dx\, g_{\mathrm{I}}^2(x)$$

$$= \frac{1}{2}\widetilde{W}_0\left(\frac{P}{2}\right) + \int_{l}^{+\infty} dx\, g_{\mathrm{I}}^2(x), \tag{35}$$

with $\widetilde{W}_0(P)$ the free energy of a noncracked strip of width $2b$. It is explicitly given by

$$\widetilde{W}_0(P) = \int_{-\infty}^{\infty}\frac{dk}{2\pi}\left\{1 - \frac{4\sinh^2[k]}{k(2k+\sinh[2k])}\right\}\frac{P^2}{k^2(k^2+P^2)}. \tag{36}$$

Note that $\widetilde{W}_0$ is independent of l. Equations (35) and (36) can be obtained by two different, but equivalent, methods: either by putting directly in Eq. (13) the solution of the above problem or by using Eq. (14) and calculating the free energy $\widetilde{W}_0$ of a noncracked strip. This can be done easily since in this simple case, the mixed boundary condition (29) is replaced by $u_y(x,0) = \hat{u}_y(k,0) = 0$.

By using Eqs. (9) and (35), one concludes that the straight crack can extend when $l \geq l_s(P)$, where $l_s(P)$ corresponds to $K_{\mathrm{I}}^{(s)}(P)$, the maximum of $K_{\mathrm{I}}(P,l)$. Therefore the no crack–straight crack transition (lower solid curve in Fig. 2) obeys the law

$$\frac{1}{K_{\mathrm{I}}^{(s)}(P)} = \sqrt{\frac{Eb}{\Gamma}}\,\alpha_T\Delta T. \tag{37}$$

This law is in agreement with the experimental observations concerning this transition [6,8].

The stress intensity factor $K_{\mathrm{I}}(P,l)$ decays rapidly to zero when $l \to \pm\infty$ and varies only in a window of width of order L_c, which will be the characteristic length of the problem. Therefore, when the crack position is behind this region, the elastic free energy is not very different from a noncracked strip, while when it is in front of this region, the strip can be approximately treated as an infinitely cracked one. The latter case is equivalent to the problem of two strips of width b. To a first approximation, one can assume a linear energy variation between these two limits across the unknown characteristic length L_c. Thus the existence of an extending straight crack is constrained by the condition

$$Eb^2\alpha_T^2(\Delta T)^2\Delta\widetilde{W} \approx \Gamma L_c, \tag{38}$$

where $\Delta\widetilde{W} = \widetilde{W}_0(P) - \widetilde{W}_0(P/2)/2$. It can easily be shown that the asymptotic behavior of $\Delta\widetilde{W}$ with respect to P is simply given by

$$\begin{aligned} \Delta\widetilde{W} &\propto P^2 \quad \text{for } P \ll 1, \\ \Delta\widetilde{W} &\approx 1 \quad \text{for } P \gg 1. \end{aligned} \tag{39}$$

Let us recall that from the beginning, we have scaled lengths by b and consequently k by $1/b$. So in these two limits, the relevant length scale is the width of the strip and the diffusion length d_{th} plays a secondary role compared to b. Therefore, in the asymptotic cases of Eqs. (39), the characteristic length is of the order of the width of the strip $L_c \propto b$. Extending straight cracks may occur when

$$\begin{aligned} b^3(\Delta T)^2V^2 &\approx Ct \quad \text{for } P \ll 1, \\ b(\Delta T)^2 &\approx Ct \quad \text{for } P \gg 1. \end{aligned} \tag{40}$$

Moreover, these scaling laws remain valid when one considers n equidistant straight cracks. This can be seen by considering the energy difference $W_{\mathrm{el}}(b) - (n+1)W_{\mathrm{el}}(b/(n+1))$. The scaling laws of Eqs. (40) reproduce qualitatively the experimental behavior of the transition to an advancing straight crack. However, the most important conclusion that can be drawn from this analytical study is that the problem of a crack in a heated strip cannot be approximated by a problem of an infinite plate in both limiting cases $b \ll d_{\mathrm{th}}$ and $b \gg d_{\mathrm{th}}$. That could explain why the analysis of Refs. [7,8] assuming an infinite strip failed to explain the straight-oscillating crack transition. Let us now study the stability of crack path under mode I loading.

IV. THE OSCILLATING CRACK

In this section we lay down the calculations needed to compute numerically the conditions (25) and Eq. (26). To introduce perturbations to the symmetric straight crack, one takes the deviation from this configuration, as given by Eq. (15). The condition $f(0) = 0$ is not restrictive since the transition occurs between a centered straight crack and an oscillating one. It is therefore sufficient to compare these two configurations at the same location in the temperature gradient. In our approach, we must solve first for the straight crack and then for the first- and second-order perturbation in the amplitude A. The perturbation method does not differ too much from that followed in [10]. The following analysis is to be compared to the linearization performed in [10] for the study of slightly curved cracks. The components of the vector normal to the crack edges are $(n_x, n_y) \propto (Af'(x), -1)$. Expanding the equilibrium equations (5) and the boundary conditions (6) and (7) near $A = 0$, one has the following two problems to solve.

The first problem is a mode II loading given by the equilibrium equations

$$\frac{\partial s_{ij}}{\partial x_j} = 0, \quad \nabla^2 s_{ii} = 0 \tag{41}$$

with the boundary conditions

$$s_{yy}(x,1) = s_{xy}(x,1) = s_{yy}(x,0) = 0; \tag{42}$$

$$s_{xy}(x,0) = \frac{\partial}{\partial x}\left[f(x)\sigma_{xx}(x,0)\right] \quad \text{for} \quad x \le 0,$$

$$v_x(x,0) = 0 \quad \text{for} \quad x \ge 0. \tag{43}$$

Note that $\lim_{x\to 0^-} \sigma_{xx}(x,0)$ is finite [$f^I_{xx}(\pm\pi) = 0$ in (1)]. This limit is equal to Σ [7], the stress in the transverse direction and near the tip, which remains once the square-root singularity has been subtracted out. By the same reasoning as in Sec. III, one finds that this problem satisfies the equation

$$\hat{s}_{xy}(k,0) = -P(k)\hat{v}_x(k,0), \tag{44}$$

where

$$P(k) = k\frac{\sinh^2 k - k^2}{\sinh 2k - 2k}. \tag{45}$$

To solve this equation, one uses again the Wiener-Hopf technique; one splits $\hat{s}_{xy}(k,0)$ as $\hat{s}^-_{xy}(k,0) + \hat{s}^-_{xy}(k,0)$ and $P(k)$ as $P^-(k)/P^+(k)$, where the signs + and − have the same meanings as in Sec. III. Then, using Eq. (43), one finds

$$\hat{v}_x(k,0) = \frac{1}{P^-(k)}\int_{-\infty}^{0} dx\, g_{II}(x)e^{ikx}, \tag{46}$$

where

$$g_{II}(x) = -\int_{-\infty}^{x} dx' \frac{d}{dx'}\left[f(x')\sigma_{xx}(x',0)\right]p^+(x-x'), \tag{47}$$

with $p^+(x) = \int_{-\infty}^{+\infty} \frac{dk}{2\pi} P^+(k)e^{-ikx}$. The stress intensity factor of this mode II loading is then given by

$$\frac{1}{A}K_{II}(P,l,\omega) \equiv g_{II}(0) = -\int_{-\infty}^{0} dx \frac{d}{dx}\left[\sigma_{xx}(x,0)\sin\omega x\right]p^+(-x). \tag{48}$$

The second problem concerns the second order (in the amplitude A) of the perturbation analysis. It is a mode I loading given by the equilibrium equations

$$\frac{\partial t_{ij}}{\partial x_j} = 0, \quad \nabla^2 t_{ii} = 0 \tag{49}$$

with the boundary conditions

$$t_{yy}(x,1) = t_{xy}(x,1) = 0; \tag{50}$$

$$t_{xy}(x,0) = \theta(-x)\frac{\partial}{\partial x}\left(f(x)\frac{\partial}{\partial x}v_x(x,0) - \frac{1}{2}f^2(x)\frac{\partial^2}{\partial x^2}u_y(x,0)\right); \tag{51}$$

$$t_{yy}(x,0) = \frac{1}{2}\frac{\partial^2}{\partial x^2}\left[f^2(x)\sigma_{xx}(x,0)\right] \quad \text{for} \quad x \le 0,$$

$$w_y(x,0) = 0 \quad \text{for} \quad x \ge 0. \tag{52}$$

It can be shown that this problem yields, after a Fourier transform,

$$\hat{t}_{yy}(k,0) = -F(k)\left[\hat{w}_y(k,0) - \nu\frac{\hat{t}_{xy}(k,0)}{-ik}\right] - F(k)H(k)\frac{\hat{t}_{xy}(k,0)}{-ik}, \tag{53}$$

which has to be solved by using the boundary conditions (51) and (52). The functions $F(k)$ and $H(k)$ are given by Eqs. (32) and thus the Wiener-Hopf decomposition of $F(k)$ is already known.

The elastic energy W_u up to the second order in A is given by

$$W_u = -\frac{1}{2}\int_{-\infty}^{\infty} dx\, T_l(x)\left\{\int_0^1 dy\,\left[\Sigma_{ii}(x,y) + \Sigma_{ii}(x,-y)\right] - Af(x)\theta(-x)\left[\Sigma_{ii}(x,0^+) - \Sigma_{ii}(x,0^-)\right] - \frac{A^2}{2}f^2(x)\theta(-x) \times \frac{\partial}{\partial y}\left[\Sigma_{ii}(x,y) + \Sigma_{ii}(x,-y)\right]\Big|_{y=0}\right\}. \tag{54}$$

Once the previous problems are solved analytically, the various quantities that appear in Eqs. (25) and (26) can be calculated numerically. The derivative of K_{II} with respect to ω is given by

$$\frac{1}{A}\frac{\partial K_{\rm II}}{\partial \omega}(P,l,\omega) = -\int_{-\infty}^{0} dx \frac{d}{dx}\left[x\sigma_{xx}(x,0)\cos\omega x\right] p^{+}(-x). \quad (55)$$

After some algebraic manipulations on Eq. (54), the correction δW is found to be equal to

$$\delta W = \frac{1}{2}Pu_y(-l,0)f^2(-l) - \int_{-\infty}^{0} dx \left\{ g_{\rm II}^2(x) - u_y(x,0)\frac{d^2}{dx^2}\left[f^2(x)\sigma_{xx}(x,0)\right]\right\}, \quad (56)$$

where the first term reflects the discontinuity of the derivative of $\sigma_{xx}(x,0)$ at $x=-l$, when the temperature field is given by Eq. (4). Note that the variation δW is calculated using the first- and second-order terms of the perturbation and does not depend on $g_{\rm II}$ only.

The numerical analysis of the previous problems is straightforward. The Wiener-Hopf decomposition needed for $F(k)$ and $P(k)$ is done as described in [16]. The other quantities are computed using Fourier transforms, after treating the singular parts separately and analytically. The results of these numerical calculations are summarized in Figs. 2 and 6. Using Eqs. (34), (48), and (55) and according to (22) and (25), one calculates the position $l_u(P)$ where the straight crack becomes unstable against a small perturbation of its shape, the corresponding stress intensity factor $K_{\rm I}(P,l_u)$, and the wavelength of the oscillation $\lambda(P)$. Using Eq. (56), the critical value $l_0(P)$ where δW starts to have a maximum instead of minimum at $\omega=0$ has also been calculated (see Fig. 5).

The only hypothesis we made to introduce the conditions (22) and (25) is the smoothness of the fracture shapes. This assumption is not too drastic and is in agreement with the experimental observations [3]. We have also assumed, as in [10], the existence of a small random stress intensity factor $K_{\rm II}$ due to the imperfections in the loading system. Because of the criterion of local symmetry, the existence of such imperfections leads automatically to deviations from the original straight crack. Therefore, the stability analysis of a preexisting straight crack under a small fluctuation in its shape is necessary before studying the shape of its extension.

V. CONCLUSION

In this paper we treated completely the instabilities of an advancing crack in a strip subjected to thermal stresses. The first instability concerned the condition of existence of extending straight cracks. We quantified this transition (lower solid curve in Fig. 2) and proved the asymptotic scaling laws analytically. Since this bifurcation is well defined, its experimental study is a good way to fix the fracture energy value and to determine the relevant length scale in the imposed temperature field.

For the more subtle transition from a straight crack to a wavy crack (upper solid curve in Fig. 2), we introduced a notion that consists of defining this bifurcation by the existence of a physical stress intensity factor of mode II loading for a small instability of the straight crack. Any quantitative comparison between this treatment, the studies based on the criterion of local symmetry [8,6], and the experiment [3] is difficult to do because even the first bifurcation has not yet been studied quantitatively. Nevertheless, our results agree rather well with the numerical simulations of [6]. Moreover, a comparison with the experimental data in the region of the phase diagram where the diffusion length $d_{\rm th}$ is the dominant length scale in the temperature field ($V\approx 3$ mm/s, $\Delta T\approx 70$ K, and $b=1.2$ cm) gives a value of the fracture energy $\Gamma\approx 7.3$ J/m^2, which is of the same order of magnitude as the value measured in [9].

The selected wavelength plotted in Fig. 6 also shows agreement with the results of [6] for $P\gg 1$. In both cases, it was found that $\lambda\approx 0.28$. For smaller P, the two wavelengths are different but still of the same order. In this limit, they have to be compared with the experimental value $\lambda\approx 0.56$ in [3]. However, since there is no information on V, one might attribute the plateau observed in this experiment to the effects of h, the spacing between the heater and the cold bath, or to three-dimensional effects [4].

ACKNOWLEDGMENTS

M.A.-B. is grateful to M. Ben Amar and V. Hakim for helpful discussions and critical comments and also thanks O. Ronsin, F. Heslot, and B. Perrin for communications about their experimental results before publication.

[1] L. B. Freund, *Dynamic Fracture Mechanics* (Cambridge University Press, New York, 1990).
[2] A. A. Griffith, Philos. Trans. R. Soc. London Ser. A **221**, 163 (1921).
[3] A. Yuse and M. Sano, Nature (London) **362**, 329 (1993).
[4] O. Ronsin, F. Heslot, and B. Perrin (unpublished).
[5] H. Furukawa, Prog. Theor. Phys. **90**, 949 (1993); Y. Hayakawa, Phys. Rev. E **49**, R1804 (1994).
[6] H. A. Bahr, A. Gerbatsch, U. Bahr, and H. J. Weiss, Phys. Rev. E **52**, 240 (1995).
[7] M. Marder, Phys. Rev. E **49**, R51 (1994).
[8] S. Sasa, K. Sekimoto, and H. Nakanishi, Phys. Rev. E **50**, R1733 (1994).
[9] K. Reddy, E. H. Fontana, and J. D Helfinstine, J. Am. Ceram. Soc. **71**, C310 (1988).
[10] B. Cotterell and J. R. Rice, Int. J. Fract. **16**, 155 (1980).
[11] J. B. Leblond, *Mécanique de la Rupture Fragile* (Cours de l'Ecole Polytechnique, Paris, 1992).
[12] Note that in [10], the crack is treated as a stable straight one if the asymptotic deviation $\lambda(x)$ from the original

path is $\lambda(x) \propto \sqrt{x}$. For an infinite geometry, this is a sufficient condition for a straight crack to be asymptotically stable. However, the existence of boundaries in our case leads to the creation of a "geometrical" shear stress. If the straight crack is not centered, it will be automatically unstable so that it will deviate towards the center. By the repetition of these processes, it is then possible to construct a wavy instability. Therefore, the condition that makes the crack stable in the infinite geometry can not be applied to the finite one [7].

[13] N. I. Muskhelishvili, *Some Basic Problems of the Mathematical Theory of Elasticity* (Noordhoff, Groningen, 1953).

[14] L. Landau and E. Lifchitz, *Théorie de l'Elasticité* (Mir, Moscow, 1967).

[15] G. R. Irwin, J. Appl. Mech. **24**, 361 (1957).

[16] Xiangming Liu and M. Marder, J. Mech. Phys. Solids **39**, 947 (1991).

Stability of Quasiequilibrium Cracks under Uniaxial Loading

Mokhtar Adda-Bedia and Martine Ben Amar

Laboratoire de Physique Statistique, Ecole Normale Supérieure, 24 rue Lhomond, F-75231 Paris Cedex 05, France*

(Received 8 August 1995)

We propose a linear stability analysis of a straight crack subjected to uniaxial loading. We argue that, under quasistatic extension conditions, the crack propagation follows a straight path until the creation of a "physical" shear stress at its tip. This instability leads to a deviation of the fracture from the direction perpendicular to the applied loading. We compare our tip criterion instability with both experimental results and previous theoretical models.

PACS numbers: 62.20.Mk, 46.30.Nz, 81.40.Np

Recently, crack propagation problems have attracted attention of the physics community. This renewal of interest was essentially caused by experimental realizations of both equilibrium [1] and dynamic fracture mechanics [2]. From the theoretical side, the study of crack propagation can be subdivided in two classes. First, for the study of dynamical fracture formation, a long-standing problem exists. According to theory [3], cracks in brittle materials are supposed to accelerate up to the Rayleigh wave speed. In experiments, however, the cracks seldom exceed half this speed [2]. Moreover, the mechanisms that govern the dynamics of cracks are not well understood, and a theory of instability does not exist yet. The second field of crack propagation concerns slow or quasiequilibrium cracks. For this case, the work of Griffith [4] is often seen as the beginning of equilibrium fracture mechanics as a quantitative science of material behavior. Recent experiments [1] have shown that a crack traveling in a strip submitted to a nonuniform, but unidirectional, thermal diffusion field undergoes numerous instabilities. It has been established that at well-defined critical values of the control parameters a moving straight crack becomes unstable after which a wavy crack path appears. In a recent theoretical work [5], in relation with that experiment, a linear stability analysis of a straight crack based on a crack tip propagation criterion was introduced. The criterion states that the crack tip will extend out of the centered straight direction as soon as it is submitted to a "physical" shear stress. In this paper, we will show that the treatment introduced in [5], which accounts for the appearance of wavy crack patterns, is not specific to this thermoelastic problem. Moreover, we generalize this criterion to the study of the stability of a straight crack subject to any uniaxial loading in two dimensions. Although the notion of stability is systematically used for hydrodynamic systems [6], it has not been performed yet for the study of fracture problems.

As an introduction, the quasiequilibrium crack problem will be posed in its general form. Then, admitting the Griffith theory [4] and the so-called principle of local symmetry [7,8], we will perform a linear stability analysis of equilibrium cracks subjected to unidirectional loading. This defines a stability criterion for the straight crack in the presence of intrinsic perturbations due to material inhomogeneities. Finally, we will apply our approach to two simple cases and a comparison with previous results, especially those of Cotterell and Rice (CR) [8], will be done.

In a two-dimensional linear isotropic elastic model, the strain tensor $\overline{\overline{E}}(x, y)$ is related to the stress tensor $\overline{\overline{\Sigma}}(x, y)$ by a relation of the form [9]

$$E_{ij} = \tfrac{1}{2}\{\partial U_i/\partial x_j + \partial U_j/\partial x_i\}$$

$$= (1/2\mu)\{\Sigma_{ij} - [\kappa - 2/2(\kappa - 1)]\,\Sigma_{kk}\delta ij\}. \quad (1)$$

Here the subscripts are two-dimensional coordinate indices; repeated indices indicate summation. $\vec{U}$ is the displacement vector and $\kappa = 2(1 - \nu)/(1 - 2\nu)$ [$\kappa = 2/(1 - \nu)$] for a plane strain (plane stress) problem. ν is the Poisson ratio, and μ is the Lamé coefficient.

The problem of an equilibrium crack of unknown shape in an elastic medium, which is opened by tractions $-\overline{\overline{p}}(x)$, at the surface, consists of solving the equilibrium equations

$$\partial\Sigma_{ij}/\partial x_j = 0 \quad \text{and} \quad \nabla^2\Sigma_{\mathrm{II}} = 0 \quad (2)$$

with the boundary conditions on the crack faces

$$(\Sigma_{ij} + p_{ij})n_j = 0, \quad (3)$$

where $\vec{n}$ is the unit vector normal to the crack edges. This load configuration can be either the present one or that necessary to superimpose on the stress field for an uncracked body to remove the stresses from the boundary of the crack. At this stage, we do not need to specify the conditions on the boundaries of the medium. Under equilibrium conditions, the crack shape depends essentially on the applied stresses. The mathematical formulation of this problem is as follows: Given the boundary conditions (3) for a crack whose shape is *a priori* unknown, the solution of the whole problem will determine the correct shape of the crack [9]. Formally, there might exist more than one solution to the global problem, and one has to select the crack shape which also satisfies two stability criteria.

First, the solution must satisfy a condition related to the energy criterion introduced by Griffith [4]. Defining the energy release rate G as the reduction in the total potential energy, which is the sum of the stored elastic energy $W_{\rm el}$ and the potential energy $-\phi$ of the external forces, associated with a small virtual crack advance ds, Griffith states that the crack is at a *critical value of incipient growth* if G is equal to the fracture energy Γ

$$G \equiv -\frac{\partial}{\partial s}(W_{\rm el} - \phi) = \Gamma\,, \text{ with } \frac{\partial G}{\partial s} \leq 0\,. \quad (4)$$

Γ is a material constant independent of the crack shape and of its dynamics.

On the other hand, the "*criterion of local symmetry*" [7,8] states that the path $y(x)$ taken by a crack in brittle homogeneous isotropic material is the one for which the local stress field at the tip is of mode I type. Let us recall that the mode I loading causes an opening of the fracture, while the mode II loading causes a shearing off. The local analysis in the neighborhood of a crack tip shows that the asymptotic stress tensor field $\overline{\overline{\Sigma}}$, in the polar coordinate system (r,θ), takes the universal form [3]

$$\Sigma_{ij}(r,\theta) = \frac{K_{\rm I}}{\sqrt{2\pi r}} f_{ij}^{\rm I}(\theta) + \frac{K_{\rm II}}{\sqrt{2\pi r}} f_{ij}^{\rm II}(\theta)\,, \quad (5)$$

where $f_{ij}^{\rm I}(\theta)$ and $f_{ij}^{\rm II}(\theta)$ are universal functions common to all configurations and loading conditions. The influence of configuration and loading are included in the asymptotic description of stress only through the scalar multipliers $K_{\rm I}$ and $K_{\rm II}$, which are the elastic stress intensity factors of the mode I and mode II loadings, respectively. The criterion of local symmetry features that, if a shear loading exists at the crack tip, $K_{\rm II} \neq 0$ and the crack will move by changing abruptly the orientation of the path.

Now consider a straight crack subjected to mode I loading and take a coordinate system so that the x axis is parallel to the crack. Nominally, $p_{ij}(x) \equiv p(x)\delta_{iy}\delta_{jy}$ and $K_{\rm II} \equiv 0$, so the criterion of local symmetry is automatically satisfied. Therefore the extension condition of the straight crack and its stability are given by Eqs. (4) only. Moreover, in this case there is a correspondence relation between the energy release rate and the stress intensity factor [10], since $G \propto K_{\rm I}^2$. In the quasistatic limit, an advancing straight crack exists if

$$K_{\rm I} = K_{\rm Ic}\,, \text{ with } \partial K_{\rm I}/\partial x \leq 0\,. \quad (6)$$

Note that only positive $K_{\rm I}$ are permitted. If $K_{\rm I} < 0$, the crack reseals and the analysis above using vanishing traction conditions on the crack faces will not be applicable.

The question at rest is: if the conditions (6) are satisfied, does the crack always grow in the x direction for any mode I loading? In fact, due to the imperfections in the system, the stress intensity factor of mode II loading will differ slightly from zero. So, the crack alignment will be slightly perturbed [7,8]. Such a deviation, due to an instability of the straight crack, will create a shear loading which may cause the crack tip to follow a path which is amplified compared to the initial perturbation. Therefore, we investigated the problem in a different manner than in [8]: we do not analyze it at the level $K_{\rm II} = 0$, but we examine when a tiny perturbation of the path is amplified.

To perform the linear stability analysis let us introduce a small smooth perturbation, with a given wavy shape:

$$y(x) \approx A f(x) + O(A^3)\,, \quad (7)$$

where A is a constant small amplitude. The crack is arranged so that the unperturbed shape is located at $y = 0$. By small deviations from a straight crack, it must be understood that $|y(x)| \ll 1$ and $|y'(x)| \ll 1$, because the length difference between the two paths must also be small. In addition to the straight crack perturbation given by Eq. (7), we introduce a supplementary condition: $f(0) = 0$ at the crack tip (supposed to be at $x = 0$). This condition is not restrictive, since the instability occurs for a straight crack. It is therefore sufficient to compare these two configurations at the same location of the crack tip.

The perturbation method we use does not differ too much from the one followed in Ref. [8] for the study of slightly curved cracks. We develop the stress and displacement fields in A:

$$\begin{aligned} \Sigma_{ij} &= \sigma_{ij} + A s_{ij} + O(A^2)\,, \\ U_i &= u_i + A v_i + O(A^2)\,, \end{aligned} \quad (8)$$

and solve first for the straight crack and then for the first order perturbation in the amplitude A. Because of the symmetry $A \to -A$, one notes that the even perturbation orders are of pure mode I type, while the odd ones are of pure mode II type. Expanding Eqs. (2) and (3) around $A = 0$, one has to solve the equilibrium equations (2) for $\overline{\overline{s}}(x,y)$, with the following conditions on the crack faces:

$$s_{yy}(x,0) = 0\,, \quad s_{xy}(x,0) = \frac{\partial}{\partial x}[f(x)\sigma_{xx}(x,0)]\,. \quad (10)$$

Using the tangential $U_t(x, y(x))$ and normal $U_n(x, y(x))$ displacements to the crack faces, one can calculate $K_{\rm I}^{\rm tot}$ and $K_{\rm II}^{\rm tot}$, the stress intensity factors of mode I and II loadings, respectively. They are [8]

$$K_{\rm I}^{\rm tot} = \alpha \lim_{x\to 0^-} \sqrt{\frac{2\pi}{-x}}\{U_n[x, y^+(x)] - U_n[x, y^-(x)]\}\,, \quad (11)$$

$$K_{\rm II}^{\rm tot} = \alpha \lim_{x\to 0^-} \sqrt{\frac{2\pi}{-x}}\{U_t[x, y^+(x)] - U_t[x, y^-(x)]\}\,, \quad (12)$$

where the superscripts $(+,-)$ design the upward and downward limits and $\alpha = \mu(\kappa - 1)/2\kappa$ is a material

constant. To leading order in A, we obtain

$$K_{\mathrm{I}}^{\mathrm{tot}} = K_{\mathrm{I}} + O(A^2), \tag{13}$$

$$K_{\mathrm{II}}^{\mathrm{tot}}/y'(0) = K_{\mathrm{II}}^{*}/y'(0) + \tfrac{1}{2}K_{\mathrm{I}} + O(A^2), \tag{14}$$

which shows that $K_{\mathrm{I}}^{\mathrm{tot}}$ is still given by K_{I}, the stress intensity factor of the straight crack. The stress intensity factor K_{II}^{*} is the shear effect introduced by the first order perturbation of the loading. It is given by the resolution of a pure mode II problem for a straight crack

$$K_{\mathrm{II}}^{*} = \alpha A \lim_{x\to 0^-} \sqrt{\frac{2\pi}{-x}}\,\{v_x(x,0^+) - v_x(x,0^-)\}. \tag{15}$$

At this stage, two remarks have to be made. First, the crack will not propagate if the Griffith energy criterion is not satisfied. The stress intensity factor $K_{\mathrm{I}}^{\mathrm{tot}}$ must still satisfy Eqs. (6). Second, the linear stability analysis will not contradict the criterion of local symmetry. On the contrary, it is based on an observation which follows from this principle. When a crack is submitted to a shear loading, its extension will deviate from the pre-existing path by an angle whose sign is opposite to the one of the stress intensity factor of the mode II loading. From this observation, the stability condition for the straight crack stated hereafter follows immediately.

Our linear stability analysis is then based on the following physical arguments. If $K_{\mathrm{II}}^{\mathrm{tot}}/y'(0)$ is found positive, this means that the stress intensity factor, $K_{\mathrm{II}}^{\mathrm{tot}}$, and the orientation of the crack tip, $y'(0)$, are of the same sign. Therefore, according to the criterion of local symmetry, the crack tip tends to follow a path for which $|y'(0)|$ decreases and, consequently, the amplitude of the perturbation will decrease. On the other hand, when $K_{\mathrm{II}}^{\mathrm{tot}}/y'(0) < 0$, the slope $|y'(0)|$ will increase in order to restore a pure mode I local stress field at the tip. So, under a small perturbation of its shape, the straight crack will be stable if $K_{\mathrm{II}}^{\mathrm{tot}}/y'(0)$ is positive and unstable elsewhere. The crack path will thus deviate from a straight propagation once $K_{\mathrm{II}}^{\mathrm{tot}}/y'(0) < 0$ is satisfied. In fact, our scheme consists of searching for conditions where a small perturbation of the linear crack can create a shear loading which amplifies the intrinsic instabilities. Of course, once this threshold is reached, the extending crack will choose a curved path which satisfies $K_{\mathrm{II}}^{\mathrm{tot}} = 0$.

Although our perturbation method is close to the one of CR [8], the two stability analyses are completely different. This difference is not due to the approximation of an infinite medium assumed in [8]. More precisely, our $K_{\mathrm{II}}^{\mathrm{tot}}$ of Eq. (14) corresponds to the k_{II} of Eq. (42) in [8]. However, CR considered a straight crack which bifurcates under the effect of k_{II}. They assumed that independently of the value of k_{II} the pre-existing crack can be treated as a straight one, an assumption that we think arguable. They found that the stability condition is related to the sign of the stress in the transverse direction near the tip, which remains once the square-root singularity has been subtracted out. But, in our approach, we represented from the beginning the inhomogeneities of the material by a perturbation of the straight crack given by a fully wavy path. We analyzed when the shear effect leads to an amplification of the intrinsic deviations of the crack alignment. In fact, our stability analysis performs the approach followed in the study of a large variety of physical systems [6].

Equation (14) shows that $K_{\mathrm{II}}^{\mathrm{tot}}/y'(0)$ is the sum of two terms: The first one, $K_{\mathrm{II}}^{*}/y'(0)$, is due to the variation of the stress field $\overline{\overline{\Sigma}}$ with $\overline{\overline{\sigma}}$. The second term of Eq. (14), $K_{\mathrm{I}}/2$, is a geometrical stabilizing effect. This quantity is always positive in the range of parameters for which a straight crack can exist, so it tends to favor the straight configuration by damping the perturbation given by Eq. (7). It is foreseeable that the instability of the straight crack occurs when the perturbation of the stress field shows a destabilizing effect. That is, when $K_{\mathrm{II}}^{*}/y'(0) < 0$, which tends to amplify the instability of the straight crack. The transition will then occur when the two effects cancel exactly. This condition gives the critical values of the control parameters for which a small deviation from the straight crack begins to introduce a physical shear loading at the crack tip. At this threshold, if it exists, the straight crack becomes unstable and a curved crack path appears.

The condition for instability for the experiment described in [1] as well as the selected wavelength have been deduced quantitatively in [5]; the agreement with experiments was shown to be favorable. On the other hand, recent attempts [11] to apply the CR criterion to the same experiment has given stability thresholds significantly different from the experimental results. However, in order to examine the generality of our linear stability analysis, we will consider below two classical crack configurations in a two-bidimensional body of infinite extent which is opened by a normal mechanical traction at the surface. This configuration is chosen for its simplicity; it can be treated using Muskhelishvili's [12] method for straight cuts.

Let us take as a first example a semi-infinite crack with $p(x) = T\theta(x + l)$, where $\theta()$ is the Heaviside function and the crack tip is located at $x = 0$. The body is also assumed to be loaded at infinity by a stress RT parallel to the crack. In this case [12], $K_{\mathrm{I}} = 2T\sqrt{2l/\pi}$ and $\sigma_{xx} = [R - \theta(x + l)]T$ on the crack surface. As a simple smooth deviation of the crack shape that may exhibit the stability properties we seek, we assume that the perturbation $f(x)$ can be $f(x) = \sin \omega x$. Then Eq. (14) gives

$$\frac{K_{\mathrm{II}}^{\mathrm{tot}}}{y'(0)} = \frac{K_{\mathrm{I}}}{2}\left\{1 - R\sqrt{\frac{\pi}{2l\omega}} + \int_0^1 \frac{\cos l\omega t}{\sqrt{t}}\,dt\right\}. \tag{16}$$

Independently of the perturbation wavelength, the quantity in brackets is always positive once R is negative. So in this case, the quasistatic propagation of the straight

crack is stable for $R \leq 0$. One notes that CR analysis would give a stability threshold $R = 1$.

The second problem is related to an experiment [13] on centrally cracked PMMA sheets loaded by a stress T normal to the crack and a stress RT parallel to it. For this case, one has $K_I = T\sqrt{\pi a}$ and $\sigma_{xx} = (R - 1)T$, where $2a$ is the crack length. Using again Muskhelishvili's [12] method one finds that Eq. (14) satisfies

$$\frac{K_{II}^{tot}}{y'(a)} = \frac{K_I}{2}\left\{1 - \frac{2}{\pi}(R - 1)\int_{-1}^{1}\frac{f'(at)}{f'(a)}\sqrt{\frac{1+t}{1-t}}\,dt\right\}. \tag{17}$$

Here the middle of the crack is chosen to be at $x = 0$. The problem is now to determine the perturbation of the straight crack path. In fact, the allowed perturbation follows from the restriction $f = 0$ at the crack extremities and from the assumption that $f(x)$ is described by a wavy smooth function. For this finite crack problem, the cases of small and large wavelength λ perturbations must be treated separately. When considering the case $\lambda \leq 2a$, the simplest form of $f(x)$ is given by $f(x) = \sin(n\pi x/a)$, with n an integer. This does not allow perturbation wavelengths larger than the crack length. Since the sought after instability is expected to derive from a large wavelength stability analysis, one must also treat the case when $f(x)$ is $f(x) = \cos\omega x - \cos\omega a$, with $\omega a \leq \pi$. If one assumes that these two forms for $f(x)$ are good representations of the perturbations, it is straightforward to show that the case of small wavelength perturbations gives a stability threshold $R = 3/2$. However, when adding the large wavelength perturbations, this threshold decreases and becomes $R = 1$. Therefore we conclude that the straight propagation of this finite crack configuration is unstable for $R > 1$ and stable for $R < 1$. This is consistent with the experimental results of [13]. Moreover, our stability threshold agrees, in this case, with that of CR [8].

In conclusion, a linear stability analysis of quasiequilibrium straight cracks subjected to an opening loading has been presented. From examination of the effect of a smooth deviation from the straight path on the various stress intensity factors, a stability criterion for the straight crack has been established. As this tip criterion compares two competitive terms which depend on the behavior of the stress field in the medium, it automatically includes the geometry and the loading conditions. This explains why in crack experiments the stability thresholds depend sensitively on the different experimental conditions. It has also been shown that the resulting stability conditions agree with both thermal [1] and mechanical [13] experiments.

The important question that remains is in what way one can extend the stability analysis to the dynamical case. To our knowledge, there is no principle equivalent to the criterion of local symmetry for a crack that is moving at velocities of the order of the Rayleigh wave speed. Attempts to find a criterion for the deviation of the dynamical straight crack tip are all related to branching instabilities [14,15]. This consists of a local analysis of the stresses near the crack tip. At this stage, criteria related to maximum stresses [14,15] in the presence (or absence) of dissipation or that of the maximum velocity allowed by the equation of motion [3] (which is an extension of the Griffith theory [4]) cannot be excluded. But since experiments often show other instabilities [2] before attaining the velocities predicted by these theories, other phenomena have to be taken into account, such as the roughness of the crack surfaces, or the acoustic emission of the crack tip.

We are very grateful to D. Bonn and Y. Pomeau for helpful discussions and critical comments.

*Associé au CNRS, aux Universités Paris VI et Paris VII.

[1] A. Yuse and M. Sano, Nature (London) **362**, 329 (1993); O. Ronsin, F. Heslot, and B. Perrin, Phys. Rev. Lett. **75**, 2352 (1995).
[2] J. Fineberg, S. P. Gross, M. Marder, and H. L. Swinney, Phys. Rev. Lett. **67**, 457 (1991); Phys. Rev. B **45**, 5146 (1992); J. F. Boudet, S. Ciliberto, and V. Steinberg, Europhys. Lett. **30**, 337 (1995); E. Sharon, S. P. Gross, and J. Fineberg, Phys. Rev. Lett. **74**, 5096 (1995).
[3] L. B. Freund, *Dynamic Fracture Mechanics* (Cambridge University Press, New York, 1990).
[4] A. A. Griffith, Philos. Trans. R. Soc. London Ser. A **221**, 163 (1921).
[5] M. Adda-Bedia and Y. Pomeau, Phys. Rev. E **52**, 4105 (1995).
[6] S. Chandrasekhar, *Hydrodynamic and Hydromagnetic Stability* (Oxford University Press, London, 1961); J. S. Langer, Rev. Mod. Phys. **52**, 1 (1980).
[7] R. V. Goldstein and R. L. Salganik, Int. J. Fract. **10**, 507 (1974).
[8] B. Cotterell and J. R. Rice, Int. J. Fract. **16**, 155 (1980).
[9] L. Landau and E. Lifchitz, *Théorie de l'Elasticité* (Editions Mir, Moscow, 1967).
[10] G. R. Irwin, J. Appl. Mech. **24**, 361 (1957).
[11] M. Marder, Phys. Rev. E **49**, R51 (1994); S. Sasa, K. Sekimoto, and H. Nakanishi, *ibid.* **50**, R1733 (1994).
[12] N. I. Muskhelishvili, *Some Basic Problems of the Mathematical Theory of Elasticity* (Noordhoff, Groningen, 1953).
[13] J. C. Radon, P. S. Leevers, and L. E. Culver, in *Fracture 1977*, edited by D. M. R. Taplin (Pergamon Press, New York, 1978), Vol. 3.
[14] E. H. Yoffe, Philos. Mag. **42**, 739 (1951); J. W. Craggs, J. Mech. Phys. Solids **8**, 66 (1960).
[15] J. S. Langer, Phys. Rev. Lett. **70**, 3592 (1993); J. S. Langer and H. Nakanishi, Phys. Rev. E **48**, 439 (1993).

Dynamic Instability of Brittle Fracture

Mokhtar Adda-Bedia,[1] Rodrigo Arias,[2] Martine Ben Amar,[1] and Fernando Lund[2]
[1]*Laboratoire de Physique Statistique de l'Ecole Normale Supérieure, 24 rue Lhomond, F-75231 Paris Cedex 05, France*
[2]*Departamento de Física, Facultad de Ciencias Físicas y Matemáticas, Universidad de Chile, Casilla 487-3, Santiago, Chile*
(Received 15 June 1998)

Using Eshelby's energy-momentum tensor, it is shown that the elastic configurational force acting on a moving crack tip does not necessarily point in the direction of crack propagation. A generalization of Griffith's approach that takes into account this fact is proposed to describe dynamic crack propagation in two dimensions. The model leads to a critical velocity below which motion proceeds in a pure opening mode, while above it, it does not. The possible relevance of this instability to recent experimental observations is discussed. [S0031-9007(99)08705-0]

PACS numbers: 62.20.Mk, 46.05.+b, 46.50.+a, 81.40.Np

When an elastic medium that contains a crack is subject to an external load, the energy stored in the elastic field is focused into the region around the crack tip. When the applied load exceeds a threshold value, the crack propagates, thereby creating new surface. According to the present theory of fracture mechanics in two dimensions [1], the crack tip should smoothly accelerate until it reaches the Rayleigh wave speed V_R, the speed at which elastic waves travel along a flat surface. Experiments in isotropic media, however, seldom show crack speeds exceeding half this value, with a trajectory that is far from smooth: a dynamic instability occurs above a well-defined critical velocity where microcracks appear, the fractured surface becomes increasingly rough, and acoustic emissions become markedly stronger [2,3]. Although there have been a number of attempts [4–7] at a theoretical understanding of these facts, it seems fair to say that no coherent explanation has been achieved yet. The purpose of this paper is to propose a model for elastodynamic crack propagation that leads to a dynamic instability.

A basic tenet of current macroscopic fracture theory [1,8] is that crack advance is governed by the fact that the change in energy per unit crack advance (also called the energy release rate G) must be equal to a material parameter, Γ, the specific fracture energy:

$$G \equiv \Gamma . \tag{1}$$

The latter parameter includes the energy associated with the creation of new crack surface, as well as with the energy associated with whatever nonlinear processes take place on a microscopic scale very near the crack tip. In thermodynamical terms, G is the generalized force conjugate to the extension of the crack, and there are two ways to compute it: the first [9,10] is through a global dissipation analysis that takes into account the fact that the fracture of a material sample is thermodynamically irreversible, while the local mechanical behavior of the bulk material may be fully elastic. The second one [11,12] directly involves the computation of the generalized or configurational force, of a *non-Newtonian* type, which acts at the tip of a crack which is considered as a defect. This is the point of view of the theory of defects and material forces on singularities introduced by Eshelby in 1951 [11].

An energy argument, being scalar, is insufficient to completely describe a crack trajectory that is allowed to deviate from a straight line. In order to complete the description of the crack motion, additional criteria, such as the principle of local symmetry [13,14], have been introduced. In this paper, we wish to explore the consequences of taking into account all components of the configurational force acting at the tip of a moving crack. In this framework, we develop a model of force balance instead of energy balance, that under minimal assumptions leads to a critical crack velocity. Below this critical velocity, the crack propagates in a direction that keeps a pure opening mode at its tip, and above it this ceases to hold, leading to a dynamic instability at the crack tip.

We consider an effectively two-dimensional elastic medium, with a crack tip in motion, close to which the elastic fields become singular. The equations of dynamic elasticity in the absence of body force can be written as Euler-Lagrange equations

$$\frac{\partial}{\partial X_\nu}\left(\frac{\partial \mathcal{L}}{\partial u_{i,\nu}}\right) = 0 , \tag{2}$$

with Lagrangian

$$\mathcal{L} = \frac{1}{2}\,\rho \dot{u}_i \dot{u}_i - \frac{1}{2}\,c_{ijkl} u_{i,j} u_{k,l} , \tag{3}$$

where ρ is the material density, c_{ijkl} the elastic constants, $u_i(X_\nu)$ the displacement field, $X_0 = t$, X_i the space coordinates, a comma means partial differentiation [15], and an overdot means partial differentiation with respect to time. For a homogeneous and stationary medium, they imply the conservation laws

$$\frac{\partial T_{\mu\nu}}{\partial X_\nu} = 0 , \tag{4}$$

with $T_{\mu\nu}$ the elastodynamic energy-momentum tensor [12]:

$$T_{\mu\nu} = -\mathcal{L}\delta_{\mu\nu} + \frac{\partial \mathcal{L}}{\partial u_{i,\nu}} u_{i,\mu} , \tag{5}$$

 0031-9007/99/82(11)/2314(4)$15.00

with T_{00} the energy density, T_{0i} the energy density flux, $-T_{i0}$ the field momentum density, and $-T_{ij}$ the field momentum density flux. Note that the field momentum $-T_{i0}$, also called quasimomentum or pseudomomentum [12], is dimensionally a linear momentum but it is not the physical one. Indeed, the physical linear momentum is defined by $\rho \dot{u}_i$, and the quantity $\rho \dot{u}_i + T_{i0}$ is the canonical momentum. Thus, the field momentum is the difference between the linear momentum and the canonical momentum [12].

Consider now a crack tip that is enclosed by a curve C that starts on one lip of the crack, ends on the other, and moves with it. The energy flow $\mathcal{F}(t)$ and the flow of field momentum F_i through the curve C into the crack tip are [16]:

$$\mathcal{F}(t) = -\lim_{C \to 0} \int_C dC[T_{0j} N_j - V_j T_{00} N_j], \qquad (6)$$

$$F_i(t) = \lim_{C \to 0} \int_C dC[T_{ij} N_j - V_j T_{i0} N_j], \qquad (7)$$

with $\vec{N}$ the unit normal at a given point of the curve C. $F_i(t)$ can be identified as a configurational force acting on the crack tip. These flows of energy and field momentum are independent of the shape of the curve C, as long as it lies close to the crack tip [16]. The configurational force $\vec{F}$ is related to the energy flow rate $\mathcal{F}$ through

$$\mathcal{F}(t) = F_i(t) V_i(t). \qquad (8)$$

This means that the work done by the configurational force $\vec{F}$ for an infinitesimal advance of the crack tip, $\vec{F} \cdot d\vec{R}$, is equal to the energy entering into the crack tip region during that time, $\mathcal{F} dt$, with $\vec{V} = d\vec{R}/dt$.

We define a local frame $\vec{e}_i$ such that $\vec{e}_1$ is in the direction of crack motion and $\vec{e}_2$ is perpendicular to it. We suppose a smooth motion of the crack front with relatively small curvature and smooth velocity $V(t)$. Substitution of the universal expressions for stress and displacement velocity near the moving crack tip [1] into Eqs. (3)–(7) gives

$$\frac{1}{V} \mathcal{F}(t) \equiv G(t) = F_1(t), \qquad (9)$$

$$F_1(t) = \frac{1}{2\mu} [A_{\mathrm{I}}(V) K_{\mathrm{I}}^2 + A_{\mathrm{II}}(V) K_{\mathrm{II}}^2], \qquad (10)$$

$$F_2(t) = -\frac{1}{2\mu} B(V) K_{\mathrm{I}} K_{\mathrm{II}}, \qquad (11)$$

K_{I} and K_{II} are the stress intensity factors; $A_{\mathrm{I}}(V)$, $A_{\mathrm{II}}(V)$, and $B(V)$ are universal functions of $V \equiv \vec{V} \cdot \vec{e}_1$:

$$A_{\mathrm{I}}(V) = \frac{a(1 - b^2)}{D(V)}, \qquad (12)$$

$$A_{\mathrm{II}}(V) = \frac{b(1 - b^2)}{D(V)}, \qquad (13)$$

$$B(V) = \frac{4ab(1 - b^4)(a - b)}{D(V)^2}, \qquad (14)$$

with $a(V) \equiv \sqrt{1 - V^2/c_d^2}$, $b(V) \equiv \sqrt{1 - V^2/c_s^2}$; c_d and c_s the dilatational and shear sound velocities respectively, and $D(V) \equiv 4ab - (1 + b^2)^2$, with $D(V_R) = 0$. Expressions (9) and (10) are standard expressions in dynamic fracture. Expression (11) does not appear to have received much attention.

In Eq. (9), we recover the anticipated result (8). Indeed, F_1 is the configurational force in the direction of motion that does work, and F_2 is perpendicular to it and does no work. The possible relevance of such forces to the understanding of crack dynamics was pointed out in Ref. [17]. As evidenced in Eq. (11), the elastic configurational force on the crack tip ceases to be in the direction of motion when in addition to mode-I loading, we have a component of mode-II loading ($K_{\mathrm{II}} \neq 0$).

From Eqs. (9) and (10), we see that the energy release rate G is equivalent in the Eshelbian approach to the configurational force per unit length of the crack front. Thus, Eq. (1) can be reinterpreted as a balance between the elastic configurational force F_1 and a resistance force to crack advance, that is Γ (all per unit length of the crack front). Usually, in addition to Eq. (1), it is assumed that cracks proceed in a purely local opening mode at the tip. This is the *principle of local symmetry* [13,14]:

$$K_{\mathrm{II}} = 0 \Longleftrightarrow \text{smooth crack propagation}. \qquad (15)$$

We wish to write down an equation of motion for two dimensional dynamic crack propagation without assuming *a priori* a principle of local symmetry. In order to do so, two equations are needed. So far, we have determined the two components of the elastic configurational forces acting on the crack tip [Eqs. (10) and (11)]. In order to write down an equation of motion for it, we will assume that it involves the crack velocity only, i.e., that the crack tip does not have inertia [1]. The elastic configurational forces must be balanced by some configurational forces acting at the crack tip region level. These forces are of a dissipative nature and should represent the resistance of the material to crack advance. Their origin should be the adjustment and breaking of bonds at an atomic level. According to our presentation, Griffith's resistance force for mode I loading is

$$\vec{F}_d = -\Gamma \vec{e}_1. \qquad (16)$$

As a generalization of this resistance force in the presence of mode II loading, we propose the following form for $\vec{F}_d$:

$$\vec{F}_d = -\Gamma(\cos \phi_d \vec{e}_1 + \sin \phi_d \vec{e}_2), \qquad (17)$$

with ϕ_d an angle to be modeled. Thus, we state that for $K_{\mathrm{II}} \neq 0$ the resistance force is not necessarily in the direction of motion, but that its magnitude will remain as Γ. The asymmetry introduced at the tip by a mode II loading, we think justifies the fact that the resistance force will not point in the direction of motion. Furthermore, we think the resistance force should be weakened in

the direction of motion by the shearing produced by the mode II loading, as it is reflected in Eq. (17).

We model the angle ϕ_d as a function of $K_{\rm II}$ (that acts as the forcing mechanism here) and the velocity of the crack tip, V [16]. In order to be nondimensioned, ϕ_d should depend on q, a parameter proportional to $K_{\rm II}/K_{\rm I}$,

$$q \equiv (b/a)\,(K_{\rm II}/K_{\rm I})\,.$$

Also, it should be an odd function of q in order to respect mode II symmetry. Therefore, one can always write

$$\tan\phi_d = -2\alpha(V) q \psi(q,V)\,, \tag{18}$$

with $\alpha(V)$ an unknown material parameter, and $\psi(q,V) = 1 + \beta(V)q^2 + \ldots$ a function that represents higher order corrections in q.

The energy balance arguments at the crack tip imply local force balance in the direction of motion. Then, it is natural to assume that this balance also holds perpendicularly to the direction of motion. Having a form for the elastic configurational force and for the resistance force, we write our equation of motion by assuming vectorial balance of forces, $\vec{F} + \vec{F}_d = 0$, thus in the following way

$$\tan\phi_d = \frac{F_2}{F_1}\,, \tag{19}$$

$$\Gamma\cos\phi_d = F_1\,. \tag{20}$$

Substitution of Eqs. (10), (11), and (18) into Eq. (19) leads to

$$2\alpha(V) q\psi(q,V) - 2C(V)\,\frac{q}{1+\frac{a}{b}\,q^2} = 0\,, \tag{21}$$

with $C(V) \equiv 2a(1+b^2)(a-b)/D(V)$. This equation can be solved for q for a given V, independently of the specific loading conditions and geometry. The function $\psi(q,V)$ for $q \ll 1$ is approximately $\psi(q,V) \simeq 1 + \beta(V)q^2$, and we assume $\beta(V) \geq 0$, i.e., the angle of the force of resistance grows with $K_{\rm II}$. We will also assume that the material parameter $\alpha(V)$ is a slowly varying function of V compared with the variation of $C(V)$. Under these assumptions on $\psi(q,V)$ and $\alpha(V)$, the solutions of Eq. (21) can be determined: for $\alpha(V) \geq 1$, there is a critical velocity V_c, given by the condition $C(V_c) = \alpha(V_c)$, such that

$$V < V_c \Longleftrightarrow K_{\rm II} = 0\,, \tag{22}$$

$$V > V_c \Longleftrightarrow K_{\rm II} = 0,\ \pm g(V) K_{\rm I}\,. \tag{23}$$

Therefore, according to the velocity of the crack tip, there exists either one solution $K_{\rm II} = 0$, or three solutions $K_{\rm II} = 0$ and $K_{\rm II} = \pm g(V) K_{\rm I}$ for Eq. (21). Notice that the approximation of $\psi(q,V)$ to order q^2 allows the calculation of $g(V)$ from Eq. (21). Indeed, $g(V) \simeq h(V_c)\sqrt{V - V_c}$ for V greater but close to V_c. Thus, the velocity V acts as a bifurcation parameter at $V = V_c$ for finding the solutions of Eq. (21) as a function of q, or $K_{\rm II}/K_{\rm I}$.

The new solutions with $K_{\rm II} \neq 0$ correspond to a continuously growing $K_{\rm II}$ as V grows over V_c, from $K_{\rm II} = 0$ at $V = V_c$. If $\alpha(V) < 1$, there would always exist three solutions to our equation (21), since $C(V) \geq 1$. We shall not consider this case since it does not appear to be related to experimental results in glass and plexiglass [2,3]. Notice also that the critical velocity V_c always satisfies $V_c < V_R$, since $C(V) \to \infty$ as $V \to V_R$.

Having found different solutions for *smooth* crack propagation for $V > V_c$, one needs to define a selection mechanism to decide which one will correspond to the path taken by the moving crack tip. Consider first a configuration of *smooth* crack propagation at $V(t) > V_c$, with $K_{\rm I} \neq 0$ and $K_{\rm II} = 0$. From Eqs. (9) and (20), the rate of energy flow needed for the propagation of this crack is $\mathcal{F}' = V\Gamma$. Consider a second configuration of *smooth* crack propagation with the same instantaneous velocity $V(t)$, but with $K_{\rm I} \neq 0$ and $K_{\rm II} = \pm g(V) K_{\rm I}$. From Eqs. (9) and (20), the rate of energy flow needed for the propagation of this crack is $\mathcal{F}'' = V\Gamma\cos\phi_d$. Clearly, $\mathcal{F}'' \leq \mathcal{F}'$. This is so because the material response to external loading provides a smaller restoring force for the second configuration than for the first one. Thus, for a given velocity V above the critical velocity V_c, the crack needs more energy to advance in a configuration with $K_{\rm II} = 0$ than in a configuration with $K_{\rm II} \neq 0$. Therefore, for $V > V_c$ the selected solutions are $K_{\rm II} = \pm g(V) K_{\rm I}$, instead of the solution $K_{\rm II} = 0$, and consequently the principle of local symmetry no longer holds for $V > V_c$.

The following scenario based on our model tries to explain some features of the experimental results in fast fracture of glass and plexiglass plates under tension [2,3]. These experiments have shown an instability appearing when the crack tip velocity surpasses a certain critical velocity. This instability is associated with the roughening of the crack surfaces and the appearance of microcracks on them. As our scenario, we propose to identify the critical velocity V_c of our model with this experimental critical velocity. For PMMA, the critical velocity has been found at $V_c \approx 0.36 V_R$ [2,3]. Using $c_d \approx \sqrt{3}\,c_s$, and from the condition $\alpha(V_c) = C(V_c)$, one finds $\alpha(V_c) \approx 1.073$, which is a reasonable value for the model. Indeed, a simple estimate based on an analogy with the branching process at low velocities [14] suggests $\alpha \approx 1$ [16].

For velocities below V_c, the only possible solution that was obtained corresponds to $K_{\rm II} = 0$. From Eq. (20), we recover the well-known equation of motion [1]:

$$\frac{1}{2\mu}\,A_{\rm I}(V) K_{\rm I}^2 = \Gamma\,, \tag{24}$$

which allows one to determine the crack tip velocity. The result $K_{\rm II} = 0$ means that the crack will propagate following a smooth path, with a pure opening mode at its tip. This is the statement of the principle of local symmetry (15). Our approach can be viewed as a derivation of this principle and as an extension of it to

velocities $V < V_c$. Considering the experimental results of [2,3], this solution corresponds to the mirror region, where the crack propagation follows a straight line.

As the velocity of the crack surpasses V_c, according to our selection mechanism the propagation satisfying $K_{\mathrm{II}} = 0$ at the crack tip should become unstable. The crack now propagates in one of the two new directions satisfying $K_{\mathrm{II}} \neq 0$, specifically $K_{\mathrm{II}} = \pm g(V) K_{\mathrm{I}}$. Notice that the allowed values of $K_{\mathrm{II}}/K_{\mathrm{I}}$ grow continuously with V from 0 at $V = V_c$, and that these new solutions correspond to *smooth* crack propagation.

Experiments [2,3] have shown that the roughness is associated with the presence of bumps on the surfaces, together with microcracks. The solution $K_{\mathrm{II}} = \pm g(V) K_{\mathrm{I}}$ means that the trajectory of the crack tip will deviate from a straight line, which in experiments [2,3] corresponds to the solution $K_{\mathrm{II}} = 0$. The appearance of microcracks at this stage can be explained as follows: on the crack faces the stress components σ_{22} and σ_{12} vanish identically. However, in the presence of a shear mode at the crack tip ($K_{\mathrm{II}} \neq 0$), the asymptotic elastic stress field σ_{11} near the moving crack tip is singular on the crack faces [1]:

$$\sigma_{11}(r, \pm\pi) \sim \mp K_{\mathrm{II}}/\sqrt{r}\,. \tag{25}$$

This means that there is a high tensile stress near the tip that will tend to open microcracks on one of the crack faces, in a direction initially perpendicular to the direction of motion of the main crack. The microcrack will initiate in a weak place; it starts perpendicularly and later deviates into a direction closer to the direction of motion of the main crack, since it will avoid the unloaded region which is left behind the crack tip.

Summarizing, we have developed an approach based on the balances of energy and field momentum [11,12] for a moving crack tip in two dimensions. We have derived the energy flow rate into the crack tip and the configurational forces acting on it. The components of the material force at the crack tip have been computed in the framework of the linear isotropic elastodynamic model. Within a Griffith-like approach, we have defined a generalized dissipative force at the crack front. By assuming forces balance at the crack front, we derived a vectorial equation of motion for it. Under minimal assumptions, we have shown that below a critical crack speed, the crack propagates in a direction that keeps a pure opening mode at its tip. Moreover, a second order dynamic instability has been predicted: above this critical velocity, the crack growth with a pure opening mode at the tip becomes unstable with respect to two new possible solutions.

Our approach is universal, in the sense that the instability mechanism is local at the crack tip as well as independent of the specific loading configuration and the geometry of the experiment. Throughout the analysis, it has not been specified that the fracture energy should be velocity independent, or that the configuration of pure opening mode of the crack tip has to be a straight line. Such a configuration could be a curved path, but an instability would still occur.

M. A.-B. wishes to thank Professor J. R. Rice for helpful discussions and critical comments. R. A. and F. L. gratefully acknowledge the support of a Cátedra Presidencial en Ciencias. This collaboration was made possible by a grant from CNRS-CONICYT. Laboratoire de Physique Statistique is associated with CNRS (UMR 8550) and Universities Paris VI and Paris VII.

[1] L. B. Freund, *Dynamic Fracture Mechanics* (Cambridge University Press, Cambridge, 1990).
[2] E. Sharon and J. Fineberg, Phys. Rev. B **54**, 7128 (1996); S. P. Gross *et al.*, Phys. Rev. Lett. **71**, 3162 (1993); J. Fineberg *et al.*, Phys. Rev. B **45**, 5146 (1992).
[3] J. F. Boudet and S. Ciliberto, Phys. Rev. Lett. **80**, 341 (1998); J. F. Boudet, S. Ciliberto, and V. Steinberg, J. Phys. II (France) **6**, 1493 (1996).
[4] X. P. Xu and A. Needleman, J. Mech. Phys. Solids **42**, 1397 (1994).
[5] M. Marder and S. P. Gross, J. Mech. Phys. Solids **43**, 1 (1995).
[6] E. S. C. Ching, J. S. Langer, and H. Nakanishi, Phys. Rev. E **53**, 2864 (1996).
[7] M. Adda-Bedia, M. Ben Amar, and Y. Pomeau, Phys. Rev. E **54**, 5774 (1996).
[8] A. A. Griffith, Philos. Trans. R. Soc. London A **221**, 163 (1920).
[9] J. R. Rice, J. Appl. Mech. **35**, 379 (1968).
[10] B. V. Kostrov and L. V. Nitkin, Arch. Mech. Stosow. **22**, 749 (1970).
[11] J. D. Eshelby, Philos. Mag. **42**, 1401 (1951).
[12] J. D. Eshelby, in *Inelastic Behaviour of Solids*, edited by M. F. Kanninen, W. F. Adler, A. R. Rosenfield, and R. I. Jaffee (McGraw-Hill, New York, 1970), pp. 77–115.
[13] R. V. Goldstein and R. L. Salganik, Int. J. Fract. **10**, 507 (1974).
[14] M. Amestoy and J. B. Leblond C. R. Acad. Sci. Ser. 2 **301**, 969 (1985); B. Cotterell and J. R. Rice, Int. J. Fract. **16**, 155 (1980).
[15] We use this notation for compactness. Greek indices do NOT label components of a four-vector.
[16] M. Adda-Bedia, R. Arias, M. Ben Amar, and F. Lund, submitted to Phys. Rev. E, Phys. Rev. E (to be published).
[17] F. Lund, Phys. Rev. Lett. **76**, 2742 (1996).

Generalized Griffith criterion for dynamic fracture and the stability of crack motion at high velocities

M. Adda-Bedia,[1] R. Arias,[2] M. Ben Amar,[1] F. Lund[2]
[1]*Laboratoire de Physique Statistique de l'Ecole Normale Supérieure, 24 rue Lhomond, F-75231 Paris Cedex 05, France*
[2]*Departamento de Física, Facultad de Ciencias Físicas y Matemáticas, Universidad de Chile, Casilla 487-3, Santiago, Chile*
(Received 18 November 1998)

We use Eshelby's energy momentum tensor of dynamic elasticity to compute the forces acting on a moving crack front in a three-dimensional elastic solid [Philos. Mag. **42**, 1401 (1951)]. The crack front is allowed to be any curve in three dimensions, but its curvature is assumed small enough so that near the front the dynamics is locally governed by two-dimensional physics. In this case the component of the elastic force on the crack front that is tangent to the front vanishes. However, both the other components, parallel and perpendicular to the direction of motion, do not vanish. We propose that the dynamics of cracks that are allowed to deviate from straight line motion is governed by a vector equation that reflects a balance of elastic forces with dissipative forces at the crack tip, and a phenomenological model for those dissipative forces is advanced. Under certain assumptions for the parameters that characterize the model for the dissipative forces, we find a second order dynamic instability for the crack trajectory. This is signaled by the existence of a critical velocity V_c such that for velocities $V<V_c$ the motion is governed by $K_{II}=0$, while for $V>V_c$ it is governed by $K_{II}\neq 0$. This result provides a qualitative explanation for some experimental results associated with dynamic fracture instabilities in thin brittle plates. When deviations from straight line motion are suppressed, the usual equation of straight line crack motion based on a Griffiths-like criterion is recovered. [S1063-651X(99)12408-5]

PACS number(s): 46.05.+b, 62.20.Mk, 46.50.+a, 81.40.Np

I. INTRODUCTION

Experiments carried out over the past ten years with thin plates of glass and plexiglass have uncovered a wealth of phenomena associated with dynamic fracture [1–5]. When the crack velocity V exceeds a critical speed V_c, a dynamic instability occurs: The velocity of the crack starts to oscillate, the crack surface becomes rough, microcracks branch out of the main crack, acoustic emission from the crack increases, velocity oscillations are amplified, and a pattern more or less correlated with the velocity oscillations appears on the fracture surface. One recent experiment [6] has focused on the role played by microcracks, while another [7] has shown that even a modest amount of acoustic energy may induce a significant change in the velocity of a running crack. Those measurements that have been performed both in glass and plexiglass indicate that, after proper normalization, those effects are the same in both materials. A remarkable fact given their very different microstructure.

Standard theoretical tools to understand crack dynamics are based on dynamic elasticity in two dimensions [8]. This theoretical framework predicts that a crack in tension will accelerate smoothly, asymptotically approaching the Rayleigh wave velocity. For quite some time, however, there have been experimental results at variance with conclusions based on this analysis [9]. The experiments mentioned in the previous paragraph are sufficiently accurate to place quantitative bounds on deviations from the smooth, straight trajectory that a simple minded two-dimensional analysis yields.

Over the last several years, there have been a number of attempts to explain the complexity of the dynamics of the crack tip. Studies based on a continuum approach to the crack problem have been made, and it has been suggested that the crack instabilities are due to three-dimensional effects [10,11], or to the effect of large deformations near the crack tip, requiring a nonlinear analysis [12]. Another point of view has emphasized that complete dynamical models of deformation and decohesion at crack tips [13,14] are necessary in order to understand the experimental observations. It has also been argued [15] that conventional continuum theories are inherently inadequate to describe crack dynamics, and lattice models have accordingly been proposed and solved (see also Ref. [16]). Finally, a number of studies have been undertaken using large scale molecular dynamics simulations [17–19]. In spite of this considerable effort, it does not seem unfair to say that there are well established experimental observations that, to date, have defied theoretical understanding.

Current theory of brittle fracture mechanics is essentially based on the determination of a characteristic quantity called the energy release rate G [8], or rate of decrease of elastodynamic energy per unit crack advance. Within purely elastic assumptions, the crack must grow in such a way that G is always equal to a newly defined quantity Γ, the dynamic fracture energy of the material [8,20]. The parameter Γ includes the energy associated with the creation of a new crack surface, as well as the energy associated with whatever nonlinear processes take place on a microscopic scale very near the crack tip. However, this is only one condition, and it is not enough to completely determine the crack tip motion that is allowed to deviate from a straight line. Effectively, the generalized Griffith criterion [8,20] is a scalar equation, while crack motion has three degrees of freedom. Therefore, in order to complete the description of crack motion, additional criteria, such as the principle of local symmetry [21,22], have been introduced.

In thermodynamics terms, G is the generalized force con-

jugate to the extension of a crack. There are two ways to compute this quantity. The first of these [23,24] is a global dissipation analysis which recognizes the fact that the fracture of a material sample is thermodynamically, irreversible while the local mechanical behavior of the bulk material may be fully elastic. The second one [25,26] directly involves the computation of the generalized, or configurational, force of a *non-Newtonian* type which acts at the tip of the crack, which is considered as a defect. This is the point of view of the theory of defects, or material inhomogeneities, and material forces on singularities introduced by Eshelby in 1951 [25]. Configurational forces in conjunction with an inequality based on the second law of thermodynamics have been recently used to propose a framework for crack propagation [27,28].

In this paper, we propose an approach based on the full consideration of all components of the configurational force at the crack front. It is found that this force does not necessarily point in the direction of crack propagation, and we propose a generalization of Griffith's approach [20] in order to take this fact into account. Within this framework, we develop a model of forces balance, instead of energy balance. Under minimal assumptions, we show that there exists a critical crack velocity, below which the crack propagates in a direction that keeps a pure opening mode at the tip. Above the critical velocity, this mode of crack propagation is no longer favored, and there appears a dynamic instability. A number of experimental results can thereby be qualitatively understood. A preliminary announcement of these results was presented in Ref. [29].

This paper is organized as follows. In Secs. II and III, we introduce the main theoretical ingredients of our analysis. We review the derivation of the Eshelby energy-momentum tensor [26,30], and we present the balance of energy and field momentum for a moving crack front. This motivates the introduction of the energy flow rate into the crack front and the material forces acting on it. The analysis of these two Sections is valid in three dimensions, and for quite general constitutive relations, including nonlinear stress-strain relations. In Sec. IV, we derive the explicit form of the material forces in a linear isotropic elastodynamic solid. The commonly used equation of motion [8] corresponds to a balance of energy at the crack front. We point out that it also corresponds to the balance of configurational forces in one direction, the direction of motion. In Sec. V, we show that within a Griffith-like approach, it is possible to define a generalized dissipative force at the crack front. Assuming that elastic and dissipative forces acting at the crack front exactly balance, we derive a vector equation of motion. In Sec. VI we show that within our model a second order dynamic instability is possible: above a critical velocity (smaller than the Rayleigh velocity), crack growth with a pure opening mode at the tip becomes unstable with respect to two new possible solutions. Section VII is devoted to the interpretation of some of the experimental results of Refs. [1–5] within the framework of this model. Concluding remarks are offered in Sec. VIII.

II. BALANCES OF ENERGY, LINEAR AND FIELD MOMENTA

In this section we review some concepts of energy and momentum balance in an elastic solid [26,30]. We will use a Lagrangian description, with variables associated to a reference, or undistorted, configuration. The volume and boundary of this reference configuration are denoted by V and S, respectively, and their points are described in terms of a Cartesian basis $\vec{E}_i$ $(i=1,2,3)$ as $\vec{X}=X_i\vec{E}_i$. The dynamics of the solid is given by the evolution of those points as a function of time. Their position is given by the current, or distorted, configuration

$$\vec{x}=\vec{\chi}(\vec{X},t)=\vec{X}+\vec{u}(\vec{X},t), \tag{1}$$

with $\vec{u}(\vec{X},t)$ the displacement field. The local balance of the linear momentum reads

$$\frac{\partial}{\partial t}(\rho_o(\vec{X})v_i(\vec{X},t))-\frac{\partial p_{ij}}{\partial X_j}(\vec{X},t)=\rho_o(\vec{X})f_i(\vec{X},t), \tag{2}$$

with $v_i(\vec{X},t)=u_{i,t}\equiv\partial u_i/\partial t$ the particle velocity, p_{ij} the nominal stress tensor, $\rho_o(\vec{X})$ the mass density per unit volume, and $\vec{f}(\vec{X},t)$ the body force per unit mass. They are all defined with respect to the reference configuration. The nominal stress tensor p_{ij} is given by

$$p_{ij}(\vec{X},t)=\frac{\partial}{\partial u_{i,j}}W(u_{k,l},\vec{X},t), \tag{3}$$

with W the strain energy per unit initial volume, and $u_{i,j}\equiv\partial u_i/\partial X_j$. The equation of motion [Eq. (2)], together with boundary conditions on the surface S,

$$\mathcal{T}_i=p_{ij}n_j,$$

where $\mathcal{T}_i$ is the traction exerted by external loads on the surface that points in the direction n_i, can also be obtained as the extremum of the action

$$\mathcal{A}=\int_{t_i}^{t_f}dt\int_V d\vec{X}[\mathcal{L}(u_{i,t},u_{i,j},X_i,t)+\rho_o(\vec{X})f_i(\vec{X},t)u_i(\vec{X},t)]+\int_{t_i}^{t_f}dt\int_S dS\,\mathcal{T}_i(\vec{X},t)u_i(\vec{X},t), \tag{4}$$

with respect to variations of $\vec{u}(\vec{X},t)$. This procedure leads to the following Euler-Lagrange equations, representing linear momentum balance:

$$\frac{\partial}{\partial t}\left(\frac{\partial\mathcal{L}}{\partial u_{i,t}}\right)+\frac{\partial}{\partial X_j}\left(\frac{\partial\mathcal{L}}{\partial u_{i,j}}\right)=\rho_o f_i. \tag{5}$$

This equation is equivalent with Eq. (2) if the Lagrangian density $\mathcal{L}$ is defined as

$$\mathcal{L}(u_{i,t},u_{i,j},X_i,t)\equiv T(u_{i,t},X_i)-W(u_{i,j},X_i,t), \tag{6}$$

where $T=\frac{1}{2}\rho_o(\vec{X})\vec{v}^2$ is the kinetic energy density.

Multiplying Eq. (2) by v_i and rearranging, the following equation of energy balance results:

$$\frac{\partial}{\partial t}(T+W)+\frac{\partial}{\partial X_j}(-p_{ij}v_i)=\rho_o f_i v_i-\left.\frac{\partial\mathcal{L}}{\partial t}\right|_{\text{expl}}, \tag{7}$$

where the subscript expl designs the explicit material derivative of the Lagrangian density. Likewise, multiplying Eq. (2) by $\partial u_i/\partial X_k$ one can obtain the following equation of field momentum balance:

$$\frac{\partial}{\partial t}\left(\rho_o v_i \frac{\partial u_i}{\partial X_k}\right)+\frac{\partial}{\partial X_j}\left(-\mathcal{L}\delta_{kj}-p_{ij}\frac{\partial u_i}{\partial X_k}\right)=\rho_o f_i \frac{\partial u_i}{\partial X_k}-\left.\frac{\partial \mathcal{L}}{\partial X_k}\right|_{\text{expl}}, \tag{8}$$

where the field momentum density is defined as $-\rho_o v_i \partial u_i/\partial X_k$ [26]. Note that this quantity is dimensionally a density of linear momentum, i.e., mass density times velocity, but it is not the ''physical'' momentum $\rho_0 v_i$. Indeed, the field momentum per unit volume of the reference configuration, also known as quasimomentum or pseudomomentum, is the difference between the linear momentum $\rho_o v_k$ and the canonical momentum $\rho_o v_k+\rho_o v_i \partial u_i/\partial X_k$ [26,30].

Equations (7) and (8) in the absence of body forces ($f_i=0$), and in an homogeneous and stationary medium ($\partial\mathcal{L}/\partial X_k|_{\text{expl}}=0$, $\partial\mathcal{L}/\partial t|_{\text{expl}}=0$) represent energy and field momentum conservation. In the absence of body forces, the energy and field momentum balance can be written in the form

$$\frac{\partial T_{\mu\nu}}{\partial X_\nu}=-\left.\frac{\partial \mathcal{L}}{\partial X_\mu}\right|_{\text{expl}}, \tag{9}$$

with $\mu,\nu=0,1,2$, and 3 and $X_0\equiv t$. Note that, although we use four-dimensional notation for convenience, Greek indices do not label the four components of vectors. The components of the Eshelby energy-momentum tensor $T_{\mu\nu}$ are [26]

$$T_{00}=T+W,\quad T_{0i}=-p_{ji}v_j,$$

$$T_{i0}=\rho_o v_j\frac{\partial u_j}{\partial X_i},\quad T_{ij}=-\mathcal{L}\delta_{ij}-p_{kj}\frac{\partial u_k}{\partial X_i}, \tag{10}$$

with T_{00} the energy density, T_{0i} the energy density flux, $-T_{i0}$ the field momentum density, and $-T_{ij}$ the field momentum density flux. These formulas can be encapsulated in the following compact form:

$$T_{\mu\nu}=-\mathcal{L}\delta_{\mu\nu}+\frac{\partial\mathcal{L}}{\partial u_{i,\nu}}u_{i,\mu}. \tag{11}$$

Note that throughout this section it has been assumed that the solid is elastic, in the sense that stresses can be obtained as gradients of a potential energy function W [Eq. (3)]. Nothing has been assumed, however, about the functional dependence of W upon strain. In particular, the solid need not be linearly elastic.

Consider now the motion of a given domain $\mathcal{B}(t)$ of the reference frame, bounded by a surface $\partial\mathcal{B}(t)$, within an homogeneous elastic body of volume $\mathcal{V}$, itself bounded by an external surface $\mathcal{S}$. The domain $\mathcal{B}$ is in motion with a velocity $\vec{V}$, measured in the reference, or undistorted, frame. We look for the energy and field momentum flow into this domain. It is allowed for this domain to contain an inhomogeneity, or a singularity of the elastic fields, or to intersect the external surface. This last possibility will be used in Sec. III,

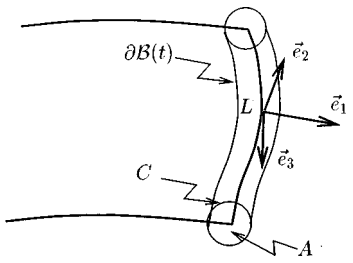

FIG. 1. Schematic representation of a crack surface. A local orthonormal basis $\vec{e}_i$ ($i=1$, 2, and 3) is associated with the crack front. The front itself is a curve whose parameter is L. Arguments involving energy and momentum balance involve a cylindrical volume around the crack front. This cylinder is bounded by a surface $\partial\mathcal{B}(t)$ of cross section A, whose rim is given by a curve C.

in which $\mathcal{B}(t)$ will surround a crack tip. Integrating Eq. (9) within the volume $\mathcal{V}$ but excluding the domain $\mathcal{B}$, and under the assumption that $\partial\mathcal{L}/\partial X_\mu|_{\text{expl}}=0$ in $\mathcal{V}-\mathcal{B}$, leads to the following equation of energy-momentum balance:

$$\frac{d}{dt}\int_{\mathcal{V}-\mathcal{B}(t)} d\vec{X}\ T_{\mu 0}=\int_{\mathcal{S}} dS_i\ T_{\mu i}+\int_{\partial\mathcal{B}(t)} dS_i[T_{\mu i}-V_i T_{\mu 0}]. \tag{12}$$

Since T_{00} is the energy density, we can interpret the $\mu=0$ component of this equation as an equation of field energy balance: the change in elastic energy within the volume $\mathcal{V}-\mathcal{B}$ per unit time is equal to the work performed at the surface $\mathcal{S}$ minus the quantity

$$\mathcal{W}=-\int_{\partial\mathcal{B}(t)} dS_i[T_{0i}-V_i T_{00}], \tag{13}$$

which can thus be identified as the rate of energy flow into the moving domain $\mathcal{B}$ through its boundary $\partial\mathcal{B}$. Similarly, since $-T_{j0}$ is the density of field momentum, taking the $\mu=j$ component of Eq. (12) yields an equation of momentum balance: the change in field momentum within $\mathcal{V}-\mathcal{B}$ is given by the elastic force performed at the surface $\mathcal{S}$ minus the quantity

$$\mathcal{P}_j=\int_{\partial\mathcal{B}(t)} dS_i[T_{ji}-V_i T_{j0}], \tag{14}$$

which can thus be identified as the rate of flow of field momentum into the moving domain $\mathcal{B}$ through its boundary $\partial\mathcal{B}$.

III. ENERGY AND FIELD MOMENTUM BALANCE FOR A MOVING CRACK

We now apply the previous formalism to a three-dimensional solid within which there is a moving crack. The crack front is a line $\vec{R}(L,t)$, with L a Lagrangian coordinate that labels points along the crack front, where elastic fields are singular. The crack front velocity is $\vec{V}(L,t)\equiv\partial\vec{R}(L,t)/\partial t$. We take as the domain $\mathcal{B}$ a thin cylinder surrounding the crack front and the surface $\partial\mathcal{B}(t)$ the surface of this cylinder; it starts on one crack lip, encircles the crack front, and ends on the other crack lip (see Fig. 1). We assume that during crack propagation both the crack surface and the

crack front remain smooth with continuously turning tangents. Otherwise, the local frame at the crack front is ill defined.

The instantaneous rate of energy flow $\mathcal{F}(L,t)$ entering into the region of the crack front per unit of its length [8,23,24] is given by the specialization of Eq. (13) to the case of a thin cylindrical surface just mentioned,

$$\mathcal{F}(L,t)\equiv\frac{d\mathcal{W}}{dL}=-\lim_{C\to 0}\int_C dC[T_{0i}N_i-V_iT_{00}N_i], \quad (15)$$

where C is a curve that encircles the crack front along the surface of the cylinder $\partial\mathcal{B}(t)$, within a plane locally perpendicular to the crack front (see Fig. 1), and N_i is the unit normal to this curve. The instantaneous rate of flow of field momentum into the region of the crack front can be identified as a configurational force $F_j(L,t)$ acting on it [26,30], whose value is found, from Eq. (14), to be

$$F_j(L,t)\equiv\frac{d\mathcal{P}_j}{dL}=\lim_{C\to 0}\int_C dC[T_{ji}N_i-V_iT_{j0}N_i]. \quad (16)$$

We emphasize that $\mathcal{F}(L,t)$ and $F_i(L,t)$ are defined *per unit length of the crack front*: the total rate of energy flow and total forces are given by $\mathcal{W}=\int_L dL\mathcal{F}(L,t)$ and $\mathcal{P}_j=\int_L dLF_j(L,t)$, respectively.

Some insight into the nature of the force $\vec{F}$ may be obtained by considering the field momentum balance for the volume *within* $\mathcal{B}(t)$, assuming that elasticity, not necessarily linear and not necessarily homogeneous but obeying the assumptions of Sec. II, holds. Simple integration gives

$$\frac{d}{dt}\int_{\mathcal{B}(t)}d\vec{X}(-T_{j0})=\int_{\mathcal{B}(t)}d\vec{X}\frac{\partial}{\partial t}(-T_{j0})+\int_{\partial\mathcal{B}(t)}dS_i(-T_{j0})V_i. \quad (17)$$

Use of the local field momentum balance [Eq. (9)], and of Eq. (14) for the field momentum flow into the domain $\mathcal{B}(t)$, leads to

$$\frac{d}{dt}\int_{\mathcal{B}(t)}d\vec{X}(-T_{j0})=\int_{\mathcal{B}(t)}d\vec{X}\left.\frac{\partial\mathcal{L}}{\partial X_j}\right|_{\text{expl}}+\mathcal{P}_j(t). \quad (18)$$

For the actual calculation of these forces and energy flow, we take the displacement field within $\mathcal{B}(t)$ to be of the form

$$u_i=u_i^o(\vec{X}-\vec{R}(L,t),t)+u_i'(\vec{X},t), \quad (19)$$

with $\partial u_i^o/\partial X_j\gg\partial u_i'/\partial X_j$, and $\partial u_i^o/\partial t\simeq -V_j\partial u_i^o/\partial X_j$. To the extent that the dominant contribution $\vec{u}^o$ leads to a divergence of T_{j0} weaker than $|\vec{X}-\vec{R}(L,t)|^{-2}$, the left hand side of Eq. (18) will be zero, and accordingly, per unit length of the crack front the following holds:

$$F_j(L,t)=-\lim_{A\to 0}\int_A\left.\frac{\partial\mathcal{L}}{\partial X_j}\right|_{\text{expl}}dA, \quad (20)$$

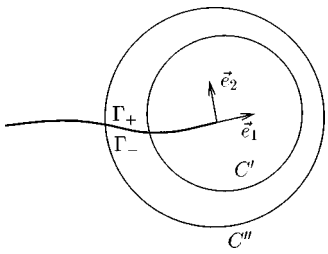

FIG. 2. Two different contours of integration C' and C'' surrounding the crack tip. A closed surface is defined by them, plus two lines Γ_+ and Γ_- along the upper and lower lips of the crack surface that lie between C' and C''.

with A the cross sectional area of $\mathcal{B}(t)$. This last relation for the material forces $F_j(L,t)$ suggests that they may be balanced by inhomogeneities of the elastic field very near the crack front.

Equations (15) and (16) must be path independent in order to have fundamental significance, and we now show that this is the case. Consider two distinct crack-tip encircling curves C' and C'', and the closed contour formed by C' and C'' plus two straight segments Γ_+ and Γ_- along the crack faces (Fig. 2). The integrand $I_{\mu i}=T_{\mu i}-V_iT_{\mu 0}$ that appears in Eqs. (15) and (16) for $\mathcal{F}$ and F_i renders a null result when integrated over the closed curve $C'+\Gamma_++C''+\Gamma_-$, provided the displacement field u_i has the near-field asymptotic behavior [Eq. (19)]. This behavior is satisfied by linear elastodynamic fields close to the crack front (see Sec. II). This result is established by applying the divergence theorem to the integral and by incorporating the energy and field momentum balances, Eqs. (7) and (8), with $f_i=0$ and $\partial\mathcal{L}/\partial X_\nu=0$. The integration of $\mathcal{F}$ over $\Gamma_\pm$ is equal to zero. The integration of F_j over Γ_+ is the negative of the integration over Γ_- and leads to a cancellation because, due to the near field behavior [Eq. (19)] $\mathcal{L}_+=\mathcal{L}_-$, with $\mathcal{L}_\pm$ the Lagrangian evaluated on the segments $\Gamma_\pm$, respectively. From this one deduces that, as long as both C' and C'' are close to the tip,

$$\mathcal{F}=-\int_{C'}dS_iI_{0i}=-\int_{C''}dS_iI_{0i},$$

$$F_j=\int_{C'}dS_iI_{ji}=\int_{C''}dS_iI_{ji}. \quad (21)$$

This proves the independence of the result on the shape of the curve C, as long as it is near the crack front [31].

The force $\vec{F}$ can be related to the energy flow rate $\mathcal{F}$ [23,26,30]. Using the explicit expressions for $T_{\mu\nu}$ from Eq. (10) and the near field behavior $v_i\simeq\partial u_i^o/\partial t\simeq -V_j\partial u_i^o/\partial X_j$ [see Eq. (19)], a direct substitution into Eqs. (15) and (16) shows that

$$\mathcal{F}(L,t)=V_i(L,t)F_i(L,t). \quad (22)$$

This important result gives a physical interpretation to the force $\vec{F}$ on the crack front; the work done by the force for an infinitesimal advance of the crack front, $\vec{F}\cdot d\vec{R}$, is *equal* to the energy entering the crack front per unit length during that time, $\mathcal{F}dt$.

IV. ENERGY FLOW AND MATERIAL FORCES FOR A GROWING CRACK

We now specialize to the case of elastodynamic crack growth within a linearly elastic material. In this case the strain energy density is $W=p_{ij}u_{i,j}/2$, with $p_{ij}=C_{ijpq}\partial u_p/\partial X_q$, where C_{ijpq} is the elastic constants tensor. We shall assume that derivatives along a direction locally parallel to the crack front are smaller than derivatives along a direction locally perpendicular to it, so that the singular structure of the elastic fields near the crack front is locally two dimensional [32].

Consider a crack front moving under loading in modes I, II (plane strain conditions), and III. Define a local frame $\vec{e}_i$ such that $\vec{e}_1$ is the local unit vector normal to the crack front along its direction of motion, $\vec{e}_3$ is the local unit vector tangent to the crack front and $\vec{e}_2=\vec{e}_3\wedge\vec{e}_1$ (see Fig. 1). In the vicinity of each point of the crack front, the universal part of the stress and displacement velocity elastic fields are well known to be [8]

$$p_{ij}(r,\theta,t)=\sum_l \frac{K_l(L,t)}{\sqrt{2\pi r}}P^l_{ij}(\theta,V), \tag{23}$$

$$v_i(r,\theta,t)=\sum_l \frac{VK_l(L,t)}{\mu\sqrt{2\pi r}}V^l_i(\theta,V), \tag{24}$$

with (r,θ) polar coordinates in the plane $(\vec{e}_1,\vec{e}_2)$ based on the crack front at the position L. $V=V_\perp(L,t)$ is the local instantaneous velocity of the crack front, normal to itself. $K_l(l,t)$ (l=I, II, and III) are the stress intensity factors corresponding to the three possible modes of local loading. $P^l_{ij}(\theta,V)$ and $V^l_i(\theta,V)$ are universal angular functions independent of the specific loading conditions and geometry.

As already mentioned, the evaluation of the rate of energy flow $\mathcal{F}$ and the forces F_i is path independent, as long as the path is close to the crack front. Thus, in Eqs. (15) and (16) we chose the curve C as a circle of small radius around the moving crack tip, such that the asymptotic values (23) and (24) hold. Using these values together with the definition (10) yields

$$\frac{1}{V}\mathcal{F}(L,t)\equiv G(L,t)=F_1(L,t), \tag{25}$$

$$F_1(L,t)=\frac{1}{2\mu}[A_I(V)K_I^2+A_{II}(V)K_{II}^2+A_{III}(V)K_{III}^2], \tag{26}$$

$$F_2(L,t)=-\frac{1}{2\mu}B(V)K_IK_{II}, \tag{27}$$

$$F_3(L,t)=0, \tag{28}$$

where μ is the elastic shear modulus. G is the *dynamic energy release rate* per unit length of the crack front [8], and

$$A_I(V)=\frac{a(1-b^2)}{D(V)}, \tag{29}$$

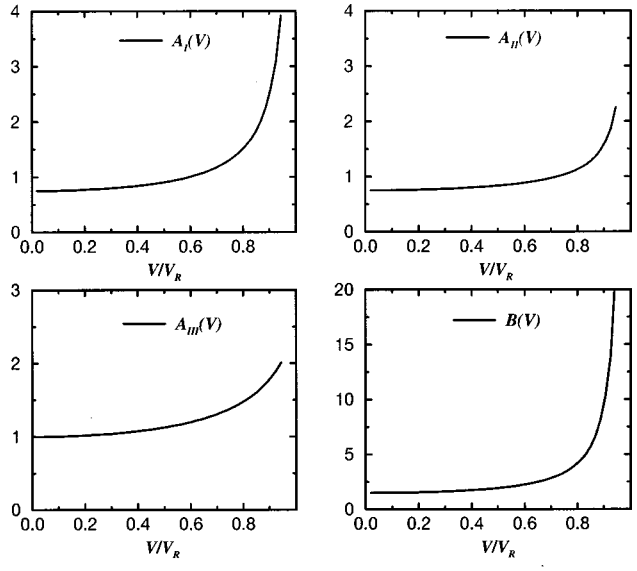

FIG. 3. Universal functions $A_i(V)$ (i=I, II, and III) and $B(V)$, given by Eqs. (29)–(32), plotted as a function of V/V_R for $C_d=\sqrt{3}C_s$.

$$A_{II}(V)=\frac{b(1-b^2)}{D(V)}, \tag{30}$$

$$A_{III}(V)=\frac{1}{b}, \tag{31}$$

$$B(V)=\frac{4ab(1-b^4)(a-b)}{D(V)^2}, \tag{32}$$

with $a(V)\equiv\sqrt{1-V^2/C_d^2}$, $b(V)\equiv\sqrt{1-V^2/C_s^2}$, and $D(V)\equiv 4ab-(1+b^2)^2$. C_d and C_s are the longitudinal and shear sound velocities, respectively. Note that the Rayleigh velocity of surface waves, V_R, is a solution of $D(V_R)=0$. The functions $A_i(V)$ and $B(V)$ are also universal in the sense that they do not depend on the details of the applied loading or the configuration of the body being analyzed. They do depend on the local *instantaneous* speed normal to the crack front and on the properties of the material. For low velocities, $V\to 0$, they have the behaviors

$$A_{I,II}\to(2(1-C_s^2/C_d^2))^{-1},\quad B\to(1-C_s^2/C_d^2)^{-1},\quad A_{III}\to 1, \tag{33}$$

while for high velocities they diverge:

$$A_{I,II}\sim(V_R-V)^{-1},\quad B\sim(V_R-V)^{-2} \tag{34}$$

when $V\to V_R$, and

$$A_{III}\sim(C_s-V)^{-1} \tag{35}$$

when $V\to C_s$. These functions are plotted in Fig. 3.

Equation (26) for $F_1(L,t)$ reproduces the result of Eq. (22): $\vec{V}\cdot\vec{F}=VF_1=\mathcal{F}$. This result gives a physical interpretation to the material force in the direction of motion of the crack front: it is the component of the force that does work [23,26,30], with the energy needed for that work being supplied by the elastic energy flow into the crack tip. This rela-

tion is well known. Expressions (27) and (28) for the forces F_2 and F_3 however, do not appear to have received much attention in the literature. They are the components of the elastic force perpendicular to the direction of motion, and they do no work. However, they can certainly influence the dynamics of the crack front. Equation (28) shows that there are no tangential forces to the crack edge, i.e., $F_3=0$, a result to be expected in a system that has local two dimensional behavior.

Equation. (27) shows that F_2 depends on the product $K_I K_{II}$ only. This suggests that if an instability mechanism for crack dynamics exists, it will be primarily two dimensional. This is not surprising in view of our assumption of local two dimensionality near the crack tip, and is consistent with the available numerical and experimental evidence. It is important to recall that $\mathcal{F}$ and $\vec{F}$ have been evaluated for a *smooth* crack front $\vec{R}(L,t)$ that propagates at a *smooth* velocity $\vec{V}(L,t)=\partial\vec{R}(L,t)/\partial t$, and also that the curvature of the crack front cannot be very large.

Since $F_2\neq 0$ if $K_{II}\neq 0$, the direction of the material force acting on the crack front is not necessarily parallel to the direction of crack propagation. The orientation of this force, $\phi(L,t)$, with respect to the normal to the crack front, $\vec{e}_1$ is given by

$$\tan\phi(L,t)\equiv\frac{F_2}{F_1}=-2C(V)\frac{q}{1+p^2+\frac{a}{b}q^2}, \tag{36}$$

where

$$q\equiv\frac{b}{a}\frac{K_{II}}{K_I}, \tag{37}$$

$$p\equiv\sqrt{\frac{A_{III}}{A_I}}\frac{K_{III}}{K_I}, \tag{38}$$

$$C(V)=\frac{2a(1+b^2)(a-b)}{D(V)}. \tag{39}$$

The function $C(V)$ is also universal in the sense that it depends on the local *instantaneous* speed normal to the crack front and on the properties of the material only (see Fig. 4). Its asymptotic behavior is given by

$$C\to 1 \text{ when } V\to 0,\quad C\sim(V_R-V)^{-1} \text{ when } V\to V_R. \tag{40}$$

On the other hand, $\tan\phi$ is an odd function of q. It vanishes when $q\to\pm\infty$, and it has extrema at $q=\pm\sqrt{(1+p^2)b/a}$.

In the study of crack growth processes in materials which fail in a purely brittle manner, the most commonly used crack growth criterion is the generalization of Griffith's critical energy release rate criterion [8,20]. According to the generalized Griffith criterion, the crack must grow in such a way that G is always equal to a newly defined quantity: the dynamic fracture energy of the material, Γ. The growth criterion is [8]

$$G=\Gamma. \tag{41}$$

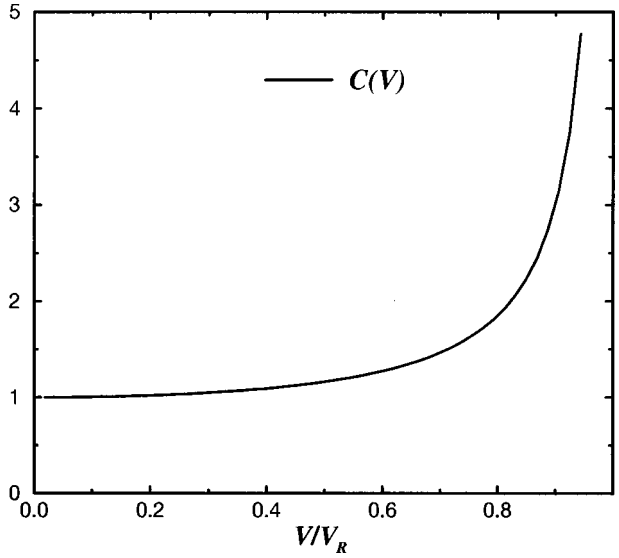

FIG. 4. Universal function $C(V)$, given by Eq. (39), plotted as a function of V/V_R for $C_d=\sqrt{3}C_s$.

This relation is called an equation of motion for the crack front. The energy release rate G is a property of the local mechanical fields. The dynamic fracture energy Γ, on the other hand, represents the resistance of the material to crack advance; it is assumed to be a property of the material determined by the energy needed to create new crack surface, including whatever nonlinear microscopic processes take place very near the crack tip. Its value can be determined only through laboratory measurements, or, eventually, by way of microscopic models.

On the other hand, Eqs. (25) and (26) show that the energy release rate G is equivalent, in Eshelby's approach, to a force per unit length of the crack front. Equation (41) can be reinterpreted as a balance between the component F_1 of the material force along the direction of motion, and a resistance force to crack advance per unit length of the crack front: $F_1=\Gamma$. As stated in Sec. I, one equation of motion is not enough to determine the trajectory of a crack that is allowed to deviate from straight line motion. A popular additional requirement to determine a crack trajectory in two dimensions is the principle of local symmetry [21,22]:

$$K_{II}=0 \quad\Leftrightarrow\quad (\text{smooth crack propagation}); \tag{42}$$

that is, that propagation without branching occurs in such a way as to keep a purely opening mode at the crack tip. This principle has been essentially developed for quasistatic regimes [22] (see also Ref. [33] for a discussion), although it has also been used in the dynamic case [34].

The fact that the usual energy criterion used to determine crack evolution can be interpreted as one component of a balance of forces suggests a different approach: Why not use a balance of forces criterion for all three components? This would give the requisite number of equations needed to determine the evolution of a crack front. In Sec. V, we shall develop this idea, in which the principle of local symmetry is not assumed to hold *a priori*.

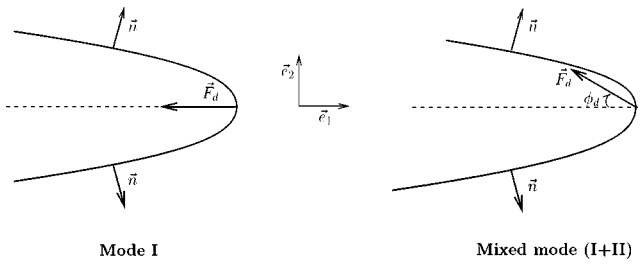

FIG. 5. A simple model of the ''shape'' of newly created surface in the vicinity of the crack tip and the associated forces of surface tension. Pure tension gives a symmetric opening. Mixed mode loading breaks this symmetry.

V. A MODEL FOR AN EQUATION OF MOTION OF THE CRACK FRONT

So far, we have determined the material forces [Eqs. (26), (27), and (28)] acting on the crack front. In order to write down an equation of motion, we will assume that these material forces are exactly balanced by dissipative forces of microscopic origin acting within the crack front region. These new forces represent the resistance of the material to crack advance. Our task is now to advance a model for these forces that will allow mathematical analysis to be performed.

Here we introduce a simple two-dimensional model of what happens within the crack front region in order to obtain some insight into the physics of the forces acting at the crack front. Our purpose is to obtain qualitative understanding, and not necessarily to provide an accurate picture of the microphysics near the crack tip. Suppose that the crack tip, even at very small scales, can be described by a continuous curve Σ of high curvature (see Fig. 5). In reality, this surface is not well defined. We assume, nevertheless, there exists an energy U associated with the creation of *curved* surface at the crack front. That is,

$$U=\gamma\int_{\Sigma}dS, \tag{43}$$

with dS an element of crack surface and γ a surface tension that will be assumed constant for simplicity. This means that U is proportional to the amount of new surface created, a reasoning that is closely analogous to the original approach of Griffith [20], who associated the energy released during crack growth to the energy required to create a unit of new surface area. If the surface of the crack is changed by displacing each element by an amount $\delta\vec{X}$, the change in the surface energy U of Eq. (43) is

$$\delta U=-\gamma\int_{\Sigma}dS\frac{\hat{n}\cdot\delta\vec{X}}{R}, \tag{44}$$

where $\hat{n}$ is the unit vector normal to the surface that points into the material, and R is the radius of curvature at each point of the original surface (it is negative if the curvature is measured with respect to a point outside the material). This allows us to identify

$$\vec{F}_d=\gamma\int_{\Sigma}dS\frac{\vec{n}}{R} \tag{45}$$

as the force originating from surface tension, that would balance the material forces in this simple model.

The implication of this simple model for mode I loading is (see Fig. 5) that the contribution to the resistance force of the upward and downward surfaces near the tip are symmetric, and thus

$$\vec{F}_d\simeq-\gamma\int_{-\theta_0}^{\theta_0}d\theta(\cos\theta\vec{e}_1+\sin\theta\vec{e}_2)=-\Gamma\vec{e}_1, \tag{46}$$

where θ is the angle between the normal to the surface and the direction $\vec{e}_1$. In Eq. (46), we have used the equality $dS=Rd\theta$. The magnitude of the dissipative force F_d is adjusted to the value already mentioned in Eq. (41), with $\Gamma\simeq 2\gamma\sin\theta_0$ and, for symmetry reasons, it points along the direction of motion.

In the presence of mode II loading, reflection symmetry with respect to the direction of motion is broken. We write then the resistance force in the mixed mode case as

$$\begin{aligned}\vec{F}_d&\simeq-\gamma\int_{-\theta_0+\phi_d}^{\theta_0+\phi_d}d\theta(\cos\theta\vec{e}_1+\sin\theta\vec{e}_2)\\&=-\Gamma(\cos\phi_d\vec{e}_1+\sin\phi_d\vec{e}_2),\end{aligned} \tag{47}$$

with ϕ_d an angle yet to be modeled. This angle takes into account the asymmetric contributions to the resistance force of the upward and downward surfaces near the tip. The direction of resistance forces is not necessarily parallel to the direction of motion. The general idea of this simple model is that the curvature created will adjust itself so as to balance the material forces acting at the tip. This hypothesis of existence of a perpendicular resistance force is reminiscent of the approaches used to generalize cohesive zone models in the presence of shear [13], or to model fracture energy of interface cracks [35].

From now on, leaving aside the specifics of the simple model just presented, we will assume that these resistance balancing forces do exist, and that they have the form suggested by Eq. (47):

$$\vec{F}_d=-\Gamma(\cos\phi_d\vec{e}_1+\sin\phi_d\vec{e}_2). \tag{48}$$

Also, we assume that the angle ϕ_d, that defines the direction of the resistance force, is a function of q, or K_{II}/K_I, the relative amount of local shear with respect to local tensile loading, and of crack velocity V, which are parameters of the forcing. For an isotropic body, it is clear that ϕ_d should be an odd function of K_{II} in order to respect the symmetry of mode II. Therefore, without loss of generality, the tangent of the angle of the crack tip force will be written as

$$\tan\phi_d=-2\alpha(V)q\psi(q,V), \tag{49}$$

where $\psi(q,V)$ is an undetermined even function of q, and $\psi(0,V)=1$. When K_{II} is small compared to K_I we can expand the function ψ for small q:

$$\psi(q,V)=1+\beta(V)q^2+\cdots. \tag{50}$$

We will assume $\beta(V)\geqslant 0$ for reasons to be explained in Sec. VI. Furthermore, $\tan\phi_d$ has been written in a suggestive

form, introducing a velocity dependent factor $\alpha(V)$ that is a local measure, at the crack front, of the competition between shear and opening, and it should be related to the micromechanics at the crack tip. The precise nature of this relation, however, is outside the scope of the present work.

A simple estimate of the order of magnitude of the parameter $\alpha(V)$ can be obtained in the quasistatic limit, by comparison with a crack having a kink. In this case evaluating Eq. (36) for $V=0$ shows that the orientation of the material force with respect to the normal to the crack front becomes $\phi \approx -2q$ for $q \ll 1$. On the other hand, in the presence of mode II loading, the principle of local symmetry (42) implies that a crack that is at a critical value of incipient growth will branch locally in a direction ϕ_B that satisfies a pure opening mode at the crack tip. When $q \ll 1$, this direction is also given by $\phi_B \approx -2q$ [33]. We take this fact as an indication that, for small velocities we shall also have $\phi_d \approx -2q$, so that

$$\alpha(0) \approx 1. \tag{51}$$

On this basis we shall take $\alpha(V)$ to be a positive function of V and of order one at low velocities.

Finally, Eqs. (26), (27), and (48) allow us to write down a set of two dynamic equations of motion on the following basis: since the usual Griffith criterion [Eq. (41)] can be interpreted as a balance of one component of the forces acting at the crack tip, we extend this requirement to hold for *both* force components: elastodynamic force must be exactly balanced by dissipative force at the crack front. That is,

$$\tan \phi_d = \tan \phi = -2C(V) \frac{q}{1+p^2+\frac{a}{b}q^2}, \tag{52}$$

$$\Gamma \cos \phi_d = F_1 = \frac{1}{2\mu}\left(1+p^2+\frac{a}{b}q^2\right) A_I(V) K_I^2. \tag{53}$$

Our assumption, implicit in Eq. (49), that material parameters depend on velocity but not on higher order time derivatives of crack tip position, implies that the crack tip has no inertia.

VI. SOLUTIONS TO THE EQUATION OF MOTION

In this section we consider the case $K_{III}=0$, i.e., $p=0$. The case $p \neq 0$ will be discussed qualitatively in Sec. VII.

If we introduce Eq. (49) into Eq. (52), we obtain

$$-2\alpha(V) q \psi(q,V) = -2C(V) \frac{q}{1+\frac{a}{b}q^2}. \tag{54}$$

Equation (54) is a local equality between the angles of the material forces and the resistance forces with the direction of crack propagation. It can be solved for q, independently of the specific loading conditions and geometry. $q=0$ is always a solution to Eq. (54) (see Fig. 6). We will also assume that $\alpha(V)$ is a slowly varying function of V compared with the variation of $C(V)$. This allows the number of solutions of Eq. (54) to be determined by the magnitude of the slope of the right and left hand sides at $q=0$. These slopes are equal

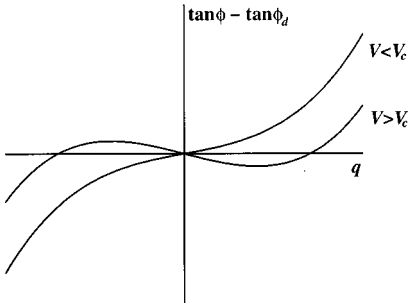

FIG. 6. Graphic solution of Eq. (54) for different values of V. The critical velocity V_c is determined by condition (55).

to $2\alpha(V)$ and $2C(V)$, respectively. Since $C(V)$ is an increasing function of velocity V with $C(0)=1$ (Fig. 4), the condition that slopes be equal at $q=0$ leads to the conclusion that, for $\alpha \geq 1$ and $\beta(V) \geq 0$ there exists a critical velocity V_c for which

$$C(V_c) = \alpha(V_c), \tag{55}$$

below which, i.e., for $V<V_c$, $K_{II}=0$ is the only solution to Eq. (54) while for $V>V_c$ there are three solutions, $K_{II}=0$ and $K_{II}=\pm g(V) K_I$ (Fig. 7),

$$V<V_c \Leftrightarrow \alpha(V)>C(V) \Leftrightarrow K_{II}=0, \tag{56}$$

$$V>V_c \Leftrightarrow \alpha(V)<C(V) \Leftrightarrow K_{II}=0, \quad K_{II}=\pm g(V) K_I. \tag{57}$$

The function $g(V)$ can be computed only if the function $\psi(q,V)$ is known. Even in the vicinity of V_c one needs to know the coefficient $\beta(V)$, in order to compute $g(V)$. However, it can be determined that for velocities V just above V_c, the function $g(V)$ behaves as $(V/V_c-1)^{1/2}$. This results from solving Eq. (54), with both sides written to order q^3. As seen in Fig. 7, the velocity V acts as a bifurcation parameter at $V=V_c$ for the solutions of Eq. (54) as a function of q, or K_{II}/K_I. As V grows over V_c, the new solutions with $K_{II} \neq 0$ are increasing functions of V, away from $K_{II}=0$ at $V=V_c$. This is a signature of a second order transition. If $\alpha(V)<1$, there would always exist three solutions to our equation [since $C(V) \geq 1$], and the above transition would be absent. Notice also that the critical velocity V_c always satisfies $V_c<V_R$, since $C(V) \to \infty$ as $V \to V_R$.

Given different solutions to the equation of motion for $V>V_c$, the question arises of what is the selection mechanism that will decide which possibility will be chosen by a

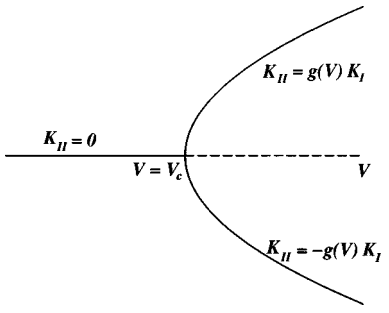

FIG. 7. Schematic phase diagram of the solutions $K_{II}(V)$ of Eq. (54), showing the second order transition.

traveling crack. Consider a first configuration of *smooth* crack propagation at an instantaneous velocity $V>V_c$, with stress intensity factors $K_I\neq 0$ and $K_{II}=0$. From Eqs. (25), (52), and (53), the rate of energy flow needed for the propagation of this crack is

$$\mathcal{F}=V\Gamma. \tag{58}$$

Consider a second configuration of *smooth* crack propagation with the same instantaneous velocity V, but with stress intensity factors satisfying $K_I\neq 0$ and $K_{II}=\pm g(V)K_I$. From Eqs. (25) and (53), the rate of energy flow needed for the propagation of this crack is

$$\mathcal{F}'=V\Gamma\cos\phi_d. \tag{59}$$

Clearly, $\mathcal{F}'\leqslant\mathcal{F}$: the material response to external loading provides less energy per unit time for the second configuration than for the first one. Above the critical velocity, the crack needs more energy to advance in a configuration at the state $K_{II}=0$ with a velocity V than in the one at the state $K_{II}\neq 0$ with the same velocity V. Therefore, above V_c, the crack propagation selects one of the solutions $K_{II}=\pm g(V)K_I$, instead of the solution $K_{II}=0$. Consequently, when the crack tip velocity is below V_c, the crack propagation satisfies the principle of local symmetry [Eq. (42)]. However, for $V>V_c$, this principle no longer holds, and the crack propagation with a pure opening mode at the tip becomes unstable with respect to solutions satisfying $K_{II}=\pm g(V)K_I$ (see Fig. 7).

To summarize, we have shown that, subject to conditions explained in detail above, there is a critical velocity at which the dynamics of a crack undergoes a transition from being determined by $K_{II}=0$ to being determined by $K_{II}\neq 0$. The trajectory itself, however, remains smooth with smoothly turning tangents. Note that nowhere in the last two sections have we made any assumption concerning a possible dependence of the fracture energy of the material Γ upon velocity.

VII. SCENARIO RELATED TO EXPERIMENTAL RESULTS

In this section we use our model to attempt an explanation of some features of the experimental results in fast fracture under mode I loading of thin plates of glass and plexiglass [1–5]. These experiments show a dynamic instability at a critical velocity that is about a third of the Rayleigh velocity of the material. This instability is associated with the roughening of the crack surfaces, the appearance of microcracks, crack tip velocity oscillations, and strong acoustic emissions. We wish to explore the consequences of identifying the critical velocity V_c of our model with the experimental critical velocity. Using $C_d\approx\sqrt{3}C_s$, and from Eqs. (39) and (55), this value can be obtained with $\alpha(V_c)\approx 1.073$, which is a reasonable value according to the estimates of Sec. V.

A. Low velocities, $V<V_c$

In this case, the only possible solution is $K_{II}=0$. From Eq. (53), and assuming $K_{III}=0$, one recovers the well known equation of motion [8]

$$\frac{1}{2\mu}A_I(V)K_I^2=\Gamma, \tag{60}$$

which determines the crack tip velocity. The result $K_{II}=0$ means that the crack will propagate following a smooth path, with a pure opening mode at the tip. This is the statement of the principle of local symmetry [Eq. (42)]. Our approach can be regarded as a derivation and an extension of this principle to nonzero velocities $V<V_c$.

This solution corresponds then to the experimentally observed mirror region, where the crack propagation follows a straight path. For a crack under uniaxial loading, this corresponds to the direction that satisfies $K_{II}=0$ during the crack propagation. Since this path appears to be stable, we expect that small perturbations away from this straight line propagation will be damped away [36].

B. High velocities, $V>V_c$

As the velocity of the crack surpasses V_c, the propagation satisfying $K_{II}=0$ at the crack tip becomes unstable. The crack now propagates in one of the two new directions satisfying $K_{II}=\pm g(V)K_I$. It is important to notice that the allowed values of K_{II}/K_I grow continuously with V from 0 at $V=V_c$, and that these new solutions correspond to *smooth* crack propagation.

Experiments show that at velocities higher than a critical value the surface left behind after rupture becomes rough, and microcracks appear. As we have noted, an experiment carried out in pure tension leads to a straight path in the case $K_{II}=0$. The solution $K_{II}=\pm g(V)K_I\neq 0$ means then that the trajectory of the crack tip will deviate from a straight line. Smooth crack propagation with $K_{II}\neq 0$ explains the observed appearance of microcracks, because on the crack faces the stress components p_{22} and p_{12} vanish identically. However, in the presence of a shear mode at the crack tip, it is seen from Eq. (23) that the near field asymptotic stress p_{11} at the moving crack tip is singular on the crack faces [8]:

$$p_{11}(r,\pm\pi)\sim\mp K_{II}/\sqrt{r}. \tag{61}$$

This means that there is a high tensile stress near the tip that, if given the chance, will tend to open microcracks on one of the crack faces in a direction that is initially perpendicular to the direction of motion of the main crack. Small perturbations may thus initiate microcracks that will start perpendicularly to the main crack, and later on will deviate into a direction closer to the direction of motion of the main crack, in order to avoid the unloaded region which is left behind the crack tip. Also, the formation of these microcracks may tend to slow down the main crack due to the expenditure of energy on surface creation [4]. As this happens the ratio K_{II}/K_I will decrease, leading to a trajectory change back toward the initial crack trajectory. This may be the reason for the appearance of bumps on the crack surfaces (see Fig. 8). This description of the microbranching process does not require any discontinuity in the velocity of the main crack.

C. Presence of a mode III

Equations (49) and (52) suggest that the presence of nonvanishing mode III loading may be taken into account within

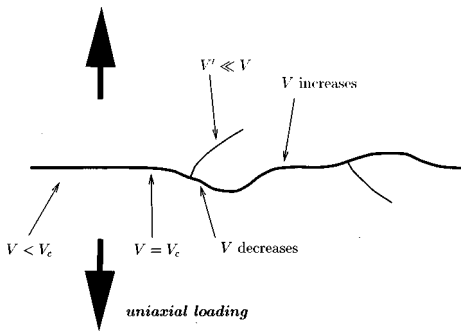

FIG. 8. Scenario for the trajectory of a crack submitted to uniaxial loading. At low velocities there is straight line propagation (mirror zone). Above the critical velocity the trajectory deviates from a straight line. $K_{II} \neq 0$ allows for microcracks to sprout behind the advancing crack tip. Their energy expenditure slows down the main crack, possibly below the critical velocity. This would reorient the crack back to straight line propagation.

the $K_{III}=0$ arguments simply by replacing the parameter α by a modified ''effective'' value α_{eff},

$$\alpha_{\text{eff}}(V)=(1+p^2)\alpha(V), \tag{62}$$

that will now determine the value of the critical velocity. Thus the presence of an out of plane mode has a stabilizing effect, in the sense that the value of the critical velocity V_c for the instability to appear is increased. In other words, the instability will appear first at points on the crack front where K_{III} vanishes. This provides a rationale to understand the experimental fact [4] that microcracks first appear near the edges of the plate. Indeed, we do expect the crack front to deviate from a straight line perpendicular to both faces of the plate. Consequently, in general, we shall have $K_{III} \neq 0$ *except* near the faces of the plate where the condition $K_{III}=0$ will be enforced by the free surface condition $p_{ij}n_j=0$. Therefore, the minimal value of α_{eff} will be at the faces of the plate, and that is where the instability will start. As the mean crack velocity increases, the roughness and microbranches increase, because more and more points on the crack front reach the critical velocity. This explains why roughness and microcrack penetration increases with increasing velocity [4].

VIII. CONCLUSION

We have developed an approach to crack dynamics based on the balance of energy and field momentum for a moving crack in three dimensions [26,30]. We have derived the energy flow rate into the crack front and the configurational forces acting on it. The components of the material force at the crack front have been computed in the framework of the linear isotropic elastodynamic model. It has been found that the orientation of this force is not necessarily in the direction of crack propagation. Within a Griffith-like approach, we have defined a generalized dissipative force at the crack front. Assuming that this dissipative force exactly balances the material force at the crack front, we derived a vector equation of motion for the crack front. Under minimal assumptions, we have shown that there exists a critical velocity below which a crack propagates in a direction that keeps a pure opening mode at the tip. At the critical velocity there is a second order dynamic instability, and above the critical velocity the crack growth with a pure opening mode at the tip becomes unstable with respect to two new possible solutions. Various experimental manifestations have been described qualitatively under the light of this model.

Our approach is universal in the sense that the instability mechanism we have presented is local at the crack tip, and it is independent of the specific loading configuration and the geometry of the experiment. It will hold for any isotropic elastic material. Throughout the analysis, it has not been specified that the configuration of the pure opening mode of the crack tip has to be a straight path. Such a configuration could be a curved path, but the instability we have discussed would still occur. The instability mechanism originates in a balance between forces of elastic origin and material dissipative forces of microscopic origin which have been modeled. A detailed microscopic justification of this modeling suggests itself as an interesting avenue for future research.

ACKNOWLEDGMENTS

M.A.-B. is grateful to Professor J.R. Rice for helpful discussions and critical comments. R.A. and F.L. gratefully acknowledge the support of a Cátedra Presidencial en Ciencias. This collaboration was made possible by a grant from CNRS, Conicyt, and Fondecyt Grant No. 1960892. Laboratoire de Physique Statistique is associated with the CNRS (UMR 8550) and Universities Paris VI and Paris VII.

[1] J. Fineberg, S.P. Gross, M. Marder, and H.L. Swinney, Phys. Rev. Lett. **67**, 457 (1991); Phys. Rev. B **45**, 5146 (1992).
[2] S.P. Gross, J. Fineberg, M. Marder, W.D. McCormick, and H.L. Swinney, Phys. Rev. Lett. **71**, 3162 (1993).
[3] E. Sharon, S.P. Gross, and J. Fineberg, Phys. Rev. Lett. **74**, 5096 (1995); **76**, 2117 (1996).
[4] E. Sharon and J. Fineberg, Phys. Rev. B **54**, 7128 (1996).
[5] J.F. Boudet, S. Ciliberto, and V. Steinberg, Europhys. Lett. **30**, 337 (1995); J. Phys. II **6**, 1493 (1996).
[6] K. Ravi-Chandar and B. Yang, J. Mech. Phys. Solids **45**, 535 (1997).
[7] J.F. Boudet and S. Ciliberto, Phys. Rev. Lett. **80**, 341 (1998).
[8] L.B. Freund, *Dynamic Fracture Mechanics* (Cambridge University Press, Cambridge, 1990).
[9] W.G. Knauss and K. Ravi-Chandar, Int. J. Fract. **27**, 127 (1985).
[10] J. R. Rice, Y. Ben-Zion, and K.-S. Kim, J. Mech. Phys. Solids **42**, 813 (1994).
[11] F. Lund, Phys. Rev. Lett. **76**, 2742 (1996).
[12] H. Gao, J. Mech. Phys. Solids **41**, 457 (1993); **44**, 1453 (1996); Philos. Mag. Lett. **76**, 307 (1997).
[13] E.S.C. Ching, J.S. Langer, and H. Nakanishi, Phys. Rev. E **53**, 2864 (1996).
[14] J.S. Langer and A.E. Lobkowsky, J. Mech. Phys. Solids **46**, 1521 (1998).
[15] M. Marder and S.P. Gross, J. Mech. Phys. Solids **43**, 1 (1995).
[16] X.P. Xu and A. Needleman, J. Mech. Phys. Solids **42**, 1397 (1994).

[17] F.F. Abraham, D. Brodbeck, R.A. Rafey, and W.E. Rudge, Phys. Rev. Lett. **73**, 272 (1994).
[18] S.J. Zhou, P.S. Lomdahl, R. Thomson, and B.L. Holian, Phys. Rev. Lett. **76**, 2318 (1996).
[19] P. Gumbsch, S.J. Zhou, and B.L. Holian, Phys. Rev. B **55**, 3445 (1997).
[20] A.A. Griffith, Philos. Trans. R. Soc. London, Ser. A **221**, 163 (1920).
[21] R.V. Gol'dstein and R.L. Salganik, Int. J. Fract. **10**, 507 (1974).
[22] M. Amestoy and J.B. Leblond, C. R. Acad. Sci., Ser. II: Mec. Phys., Chim., Sci. Terre Univers **301**, 969 (1985).
[23] J.R. Rice, J. Appl. Mech. **35**, 379 (1968).
[24] B.V. Kostrov and L.V. Nitkin, Arch. Mech. Stosow. **22**, 749 (1970).
[25] J.D. Eshelby, Philos. Mag. **42**, 1401 (1951).
[26] J.D. Eshelby, in *Inelastic Behavior of Solids*, edited by M. F. Kanninen, W.F. Adler, A.R. Rosenfield, and R.I. Jaffee (McGraw-Hill, New York, 1970), p. 77.
[27] M.E. Gurtin and P. Podio-Guidugli, J. Mech. Phys. Solids **44**, 905 (1996); **46**, 1343 (1998).
[28] M.E. Gurtin and M.M. Shvartsman, J. Elast. **48**, 167 (1997).
[29] M. Adda-Bedia, R. Arias, M. Ben Amar, and F. Lund, Phys. Rev. Lett. **82**, 2314 (1999).
[30] G.A. Maugin, Acta Mech. **105**, 33 (1994).
[31] We have, however, considered curves C, whose end points coincide, i.e., they are on exactly opposite sides of the crack surface. The question naturally arises as to what happens if this is not the case. This is a subtle question. Let the length of the curve be of order ϵ, a quantity small compared to any length scale relevant to the problem such as crack length or acoustic wavelength. For a smooth curve, ϵ will also be the order of magnitude of the distance between points on the curve and crack tip. Now let δ be the nonzero distance, measured along the crack surface, between the beginning and end of C. If δ is of order smaller than order ϵ, the contribution from this extra surface vanishes, and the independence of Eqs. (15) and (16) from the integration path still holds. If δ is of order ϵ or larger, it does not. What this means is that the dynamical variable whose equation of motion we are trying to find is actually a small region enclosed within a smooth boundary that encircles the crack tip, whose end points are not very far from each other. This is our operational definition of ''crack tip.''
[32] R. Dmowska and J.R. Rice, in *Continuum Theories in Solid Earth Physics*, edited by R. Teisseyre, Physics and Evolution of the Earth's Interior Vol. 3 (Elsevier, Amsterdam, 1986), p. 187.
[33] B. Cotterell and J. Rice, Int. J. Fract. **16**, 155 (1980).
[34] M. Adda-Bedia, M. Ben Amar, and Y. Pomeau, Phys. Rev. E **54**, 5774 (1996).
[35] A.G. Evans, M. Rühle, B.J. Dalgleish, and P.G. Charalambides, Mater. Sci. Eng., A **126**, 53 (1990).
[36] For a discussion of the stability of straight line crack motion within the context of thermal fracture, see M. Adda-Bedia and Y. Pomeau, Phys. Rev. E **52**, 4105 (1995).

Fracture Spacing in Layered Materials

M. Adda-Bedia[1] and M. Ben Amar[1,2]

[1]*Laboratoire de Physique Statistique de l'Ecole Normale Supérieure, 24 rue Lhomond, 75231 Paris, France*
[2]*Department of Mechanical Engineering, Massachusetts Institute of Technology, 77 Massachusetts Avenue, Cambridge, Massachusetts 02139*

(Received 18 November 2000)

We perform an elastostatic analysis of a periodic array of cracks under constant loading. We give an analytical solution and show that there is a limitation to the fracture spacing, due to a transition from an opening to a compressive loading. For this configuration, the threshold of the fracture spacing depends on neither the applied strain nor the elastic parameters of the material. This result shows that, in the general case of layered materials, the physical mechanism that is responsible for the limitation in the density of fractures is related mainly to the geometry of the problem. This is in agreement with observations and with recent numerical results.

DOI: 10.1103/PhysRevLett.86.5703 PACS numbers: 46.50.+a, 62.20.Mk, 91.35.–x, 91.60.Ba

Parallel open mode brittle fractures, or joints, in layers are common structures in Nature (see Fig. 1). They are currently observed in the Earth's crust such as in sedimentary rocks [1]. They are also present in laminated engineering materials [2]. In most cases, it is observed that the ratio s of the crack spacing to the layer thickness cannot decrease below a certain threshold value [3], although the physical intuition suggests that the spacing should decrease with increasing applied loading. Indeed, since the joints are stopped by the neighboring layers, fracturing new joints would be the only way to dissipate the stored energy. Therefore, as the tension increases, it seems that there is no limitation to the density of cracks.

A recent finite element analysis has shown that there is a limitation to the density of fractures [4]. This threshold was explained by the change from an opening to a compressive mode at the middle of the spacing (at half the wavelength). So a new fracture cannot occur. This analysis is in agreement with other simulations and experiments on the permeability of joints in the geophysics literature [5]. However, these numerical treatments do not allow one to set the control parameters which fix the spacing bound. In the following, we propose an exact treatment of this crack problem in a model situation, where the different layers have the same elastic properties, which is also the case considered in the numerical simulations of [4]. We show the existence of the instability from tension to compression as the spacing decreases. Moreover, in our model the spacing threshold is of order 1, and does not depend on either the applied loading or the elastic parameters of the material layers. It turns out that this elastic instability is a generic feature which is related mainly to the geometry of the problem. This result suggests that for layered materials with different elastic properties, the physical mechanism that is responsible for the limitation to the density of fractures is purely geometrical. However, the spacing threshold in the general case will depend on the elastic mismatch parameters between the layers.

In our approach, we consider a material sample with an infinite array of parallel fractures equally separated by a distance λ. We choose half the wavelength as the length unit. The crack spacing s is then given by $1/a$, where $2a$ is the length of the cracks in dimensionless units (see Fig. 2). Fixing the ends of the fractures is a way to mimic the effect of the neighboring layers, since the observed cracks do not cross the neighboring interfaces. We assume that the sample is loaded in the y direction by an average strain ϵ_∞ which represents the tension supported by the layer. We perform a classical elastostatic analysis and show that the fracture spacing threshold does not depend on either the applied strain or the elastic parameters of the material, which are the Young modulus E and the Poisson ratio ν.

Under plane stress conditions, the two-dimensional strain tensor $\overline{\overline{\epsilon}}$ is related to the stress tensor $\overline{\overline{\sigma}}$ by

$$\sigma_{ij} = \frac{2}{1-\nu^2}[(1-\nu)\epsilon_{ij} + \nu\epsilon_{kk}\delta ij]. \qquad (1)$$

The plane strain configuration is recovered by a suitable change of the Poisson ratio. For convenience, all the quantities in Eq. (1) are dimensionless: $\overline{\overline{\sigma}}$ is scaled by

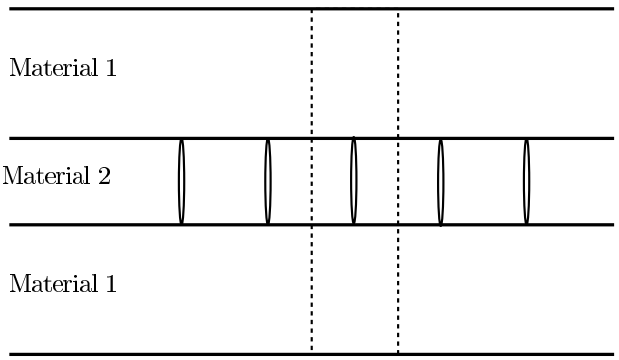

FIG. 1. Schematic representation of a layered system with a periodic array of cracks generated in the less compliant material. The dotted region represents the unit cell that will be studied.

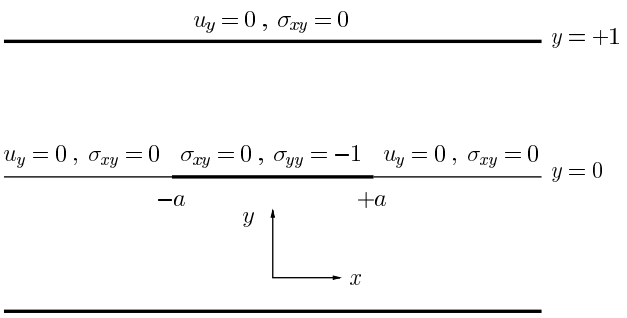

FIG. 2. Schematic representation of the elastostatic problem.

$E\epsilon_\infty/(1-\nu^2)$ and $\bar{\bar{\epsilon}}$ is scaled by $2\epsilon_\infty/(1-\nu^2)$. The body is loaded by means of a uniform remote tension of magnitude $\sigma_\infty = 1$. Since the cracks' faces are traction-free, it is convenient to superimpose this solution with the one where the cracks are subject to compressive stresses of the same magnitude. Moreover, due to the periodicity of the configuration, it is enough to solve the problem for the stress field in the region $0 \le y \le 1$.

The equilibrium equations in the absence of body force are given by

$$(1-\nu)\Delta u_i + (1+\nu)\frac{\partial^2 u_j}{\partial x_i \partial x_j} = 0\,, \tag{2}$$

where $\vec{u}$ is the displacement field. The boundary conditions for this problem are simply given by

$$\sigma_{xy}(x,1) = u_y(x,1) = 0\,, \tag{3}$$

$$\sigma_{xy}(x,0) = 0\,, \tag{4}$$

$$u_y(|x| > a, 0) = 0\,, \tag{5}$$

$$\sigma_{yy}(|x| < a, 0) = -1\,. \tag{6}$$

The conditions on the displacement and stress fields in Eq. (3) are imposed by the periodicity of the configuration, while Eqs. (4) and (5) are imposed by the symmetry of the opening mode loading. Finally, Eq. (6) comes from the fact that the total solution of the present problem has to satisfy traction-free boundary conditions on the cracks' faces. At this stage, the problem depends only on the Poisson ratio ν and on the dimensionless crack length a.

The strip geometry and the boundary conditions suggest the use of Fourier sine and cosine transforms [6]. Because of the symmetry of the problem one can write the displacement field in the form

$$u_x(x,y) = \sqrt{\frac{2}{\pi}}\int_0^\infty f(k,y)\sin kx\,dk\,, \tag{7}$$

$$u_y(x,y) = \sqrt{\frac{2}{\pi}}\int_0^\infty g(k,y)\cos kx\,dk\,. \tag{8}$$

Also, we define the Fourier transform of $\sigma_{yy}(x,y)$ by

$$\sigma_{yy}(x,y) = \sqrt{\frac{2}{\pi}}\int_0^\infty s(k,y)\cos kx\,dk\,. \tag{9}$$

The equations satisfied by the functions $f(k,y)$ and $g(k,y)$ are readily derived from Eq. (2)

$$(1-\nu)f'' - 2k^2 f - (1+\nu)kg' = 0\,, \tag{10}$$

$$2g'' - (1-\nu)k^2 g + (1+\nu)kf' = 0\,, \tag{11}$$

where the derivatives are with respect to y. After some algebraic manipulations, one finds that

$$\frac{f(k,y)}{g(k,0)} = \frac{1+\nu}{2}\left\{\left[ky - \frac{1-\nu}{1+\nu}\coth k + \frac{k}{\sinh^2 k}\right]\cosh ky + \left[\frac{1-\nu}{1+\nu} - ky\coth k\right]\sinh ky\right\}, \tag{12}$$

$$\frac{g(k,y)}{g(k,0)} = \frac{1+\nu}{2}\left\{\left[\frac{2}{1+\nu} + ky\coth k\right]\cosh ky - \left[ky + \frac{2}{1+\nu}\coth k + \frac{k}{\sinh^2 k}\right]\sinh ky\right\}. \tag{13}$$

Written under this form, one can verify that the functions $f(k,y)$ and $g(k,y)$ satisfy the bulk equations (10) and (11) and the boundary conditions (3) and (4). We also obtain, using Eq. (1),

$$\frac{s(k,y)}{g(k,0)} = -\frac{k}{2\sinh^2 k}[ky\cosh k(2-y) + k(2-y)\cosh ky + \sinh k(2-y) + \sinh ky]. \tag{14}$$

Note that $s(k,y)$, and thus $\sigma_{yy}(x,y)$, does not depend on the Poisson ratio. So it is completely independent of the material properties. In the following, the two main functions that will be manipulated are $s(k,0)$ and $s(k,1)$. They are easily calculated from Eq. (14):

$$s(k,0) = -[k + F(k)]g(k,0)\,, \tag{15}$$

$$s(k,1) = -G(k)g(k,0)\,, \tag{16}$$

where

$$F(k) = \frac{k}{\sinh^2 k}[k + e^{-k}\sinh k], \tag{17}$$

$$G(k) = \frac{k}{\sinh^2 k}[k\cosh k + \sinh k]. \tag{18}$$

Note that $\sigma_{yy}(x,1)$ is the key quantity of this problem, since the sign of $[1 + \sigma_{yy}(x,1)]$ indicates if the middle of the spacing between two fractures is under tension or compression. If it is under tension, one can expect nucleation

of a new fracture, which will be responsible for defining a new wavelength (half the previous one). However, if it is under compression, the breaking process stops and the elastic energy must be dissipated according to a different scenario. It is generally believed that this elastic energy is used for the opening of the preexisting cracks and induces a full compression of the horizontal layer in the y direction [5].

In order to solve the problem completely, the determination of the function $g(k,0)$ is needed. This is done by using the boundary conditions (5) and (6), which can be expressed as

$$\sqrt{\frac{2}{\pi}} \int_0^\infty g(k,0) \cos kx \, dk = 0, \qquad |x| > a\,, \tag{19}$$

$$\sqrt{\frac{2}{\pi}} \int_0^\infty [k + F(k)] g(k,0) \cos kx \, dk = 1, \qquad |x| < a\,. \tag{20}$$

This is a set of dual integral linear equations whose analytical solutions are not available. A compilation of known solutions of such equations can be found in [7]. The condition (19) is automatically satisfied if the function $g(k,0)$ is given by

$$g(k,0) = \sqrt{\frac{\pi}{2}} \int_0^a \Phi(t) J_0(kt) \, dt\,, \tag{21}$$

where J_0 is the Bessel function, and $\Phi(t)$ is a yet unknown function. Replacing $g(k,0)$ as given by Eq. (21) in Eq. (20) leads to an integral equation for Φ:

$$\frac{d}{dx} \int_0^x \frac{\Phi(t)}{\sqrt{x^2 - t^2}} \, dt + \int_0^a dt \, \Phi(t) \int_0^\infty dk \, F(k) J_0(kt) \cos kx = 1, \qquad |x| < a\,. \tag{22}$$

This equation can be simplified by using Abel inversion transforms [6]. One obtains a Freedholm integral equation for $\Phi(t)$, given by

$$\Phi(t) = t - t \int_0^a H(t,u) \Phi(u) \, du, \qquad 0 < t < a\,, \tag{23}$$

where

$$H(t,u) = \int_0^\infty F(k) J_0(kt) J_0(ku) \, dk\,. \tag{24}$$

Despite many attempts, we did not succeed in finding an analytical solution for Eq. (23). However, the numerical resolution of this integral equation is straighforward.

Once the integral equation is solved for each value of a, one can determine the displacement and stress fields at any location. As an example, one can calculate the stress intensity factor, which is a quantity of interest in the field of fracture mechanics. In this case, the dimensionless stress intensity factor K_I is given by [6]

$$K_I(a) = \sqrt{\frac{\pi}{a}} \, \Phi(a)\,. \tag{25}$$

Figure 3 shows the variation of the stress intensity factor as a function of the crack length a.

The quantity of interest in the present problem is $\sigma_{yy}(0,1)$, the stress at the middle spacing between two successive cracks. It is simply given by

$$\sigma_{yy}(0,1) = - \int_0^a dt \, \Phi(t) \int_0^\infty dk \, G(k) J_0(kt)\,. \tag{26}$$

The sign of $1 + \sigma_{yy}(0,1)$ determines whether there is a tensile or a compressive loading. It is clear that for $a = 0$,

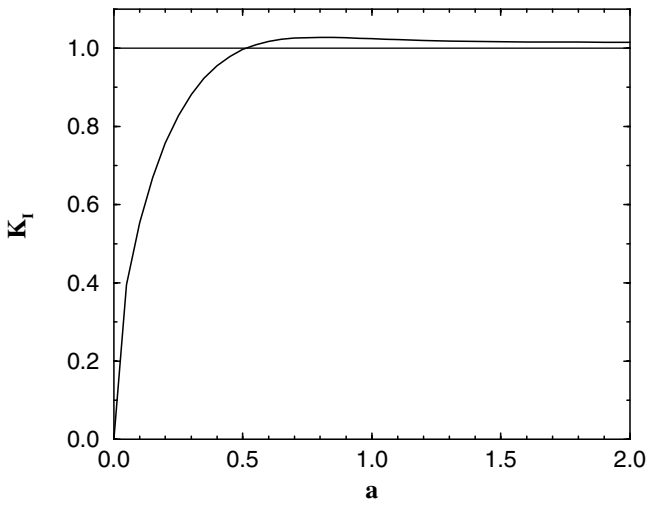

FIG. 3. The dimensionless stress intensity factor K_I as a function of the crack length a.

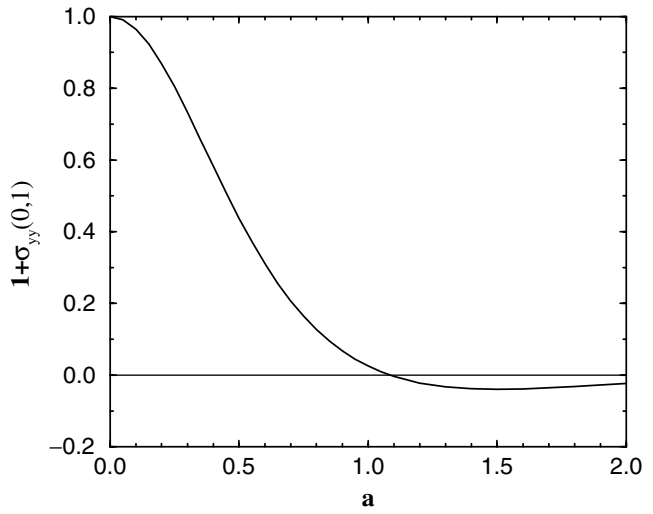

FIG. 4. The magnitude of the total stress at the point $x = 0$ and $y = 1$ as a function of the crack length a.

$\sigma_{yy}(0,1) = 0$ [see Eq. (26)], and for $a \gg 1$, the sample is completely broken, so one must have $1 + \sigma_{yy}(0,1) \rightarrow 0$. This behavior is in agreement with Fig. 4, which represents the total stress at the middle of the spacing as a function of the crack length a. Figure 4 also shows that at $a \approx 1$, or equivalently $s \approx 1$, the stress changes effectively from an opening to a compresssive mode, as has been found numerically for a particular case [4]. The transition point does not depend on any material parameter. This threshold does not even depend on the Poisson ratio in our model. This is an intrinisic instability which is due only to the geometry of the loading.

This simple model which can be solved exactly shows a well-known feature of fracture in layered materials. Our numerical value for the spacing applies for identical layers. The physical origin of the instability lies in the exchange of the elastic energy from fracturing to opening of the existing cracks. Note that introducing layers of different elastic constants will not modify the generic feature of the instability. Evidently, the spacing threshold will depend on the ratios of the elastic constants but the instability should always occur, since its origin lies in the geometry of the cracks' patterns.

[1] N. Narr and J. Suppe, J. Struct. Geol. **13**, 1037 (1991).
[2] A. Parvizi and J. E. Bailey, J. Mater. Sci. **13**, 2131 (1978).
[3] H. Wu and D. D. Pollard, J. Struct. Geol. **17**, 887 (1995).
[4] T. Bal, D. D. Pollard, and H. Gao, Nature (London) **403**, 753 (2000).
[5] L. N. Germanovich and D. K. Astakhov, "Fracture Closure in Extension and Stress Dependent Permeability" (to be published).
[6] I. N. Sneddon and R. P. Srivastav, Int. J. Eng. Sci. **9**, 479 (1971).
[7] B. N. Mandal and N. Mandal, *Advances in Dual Integral Equations* (Chapman and Hall, London, 1999).

Eur. Phys. J. B **28**, 135–138 (2002)
DOI: 10.1140/epjb/e2002-00211-1

THE EUROPEAN PHYSICAL JOURNAL B

The leaf venation as formed in a tensorial field

Y. Couder[1,a], L. Pauchard[2], C. Allain[2], M. Adda-Bedia[1], and S. Douady[1]

[1] Laboratoire de Physique Statistique[b], École Normale Supérieure, 24 rue Lhomond, 75231 Paris Cedex 05, France
[2] Laboratoire FAST[c], Campus Universitaire, 91405 Orsay Cedex, France

Received 11 March 2002
Published online 19 July 2002 –

Abstract. The veins of plant leaves exhibit a large variety of morphologies. They are often thought to result from their growth in a concentration scalar field. It is shown here that the topology of these patterns rather corresponds to what is expected from growth in a tensorial stress field. This is demonstrated by analogic experiments performed on crack formation in gel films where many characteristic venation patterns, of both dicotyledons and monocotyledons, were reproduced. This suggests, for the origin of the veins formation, a set of hypotheses which is new but supported by known physiological data.

PACS. 87.18.La Morphogenesis – 62.20.Mk Fatigue, brittleness, fracture, and cracks – 05.45.Df Fractals

Rapid Note

The spontaneous formation of patterns in nature corresponds to various types of breaking of symmetry of initially homogeneous systems. Very different processes can be reduced to a similar mathematical structure and lead to the formation of similar patterns. A large and widely studied family of patterns results from growth in various Laplacian or diffusive scalar fields [1] in such phenomena as *e.g.* viscous fingering, crystal growth, diffusion limited aggregation or landform erosion. Although the patterns produced have in each case some specificities, they all share the same characteristic topology: they are hierarchised *tree-like branched patterns*. Vein formation in plants is also assumed by the existing models [2–4] to be part of the same family of diffusive processes, (except for a simulation [5] based on a Turing type diffusion-reaction process). In these theories, a hormone is generated, diffuses through the tissues, inducing a local differentiation into veins which progressively canalise the flow [6]. The simulation of these models leads to complex branched patterns. An essential characteristics of these patterns is that the extremities of the branches are free: they never reconnect to form closed loops [7].

However, in reality, the leaf venations [8–10], in spite of the variety of their patterns, always present such reconnections as observed in the three examples shown in Figure 1. They are thus different from tree-like branched patterns and can be seen as variants of a different morphology, the *net-like structures* which are dominated by the systematic reconnections to form a reticulum. It can be noted that in mature leaves this morphology leads to a redundancy in the flow paths which is physiologically beneficial. There exists a physical archetype of patterns with a net-like structure: the 2D cracks patterns. Beautiful structures of this type can, for instance, be observed in the glazes of ceramics. In cracks, the origin of the formation of a reticulum is directly related to the tensorial nature of the stress field and can be easily explained. In a homogeneously 2D stretched medium (Fig. 2), the stress field is a tensor of rank 2. A first crack, propagating along the x-direction, relaxes the stress components σ_{yy} and σ_{xy}. But the stress parallel to the crack direction, σ_{xx}, is only weakly affected. Later, if a second crack grows in the vicinity of the first one, it will propagate so as to relax σ_{xx} and will thus collide at a right angle with the first fracture.

The first aim of the present letter is to show that the main morphologies of the leaf venation can be obtained [11] in crack growth experiments. We use variants of experiments (Allain *et al.* [12,13]) performed with concentrated colloidal suspensions of latex particles of diameter 0.1 μm in water (with volume fraction 0.50 and 0.25). These suspensions are deposited on a glass plate or on a silicon wafer and left to desiccate by evaporation, a process which is limited by diffusion of water into air [14]. The suspension first becomes a gel which then tends to shrink as it dries. It is prevented from doing so by the adhesive forces on the substrate. This growing mismatch results in stresses which are at the origin of the crack formation. For the sake of comparison with botanical patterns we explore the morphologies of these cracks with various boundaries and growth conditions.

The arrays of smaller veins of dicotyledons (Fig. 1a) form at a late stage when the leaf growth has become

[a] e-mail: couder@physique.ens.fr
[b] Associé au CNRS et aux Universités Paris VI et Paris VII
[c] Unité mixte de Recherche Paris VI, Paris XI et CNRS, bâtiment 502

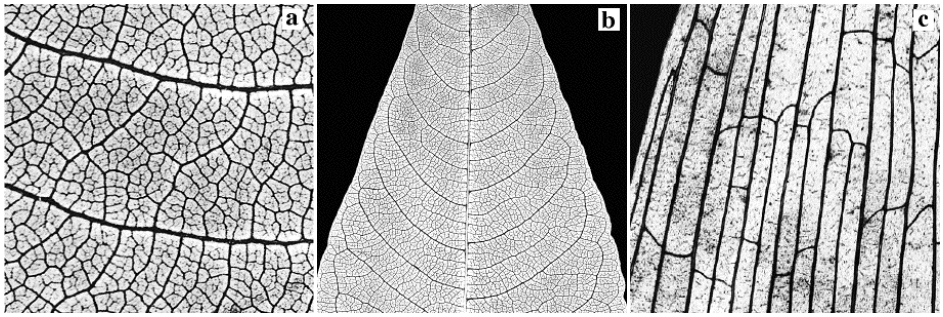

Fig. 1. Three examples of venation patterns. (a) The polygonal net-like structure of the small veins of a leaf of *Polygonum Polystachium*. (b) The secondary veins of *Polygonum Polystachium* are all connected to each other by loops located near the leaf margin. This is the 'brochidodromous' organisation [10]. (c) A detail of the venation of Lily of the valley, *Convallaria Maialis*, a monocotyledon.

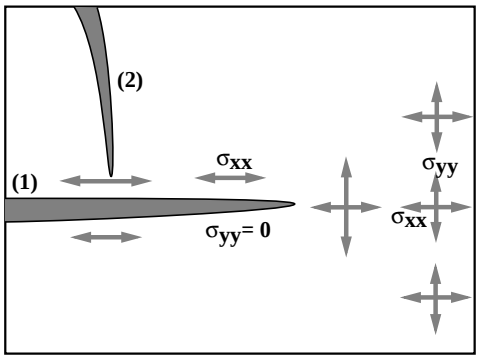

Fig. 2. Sketch of the growth of fractures in an initially homogeneously stretched medium. The reverse situation, of a compressed cellular medium, leads to the crushing of strips of material. The situation then corresponds to this sketch with all the stresses having the opposite directions.

homogeneous and isotropic [8,9,15]. They should thus be compared to crack patterns grown in homogeneous and isotropic conditions. Such patterns are obtained (Fig. 3a) in the drying of large and thin layers (of thickness $e \sim 10 - 100$ μm) far from the boundaries. Dynamically, the order of formation of the successive cracks is responsible for a hierarchy of structures, the first cracks to form being the longer. As new cracks keep forming, their length is limited because they grow in a domain limited by the older ones. They collide with them at right angle, forming an increasingly complex polygonal pattern with a typical spacing between cracks approximately equal to 4e. Both this hierarchical dynamics and the resulting topology of the patterns are the same for cracks and veins (see Fig. 3a and Fig. 1a). The only difference between the two patterns lies in the number of successive orders. During its growth a leaf expands by several order of magnitudes (*e.g.* from 0.1 mm to 100 mm) so that a much larger range of veins of successive order is generated than for a gel which shrinks only by approximately 10%. In the case of thin gel layers (≤ 10 μm), at the end of the pattern formation, when little elastic energy is left, the last cracks stop growing. Thus they fail to cross the polygons formed by their older neighbours and remain open ended (Fig. 3a). This is observed in leaves where the last veinlets remain open ended in the smallest areoles [8,9].

We can now focus on the organisation of the main veins (Fig. 1b). They are the first to form: the central (primary) vein when the leaf is still a peg-like shaped primordium, the secondary veins when the blade starts growing. In the most common organisation of dicotyledons, the main vein is axial and the secondary ones are pinnately organised. The main two archetypes are related to the morphology of the secondary veins. In the 'brochidodromous' organisation they form loops near the border (Fig. 1b) while in the 'craspedodromous' organisation they go straight to it.

These structures form in a tightly confined medium where the role of the boundaries is essential. We thus investigate the behaviour of cracks in confined media where they interact with boundaries. Our samples are now long and narrowing bands of suspension deposited on the glass plate. During drying, the meniscus bordering the deposited fluid is strongly pinned onto the substrate. The first fracture, longitudinal and centred, releases the transverse stress. Due to the remaining stress, transverse secondary cracks then form which can exhibit two behaviours. When the contact angle of the solution with the substrate is low ($\sim 25°$) the cracks which grow towards the border, rotate away from it. The resulting pattern is then formed of a series of loops due to the collision of each secondary crack with its neighbour. Comparison of Figure 3b with Figure 1b shows that we have thus obtained the brochidodromous organisation. The contact angle of our latex suspension can be modified by adding salt to the solution. Values up to $\sim 45°$ are thus obtained. In this case, the layer is thick near the meniscus and the fractures move straight to it, simulating the craspedodromous organisation.

These behaviours can be modelled by a simple 2D elastostatic model where the stresses in the strip, averaged throughout the thickness, are induced by the inhomogeneity of the concentration field. The differences between the small and large contact angles can be embedded in the boundary conditions. For small contact angles, the volume effect of the pinning is strong and induces a zero

Rapid Note

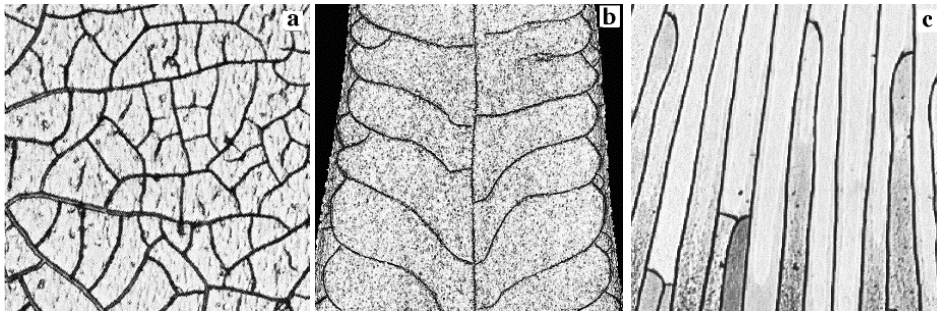

Fig. 3. (a) A pattern of cracks formed in a thin layer of gel, about 20 μm thick in which the drying is spatially homogeneous. The typical spacing of the cracks is 80 μm. (b) The cracks resulting from the drying of a wedge shaped strip of gel deposited on a silicon wafer. (c) A pattern of cracks obtained in a gel layer having a constant thickness gradient. The drying of the gel proceeds from the thin region (at the bottom) to the thick one. When a crack stops growing it connects perpendicularly, first to one of its neighbour (top of the photograph), then to the other (bottom).

displacement in the direction perpendicular to the border. One can easily show that in this case the stress component normal to the border increases in its vicinity. The criterion due to Cotterell and Rice [16] states that the crack propagation becomes unstable when the stress parallel to the crack exceeds the opening stress. This argument explains that the crack, when approaching the border, rotates in order to keep releasing the main stress. In contrast, when the contact angle is large, the volume effect of the pinning is weak so that the boundaries of the strip can be considered as traction free. Thus the stress component parallel to the crack decreases when approaching the border. This explains the stable propagation of the crack in this region.

A third experiment is meant to simulate the most usual type of venation of monocotyledons where the main veins are parallel to each other (Fig. 1c). In order to obtain an anisotropic growth we performed directional drying of the gel layer. This is obtained with a large layer having a thickness gradient. The initial cracks form in the thinner region and propagate in the gradient direction [12], forming an array of parallel and equidistant fractures. After the propagation of these cracks, there remains a mismatch between the shrunken gel and the substrate, resulting in a longitudinal stress. A series of secondary fractures, perpendicular to the initial ones, will form and the final pattern will be similar to monocotyledons veins. Another detail of this type of venation can be reproduced. In *e.g.* bread wheat [17], or lily of the valley (Fig. 1c) the number of longitudinal veins reduces as the leaf becomes narrower near its tip. A stopped vein is connected with both its two neighbours. This situation can be simulated by giving a narrowing width to the sample. The cracks, as they grow, are forced to be nearer to each other than needed to release the stress. When a crack stops growing it connects perpendicularly with one of its neighbours, then with the other (Fig. 3c). The pattern is identical to that of leaves (Fig. 1c).

The fact that a large variety of venation patterns can be obtained with cracks suggests that the vein formation occurs in a tensorial field. In order to seek the possible origin of this field we must now recall some facts about plant physiology. A cross section of a leaf is characterised by two epidermial layers separated by an inner tissue, the mesophyll. The veins are located in the mesophyll region. In their mature state they are complex bundles associating xylem and phloem which transport sieve and sap respectively. But what must be examined here is the period of formation. At the initial stage, the precursor of a future vein appears in the central region of the mesophyll when some cells differentiate into a specific tissue: the procambium. This procambium [8,9] is only weakly differentiated from the surrounding mesophyll and is characterised by strands of elongated cells with specific cell divisions. At this point it does not have transport properties. It is only later that procambium will differentiate into xylem and phloem and acquire them. Since the procambium forms the draft of the vascular system, the problem is that of its genesis.

From the previous study, a natural idea is that the mechanical stresses play a role in the differentiation of procambium. The mechanical stresses in botanical tissues have been shown to be very large and they have already been considered by botanists as being important in other morphogenetic problems such as phyllotaxis [18]. Several works [19,20] on growing organs, stems or hypocotyls, have shown that the parallel growth of the epidermis and of the inner tissues, generates growing stresses of opposite signs in these tissues. The stress is tensile in the epidermis and compressive in the inner tissues. The situation is similar in leaves where the mesophyll is submitted to a compressive stress which increases as the leaf grows in size.

We present the hypothesis that the differentiation into procambium is the response of mesophyll cells submitted to a compressive stress exceeding a threshold value. It is thus somewhat similar to the breakdown of physical cellular solids under compression [21] which is known to form localised squeezed bands of collapsed cells. The difference is that here we rather assume that when the compressive stress becomes large, the cells of band shaped regions react by having specific cell divisions where the newly formed partition is perpendicular to the main stress. This process has already been observed in a different context. Experiments [22,23] performed on botanical tissues have clearly

shown that oriented cell divisions can be forced by an externally applied compressive stress. In these situations, as in our hypothesis, the new wall forms perpendicularly to the direction of main compression, a shear free direction.

Within this model the analogy of the morphology of the veins with the fractures is reduced to a basic origin: both grow in tensorial stress fields. We can add three remarks. (i) Since the increase of the stresses is due to the leaf expansion, the model links directly the formation of veins to the growth. As a result the homogeneity of the venation is guaranteed. (ii) At the leaf edge the two epidermis meet; the stress, which comes from the mismatch between the mesophyll and the two epidermis, vanishes so that the border is analogous to the menisci of our experiments. (iii) While the cracks meet exactly at right angle, other angles are possible for veins because, once formed, they keep a role in the mechanical properties of the tissue, while cracks correspond to a complete disruption of this material. These angles are investigated elsewhere [24].

A large number of works have discussed the roles of biochemical [2,3] and mechanical [18] processes in the morphogenesis of plants. While the former has been demonstrated by many experiments [25], the direct evidence for the latter is scarcer. This is the context which gives its meaning to our results, since they suggest that the mechanical stresses in growing tissues determine the geometry of procambial strands. The reality is certainly complex with an interplay of mechanics and biochemistry since the hormones which have strong morphological effects, auxins or expansins [25], are known to modify the mechanical properties of the cells. More work is needed to characterize this interplay which is certainly essential in the regulation of a coherent tissue growth.

References

1. Y. Couder, in: *Perspectives in Fluid Dynamics*, edited by G.K. Batchelor *et al.* (Cambridge University Press, 2000)
2. G.J. Mitchison, Proc. Roy. Soc. London B **207**, 79 (1980)
3. T. Sachs, *Pattern formation in plant tissues* (Cambridge University Press, Cambridge, 1991)
4. M.E. Gottlieb, in: *Growth patterns in physical sciences and biology*, edited by J.M. Garcia Ruiz *et al.* (Plenum Press, New York, 1993)
5. H. Meinhardt, in: *Positional controls in plant development*, edited by W. Barlow, D.J. Carr (Cambridge University Press, 1984)
6. The diffusive models rely on experiments where the local application of a hormone, auxin, is responsible for the formation of veins. However these experiments are done in mature tissues so that what is observed is not the formation of procambium preceeding the transformation into xylem and phloem but the direct formation of xylem and phloem from ground cells
7. There has been attempts to obtain loops in the diffusive models. In reference [3] it is suggested that this could result from the successive diffusion of different hormones. As for the numerical model of reference [4] it is based on the idea of reconnection to the closest vein. Closed loops can be obtained but they are directly related to the use of discrete time steps in the computations
8. K. Esau, *Plant anatomy* (John Wiley, New York 1953)
9. T. Nelson, N. Dengler, The Plant Cell. **9**, 1121 (1997)
10. L.J. Hickey, Amer. J. Bot. **60**, 17 (1973)
11. Y. Couder in: *Branching in Nature*, edited by V. Fleury *et al.* (Springer-EDP Sciences, 2001)
12. C. Allain, L. Limat, Phys. Rev. Lett. **74**, 2981 (1995)
13. L. Pauchard, F. Parisse, C. Allain, Phys. Rev. E. **59**, 3737 (1999)
14. R.D. Deegan, O. Bakajin, T.F. Dupont, G. Huber, S.R. Nagel, T.A. Witten, Nature **389**, 827 (1997)
15. G.S. Avery, Amer. J. Bot. **20**, 513 (1933)
16. B. Coterell, J.R. Rice, Int. J. Fract. **16**, 155 (1980)
17. E. Blackman, Ann. Bot. **35**, 653 (1971)
18. P. Green, Int. J. Plant Sci. **153**, S59–S75 (1992)
19. W.S. Peters, A.D. Tomos, Ann. Bot. **77**, 657 (1996)
20. Z. Hejnowicz, J. Sievers, Exp. Bot. **46**, 1045 (1995)
21. M.F. Ashby, Metallurgical Trans. A **14**, 1755 (1983)
22. C.L. Brown, K. Sax, Amer. J. Bot. **49**, 683 (1962)
23. P.M. Lintilhac, T.B. Vesecky, Amer. J. Bot. **68**, 1222 (1981)
24. S. Bohn, B. Andreotti, S. Douady, J. Munzinger, Y. Couder, preprint, to appear in Phys. Rev. E (2002)
25. S. Pien, J. Wyrzykowska, S. McQueen-Mason, C. Smart, A. Fleming, Proc. Nat. Acad. Sci. **98**, 11812 (2001)


PERGAMON

Journal of the Mechanics and Physics of Solids
51 (2003) 1849–1861

JOURNAL OF THE
MECHANICS AND
PHYSICS OF SOLIDS

www.elsevier.com/locate/jmps

Self-sustained slip pulses of finite size between dissimilar materials

M. Adda-Bedia*, M. Ben Amar

Laboratoire de Physique Statistique de l'Ecole Normale Supérieure, 24 rue Lhomond, F-75231 Paris Cedex 05, France

Received 11 April 2002; accepted 31 March 2003

Abstract

The problem of a steady-state slip pulse of finite size between dissimilar materials is studied. It is shown that for a Coulomb friction law, there is a continuous set of possible solutions for any slip propagation velocity and any slip length. These solutions are, however, nonphysical because they show a singular behaviour of the slip velocity at one extremity of the pulse, which implies a crack-like behaviour. In order to regularize these solutions, we introduce a modified friction law due to Prakash and Clifton (Experimental Techniques in the Dynamics of Deformable Solids, Vol. AMD-165, pp. 33–48; J. Tribol. 120 (1998) 97), which consists in introducing in the Coulomb friction law a relaxation time for the response of the shear stress to a sudden variation of the normal stress. Then, we show that even for a slip velocity-dependent characteristic time, the degeneracy of the solutions is not suppressed and a physical pulse is not selected. This result shows the absence of steady state self-healing pulses within the modified friction law and is consistent with recent finite-difference calculations (J. Geophys. Res. 107 (2002) 10).

Keywords: A. Dynamics; B. Friction; Elastic material; C. Well-posedness

1. Introduction

Ruptures in fault zones separating dissimilar materials may provide a naturally unified explanation to some fundamental observations on earthquake and fault behaviour (Andrews and Ben-Zion, 1997; Ben-Zion and Andrews, 1998; Ben-Zion and Huang, 2002; Cochard and Rice, 2000). Effectively, there is a number of problems that are

* Corresponding author. Tel.: +33-1-44-32-25-26; fax: +33-1-44-32-34-33.
E-mail address: adda@lps.ens.fr (M. Adda-Bedia).

0022-5096/03/$ - see front matter
doi:10.1016/S0022-5096(03)00068-1

not completely explained in terms of ruptures in a homogeneous solid and that might be related to ruptures along bi-material interfaces. The interest of bi-material studies in seismology is reinforced by the fact that many earthquakes seem to have rise times much shorter than would be expected from classical crack models (Heaton, 1990). Furthermore, processes induced by heterogeneous fault zones allow earthquake ruptures to propagate at shear stresses which are low compared to friction threshold. This provides a possible explanation to the apparent lack of observed heat flow from some major faults (Lachenbruch and Sass, 1992). See the introduction of Andrews and Ben-Zion (Ben-Zion and Andrews, 1998) and of Cochard and Rice (2000) for a thorough discussion of other involved issues.

Weertman (1980) has shown that a coupling between slip and normal stress exists in a frictional interface between dissimilar materials. He concluded that a self-healing pulse can propagate along the frictional interface between dissimilar elastic solids, even when the remote shear stress is less than the frictional stress of the interface. A family of steady-state pulses at a bi-material interface under Coulomb friction law has been computed by Adams (1995, 1998, 2001). However, he has also shown that these solutions are often linearly unstable (Adams, 1995). Ranjith and Rice (2001) have shown a connection between the existence of the generalized Rayleigh wave speed and the ill-posed nature of the problem. When the material pair is such that the generalized Rayleigh wave speed is defined, the problem is ill-posed for any value of the friction coefficient, whereas when it is not defined the problem remains ill-posed for values of the friction coefficient larger than a critical value.

In a numerical study, Andrews and Ben-Zion (Andrews and Ben-Zion, 1997; Ben-Zion and Andrews, 1998) examined wrinkle like propagation using Coulomb friction law, and encountered numerical problems. Cochard and Rice (2000) found that the Adams instability was responsible for those numerical problems: the cases studied by Andrews and Ben-Zion fall precisely in the range in which the generalized Rayleigh wave speed is defined, and are thus certainly ill-posed. In order to regularize the problem, the Coulomb friction law has been replaced by an experimentally based friction law due to Prakash and Clifton (Prakash and Clifton, 1993; Prakash, 1998). This law smooths into a continuous transition with time or slip the otherwise instantaneous variation of shear strength that would follow from an instantaneous variation in normal stress if the Coulomb law was used. Ranjith and Rice (2001) have shown that this law can provide a regularization for the linear stability analysis. However, when solving the full time-dependent problem, the different numerical results (Andrews and Ben-Zion, 1997; Ben-Zion and Andrews, 1998; Ben-Zion and Huang, 2002; Cochard and Rice, 2000) do not all lead to a rupture generated by the propagation of steady state self-sustained slip pulses of finite size.

Once regularized, the physical problem is no longer exactly the same as it was originally when the Coulomb law was used. The main purpose of this paper is to provide a complete analytical study of this problem. In the next section, we present the formulation of the steady state slip pulse problem. In Section 3, we show that for a Coulomb friction law, there is a continuous set of solutions for any slip propagation velocity and any slip length. As expected, these solutions turn out to be nonphysical. In Section 6, we use the so-called Prakash–Clifton friction law in order to regularize

these solutions. Then, we show that this law *does not suppress* the degeneracy of the solutions and *does not select* a physical pulse.

2. The steady-state slip pulse problem

We consider the dynamic problem of 2D in-plane slip (plane strain deformation, Mode II rupture) along a frictional interface on the plane $Y=0$ separating two linear isotropic elastic half-spaces (Fig. 1).

The loading, particle motion, and rupture propagation are in the X-direction and all variables are functions of X, Y and t only. Shear and dilatational wave velocities are $c_{sn}=\sqrt{2\mu_n/\rho_n}$ and $c_{dn}=\sqrt{(\lambda_n+2\mu_n)/\rho_n}$, where ρ_n is mass density, λ_n and μ_n are Lamé coefficients, and subscripts $n=1,2$ denote the top ($Y>0$) and bottom ($Y<0$) materials, respectively. Shear and normal stresses on the fault are $\tau(X,t)=\sigma_{xy}(X,Y=0,t)$ and $\sigma(X,t)=\sigma_{yy}(X,Y=0,t)$. Applied shear stress and normal stress at the remote boundaries are τ^∞ and $-\sigma^\infty$, such that $\tau^\infty<f\sigma^\infty$, where f is the Coulomb dynamic coefficient of friction. Slip and slip velocity across the fault are $\delta(X,t)=u_x(X,Y=0^+,t)-u_x(X,Y=0^-,t)$ and $V(X,t)=\partial\delta/\partial t$.

Let us consider an in-plane rupture that propagates with a constant subsonic velocity c along a material interface. Rupture propagation occurs in this problem only in one direction, that of slip in the more compliant material. Since the problem is steady state, the solution depends only on $x=X-ct$ and Y. The shear and normal stress on the fault in the solution of Weertman are (Weertman, 1980)

$$\sigma(x)=-\sigma^\infty+\frac{\mu^*}{c}V(x), \tag{1}$$

$$\tau(x)=\tau^\infty-\frac{\bar{\mu}}{c}\int_{-\infty}^{\infty}\frac{V(x')}{x'-x}\frac{\mathrm{d}x'}{\pi}, \tag{2}$$

where the integral is taken in the sense of Cauchy principal value, and

$$\mu^*=\frac{1}{\Delta}[(1+b_1^2-2a_1b_1)\mu_2D_2-(1+b_2^2-2a_2b_2)\mu_1D_1], \tag{3}$$

$$\bar{\mu}=\frac{1}{\Delta}[(1-b_1^2)a_1\mu_2D_2+(1-b_2^2)a_2\mu_1D_1] \tag{4}$$

with

$$a_n=\sqrt{1-c^2/c_{dn}^2}, \tag{5}$$

$$b_n=\sqrt{1-c^2/c_{sn}^2}, \tag{6}$$

$$D_n=4a_nb_n-(1+b_n^2)^2 \tag{7}$$

and Δ is a known function of the propagation velocity and of the materials parameters (Weertman, 1980), whose explicit behaviour does not influence the subsequent analysis.

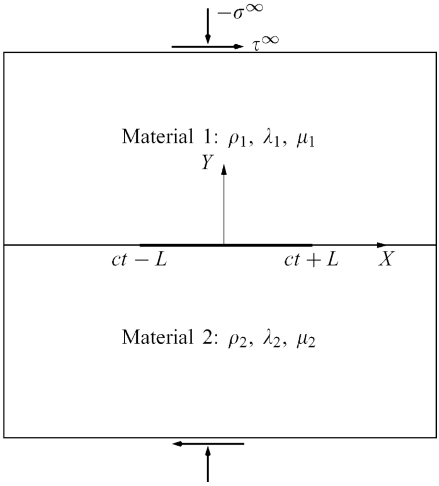

Fig. 1. The model problem for 2D in-plane steady-state rupture along the interface between different elastic solids.

The coefficient $\bar{\mu}$ decreases with increasing c and its zero defines a generalized Rayleigh speed, c_{GR}, for the materials pair. When the two materials are the same, c_{GR} reduces to the regular Rayleigh velocity. As the velocity contrast increases, the zero intersects of $\bar{\mu}$ increases and for large enough contrast $\bar{\mu}$ is positive for all subsonic values of c and c_{GR} is not defined. A steady-state Weertman pulse propagating at $c = c_{\mathrm{GR}}$, when such a speed exists, produces no changes of shear stress on the fault. When the two materials are identical, $\mu^* = 0$, and there is no coupling between slip and changes of normal stress on the fault. However, when the two materials differ, $\mu^* > 0$ and nonuniform slip produces a dynamic reduction of normal stress that is proportional to the local slip velocity.

Eqs. (1) and (2) result from applying the conditions of continuity of normal displacements and shear and normal stresses along the interface $Y = 0$. These boundary conditions allow to write the stresses at the interface as functions of the slip velocity only. In order to solve the slip pulse problem, one has to prescribe the slip conditions and/or the friction law along the interface. We impose that the pulse has a finite size $2L$. Thus outside this region, the slip velocity $V(x)$ identically vanishes,

$$V(x) = 0, \quad |x| > L. \tag{8}$$

Along the pulse, a friction law which relates the shear stress to the normal loading at the interface should be prescribed. For this, we use a simplified version of the Prakash–Clifton friction law (Prakash and Clifton, 1993; Prakash, 1998), which consists on introducing in the Coulomb friction law a slip velocity dependent relaxation time $t_0(V)$ for the response of the shear stress to a sudden variation of the normal stress

$$-t_0(V)\frac{\mathrm{d}}{\mathrm{d}t}\tau(x) \equiv L_0(V)\frac{\mathrm{d}}{\mathrm{d}x}\tau(x) = \tau(x) + f\sigma(x), \quad |x| < L, \tag{9}$$

where $L_0 \equiv ct_0$ is a characteristic length scale. A thorough discussion of the Prakash–Clifton law can be found in (Cochard and Rice, 2000; Ranjith and Rice, 2001). Note that if renewal of the asperity contact population is the underlying mechanism leading to loss of frictional "memory" of prior strength, then one expects that $t_0(V)$ should vary inversely with V at high slip rates, basically as $L^*/|V|$, where L^* is a characteristic sliding distance to renew the contact population. In order to match the behaviour at high slip rates without introducing singular behaviour at low slip rates, the Prakash–Clifton law used in the previous studies (Ben-Zion and Huang, 2002; Cochard and Rice, 2000; Ranjith and Rice, 2001) replaces the characteristic time scale $t_0(V)$ by a slip velocity dependent function $L^*/(V^* + |V(x)|)$, where L^* and V^* are characteristic length and velocity scales.

The slip velocity can now be determined from Eqs. (1), (2), (8) and (9). Let us take L as the length scale, and define a nondimensioned slip velocity $S(x)$ by

$$V(x) = \frac{(f\sigma^\infty - \tau^\infty)c}{\mu^* f} S(x). \tag{10}$$

Note that for similar materials the scaling (10) is not adequate, since μ^* vanishes in this case. Using Eqs. (1) and (2), conditions (8) and (9) become

$$S(x) = 0, \quad |x| > 1, \tag{11}$$

$$S(x) = 1 + K\left(1 - \eta(S)\frac{\mathrm{d}}{\mathrm{d}x}\right)\int_{-1}^{1} \frac{S(x')}{x' - x}\frac{\mathrm{d}x'}{\pi}, \quad |x| < 1, \tag{12}$$

where $\eta(S)$ and K are the pertinent parameters of the present problem. They are defined by

$$\eta(S) = \frac{L_0}{L}, \tag{13}$$

$$K(c) = \frac{\overline{\mu(c)}}{f\mu^*(c)}. \tag{14}$$

The function $\eta(S)$ can be seen as the inverse of the pulse size in units of the characteristic length scale L_0. The influence of the elastic parameters of the two materials are embedded in the parameter $K(c)$, whose behaviour is shown in Fig. 2. When the generalized Rayleigh speed is not defined, $K(c)$ is always positive. On the other hand, when the generalized Rayleigh speed exists, $K(c)$ is positive for a wide range of propagation velocities $0 < c < c_{\mathrm{GR}}$, and it takes finite negative values for propagation velocities $c_{\mathrm{GR}} < c \leqslant c_{\mathrm{s1}}$.

The main equations of this section are well known. They have been used for stability studies of homogeneous slips along the interface between different materials (Adams, 1995, 1998, 2001; Ranjith and Rice, 2001). In contrast, our goal consists in finding the properties of inhomogeneous slips along the interface, by introducing a slip length which is different from the fault size. Of course, the final goal would be to relate the properties of the self-sustained slip pulses to the self-healing pulses deduced by Heaton from geological observations (Heaton, 1990). Indeed, recent numerical studies (Andrews and Ben-Zion, 1997; Ben-Zion and Andrews, 1998; Ben-Zion and Huang,

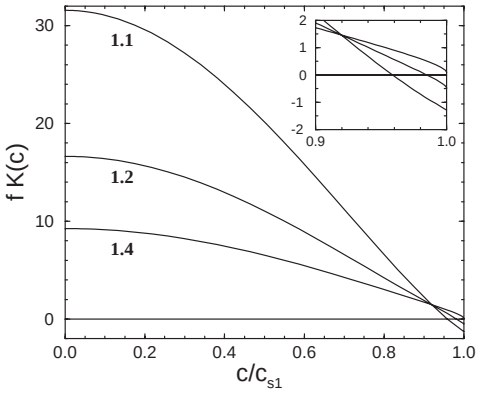

Fig. 2. The behaviour of $K(c)$, defined by Eq. (14), as a function of the subsonic propagation speed c, for ratios of c_{s2}/c_{s1} equal to 1.1, 1.2, and 1.4. The other materials coefficients are taken such that $\mu_1 = \mu_2$, $c_{d1} = \sqrt{3}c_{s1}$, $c_{d2} = \sqrt{3}c_{s2}$. The inset is a close-up of the curves in the region $0.9c_{s1} \leqslant c \leqslant c_{s1}$.

2002; Cochard and Rice, 2000) have been controversial about the conditions of existence of steady-state self-sustained slip pulses of finite size. It was found in (Ben-Zion and Huang, 2002) that the self-sharpening and divergent behaviour found earlier by Cochard and Rice (2000) with Coulomb friction law exists also with regularized friction for large enough propagation distance, or equivalently for long times. The parameters of the regularized friction law had to be fine tuned to produce apparent stability for a given propagation distance. However, eventually, the pulse always dies or diverges.

When the material pair is such that the generalized Rayleigh wave speed is defined, Adams (1998) has shown that in the framework of the classical Coulomb friction law, there exists a continuous family of steady-state pulses at a bi-material interface propagating at $c = c_{GR}$. However, Ranjith and Rice (2001) have shown that these solutions are linearly unstable for any value of the friction coefficient. In the following, we look for possible steady-state solutions by focussing on the cases when $K(c) \neq 0$. We study the singular integro-differential Eqs. (11) and (12), using a pure Coulomb friction law ($\eta = 0$), and the Prakash–Clifton law ($\eta \neq 0$) for two model cases: $\eta(S) = \eta_0$, $\eta(S) = \eta_0 + \eta_1 S$, where η_0 and η_1 are constants. We also point out that the use of a more general form of $\eta(S)$ give similar results to the latter cases. Note, however, that the possible solutions of Eqs. (11) and (12) always coexist with the trivial solution $S(x) = 0$ for all x, since we prescribed $\tau^\infty < f\sigma^\infty$. Then, the absence of solutions for these equations implies an absence of slipping along the whole interface.

3. The Coulomb friction law ($\eta = 0$)

For this case, Eq. (12) is reduced to

$$S(x) = 1 + K \int_{-1}^{1} \frac{S(x')}{x' - x} \frac{\mathrm{d}x'}{\pi}, \quad |x| < 1. \tag{15}$$

Using usual techniques of singular integral equations (Muskhelishvili, 1953), the solution of Eq. (15) is straightforward. Define a complex function $F(z)$; $z = x + \mathrm{i}y$; such that

$$F(z) = \int_{-1}^{1} \frac{S(x)}{x - z} \frac{\mathrm{d}x}{2\mathrm{i}\pi}, \tag{16}$$

whose behaviour for $|z| \to \infty$ is readily given by

$$F(z) \sim -\frac{1}{2\mathrm{i}\pi z} \int_{-1}^{1} S(x)\,\mathrm{d}x. \tag{17}$$

The function $F(z)$ is holomorphic everywhere except on the interval $[-1, 1]$ of the real axis, where it satisfies

$$F(x + \mathrm{i}0) - F(x - \mathrm{i}0) = S(x), \tag{18}$$

$$F(x + \mathrm{i}0) + F(x - \mathrm{i}0) = \int_{0}^{1} \frac{S(x')}{x' - x} \frac{\mathrm{d}x'}{\mathrm{i}\pi}. \tag{19}$$

Then combining these two conditions with Eq. (15) yields

$$\mathrm{e}^{-\mathrm{i}\alpha} F(x + \mathrm{i}0) - \mathrm{e}^{\mathrm{i}\alpha} F(x - \mathrm{i}0) = \cos\alpha, \tag{20}$$

where the parameter α is related to K by

$$\tan\alpha = K, \quad -\pi/2 < \alpha < \pi/2. \tag{21}$$

The holomorphic function that satisfies the jump condition (20) and the asymptotic behaviour (17) is readily given by (Muskhelishvili, 1953)

$$F(z) = \frac{\mathrm{i}}{2\tan\alpha} \left[1 - \left(\frac{z-1}{z+1}\right)^{\alpha/\pi}\right] \tag{22}$$

and the solution $S(x)$ follows directly from Eq. (18)

$$S(x) = \cos\alpha \left(\frac{1-x}{1+x}\right)^{\alpha/\pi}, \quad |x| < 1. \tag{23}$$

Therefore, a Coulomb friction law leads to a continuous set of solutions, where neither the length of the pulse nor its propagation velocity are selected. For each value of the parameter α, corresponding to a given value of K, there exists a "mathematical" solution $S(x)$ satisfying the Coulomb friction law. However, these solutions are clearly nonphysical ones, since $S(x)$ diverges near $x = -1$ (resp. $x = 1$) for $\alpha > 0$ (resp. $\alpha < 0$). Moreover, as seen in Fig. 3, due to the singularity of the slip velocity, the normal stress changes its sign, which induces an opening loading, and thus a crack-like behaviour, in a certain region of the pulse. This clearly violates the boundary condition of continuity of the normal displacement embedded in the solution of Weertman (1980). Therefore, a pure Coulomb friction law is inconsistent with a condition of slip without opening.

Moreover, when the material pair is such that the generalized Rayleigh wave speed is defined, one has $\alpha = 0$. For this special case, Eq. (23) shows that $S(x) = 1$ for

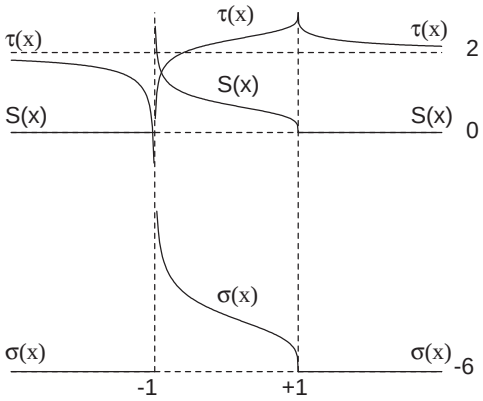

Fig. 3. The behaviour of the slip velocity $S(x)$, the normal and shear stress $\sigma(x)$ and $\tau(x)$ at the interface. The values are taken such that $\alpha = \pi/4$, $\tau^{\infty} = \sigma^{\infty}/3$ and $f = 0.5$.

$|x| < 1$ and it is discontinuous at $x = \pm 1$. The corresponding solutions do not contain infinities of the normal stress or slip rate. Such discontinuities are acceptable since they propagate at the relevant wave speed. Therefore, there exists a continuous family of steady-state pulses at a bi-material interface propagating at $c = c_{GR}$ (Adams, 1998; Rice, 1997). However, Ranjith and Rice (2001) have shown that these solutions are linearly unstable for any value of the friction coefficient.

In the following section, we will use the Prakash–Clifton friction law as a possible regularizing procedure of the simple Coulomb friction law. However, we will see that even when using a slip velocity-dependent characteristic time, the degeneracy of the solutions, found for $\eta = 0$, is not suppressed and a physical pulse cannot be selected.

4. The Prakash–Clifton friction law ($\eta \neq 0$)

The presence in Eq. (12) of the differential operator, $\partial/\partial x$, introduces an additional degree of freedom in the problem, since one has to fix a constant of integration; this operator does not appear in the case of the Coulomb friction law ($\eta = 0$). These two ingredients together are a signature of a possible eigenvalue problem, where in the case of the existence of solutions, the parameter K should be determined as a function of η.

For $\eta \neq 0$, we assume that the propagation speed does not coincide with c_{GR}, and thus $K(c) \neq 0$. Moreover, we do not explore solutions which allow loss of contact along the interface, since we are interested in studying the Weertman pulse (Weertman, 1980) for which the normal displacement is continuous. Since Eq. (11) imposes that the slip velocity vanishes outside the rupture region, one expects continuous matching of $S(x)$ at the rupture edges. Indeed, the slip rate $S(x)$, which by definition is always positive, should not diverge at $x = \pm 1$, since it leads to an opening loading $\sigma(x)$, which violates the boundary condition of continuity of the normal displacement. Moreover, if $S(\pm 1) \neq 0$, the integral part of Eq. (11) induces a singular logarithmic behaviour in

the vicinity of the rupture edges. Therefore, necessary conditions for physical solutions are given by

$$S(\pm 1) = 0. \tag{24}$$

These conditions will be used to fix the integration constant of Eq. (30), and the parameter K as functions of η. Therefore, if physical solutions exist, the pulse size would be selected as a function of its propagation speed and of the physical parameters. This is in contrast with the case $\eta = 0$, where K was undetermined and the continuity conditions of the slip velocity could not be satisfied simultaneously at the two rupture edges. This problem is similar to the so-called Saffman–Taylor problem (McLean and Saffman, 1981), where a fluid penetrates into a thin cell that contains a more viscous liquid. The introduction of a nonzero η in the present problem is similar to the introduction of capillary effects in the Saffman–Taylor problem, which suppresses the degeneracy of the solutions found at vanishing capillary number (McLean and Saffman, 1981).

Let us first fix the asymptotic behaviour of $S(x)$ in the vicinity of the endpoints $x = \pm 1$. Conditions (24) impose to $S(x)$ to behave as

$$S(x) \sim (1+x)^{\beta_0}, \quad x \to -1, \tag{25}$$

$$S(x) \sim (1-x)^{\beta_1}, \quad x \to 1, \tag{26}$$

where β_0 and β_1 are real positive constants. Without loss of generality, we can prescribe that $0 < \beta_0 < 1$ and $0 < \beta_1 < 1$. Let us also note the following results:

$$\int_{-1}^{1} \frac{(1-x')^{\beta_1}}{x'-x}\,\mathrm{d}x' = -\frac{2^{\beta_1}}{\beta_1} + \pi(1-x)^{\beta_1}\cot \pi\beta_1 - \frac{2^{(\beta_1-1)}(1-x)}{\beta_1 - 1} + O((1-x)^2), \tag{27}$$

for $x \to 1$, and

$$\int_{-1}^{1} \frac{(1+x')^{\beta_0}}{x'-x}\,\mathrm{d}x' = \frac{2^{\beta_0}}{\beta_0} - \pi(1+x)^{\beta_0}\cot \pi\beta_0 + \frac{2^{(\beta_0-1)}(1+x)}{\beta_0 - 1} + O((1+x)^2), \tag{28}$$

for $x \to -1$. Using Eq. (30), one can determine the values of the constants β_0 and β_1. For this, one has to fix the form of $\eta(S)$. In the following, we will study some particular cases.

4.1. Case $\eta(S) = \eta_0$

For this simple case, Eq. (11) is transformed into

$$S(x) = 1 + K(c)\left(1 - \eta_0 \frac{\mathrm{d}}{\mathrm{d}x}\right)\int_{-1}^{1} \frac{S(x')}{x'-x}\frac{\mathrm{d}x'}{\pi}, \quad |x| < 1. \tag{29}$$

It is easy to verify that whatever are the values of β_0 and β_1, Eq. (29) cannot be fullfiled in the vicinity of the endpoints $x = \pm 1$. This is due to the presence of the differential operator which gives the highest-order singular contribution that is not balanced by any

other term in Eq. (29). Therefore, one concludes that a constant $\eta(S)$ in the Prakash–Clifton law does not allow physical solutions with the appropriate asymptotic behaviour imposed by conditions (24). In the following, we modify slightly the Prakash–Clifton law by introducing a weak nonlinearity in $\eta(S)$.

4.2. Case $\eta(S) = \eta_0 + \eta_1 S$

Then, Eq. (11) is transformed into

$$S(x) = 1 + K(c)\left(1 - (\eta_0 + \eta_1 S(x))\frac{\mathrm{d}}{\mathrm{d}x}\right)\int_{-1}^{1}\frac{S(x')}{x'-x}\frac{\mathrm{d}x'}{\pi}, \quad |x| < 1, \tag{30}$$

Using identities (27) and (28), one finds that Eq. (30) may admit solutions that satisfy conditions (24) if and only if

$$\beta_0 = \beta_1 = \tfrac{1}{2}, \tag{31}$$

which leads to a square root behaviour of the slip velocity at the rupture edges. Since the function $S(x)$ is defined in the interval $[-1, 1]$, one can decompose the slip velocity in terms of Chebyshev polynomials by writing

$$S(x) = \sqrt{1-x^2}\sum_{n=0}^{\infty} a_n U_n(x), \tag{32}$$

where $U_n(x)$ are the Chebyshev polynomials of the second kind. Let us recall the following Hilbert transform property of this class of polynomials

$$\int_{-1}^{1}\frac{\sqrt{1-x'^2}U_n(x')}{x'-x}\frac{\mathrm{d}x'}{\pi} = -T_{n+1}(x), \tag{33}$$

where T_n are Chebyshev polynomials of the first kind. Using decomposition (32) and identity (33), Eq. (30) becomes

$$\sqrt{1-x^2}\sum_{m=0}^{\infty} a_m U_m(x)\left[1 - K\eta_1\sum_{n=0}^{\infty} a_n T'_{n+1}(x)\right]$$
$$= 1 - K\sum_{n=0}^{\infty} a_n T_{n+1}(x) + K\eta_0\sum_{n=0}^{\infty} a_n T'_{n+1}(x). \tag{34}$$

Isolating the square-root behaviour from the integer power behaviour in Eq. (34) leads to the following identities:

$$K\eta_1\sum_{n=0}^{\infty} a_n T'_{n+1}(x) \equiv K\eta_1\sum_{n=0}^{\infty}(n+1)a_n U_n(x) = 1, \tag{35}$$

$$K\sum_{n=0}^{\infty} a_n T_{n+1}(x) - K\eta_0\sum_{n=0}^{\infty}(n+1)a_n U_n(x) = 1. \tag{36}$$

Eq. (35) admits the unique solution $K\eta_1 a_0 = 1$, and $a_n = 0$ for all $n > 0$. However, this solution is not satisfied by Eq. (36). Therefore, a weak nonlinearity in the friction law as given above is not sufficient for regularizing the slip pulse solution at the endpoints $x \pm 1$. Since the form $\eta(S) = \eta_0 + \eta_1 S$ can be seen as an expansion of any nonlinear behaviour one can wonder if the absence of physical solutions persists when one takes into account a more general friction law.

4.3. Case of a general $\eta(S)$

It is rather unlikely that the nonlinear integrodifferential equation (11) has a solution with enough regular endpoints. As an example, let us write

$$\eta(S) = \eta_0 + \eta_1 S(x) F(S(x)), \tag{37}$$

where η_0 and η_1 are arbitrary constants, and F is any function of $S(x)$ that satisfies $F(S(\pm 1)) \equiv F(0) = 1$. The asymptotic analysis in the vicinity of $x = \pm 1$ is similar to the case where $F(S(x)) = 1$ and Eqs. (35) and (36) are transformed into

$$K\eta_1 F(S(x)) \sum_{n=0}^{\infty} a_n T'_{n+1}(x) = 1, \tag{38}$$

$$K \sum_{n=0}^{\infty} a_n T_{n+1}(x) - K\eta_0 \sum_{n=0}^{\infty} a_n T'_{n+1}(x) = 1. \tag{39}$$

Introducing the function defined for $|x| < 1$:

$$Q(x) = \sum_{n=0}^{\infty} a_n T_{n+1}(x). \tag{40}$$

Eq. (39) is then a linear differential equation of first order for $Q(x)$ which has an explicit solution

$$Q(x) = \frac{1}{K}[1 - \exp(x/\eta_0)]. \tag{41}$$

Therefore, the coefficients in the series expansion following Eq. (40) can be determined, and so the function $S(x)$. On the other hand, Eq. (38) gives

$$F(S(x)) = -\frac{\eta_0}{\eta_1} \exp(-x/\eta_0). \tag{42}$$

At $x = \pm 1$, Eq. (42) gives $F(S(\pm 1)) = -(\eta_0/\eta_1)\exp(\mp 1/\eta_0)$, which is in contradiction with the condition $F(S(\pm 1)) \equiv F(0) = 1$. Therefore, we conclude that even within a general nonlinear friction law, solutions of finite size steady-state slip pulses are not allowed.

Finally, whatever the nonlinearities included in the friction law (we also checked a law of the form $\eta(S) = \eta_0/S$), excluding some peculiar and probably unphysical cases, it seems hopeless to find a regular solution to the steady-state slip pulse.

5. Discussion

We have studied the problem of the existence of solutions for steady-state slip pulse of finite size between dissimilar materials. We have shown that for a Coulomb friction law, there is a continuous set of solutions that are however nonphysical because they show a singular behaviour of the slip velocity. We have shown that even within the Prakash–Clifton friction law, the degeneracy of the solutions is not suppressed and a physical pulse is not selected. This analytical result is consistent with recent finite-difference calculations (Ben-Zion and Huang, 2002). Of course, when the material pair is such that the generalized Rayleigh wave speed is defined, there exists a family of steady-state pulses at a bi-material interface propagating at $c = c_{GR}$ (Adams, 1998; Rice, 1997). However, these solutions are nonphysical within a Coulomb friction law because they are linearly unstable (Ranjith and Rice, 2001).

When the two materials on each side of a planar fault are identical, unstable slip is impossible if the interface is governed by the classical Coulomb friction law; it requires more elaborate friction laws for which, under constant normal stress, the friction stress at some point decreases as the slip displacement or slip velocity increases (Perrin et al., 1995). A simple argument of the crack-like behaviour can be found in the steady-state slip pulse solution between similar materials. Using a pure Coulomb friction law, one can easily show that these solutions are given by

$$V(x) \propto \frac{1}{\sqrt{1-x^2}} \tag{43}$$

and the use of the Prakash–Clifton law will not regularize the problem. The presence of the square root singularity reflects such a crack-like behaviour, which means that once the slip pulse exceeds a critical length, it will propagate through the whole fault plane. Thus, such models cannot produce complexity since they introduce one characteristic length scale only; the nucleation size.

Our main conclusion is that the dissimilarity between the materials on each side of the planar fault is not sufficient to produce steady state self-sustained slip pulses of finite size, because it does not introduce an additional length scale against which the pulse size can be scaled. Two recent approaches have been proposed in order to explain the existence of self-healing slip pulses, by adding a new length scale in their models. The first approach assumes that rupture occurs within an interface between a compliant fault zone layer and a stiffer surrounding solid (Ben-Zion and Huang, 2002). The additional length scale in this approach being the thickness of the layer. The second approach does not impose a priori the continuity of the normal displacement in the rupture region (Gerde and Marder, 2001). This allows the rupture to occur by opening in certain regions and slipping in others.

Acknowledgements

We thank J.R. Rice for enlightening discussions. Laboratoire de Physique Statistique is “associé au CNRS (UMR 8550) et aux Universités Paris VI et Paris VII”.

References

Adams, G.G., 1995. Self-excited oscillations of two elastic half-spaces sliding with a constant coefficient of friction. ASME J. Appl. Mech. 62, 867–872.

Adams, G.G., 1998. Steady sliding of two elastic half-spaces with friction reduction due to interface stick-slip. ASME J. Appl. Mech. 65, 470–475.

Adams, G.G., 2001. An intersonic slip pulse at a frictional interface between dissimilar materials. ASME J. Appl. Mech. 68, 81–86.

Andrews, D.J., Ben-Zion, Y., 1997. Wrinkle-like slip pulse on a fault between different materials. J. Geophys. Res. 102, 553–571.

Ben-Zion, Y., Andrews, D.J., 1998. Properties and implications of dynamic rupture along a material interface. Bull. Seismol. Soc. Am. 88, 1085–1094.

Ben-Zion, Y., Huang, Y., 2002. Dynamic rupture on an interface between a compliant fault zone layer and a stiffer surrounding solid. J. Geophys. Res. 107, 10. 1029/2001JB000254.

Cochard, A., Rice, J.R., 2000. Fault rupture between dissimilar materials: ill-posedness, regularization, and slip pulse response. J. Geophys. Res. 105, 25891–25907.

Gerde, E., Marder, M., 2001. Friction and fracture. Nature 413, 285–288.

Heaton, T.H., 1990. Evidence for and implications of self-healing pulses of slip in earthquake rupture. Phys. Earth Planet. Inter. 64, 1–20.

Lachenbruch, A.H., Sass, J.H., 1992. Heat flow from Cajon Pass, fault strength and tectonic implications. J. Geophys. Res. 97, 4995–5030.

McLean, J.W., Saffman, P.G., 1981. The effect of surface tension on the shape of fingers in a Hele–Shaw cell. J. Fluid Mech. 102, 455–469.

Muskhelishvili, N.I., 1953. Singular Integral Equations. Noordhoff, Groningen.

Perrin, G., Rice, J.R., Zheng, G., 1995. Self-healing slip pulse on a frictional surface. J. Mech. Phys. Solids 43, 1461–1495.

Prakash, V., 1998. Frictional response of sliding interfaces subjected to time varying normal pressures. J. Tribol. 120, 97–102.

Prakash, V., Clifton, R.J., 1993. Time resolved dynamic friction measurements in pressure-shear. In: Experimental Techniques in the Dynamics of Deformable Solids, Vol. AMD-165. Appl. Mech. Div., ASME, New York, pp. 33–48.

Ranjith, K., Rice, J.R., 2001. Slip dynamics at an interface between dissimilar materials. J. Mech. Phys. Solids 49, 341–361.

Rice, J.R., 1997. Slip pulse at low driving stress along a frictional fault between dissimilar media. EOS Trans. Am. Geophys. Union 78, F464.

Weertman, J.J., 1980. Unstable slippage across a fault that separates elastic media of different elastic constants. J. Geophys. Res. 85, 1455–1461.


PERGAMON

Journal of the Mechanics and Physics of Solids
51 (2003) 1287–1304

JOURNAL OF THE
MECHANICS AND
PHYSICS OF SOLIDS

www.elsevier.com/locate/jmps

Brittle fracture dynamics with arbitrary paths I. Kinking of a dynamic crack in general antiplane loading

M. Adda-Bedia[a,*], R. Arias[b]

[a] *Laboratoire de Physique Statistique de l'Ecole Normale Supérieure, 24 rue Lhomond, F-75231 Paris Cedex 05, France*

[b] *Departamento de Física, Facultad de Ciencias Físicas y Matemáticas, Universidad de Chile, Casilla 487-3 Santiago, Chile*

Received 11 April 2002; accepted 29 January 2003

Abstract

We present a new method for determining the elasto-dynamic stress fields associated with the propagation of anti-plane kinked or branched cracks. Our approach allows the exact calculation of the corresponding dynamic stress intensity factors. The latter are very important quantities in dynamic brittle fracture mechanics, since they determine the crack path and eventual branching instabilities. As a first illustration, we consider a semi-infinite anti-plane straight crack, initially propagating at a given time-dependent velocity, that changes instantaneously both its direction and its speed of propagation. We will give the explicit dependence of the stress intensity factor just after kinking as a function of the stress intensity factor just before kinking, the kinking angle and the instantaneous velocity of the crack tip.

Keywords: A. Crack branching and bifurcation; Dynamic fracture; Stress intensity factors; B. Crack mechanics; C. Analytic functions

1. Introduction

In many experimental situations, cracks propagate by following curved or kinked paths (Broberg, 1999; Freund, 1990; Lawn, 1993). Another well-known phenomenon in brittle crack propagation is the possible emergence from a single crack tip of two

* Corresponding author. Present address: DAMTP, Center for Mathematical Sciences, Wilberforce Road, Cambridge CB3 0WA, UK. Fax: +44-1223-765900.

E-mail address: m.adda-bedia@damtp.cam.ac.uk (M. Adda-Bedia).

0022-5096/03/$ - see front matter
doi:10.1016/S0022-5096(03)00022-X

or more branches. Experiments in PMMA and glass plates (Ravi-Chandar and Knauss, 1984; Sharon and Fineberg, 1996, 1999) have shown that this phenomenon occurs for fast single propagating cracks after they surpass a critical velocity that is a fraction of the Rayleigh wave speed of these materials. Above this critical speed, a dynamical instability sets in marked by the appearance of micro-branches, roughness of the crack surfaces, sound emission, and eventual macro-branches at higher speeds.

The knowledge of the instantaneous stress fields in the vicinity of the crack tip is necessary for the theoretical prediction of a crack path. Therefore, the determination of the elasto-dynamic fields associated with the propagation of kinked or branched cracks is an unavoidable step in the study of brittle fracture dynamics. Unfortunately, a general solution to the dynamical kinking or branching problem is not available yet. Up to now, efforts have been dedicated to the study of elasto-static solutions of kinked or branched cracks (Sih, 1965; Amestoy and Leblond 1992; Leblond, 1989). Also, in addition to the well established solutions of straight crack propagation (Freund, 1990; Kostrov, 1966; Kostrov, 1975; Eshelby, 1969), the only known elasto-dynamic solutions related with the kinking or branching problem deal with a semi-infinite crack that starts to propagate from rest by kinking or branching under the action of a stress pulse loading (Dempsey et al., 1982; Burgers, 1982, 1983).

The aim of this paper is to present a new method to calculate the dynamic stress intensity factors associated with the propagation of anti-plane kinked or branched cracks. As a first application, we consider the dynamic kinking of an initially semi-infinite straightly propagating crack. We will give the explicit dependence of the stress intensity factor just after kinking as a function of the stress intensity factor prior to kinking, the kinking angle and the instantaneous velocity of the crack tip. This method can be generalized to the case of an initially propagating anti-plane crack that branches into two or more cracks. The case of two cracks that branch symmetrically from a single crack will be the subject of the next application of our method.

The paper is organized as follows. In the next section, we introduce our approach to the dynamical kinked crack problem under mode III loading, and we derive the corresponding model problem. In Section 3, we detail the self-similar solution that it admits. The present work can be considered as an extension of the self-similar analysis of dynamic crack growth initiated by Broberg (Broberg, 1999) and Achenbach (Dempsey et al., 1982) among others. A detailed discussion of the analysis of self-similar mixed boundary value problems in elasto-dynamics can also be found in the work of Willis (1973). In the present case, the self-similar solution of the dynamic crack kinking problem is given by an integral representation, which is a convolution between a known kernel and a harmonic function, which is determined by the real part of a holomorphic function. In Section 4, the harmonic function is mapped into an upper complex half-plane, with boundary conditions on the real axis, and an intermediate exact solution is given. In Section 5, the numerical resolution of the integral equation is presented. The results for the stress intensity factor just after kinking are given for arbitrary angles and velocities. Finally, we discuss our results, especially the difference between our solution and the elasto-static solution, and the consequences of this discrepancy for the selection of crack paths in quasi-static situations.

2. The dynamical kinked crack under mode III loading

Consider an elastic body which contains a half-plane kinked crack but which is otherwise unbounded (see Fig. 1). Introduce a cylindrical coordinate system (r,θ,z) so that the z-axis lies along the crack edge. The upward (resp. downward) semi-infinite crack surface occupies the half-plane $\theta=\pi$ (resp. $\theta=-\pi$). Suppose that the material is subjected to a loading which produces a state of anti-plane shear deformation in the body. Thus the only nonzero component of displacement is the z-component $u_z(r,\theta,t)\equiv w(r,\theta,t)$, which is independent of z.

The scenario of crack kinking is developed as follows. A semi-infinite straight crack that propagates at a speed $v(t)$ for $t<-\tau$ (with $\tau\to 0^+$) suddenly stops at $t=-\tau$. At $t\to 0^+$, the crack kinks locally with a kinking angle equal to $\lambda\pi$, with $-1<\lambda<1$. For $t>0^+$, the new branch propagates straightly at a velocity $v'(t)$, following this new direction. The magnitudes of the crack speeds v and v' are restricted by $0<v<c$ and $0<v'<c$, where c denotes the elastic shear wave speed. It is well known (Freund, 1990; Kostrov, 1966, 1975; Eshelby, 1969) that the mode III dynamic stress intensity factor, $K(t)$, of the straight crack prior to kinking is related to the rest stress intensity factor, $K_0(t)$, of the same configuration by

$$K(t)=k(v)K_0(t), \tag{1}$$

where $k(v)$ is a universal function of the instantaneous crack tip speed given by

$$k(v)=\sqrt{1-v/c}. \tag{2}$$

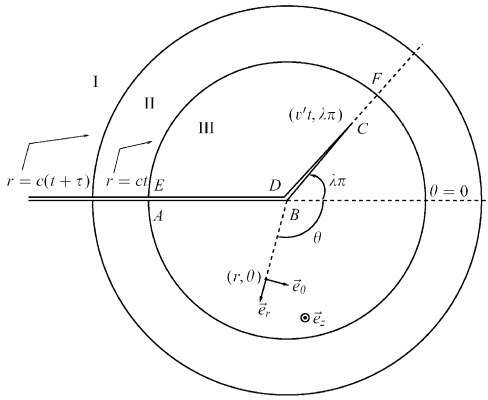

Fig. 1. Schematic representation of an anti-plane kinked crack problem. A half-plane crack that propagates at a speed v for $t<-\tau$ suddenly stops at $t=-\tau$, at $r=0$. For $t>0$, the new branch propagates straightly at a velocity v', following the direction $\lambda\pi$. The orthonormal basis $(\vec{e}_r,\vec{e}_\theta,\vec{e}_z)$ corresponding to the cylindrical coordinate system (r,θ,z) is shown. The cylindrical waves originated at the crack's arrest $(r=c(t+\tau))$ and at the start of kink propagation $(r=ct)$ divide the material into three regions. In the region labelled I, the stress field comes only from the dynamical straight crack propagation, since the effects of the crack's arrest and the crack's kinking are not experienced there. The region II is influenced by the crack arrest only, thus the stress field there is a static one (Freund, 1990; Eshelby, 1969). It is only the region III that is influenced by the crack's kinking. Thus, one has to solve the kinked crack problem only in this latter region.

We are interested in the dynamic stress intensity factor just after kinking, K', as a function of the kinking angle, the crack tip speeds (prior and after kinking), the material parameters and of the applied load. According to our description of crack kinking, K' should be defined as

$$K'(\lambda, v, v', c, \ldots) = \lim_{\tau\to 0^+} \lim_{t\to 0^+} \lim_{(r-v't)\to 0^+} \sqrt{2\pi(r-v't)}\sigma_{\theta z}(r, \lambda\pi, t). \tag{3}$$

We emphasize the importance of the order in which the limits in Eq. (3) should be taken. The decomposition of the crack kinking process as described above imposes that the limit $t \to 0^+$ must be taken before the limit $\tau \to 0^+$.

In the limit $t \to 0^+$, the length of the kinked part of the crack is vanishingly small, so that the breaking process after kinking occurs in the region determined by the square root singular stress intensity factor field of the semi-infinite crack. Therefore, the applied loads on the kink involve only the stress intensity scale, and the physical system does not involve either a characteristic time scale or a characteristic length scale. This imposes that the stress intensity factor just after kinking should be written as

$$K' = H_{33}(\lambda, v/c, v'/c)K_0, \tag{4}$$

where H_{33} is an unknown dimensionless function of the kinking angle $\lambda\pi$ and of the crack tip speeds v and v'. As in the quasi-static case (Leblond, 1989), the function H_{33} is universal in the sense that it does not depend either on the loading configuration or on the geometry of the body. Effectively, in the limits $t \to 0^+$ and $\tau \to 0^+$ that we consider, the dynamic kinking problem does not involve incoming radiation effects, so it is always equivalent to a crack propagating in an unbounded body. On the other hand, due to the absence in linear elasticity theory of intrinsic times or length scales, this problem becomes of general validity since it is not necessary for the crack or the kink to be straight. Effectively, we can generalize the quasi-static analysis (Leblond, 1989) so that Eq. (4) is also valid for dynamic curved cracks; H_{33} does not depend on the local curvature of the crack prior or after kinking.

For the mode III case, when the initial crack stops, a static stress distribution is restored behind a wave front that propagates from the crack tip at the shear wave speed (Eshelby, 1969), (see Fig. 1). Thus for $t > 0$, the propagation of the kinked crack occurs within a stationary stress field. Our kinking problem is then equivalent to solving the problem of a kink that emerges from a pre-existing stationary straight crack, and that started to propagate at time $t = 0^+$, in the direction $\lambda\pi$, with a velocity v', under the action of a time-independent loading. Moreover, in order to compute the stress intensity factor just after kinking given by Eq. (4), it is enough to solve this problem by considering the static stress distribution $\sigma^s_{\theta z}(r, \theta)$, which in the vicinity of the stationary initial crack tip has a square root singular stress intensity factor field given by (Williams, 1952)

$$\sigma^s_{\theta z}(r, \theta) = \frac{K_0}{\sqrt{2\pi r}} \cos\frac{\theta}{2}, \tag{5}$$

where K_0 is the rest stress intensity factor of the crack tip prior to kinking, which is related to the dynamic stress intensity factor, K, just before kinking through Eq. (1).

A straightforward consequence of these previous arguments is that the universal function H_{33} must be independent of the velocity prior to kinking

$$H_{33}(\lambda, v/c, v'/c) \equiv H_{33}(\lambda, v'/c). \tag{6}$$

Also, it is clear that H_{33} should satisfy the following property

$$\lim_{\lambda \to 0} H_{33}(\lambda, v'/c) = k(v'), \tag{7}$$

for all values of v' (Kostrov, 1966; Eshelby, 1969).

2.1. The model problem of dynamic crack kinking

The process of crack advance in the situation depicted in Fig. 1 can be viewed as the process of negating the traction distribution on the newly broken surface produced by the stress field distribution of the stationary crack given by Eq. (5). For $t < 0$, it is assumed that the crack is at rest and that the material is loaded according to Eq. (5). As the crack advances for $t > 0$, the component of displacement $w(r, \theta, t)$ satisfies the wave equation in two-space dimensions and time,

$$\Delta w \equiv \frac{1}{r}\frac{\partial}{\partial r}\left(r\frac{\partial w}{\partial r}\right) + \frac{1}{r^2}\frac{\partial^2 w}{\partial \theta^2} = \frac{1}{c^2}\frac{\partial^2 w}{\partial t^2}, \tag{8}$$

with the boundary conditions on the displacement field $w(r, \theta, t)$, for $r \leqslant ct$, given by

$$\sigma_{\theta z}(r, \pm\pi, t) = 0, \tag{9}$$

$$\sigma_{\theta z}(r < v't, \lambda\pi \pm \varepsilon, t) = 0, \tag{10}$$

$$w(ct, \theta, t) = \frac{2K_o}{\mu}\sqrt{\frac{ct}{2\pi}}\sin\frac{\theta}{2}. \tag{11}$$

Here (and elsewhere), ε is a vanishingly small positive constant, μ is the shear modulus, and

$$\sigma_{\theta z} = \frac{\mu}{r}\frac{\partial w}{\partial \theta}. \tag{12}$$

Condition (11) is a consequence of the continuity of the displacement field $w(r, \theta, t)$ at the wave front $r = ct$, that follows from Eq. (5). Notice that continuity of $\sigma_{\theta z}$ across the wave front follows from continuity of the displacement $w(r, \theta, t)$ there, and from Eq. (12). Moreover, there is a jump condition across the wave front $r = ct$ given by (Dempsey et al., 1982)

$$[\sigma_{rz}]_{r=ct} + \frac{\mu}{c}\left[\frac{\partial w}{\partial t}\right]_{r=ct} = 0, \tag{13}$$

where $[f]_r \equiv f(r + \varepsilon) - f(r - \varepsilon)$, with $\varepsilon \to 0$, and

$$\sigma_{rz} = \mu\frac{\partial w}{\partial r}. \tag{14}$$

Of interest is to establish the kind of singularity of the stress $\sigma_{\theta z}$ to be expected in the vicinity of the edge points B and D in Fig. 1, once the kink develops. Indeed,

the Williams expansion (Williams, 1952) imposes that the singularity of this stress component in the vicinity of these edge points should be given by

$$\sigma_{\theta z}(r,\theta,t) \sim r^p \quad \text{as } r \to 0, \tag{15}$$

where

$$p = \begin{cases} \dfrac{\lambda}{1-\lambda}, & \text{for } \lambda\pi < \theta < \pi, \\ \dfrac{-\lambda}{1+\lambda}, & \text{for } -\pi < \theta < \lambda\pi. \end{cases} \tag{16}$$

Finally, the asymptotic behavior of the stress field near the propagating crack tip is given by (Freund, 1990)

$$\sigma_{\theta z}(r,\lambda\pi \pm \varepsilon,t) = \left[\frac{K'}{\sqrt{2\pi(r-v't)}} + O(\sqrt{r-v't})\right] H(r-v't) \quad \text{as } r \to v't, \tag{17}$$

with K' the stress intensity factor after kinking and H the heaviside function.

3. Resolution of the dynamic crack kinking problem

3.1. Self-similar analysis

As a solution of the elasto-dynamic problem established in Eqs. (8)–(11), scaling analysis and the linearity of the wave equation imposes the following self-similar form for the displacement field:

$$w(r,\theta,t) = \frac{K_o}{\mu}\sqrt{\frac{r}{2\pi}}\left[2\sin\frac{\theta}{2} + W(r,\theta,t)\right], \tag{18}$$

where W is a dimensionless function of its arguments. Equivalently, the stress field takes the following form:

$$\sigma_{\theta z}(r,\theta,t) = \frac{K_o}{\sqrt{2\pi r}}\left[\cos\frac{\theta}{2} + S(r,\theta,t)\right], \tag{19}$$

with

$$S(r,\theta,t) = \frac{\partial W}{\partial\theta}(r,\theta,t). \tag{20}$$

Except for the stress intensity factor scale introduced by the boundary condition (11), there is neither a characteristic length nor a characteristic time against which the independent variables r, θ and t can be scaled. Therefore, W and S can only depend on dimensionless combinations of r, θ and t. These dimensional arguments determine the displacement function W and the stress function S to be written as

$$W(r,\theta,t) = W(\chi,\theta), \quad S(r,\theta,t) = S(\chi,\theta), \tag{21}$$

where

$$\chi \equiv \frac{ct}{r}, \quad \chi \geqslant 1. \tag{22}$$

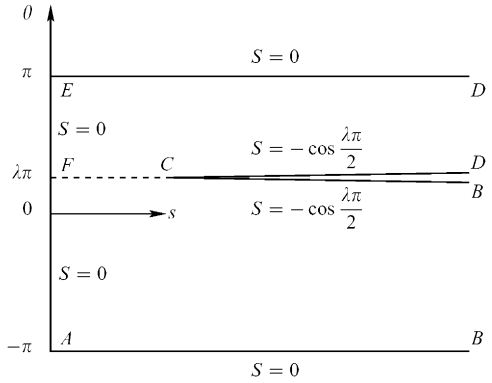

Fig. 2. The (s,θ)-plane, with $s \geqslant 0$ and $-\pi \leqslant \theta \leqslant \pi$, that maps the region III of (r,θ,t)-space, corresponding to $r \leqslant ct$, $-\pi \leqslant \theta \leqslant \pi$, and $t > 0$ (see Fig. 1).

Using Eqs. (8) and (18), and taking into account the explicit dependence of χ on r and t, one finds that W satisfies the following partial differential equation:

$$(\chi^2 - 1)\frac{\partial^2 W}{\partial \chi^2} + \frac{\partial^2 W}{\partial \theta^2} + \frac{1}{4}W = 0. \tag{23}$$

Let us make a new change of variable $\chi(s)$, by using the well-known Chaplygin's transformation (Dempsey et al., 1982; Broberg, 1999; Freund, 1990)

$$\chi(s) \equiv \cosh s, \quad s \geqslant 0. \tag{24}$$

In Fig. 2, the transformation from the coordinates system (r,θ,t) to the (s,θ)-plane is shown. Thus, in the space of coordinates (s,θ), Eq. (23) becomes

$$\frac{\partial^2 W}{\partial s^2} - \coth s \frac{\partial W}{\partial s} + \frac{\partial^2 W}{\partial \theta^2} + \frac{1}{4}W = 0. \tag{25}$$

The boundary conditions (9)–(11) can be easily re-expressed as boundary conditions on the displacement and stress functions W and S. In the new coordinates system, they take the form

$$W(s = 0, \theta) = 0, \tag{26}$$

$$S(s, \theta = \pm\pi) = 0, \tag{27}$$

$$S(s > b, \theta = \lambda\pi \pm \varepsilon) = -\cos\frac{\lambda\pi}{2}, \tag{28}$$

where

$$b \equiv \cosh^{-1}(c/v'). \tag{29}$$

The Williams expansion imposes that the asymptotic behavior of $\sigma_{\theta z}(r,\theta,t)$ in the vicinity of the edge points B and D should be weaker than the square root singularity;

the singularity of the stress field there is given by Eqs. (15) and (16). Therefore, in the vicinity of B and D the function $S(s,\theta)$ must satisfy

$$S(s,\theta) = -\cos\frac{\theta}{2} + O\left(\exp-\left(p+\frac{1}{2}\right)s\right) \quad \text{as } s\to+\infty, \tag{30}$$

with p given by Eq. (16). On the other hand, the asymptotic behavior near the crack tip, given by Eq. (17), imposes the following asymptotic behavior in the (s,θ)-plane:

$$S(s,\lambda\pi\pm\varepsilon) = -\cos\frac{\lambda\pi}{2} + \left[\frac{K'}{K_o}\frac{\sqrt{\coth b}}{\sqrt{b-s}} + O(\sqrt{b-s})\right]H(b-s) \quad \text{as } s\to b. \tag{31}$$

Finally, once the displacement field $w(r,\theta,t)$ is written in the form of Eqs. (18) and (21), the jump condition (13) across the cylindrical wave front $s=0$, corresponding to $r=ct$, is automatically satisfied.

3.2. Integral representation of the self-similar solution

Using the linearity of Eq. (25), it can be shown that the displacement function $W(s,\theta)$ admits solutions of the form

$$W(s,\theta) = \sinh s\, P^{-1}_{-1/2+\mathrm{i}v}(\cosh s)\Theta_v(\theta), \tag{32}$$

where v is a complex constant, and $P^{-1}_{-1/2+\mathrm{i}v}$ is the associated Legendre function of the first kind (Gradshteyn and Ryzhik, 1994). On the other hand, the function Θ_v satisfies the simple second order differential equation given by

$$\frac{\mathrm{d}^2\Theta_v}{\mathrm{d}\theta^2} - v^2\Theta_v = 0, \tag{33}$$

whose solution is a superposition of the functions $\sinh v\theta$ and $\cosh v\theta$. Notice that in Eq. (32), we did not take into account the solutions that contain the associated Legendre function of the second kind $Q^{-1}_{-1/2+\mathrm{i}v}(\cos s)$ (Gradshteyn and Ryzhik, 1994). This is due to the fact that only outgoing waves from $r=0$, corresponding to $s\to\infty$, are present in our problem. These waves are represented by the $P^{-1}_{-1/2+\mathrm{i}v}$ contribution. The absence of incoming radiation towards $r=0$, automatically cancels the $Q^{-1}_{-1/2+\mathrm{i}v}$ contribution. Using the integral representation of the associated Legendre functions given by (Gradshteyn and Ryzhik, 1994)

$$P^{\beta}_{\alpha}(\cosh s) = \sqrt{\frac{2}{\pi}}\frac{\sinh s^{\beta}}{\Gamma(\frac{1}{2}-\beta)}\int_0^s \frac{\cosh(\alpha+\frac{1}{2})s'}{(\cosh s-\cosh s')^{\beta+1/2}}\,\mathrm{d}s', \tag{34}$$

one can rewrite ($\beta=-1$, $\alpha=-1/2+\mathrm{i}v$), without loss of generality, the complete solution of Eq. (25) in the form

$$W(s,\theta) = \frac{2}{\pi}\int_0^s \sqrt{\cosh s-\cosh s'}\, f(s',\theta)\,\mathrm{d}s', \tag{35}$$

where $f(s,\theta)$ is an unknown function that satisfies the harmonic equation

$$\left[\frac{\partial^2}{\partial s^2}+\frac{\partial^2}{\partial\theta^2}\right] f(s,\theta)=0, \tag{36}$$

and the additional boundary condition.

$$\left[\frac{\partial}{\partial s} f(s,\theta)\right]_{s=0}=0. \tag{37}$$

It is straightforward to confirm a posteriori that the latter integral representation of $W(s,\theta)$, combined with conditions (36) and (37), is an exact solution of Eq. (25).

Also, notice that once the displacement function $W(s,\theta)$ is written in the form (35), the boundary condition (26) at the cylindrical wave front $s=0$ is automatically satisfied. The problem as it is posed now is tractable, at least numerically, because it allows the use of complex analysis and conformal mapping techniques.

3.3. Boundary conditions and asymptotic behavior

The solution of the dynamic kinking problem within the representation of Eqs. (35)–(37) of $W(s,\theta)$ is reduced to the determination of $f(s,\theta)$. Harmonicity of $f(s,\theta)$ means that it can be written as the real part of a complex function $F(\gamma=s+\mathrm{i}\theta)$, which is holomorphic inside the contour *DCBAED* (see Fig. 2):

$$f(s,\theta)=\mathrm{Re}[F(\gamma)]\equiv\frac{1}{2}[F(\gamma)+\overline{F(\gamma)}],\quad \gamma=s+\mathrm{i}\theta. \tag{38}$$

Using Eqs. (20) and (38) and the Cauchy identities for holomorphic functions, the function $S(s,\theta)$ can be written in the form

$$S(s,\theta)=\frac{2}{\pi}\sqrt{\cosh s-1}\,\mathrm{Im}[F(\mathrm{i}\theta)]-\int_0^s\frac{\sinh s'\,\mathrm{Im}[F(s'+\mathrm{i}\theta)]}{\sqrt{\cosh s-\cosh s'}}\,\frac{\mathrm{d}s'}{\pi}. \tag{39}$$

Condition (30) implies that the stress function $S(s,\theta)$ does not diverge as $s\to+\infty$. This imposes that

$$\mathrm{Im}[F(\mathrm{i}\theta)]=0. \tag{40}$$

Using again the Cauchy relations for holomorphic functions, one finds that Eq. (40) is sufficient for satisfying the boundary condition (37). Therefore, Eq. (39) is reduced to

$$S(s,\theta)=-\int_0^s\frac{\sinh s'\,\mathrm{Im}[F(s'+\mathrm{i}\theta)]}{\sqrt{\cosh s-\cosh s'}}\,\frac{\mathrm{d}s'}{\pi}. \tag{41}$$

Using Eq. (41), Expansions (30) in the vicinity of the wedge points B and D are completely recovered if the function F satisfies

$$\mathrm{Im}[F(\gamma)]=\sqrt{2}\exp\left[-\frac{s}{2}\right]\cos\frac{\theta}{2}+O(\exp-(p+1)s)\quad \text{as } s\to\infty. \tag{42}$$

The asymptotic behavior of the stress function $S(s,\theta)$ near the crack tip embodied in Eq. (31) imposes a specific behavior of $F(\gamma)$ in the neighborhood of the corresponding point $\gamma_C \equiv b + \mathrm{i}\lambda\pi$. This can be obtained by an Abel inversion of Eq. (41), or by noting the equality (Gradshteyn and Ryzhik, 1994)

$$\int_0^s \frac{\sinh(s'/2)\sinh s'\,\mathrm{d}s'}{\sqrt{\cosh s-\cosh s'}(\cosh s'-\cosh b\pm \mathrm{i}\varepsilon)} = \frac{\pi}{\sqrt{2}}\left[1-\frac{\sqrt{2}\sinh(b/2)}{\sqrt{\cosh b-\cosh s\mp \mathrm{i}\varepsilon}}\right]. \tag{43}$$

Identifying the behavior of Eq. (43) when $s \to b$ with that of Eq. (31), one concludes that $F(\gamma)$ behaves as

$$F(\gamma) \simeq \frac{\mathrm{i}a}{\gamma-\gamma_C} + O((\gamma-\gamma_C)^0) \quad \text{as } \gamma \to \gamma_C \equiv b + \mathrm{i}\lambda\pi, \tag{44}$$

where a is a real constant related to the stress intensity factor just after kinking, K', by

$$a = \frac{\sqrt{\cosh b}}{\sinh b}\frac{K'}{K_o}. \tag{45}$$

Thus, the function F has a simple pole at $\gamma = \gamma_C$. Also, the higher order terms in expansion (44) of $F(\gamma)$ are prescribed by the higher order terms in expansion (31) of the stress field S in the vicinity of the crack tip. In particular, logarithmic singularities of the form $\log(b-s)$ and terms of the form $(b-s)^\mu$, with $-1/2 < \mu < 1/2$, are forbidden.

We now turn to the condition imposed on $F(\gamma)$ by the boundary conditions (27) and (28) satisfied by S. The boundary conditions (27) on S implies that $F(\gamma)$ must satisfy

$$\mathrm{Im}[F(s \pm \mathrm{i}\pi)] = 0. \tag{46}$$

The boundary condition Eq. (28) of S means that $\mathrm{Im}[F]$ satisfies the following integral equation for $s > b$:

$$\int_b^s \frac{\sinh s'\,\mathrm{Im}[F(s'+\mathrm{i}(\lambda\pi\pm\varepsilon))]}{\sqrt{\cosh s-\cosh s'}}\frac{\mathrm{d}s'}{\pi} = g(s) \tag{47}$$

with

$$g(s) \equiv \cos\frac{\lambda\pi}{2} - \int_0^b \frac{\sinh s'\,\mathrm{Im}\,[F(s'+\mathrm{i}\lambda\pi)]}{\sqrt{\cosh s-\cosh s'}}\frac{\mathrm{d}s'}{\pi}. \tag{48}$$

We write this integral equation differently by noticing that Eq. (47) is in the form of an Abel integral equation (Freund, 1990). Thus, one can invert Eq. (47) to obtain

$$\mathrm{Im}[F(s+\mathrm{i}(\lambda\pi\pm\varepsilon))] = \frac{1}{\sinh s}\frac{\mathrm{d}}{\mathrm{d}s}\int_b^s \frac{\sinh s'\,g(s')}{\sqrt{\cosh s-\cosh s'}}\,\mathrm{d}s'. \tag{49}$$

Then using Eq. (48) for $g(s')$, one finally gets

$$\sqrt{\cosh s - \cosh b}\,\mathrm{Im}\,[F(s + \mathrm{i}(\lambda\pi \pm \varepsilon))]$$
$$= \cos\frac{\lambda\pi}{2} - \int_0^b \frac{\sqrt{\cosh b - \cosh s'}}{\cosh s - \cosh s'} \sinh s'\,\mathrm{Im}\,[F(s' + \mathrm{i}\lambda\pi)]\,\frac{\mathrm{d}s'}{\pi}. \tag{50}$$

The next step in solving our problem is to transform the strip geometry of Fig. 2 into a half-plane geometry by use of a conformal transformation of coordinates that is detailed in the following. The boundary conditions will be applied on the real axis of the new coordinate system.

4. Solution of the dynamic crack kinking problem

4.1. Conformal mapping

Let us map the interior of the contour $DCBAED$ in the γ-plane into the upper half-plane of a new coordinates system (ξ, η). The conformal mapping associated with this transformation is given by (Dempsey et al., 1982)

$$\gamma(\zeta) = (1+\lambda)\ln\left[\frac{1 + \xi_B\zeta + \sqrt{(1-\xi_B^2)(1-\zeta^2)}}{\zeta + \xi_B}\right]$$
$$+ (1-\lambda)\ln\left[\frac{1 - \xi_D\zeta + \sqrt{(1-\xi_D^2)(1-\zeta^2)}}{\zeta - \xi_D}\right] + \mathrm{i}\pi, \tag{51}$$

where $\zeta = \xi + \mathrm{i}\eta$. Fig. 3 shows the ζ-plane and the locations, on the ξ-axis, of the points corresponding to the vertices of the polygon $DCBAFED$, in the γ-plane. The conditions satisfied by ξ_B, and ξ_D are given by (Dempsey et al., 1982)

$$(1+\lambda)\frac{\sqrt{1-\xi_B^2}}{\xi_B} - (1-\lambda)\frac{\sqrt{1-\xi_D^2}}{\xi_D} = 0, \tag{52}$$

$$(1+\lambda)\cosh^{-1}\left[\frac{1}{\xi_B}\right] + (1-\lambda)\cosh^{-1}\left[\frac{1}{\xi_D}\right] = b. \tag{53}$$

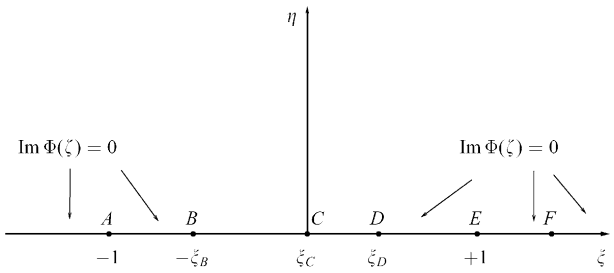

Fig. 3. The ζ-plane corresponding to the conformal mapping $\gamma(\zeta)$.

On the other hand, when $\gamma \to \gamma_C$, or equivalently $\zeta \to 0$, one has

$$\gamma(\zeta) \simeq \gamma_C + \frac{\gamma_2}{2}\,\zeta^2 + \frac{\gamma_3}{6}\,\zeta^3 + O(\zeta^4), \tag{54}$$

with

$$\gamma_2 \equiv \gamma''(0) = (1+\lambda)\,\frac{\sqrt{1-\xi_B^2}}{\xi_B}\left[\frac{1}{\xi_B} + \frac{1}{\xi_D}\right], \tag{55}$$

$$\gamma_3 \equiv \gamma'''(0) = 2(1+\lambda)\,\frac{\sqrt{1-\xi_B^2}}{\xi_B}\left[\frac{1}{\xi_D^2} - \frac{1}{\xi_B^2}\right]. \tag{56}$$

4.2. Solution in the ζ-space

We look for the analytic function $F(\gamma)$ on the new half-space, and we call it $\Phi(\zeta) \equiv F(\gamma(\zeta))$, with $\zeta = \xi + i\eta$. The function $\Phi(\zeta)$ is now holomorphic for $\mathrm{Im}[\zeta] > 0$, and the conditions it satisfies on the real axis of the ζ-plane are readily given from those of $F(\gamma)$ in the γ-plane. Eqs. (40) and (46) imply that

$$\mathrm{Im}[\Phi(\xi)] = 0 \quad \text{for } \xi > \xi_D \text{ or } \xi < -\xi_B. \tag{57}$$

Moreover, the function $\Phi(\zeta)$ should also satisfy

$$\lim_{|\zeta|\to\infty} \mathrm{Im}[\Phi(\zeta)] = 0. \tag{58}$$

This condition follows from the fact that $|\zeta| \to \infty$ corresponds to a point lying on the imaginary axis of the γ-plane ($s = 0$), where $\mathrm{Im}[F] = 0$. The behavior (42) of $F(\gamma)$, in the vicinity of the points D and B, leads to the two following limiting behaviors of $\Phi(\zeta)$:

$$\Phi(\zeta) \approx \beta_D + \alpha_D(\zeta - \xi_D)^{(1/2)(1-\lambda)} \quad \text{as } \zeta \to \xi_D, \tag{59}$$

$$\Phi(\zeta) \approx \beta_B - \alpha_B(-\zeta - \xi_B)^{(1/2)(1+\lambda)} \quad \text{as } \zeta \to -\xi_B, \tag{60}$$

where β_B and β_D are real unknown constants, and α_B and α_D are real constants given by

$$\alpha_D = \frac{2^{\lambda/2}(\xi_D + \xi_B)^{(1+\lambda)/2}}{(1-\xi_D^2)^{(1-\lambda)/2}(1 + \xi_B\xi_D + \sqrt{(1-\xi_B^2)(1-\xi_D^2)})^{(1+\lambda)/2}}, \tag{61}$$

$$\alpha_B = \frac{(\xi_B + \xi_D)^{(1-\lambda)/2}}{2^{\lambda/2}(1-\xi_B^2)^{(1+\lambda)/2}(1 + \xi_B\xi_D + \sqrt{(1-\xi_B^2)(1-\xi_D^2)})^{(1-\lambda)/2}}. \tag{62}$$

On the other hand, using Eq. (54), the behavior (44) of $F(\gamma)$ when $\gamma \to \gamma_C$ imposes the following behavior of $\Phi(\zeta)$ in the ζ-plane:

$$\Phi(\zeta) \simeq \frac{\mathrm{i}\alpha}{\zeta^2}(1+\beta\zeta) + O(\zeta^0) \quad \text{as } \zeta \to 0, \tag{63}$$

where α and β are real constants given by

$$\alpha = \frac{2a}{\gamma_2} = \frac{2\sqrt{\cosh b}}{\gamma_2 \sinh b}\frac{K'}{K_o}, \tag{64}$$

$$\beta = -\frac{\gamma_3}{3\gamma_2} = -\frac{2}{3}\left[\frac{1}{\xi_D} - \frac{1}{\xi_B}\right]. \tag{65}$$

In the region $-\xi_B < \xi < \xi_D$, the function Φ satisfies an integral equation given by the transformation of Eq. (50) in the ζ-plane.

4.3. A practical representation of the solution $\Phi(\zeta)$

It is possible to write a representation of $\Phi(\zeta)$, which satisfies the boundary conditions (57) and (58), and has the appropriate limiting behaviors of Eqs. (59), (60) and (63). Let us write a priori $\Phi(\zeta)$ as (Muskhelishvili, 1953)

$$\Phi(\zeta) = \alpha[\Phi_1(\zeta) + \Phi_2(\zeta)], \tag{66}$$

with α the constant of Eq. (64) that is proportional to the stress intensity factor K', and where $\Phi_1(\zeta)$ and $\Phi_2(\zeta)$ are two holomorphic functions for $\eta > 0$ given by

$$\Phi_1(\zeta) = \frac{a_0}{\zeta^2} + \frac{a_1}{\zeta} + \left[\frac{b_0}{\zeta^2} + \frac{b_1}{\zeta}\right]\Omega(\zeta), \tag{67}$$

$$\Phi_2(\zeta) = \int_{-\xi_B}^{\xi_D} \frac{\Omega_R(t)\psi(t)}{t-\zeta}\,\mathrm{d}t, \tag{68}$$

where

$$\Omega(\zeta) \equiv (\zeta - \xi_D)^{(1/2)(1-\lambda)}(\zeta + \xi_B)^{(1/2)(1+\lambda)}, \tag{69}$$

$$\Omega_R(t) \equiv (\xi_D - t)^{(1/2)(1-\lambda)}(\xi_B + t)^{(1/2)(1+\lambda)}. \tag{70}$$

Here, a_j and b_j are real constants, and $\psi(t)$ is a real continuous function in the interval $[-\xi_B, \xi_D]$. Written in the forms (67) and (68), the functions $\Phi_1(\zeta)$ and $\Phi_2(\zeta)$, and consequently $\Phi(\zeta)$, satisfy automatically condition (57). Moreover, when $|\zeta| \to \infty$, condition (58) is satisfied since all the constants a_1, a_2, b_1, b_2 are real, as well as $\psi(t)$. The real constants a_j and b_j are determined by condition (63) satisfied by $\Phi(\zeta)$, and consequently by $\Phi_1(\zeta)$, in the vicinity of $\zeta = 0$. After simple algebraic manipulations

one finds that

$$a_0 = -\tan[\lambda\pi/2], \tag{71}$$

$$b_0 = \frac{\sec[\lambda\pi/2]}{\xi_B^{(1+\lambda)/2}\,\xi_D^{(1-\lambda)/2}}, \tag{72}$$

$$a_1 = \beta a_0, \tag{73}$$

$$b_1 = \left[\beta + \frac{1-\lambda}{2\xi_D} - \frac{1+\lambda}{2\xi_B}\right] b_0. \tag{74}$$

The power law behavior of $\Phi(\zeta)$ for ζ close to $-\xi_B$ and ξ_D, as given by Eqs. (59) and (60), is readily satisfied by $\Phi_1(\zeta)$. On the other hand, the function $\Phi_2(\zeta)$ is the most general representation of an analytic function in the upper half-plane that satisfies the required behavior at $\zeta \simeq -\xi_B$ and at $\zeta \simeq \xi_D$, and whose imaginary part is zero on the segments of the real axis $\xi > \xi_D$ and $\xi < -\xi_B$. Indeed, for $-\xi_B < \xi < \xi_D$, one has (Muskhelishvili, 1953)

$$\mathrm{Im}[\Phi_2(\xi + \mathrm{i}\varepsilon)] = \frac{1}{2\mathrm{i}}[\Phi_2(\xi + \mathrm{i}\varepsilon) - \overline{\Phi_2}(\xi - \mathrm{i}\varepsilon)] = \pi\Omega_R(\xi)\psi(\xi), \tag{75}$$

a simple relation that guarantees the right behavior of $\Phi(\zeta)$ in the vicinity of the points B and D, and which also fixes, through Eqs. (59) and (60), the values of $\psi(-\xi_B)$ and $\psi(\xi_D)$.

Notice that the behavior of $\Phi(\zeta)$ for $\zeta \simeq 0$, as given by Eq. (63), is related to the behavior of $\psi(\xi)$ for $\xi \simeq 0$. Furthermore, let us recall that expansion (63) of $\Phi(\zeta)$ is prescribed by expansion (31) of the stress field S in the vicinity of the crack tip, where logarithmic singularities of the form $\log(b-s)$ and terms of the form $(b-s)^\mu$, with $-1/2 < \mu < 1/2$, are forbidden. Since the singular parts of $\Phi(\zeta)$ are already embedded in the function $\Phi_1(\zeta)$, the function $\Phi_2(\zeta)$ must not exhibit poles or singular behavior at $\zeta \simeq 0$. This result imposes that the function $\psi(\xi)$ must be of class C^1 for all $-\xi_B < \xi < \xi_D$ (i.e. continuous and with first derivative also continuous). This condition will be used in our numerical study in order to identify the proper stress intensity factor of the kinking problem.

Therefore, the problem of determining the solution $\Phi(\zeta)$ is now reduced to the determination of the real function $\psi(t)$ and of the real constant α. They are fixed by the integral equation (50) satisfied by Φ (or $\psi(t)$) in the region $-\xi_B < \xi < \xi_D$, combined with the complementary condition of the function $\psi(t)$ being of class C^1. Once the constant α is determined by this procedure, the stress intensity factor just after kinking is determined through the relation

$$\frac{K'(\lambda, v')}{K_o} \equiv H_{33}(\lambda, v'/c) = \frac{\sinh b}{\sqrt{\cosh b}}\, a = \frac{\sinh b}{2\sqrt{\cosh b}}\, \gamma_2\, \alpha. \tag{76}$$

A complete analytical solution cannot be derived in the general case. For the straight crack case ($\lambda = 0$), one can easily verify that the exact solution as found by Eshelby and Kostrov (Kostrov, 1966; Eshelby, 1969), is given in our approach by $\psi(t) = 0$ and a

stress intensity factor $K' = K_0\sqrt{1-v/c}$. For the general case, this problem will be solved numerically in the next section.

5. The stress intensity factor of the kinked crack

In our representation, the numerical problem consists in finding the function $\psi(t)$ and the real constant α using Eq. (50) and the condition of $\psi(t)$ being of class C^1. Except for α, the number of unknowns is equal to the number of available equations. Due to the presence of a singular behavior in the vicinity of the crack tip, and for numerical purpose, we modify in the following Eq. (50) into a more suitable integral equation.

Using Eq. (43), one can subtract the square root singular behavior in the integral equation (50), when $s \simeq b$. This leads to

$$\sqrt{\cosh s - \cosh b}\,[\mathrm{Im}[F(s + \mathrm{i}(\lambda\pi \pm \varepsilon))] - G(s)] = \cos\frac{\lambda\pi}{2} - \sqrt{2}a\cosh(b/2) - \int_0^b \frac{\sqrt{\cosh b - \cosh s'}}{\cosh s - \cosh s'}\sinh s'\,[\mathrm{Im}[F(s' + \mathrm{i}\lambda\pi)] - G(s')]\,\frac{\mathrm{d}s'}{\pi}, \tag{77}$$

where

$$G(s) = \frac{2a\sinh(s/2)\cosh(b/2)}{\cosh s - \cosh b}. \tag{78}$$

The integral appearing in the integral equation (77) can be written in a different form in order to avoid a numerical singularity when $s \simeq s' \simeq b$. The integral is first written using a complex variable representation as

$$I(s) \equiv \int_0^b \frac{\sqrt{\cosh b - \cosh s'}}{\cosh s - \cosh s'}\sinh s'\,[\mathrm{Im}\,[F(s' + \mathrm{i}\lambda\pi)] - G(s')]\,\frac{\mathrm{d}s'}{\pi} = \mathrm{Im}\int_\Gamma \frac{\sqrt{\cosh b - \cosh(\gamma - \mathrm{i}\lambda\pi)}}{\cosh s - \cosh(\gamma - \mathrm{i}\lambda\pi)}\sinh(\gamma - \mathrm{i}\lambda\pi)[F(\gamma) - \mathrm{i}G(\gamma - \mathrm{i}\lambda\pi)]\frac{\mathrm{d}\gamma}{\pi}, \tag{79}$$

where Γ is a curve in γ-space, with $\gamma = s' + \mathrm{i}\lambda\pi$ and $0 \leqslant s' \leqslant b$. This integration over Γ is now written in ζ-space, where the curve Γ starts on the ξ axis at the point F, enters into the upper half-plane and finishes at the point C that corresponds to the crack tip. Useful in this transformation of variables is the expression for $\gamma'(\zeta) = \mathrm{d}\gamma/\mathrm{d}\zeta$:

$$\gamma'(\zeta) = \frac{\mathrm{d}\gamma}{\mathrm{d}\zeta} = \frac{\gamma_2\zeta}{(1 + \zeta/\xi_B)(1 - \zeta/\xi_D)\sqrt{1-\zeta^2}}. \tag{80}$$

Since the integrand of (79) is an analytic function for $\mathrm{Im}[\zeta] > 0$, the contour of integration Γ in ζ-space can be deformed. Closing the integral with a segment on the ξ axis from F to infinity and then with quarter of a circle at infinity and finishing with the

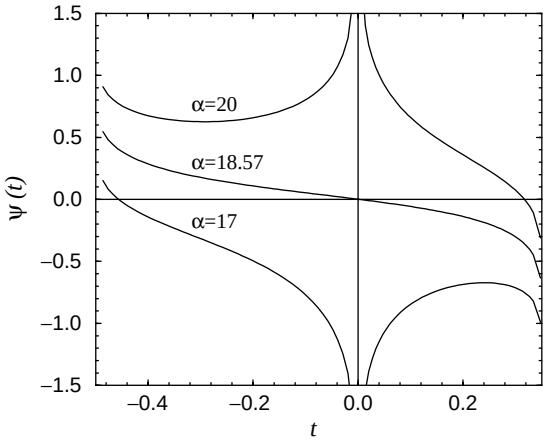

Fig. 4. Plot of the function $\psi(t)$ for $\lambda = 0.2$, $v'/c = 0.1$, and for different values of α.

vertical axis $\xi = 0$, one finds that the first two segments do not contribute, and the integral becomes

$$I(s) = -\mathrm{Im}\int_0^\infty \frac{\mathrm{i}d\eta}{\pi}\,\frac{\sqrt{\cosh b - \cosh(\gamma(\mathrm{i}\eta) - \mathrm{i}\lambda\pi)}}{\cosh s - \cosh(\gamma(\mathrm{i}\eta) - \mathrm{i}\lambda\pi)}\sinh(\gamma(\mathrm{i}\eta) - \mathrm{i}\lambda\pi)\gamma'(\mathrm{i}\eta)$$
$$\times[F(\gamma(\mathrm{i}\eta)) - \mathrm{i}G(\gamma(\mathrm{i}\eta) - \mathrm{i}\lambda\pi)]. \tag{81}$$

Using this new representation of the integral, the numerical resolution of Eq. (50) can be done without difficulty. For each value of α, one finds a function $\psi(t)$ that satisfies the integral equation (77), and one varies α until the condition of no singular behavior of $\psi(t)$ (or $\psi(t)$ of class C^1) at $t = 0$ is satisfied. The corresponding value of α being the one we are looking for. In Fig. 4, we show examples of functions $\psi(t)$ for fixed values of λ and v' and for different values of α. It is seen that $\psi(t)$ presents a singularity at $t = 0$ that is incompatible with the physical expansion (17) of the stress field in the vicinity of the crack tip. This singularity is absent for a unique value of α, the desired one, where the function $\psi(t)$ satisfies the condition of being of class C^1. In Fig. 5, we plot the stress intensity factor K' as function of the kinking angle and for different velocities.

6. Discussion

In this paper, we presented a general method for determining the elasto-dynamic stress fields associated with the propagation of anti-plane kinked or branched cracks. As a first illustration, we considered a semi-infinite anti-plane straight crack, initially propagating at a given time-dependent velocity, that changes instantaneously both its direction and its speed of propagation. This work can be considered as a continuation and a generalization of the works on equilibrium of star shaped cracks, cases that

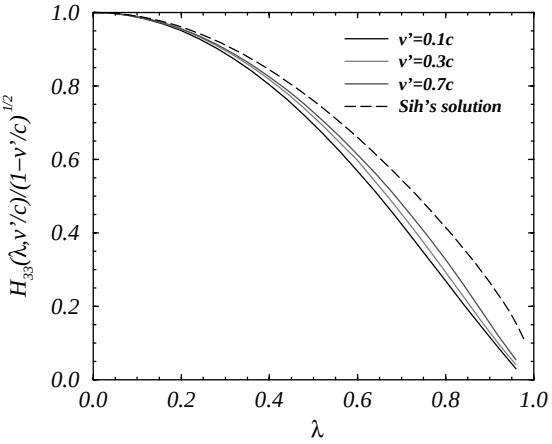

Fig. 5. Plot of the stress intensity factor function H_{33} as a function of the kinking angle and for different values of the crack tip velocity. Also shown in this figure, Sih's solution associated with the elasto-static kinking problem (Sih, 1965).

have been extensively studied (Sih, 1965; Amestoy and Leblond, 1992). It is also a generalization of the solutions found by Eshelby and Kostrov for the mode III straight dynamic crack (Eshelby, 1969; Kostrov, 1966, 1975; Freund, 1990). It also extends the class of self-similar solutions that were found for crack problems (Dempsey et al., 1982; Broberg, 1999; Willis, 1973).

Our approach allowed the exact calculation of the dynamic stress intensity factor for the dynamical kinked crack problem. The most important result of this study is displayed in Fig. 5. It is shown that our solution for vanishingly small velocity is different from the elasto-static solution, as given by Sih (1965), where the static stress intensity factor just after kinking, K_s', is related to the one just before kinking, K_0, by

$$K_s' = \left(\frac{1-\lambda}{1+\lambda}\right)^{\lambda/2} K_0. \tag{82}$$

This discrepancy was to be expected, since in this case the length of the kink is not time dependent and the propagating wave character of the solution is lost. Indeed, in Sih's solution, any small kink will modify the stress field all throughout the material, while in our representation of the kinking mechanism, the stress field is modified only within a cylindrical region limited by the cylindrical wave ct. Outside this region, the stress field remains unchanged with respect to the kinking process. Therefore, the propagation of bifurcated cracks should be seen as an intrinsically time dependent process, even if it occurs at vanishingly small speeds.

Although the equivalent in-plane dynamical kinked crack solutions remain to be found, the observed discrepancy between the elasto-static solution and the elasto-dynamic one with vanishingly small velocity, is expected to persist in that case also. Therefore, criteria of the path selection, such as the principle of local symmetry or the maximum energy release rate criterion, that have been developed for quasi-static crack

propagation, using elasto-static solutions (Amestoy and Leblond, 1992; Leblond, 1989) be reviewed at least for quantitative facts.

In order to study the dynamic branching instability, the next step of this work will be the determination of the stress fields associated with the anti-plane symmetrical branching problem.

Acknowledgements

M.A.-B. wishes to thank M. Ben Amar and J.R. Rice for enlightening discussions. This work was financed by an international collaboration CNRS-CONICYT. Laboratoire de Physique Statistique de l'Ecole Normale Supérieure is associé au CNRS (UMR 8550), et aux Universités Paris VI et Paris VII.

References

Amestoy, M., Leblond, J.B., 1992. Crack paths in plane situations—II. Detailed form of the expansion of the stress intensity factors. Int. J. Solids Struct. 29 (4), 465–501.

Broberg, K.B., 1999. Cracks and Fracture. Academic Press, London.

Burgers, P., 1982. Dynamic propagation of a kinked or bifurcated crack in antiplane strain. J. Appl. Mech. 49, 371–376.

Burgers, P., 1983. Dynamic kinking of a crack in plane strain. Int. J. Solids Struct. 19, 735–752.

Dempsey, J.P., Kuo, M.K., Achenbach, J.D., 1982. Mode III kinking under stress wave loading. Wave Motion 4, 181–190.

Eshelby, J.D., 1969. The elastic field of a crack extending nonuniformly under general anti-plane loading. J. Mech. Phys. Solids 17, 177–199.

Freund, L.B., 1990. Dynamic Fracture Mechanics. Cambridge University Press, New York.

Gradshteyn, I.S., Ryzhik, I.M., 1994. In: Jeffrey, A. (Ed.), Table of Integrals, Series, and Products, 5th Edition. Academic Press, New York.

Kostrov, B.V., 1966. Unsteady propagation of longitudinal shear cracks. Appl. Math. Mech. 30, 1241–1248.

Kostrov, B.V., 1975. On the crack propagation with variable velocity. Int. J. Fracture 11, 47–56.

Lawn, B., 1993. Fracture of Brittle Solids. Cambridge University Press, New York.

Leblond, J.B., 1989. Crack paths in plane situations—I. General form of the expansion of the stress intensity factors. Int. J. Solids Struct. 25, 1311–1325.

Muskhelishvili, N.I., 1953. Some Basic Problems of the Mathematical Theory of Elasticity. Noordhoff, Groningen.

Ravi-Chandar, K., Knauss, W.G., 1984. An experimental investigation into dynamic fracture—III. On steady-state crack propagation and crack branching. Int. J. Fracture 26, 141–154.

Sharon, E., Fineberg, J., 1996. Microbranching instability and the dynamic fracture of brittle materials. Phys. Rev. B 54, 7128–7139.

Sharon, E., Fineberg, J., 1999. Confirming the continuum theory of dynamic brittle fracture for fast cracks. Nature 397, 333–335.

Sih, G.C., 1965. Stress distribution near internal crack tips for longitudinal shear problems. J. Appl. Mech. 32, 51–58.

Williams, M.L., 1952. Stress singularities resulting from various boundary conditions in angular corners of plates in extension. J. Appl. Mech. 19, 526–528.

Willis, J.R., 1973. Self-similar problems in elastodynamics. Philos. Trans. R. Soc. (London) 274, 435–491.

ELSEVIER

Journal of the Mechanics and Physics of Solids
52 (2004) 1407–1420

JOURNAL OF THE
MECHANICS AND
PHYSICS OF SOLIDS

www.elsevier.com/locate/jmps

Brittle fracture dynamics with arbitrary paths. II. Dynamic crack branching under general antiplane loading

M. Adda-Bedia*

Laboratoire de Physique Statistique de l'Ecole Normale Supérieure, 24 rue Lhomond, F-75231 Paris Cedex 05, France

Received 12 June 2003; accepted 15 October 2003

Abstract

The dynamic propagation of a bifurcated crack under antiplane loading is considered. The dependence of the stress intensity factor just after branching is given as a function of the stress intensity factor just before branching, the branching angle and the instantaneous velocity of the crack tip. The jump in the dynamic energy release rate due to the branching process is also computed. Similar to the single crack case, a growth criterion for a branched crack is applied. It is based on the equality between the energy flux into each propagating tip and the surface energy which is added as a result of this propagation. It is shown that the minimum speed of the initial single crack which allows branching is equal to $0.39c$, where c is the shear wave speed. At the branching threshold, the corresponding bifurcated cracks start their propagation at a vanishing speed with a branching angle of approximately 40°.

Keywords: A. Crack branching and bifurcation; Dynamic fracture; Stress intensity factors; B. Crack mechanics; C. Analytic functions

1. Introduction

In a previous paper (Adda-Bedia and Arias, 2003), a method for determining the elastodynamic stress fields associated with the propagation of antiplane kinked or branched cracks was developed. As a first illustration, the case of a semi-infinite antiplane straight crack, initially propagating at a given time-dependent velocity, that changes instantaneously both its direction and its speed of propagation was considered. The aim of the

* Tel.: +33-1-44-32-25-26; fax: +33-1-44-32-34-33.
E-mail address: adda@lps.ens.fr (M. Adda-Bedia).

0022-5096/$ - see front matter © 2003 Elsevier Ltd. All rights reserved.
doi:10.1016/j.jmps.2003.10.001

present paper is to apply this method to the case of an initially propagating antiplane crack that branches into two cracks that merge symmetrically. The explicit dependence of the stress intensity factor just after branching is given as a function of the stress intensity factor just before branching, the branching angle and the instantaneous velocity of the crack tip.

A growth criterion for a branched crack must be based on the equality between the energy flux into the two propagating tips and the surface energy which is added as a result of this propagation. Eshelby proposed this approach (Eshelby, 1970; Rice et al., 1994) posing the question how large must be the single crack speed so that there will be enough energy available to form two slow cracks instead of the single fast one. Using the exact solution, the jump in the dynamic energy release rate due to the branching process is computed. It is shown that the minimum speed of the initial single crack which allows branching is equal to $0.39c$, where c is the shear wave speed. The corresponding bifurcated cracks start their propagation at a vanishing speed with a branching angle of 39.6°.

The paper is organized as follows. The next section summarizes the approach to the branched crack dynamics under mode III loading. The corresponding model problem is presented, and the self-similar solution that it admits is derived. The analysis of this section is similar to the dynamical kinked crack problem, and a detailed discussion can be found in Adda-Bedia and Arias (2003). In Section 3, the dynamic crack branching problem is completely solved. The self-similar solution of the corresponding problem is given by an integral representation, which is a convolution between a known kernel and a harmonic function, which is determined by a different method than that used for the kinked crack case (Adda-Bedia and Arias, 2003). It is shown that the problem can be reduced to the determination of a real function that satisfies a simple integral equation. Once the integral equation is solved, the stress intensity factor just after branching is computed a posteriori using an additional condition. In the last section, the stress intensity factor just after branching and the jump in the dynamic energy release rate due to the branching process are given for arbitrary angles and velocities. Finally, following Eshelby's approach (Eshelby, 1970; Rice et al., 1994), the growth criterion for a branched crack is applied, and the minimum speed of the initial single crack which can allow branching is computed.

2. The dynamical branched crack under mode III loading

Consider an elastic body which contains a branched crack but which is otherwise unbounded (see Fig. 1). Introduce a cylindrical coordinate system (r,θ,z) so that the z-axis lies along the crack edge. Suppose that the material is subjected to a loading which produces a state of antiplane shear deformation in the body. Thus the only nonzero component of displacement is the z-component $u_z(r,\theta,t) \equiv w(r,\theta,t)$, which is independent of z.

The scenario of crack branching is decomposed as follows. A semi-infinite straight crack that propagates at a speed $v(t)$ for $t < -\tau$, with $\tau \to 0^+$, suddenly stops at $t = -\tau$. At $t \to 0^+$, the crack branches locally with a branching angle equal to $\lambda\pi$,

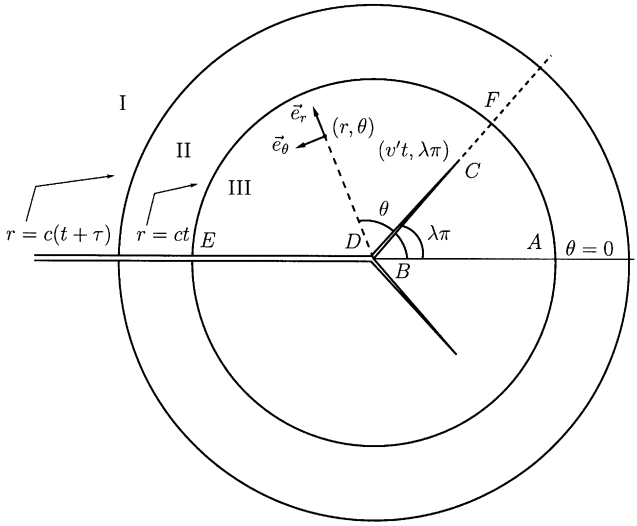

Fig. 1. A half-plane crack that propagates at a speed v for $t<-\tau$ suddenly stops at $t=-\tau$. For $t>0$, the new branches propagate straightly from the position $r=0$ at a velocity v', following the directions $\pm\lambda\pi$. The orthonormal basis $(\vec{e}_r,\vec{e}_\theta,\vec{e}_z)$ corresponding to the cylindrical coordinate system (r,θ,z) is shown. The cylindrical waves originated at the crack's arrest ($r=c(t+\tau)$) and at the start of branches propagation ($r=ct$) divide the material into three regions. In the region labelled I, the stress field comes only from the dynamical straight crack propagation, since the effects of the crack's arrest and the crack's branching are not experienced there. The region II is influenced by the crack arrest only, thus the stress field there is a static one (Eshelby, 1969; Freund, 1990). It is only the region III that is influenced by the crack's branching. Thus, one has to solve the branched crack problem only in this latter region.

with $0<\lambda<1$. For $t>0$, the new branches propagate straightly at a velocity $v'(t)$, following the new directions $\pm\lambda\pi$. The magnitude of the crack speed v and v' are restricted by $0<v<c$ and $0<v'<c$, where c denotes the shear wave speed. The mode III dynamic stress intensity factor, $K(t)$, of the straight crack prior to branching is related to the rest stress intensity factor, $K_0(t)$, of the same configuration by (Eshelby, 1969; Kostrov, 1966; Freund, 1990)

$$K(t)=k(v)K_0(t), \tag{1}$$

where $k(v)$ is a universal function of the instantaneous crack tip speed given by

$$k(v)=\sqrt{1-v/c}. \tag{2}$$

According to the latter description of crack branching, the dynamic stress intensity factor, K', just after branching should be defined by

$$K'(\lambda,v,v',c,\cdots)=\lim_{\tau\to0^+}\lim_{t\to0^+}\lim_{(r-v't)\to0^+}\sqrt{2\pi(r-v't)}\sigma_{\theta z}(r,\lambda\pi,t). \tag{3}$$

When the initial crack stops, a static stress distribution is restored behind a wave front that propagates from the crack tip at the shear wave speed (Eshelby, 1969; Freund, 1990), (see Fig. 1). Moreover, in the limit $t\to0^+$, the lengths of the branched

parts of the crack are vanishingly small, so that the breaking process after branching occurs in the region determined by the square root singular stress intensity factor field of the semi-infinite straight crack. Therefore, the branching problem consists in two symmetric branches reminiscent from a preexisting stationary straight crack, that start to propagate at time $t=0^+$, in the directions $\pm\lambda\pi$, with a velocity v', under the action of a time-independent loading, $\sigma^{\rm s}_{\theta z}(r,\theta)$, given by (Adda-Bedia and Arias, 2003)

$$\sigma^{\rm s}_{\theta z}(r,\theta)=\frac{K_0}{\sqrt{2\pi r}}\cos\frac{\theta}{2}, \tag{4}$$

where K_0 is the rest stress intensity factor of the crack tip prior to branching. A straightforward consequence of these dimensional arguments is that the stress intensity factor just after branching must be written as (Adda-Bedia and Arias, 2003)

$$K'=k(v')H_{33}(\lambda,v'/c)\,K_0, \tag{5}$$

where H_{33} is an unknown dimensionless function of the branching angle $\lambda\pi$ and of the crack tip speed v' only. The function H_{33} is universal in the sense that it depends on neither the loading configuration nor on the geometry of the body. Effectively, in the limits $t\to 0^+$ and $\tau\to 0^+$ that we consider, the dynamic branching problem does not involve radiation effects. So it is always equivalent to a crack propagating in an unbounded body. On the other hand, due to the absence of intrinsic time or length scales in linear elasticity theory, this problem becomes of general purpose, because it is not necessary for the crack and for the branches to be straight. H_{33} does not depend on the local curvature of the crack prior to or after branching (Adda-Bedia and Arias, 2003).

2.1. The model problem of dynamic crack branching

The process of crack advance in the situation depicted in Fig. 1 can be viewed as follows. For $t<0$, it is assumed that the crack is at rest and that the material is loaded according to Eq. (4). As the crack advances for $t>0$, the component of displacement $w(r,\theta,t)$ satisfies the wave equation

$$\frac{1}{r}\frac{\partial}{\partial r}\left(r\frac{\partial w}{\partial r}\right)+\frac{1}{r^2}\frac{\partial^2 w}{\partial\theta^2}=\frac{1}{c^2}\frac{\partial^2 w}{\partial t^2} \tag{6}$$

with boundary conditions on the displacement field $w(r,\theta,t)$, for $r\le ct$, given by

$$\sigma_{\theta z}(r,\pi,t)=0, \tag{7}$$

$$w(r,0,t)=0, \tag{8}$$

$$\sigma_{\theta z}(r<v't,\lambda\pi\pm\varepsilon,t)=0, \tag{9}$$

$$w(ct,\theta,t)=\frac{2K_0}{\mu}\sqrt{\frac{ct}{2\pi}}\sin\frac{\theta}{2}. \tag{10}$$

Here (and elsewhere), ε is a vanishingly small positive constant, μ is the shear modulus, and

$$\sigma_{\theta z}=\frac{\mu}{r}\frac{\partial w}{\partial\theta}.$$

Condition (8) follows from the symmetry property of $w(r,\theta,t)$ with respect to reflection in the plane $\theta=0$. Condition (9) is a consequence of the continuity of the displacement field $w(r,\theta,t)$ at the wave front $r=ct$. Moreover, the dynamic jump condition across the wave front $r=ct$ is given by (Dempsey et al., 1982)

$$[\sigma_{rz}]_{r=ct}+\frac{\mu}{c}\left[\frac{\partial w}{\partial t}\right]_{r=ct}=0, \tag{11}$$

where

$$\sigma_{rz}=\mu\frac{\partial w}{\partial r}.$$

The Williams expansion (Williams, 1952) imposes that the singularity of $\sigma_{\theta z}(r,\theta,t)$ in the vicinity of the edge points B and D should be given by

$$\sigma_{\theta z}(r,\theta,t)\sim r^{p} \quad \text{as} \quad r\to 0, \tag{12}$$

where

$$p=\begin{cases}\dfrac{\lambda}{1-\lambda} & \text{for } \lambda\pi<\theta<\pi,\\[2ex] -1+\dfrac{1}{2\lambda} & \text{for } 0<\theta<\lambda\pi.\end{cases} \tag{13}$$

The asymptotic behavior of the stress field near the propagating crack tip is given by (Freund, 1990)

$$\sigma_{\theta z}(r,\lambda\pi\pm\varepsilon,t)=\left[\frac{K'}{\sqrt{2\pi(r-v't)}}+O(\sqrt{r-v't})\right]H(r-v't)$$
$$\text{as} \quad r\to v't, \tag{14}$$

where H is the heaviside function.

2.2. Self-similar analysis

Except the stress intensity factor scale introduced by the boundary condition (10), there is neither a characteristic length nor a characteristic time against which the independent variables r and t can be scaled. Therefore, the displacement field takes the following self-similar form (Adda-Bedia and Arias, 2003):

$$w(r,\theta,t)=\frac{K_0}{\mu}\sqrt{\frac{r}{2\pi}}\left[2\sin\frac{\theta}{2}+W(s,\theta)\right], \tag{15}$$

where

$$s\equiv\cosh^{-1}\left(\frac{ct}{r}\right), \quad s\geqslant 0 \tag{16}$$

and W is a dimensionless function of its arguments (Miles, 1960; Dempsey et al., 1982; Broberg, 1999). Equivalently, the stress field takes the following form:

$$\sigma_{\theta z}(r,\theta,t)=\frac{K_0}{\sqrt{2\pi r}}\left[\cos\frac{\theta}{2}+S(s,\theta)\right] \tag{17}$$

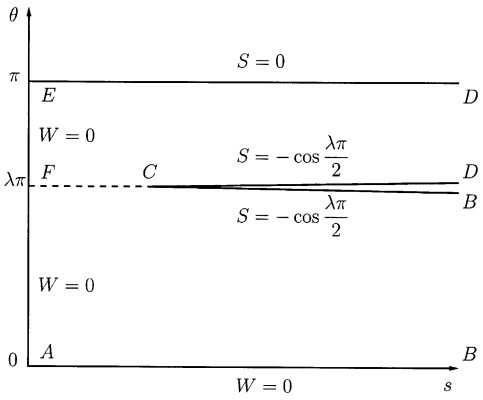

Fig. 2. The (s,θ)-plane, with $s \geqslant 0$ and $0 \leqslant \theta \leqslant \pi$, that maps the region III of (r,θ,t)-space, corresponding to $r \leqslant ct$, $0 \leqslant \theta \leqslant \pi$, and $t > 0$ (see Fig. 1).

with

$$S(s,\theta) = \frac{\partial W}{\partial \theta}(s,\theta). \tag{18}$$

In Fig. 2, the transformation from the coordinates system (r,θ,t) to the (s,θ)-plane is shown. Taking into account the explicit dependence of s on r and t, one finds that W satisfies the partial differential equation

$$\frac{\partial^2 W}{\partial s^2} - \coth s \frac{\partial W}{\partial s} + \frac{\partial^2 W}{\partial \theta^2} + \frac{1}{4} W = 0. \tag{19}$$

The singularity of the stress field in the vicinity the edge points B and D, as given by Eq. (12), imposes the behavior to the function $S(s,\theta)$

$$S(s,\theta) = -\cos\frac{\theta}{2} + O\left(\exp - \left(p + \frac{1}{2}\right) s\right) \quad \text{as } s \to +\infty, \tag{20}$$

On the other hand, the asymptotic behavior near the crack tip (14) imposes the following asymptotic behavior in the (s,θ)-plane:

$$S(s,\lambda\pi \pm \varepsilon) = -\cos\frac{\lambda\pi}{2} + \left[\frac{K'}{K_0}\frac{\sqrt{\coth b}}{\sqrt{b-s}} + O\left(\sqrt{b-s}\right)\right] H(b-s)$$

$$\text{as} \quad s \to b, \tag{21}$$

where

$$b \equiv \cosh^{-1}(c/v'). \tag{22}$$

The boundary conditions (7)–(10) are easily transformed into conditions on W and S. They are given by

$$S(s,\pi) = 0, \tag{23}$$

$$W(s,0) = 0, \tag{24}$$

$$S(s > b, \lambda\pi \pm \varepsilon) = -\cos\frac{\lambda\pi}{2}, \tag{25}$$

$$W(0,\theta) = 0. \tag{26}$$

Once the displacement field $w(r,\theta,t)$ is written under the form (15), the jump condition (11) across the cylindrical wave front $s = 0$, corresponding to $r = ct$, is automatically satisfied.

3. Solution of the dynamic crack branching problem

In Adda-Bedia and Arias (2003), it has been shown that Eq. (19) admits solutions of the form

$$W(s,\theta) = \frac{2}{\pi}\int_0^s \sqrt{\cosh s - \cosh s'}\,\Phi(s',\theta)\,\mathrm{d}s', \tag{27}$$

where $\Phi(s,\theta)$ is an unknown function that satisfies the harmonic equation

$$\left[\frac{\partial^2}{\partial s^2} + \frac{\partial^2}{\partial\theta^2}\right]\Phi(s,\theta) = 0, \tag{28}$$

and the additional boundary condition

$$\left[\frac{\partial}{\partial s}\Phi(s,\theta)\right]_{s=0} = 0. \tag{29}$$

Note that once the displacement function $W(s,\theta)$ is written in the form (27), the boundary condition (26) at the cylindrical wave front $s = 0$ is automatically satisfied. Eq. (28) implies that the function $\Phi(s,\theta)$ is readily given by the real part of a complex function $F(\gamma = s + \mathrm{i}\theta)$, which is holomorphic inside the contour $DCBAED$ (see Fig. 2):

$$\Phi(s,\theta) = \mathrm{Re}[F(\gamma)] \equiv \frac{1}{2}[F(\gamma) + \overline{F(\gamma)}], \quad \gamma = s + \mathrm{i}\theta. \tag{30}$$

Using Eq. (30) and Cauchy relations for holomorphic functions, the function $S(s,\theta)$ can thus be written in the form

$$S(s,\theta) = \frac{1}{\pi}\sqrt{\cosh s - 1}\,\mathrm{Im}[F(\mathrm{i}\theta)] - \int_0^s \frac{\sinh s'\,\mathrm{Im}[F(s' + \mathrm{i}\theta)]}{\sqrt{\cosh s - \cosh s'}}\,\frac{\mathrm{d}s'}{\pi}. \tag{31}$$

Condition (20) imposes that the stress function $S(s,\theta)$ is not diverging at $s \to +\infty$. This imposes that

$$\mathrm{Im}[F(\mathrm{i}\theta)] = 0. \tag{32}$$

Moreover, Eq. (32) is a sufficient condition for satisfying the boundary condition (29). Therefore, Eq. (31) is reduced to

$$S(s,\theta) = -\int_0^s \frac{\sinh s'\,\mathrm{Im}[F(s' + \mathrm{i}\theta)]}{\sqrt{\cosh s - \cosh s'}}\,\frac{\mathrm{d}s'}{\pi}. \tag{33}$$

Using Eq. (33), expansion (20) in the vicinity of the wedge points B and D are recovered if the function F satisfies the following behavior:

$$\mathrm{Im}[F(\gamma)] \to \sqrt{2}\exp\left[-\frac{s}{2}\right]\cos\frac{\theta}{2} \quad \text{as } \gamma \to \infty. \tag{34}$$

The asymptotic behavior near the crack tip embodied in Eq. (21) imposes a specific behavior of $F(\gamma)$ in the neighborhood of the corresponding point $\gamma_C \equiv b + \mathrm{i}\lambda\pi$. It can be shown that $F(\gamma)$ behaves as (Adda-Bedia and Arias, 2003)

$$F(\gamma) = \frac{\mathrm{i}a}{\gamma - \gamma_C} + O((\gamma - \gamma_C)^0) \quad \text{as} \quad \gamma \to \gamma_C \equiv b + \mathrm{i}\lambda\pi, \tag{35}$$

where a is a real constant that satisfies

$$a = \frac{\sqrt{\cosh b}}{\sinh b}\frac{K'}{K_0}. \tag{36}$$

Thus, the function F has a simple pole at $\gamma = \gamma_C$. The boundary conditions (23), (24) on S imply that $F(\gamma)$ must satisfy

$$\mathrm{Im}[F(s + \mathrm{i}\pi)] = 0, \tag{37}$$

$$\mathrm{Re}[F(s)] = 0. \tag{38}$$

Finally, the transformation of the boundary condition (25) on S onto a condition satisfied by F leads to (Adda-Bedia and Arias, 2003)

$$\sqrt{\cosh s - \cosh b}\,\mathrm{Im}\,[F(s + \mathrm{i}(\lambda\pi \pm \varepsilon))] = \cos\frac{\lambda\pi}{2} - \int_0^b \frac{\sqrt{\cosh b - \cosh s'}}{\cosh s - \cosh s'}\sinh s'\,\mathrm{Im}\,[F(s' + \mathrm{i}\lambda\pi)]\frac{\mathrm{d}s'}{\pi}, \quad s > b. \tag{39}$$

The holomorphic function $F(\gamma)$ is uniquely determined by conditions (32), (34), (35), (37)–(39). On the other hand, using Eq. (36), the stress intensity factor just after branching, K', is determined once the real constant a is fixed.

In the following, the dynamic crack branching problem will be solved using a different method than the one for the dynamic kinked crack problem (Adda-Bedia and Arias, 2003). For the present case, it is possible to get a suitable representation of the function $F(\gamma)$ without mapping it into a complex half-plane (Adda-Bedia and Arias, 2003). An intermediate solution of $F(\gamma)$, which satisfies the conditions (32), (35), (37), (38), is given by

$$F(\gamma) = 2a\cosh(b/2)\,[F_1(\gamma) + F_2(\gamma)], \tag{40}$$

where $F_1(\gamma)$ and $F_2(\gamma)$ are holomorphic functions inside the contour $DCBAED$, given by

$$F_1(\gamma) = \mathrm{i}\left[\frac{\sinh((\gamma - \mathrm{i}\lambda\pi)/2)}{\cosh(\gamma - \mathrm{i}\lambda\pi) - \cosh(b)} + \frac{\sinh((\gamma + \mathrm{i}\lambda\pi)/2)}{\cosh(\gamma + \mathrm{i}\lambda\pi) - \cosh(b)}\right], \tag{41}$$

$$F_2(\gamma) = \mathrm{i}\int_b^\infty \left[\frac{\sinh((\gamma - \mathrm{i}\lambda\pi)/2)}{\cosh(\gamma - \mathrm{i}\lambda\pi) - \cosh(t)} + \frac{\sinh((\gamma + \mathrm{i}\lambda\pi)/2)}{\cosh(\gamma + i\lambda\pi) - \cosh(t)}\right] f(t)\,\mathrm{d}t, \tag{42}$$

with $f(t)$ a real continuous function defined for $t > b$. Written in the forms (41), (42), the functions $F_1(\gamma)$ and $F_2(\gamma)$, and consequently $F(\gamma)$, satisfy automatically the conditions (32), (37), (38). Also, condition (35) is automatically satisfied by $F(\gamma)$, through $F_1(\gamma)$. Finally, notice that $F_2(\gamma)$, as given by Eq. (42), is the most general representation of a holomorphic function that satisfy the conditions (32), (37), (38).

Therefore, the complete determination of the function $F(\gamma)$ is now reduced to finding the real function f and the real constant a. They are fixed by the integral equation (39) satisfied by F (or f), combined with the additional condition (34), which can be rewritten as

$$2\sqrt{2}\,a\cos(\lambda\pi/2)\cosh(b/2)\left[1+\int_b^\infty f(t)\,\mathrm{d}t\right]=1. \tag{43}$$

Using Eqs. (36) and (43), the stress intensity factor just after branching, K', is then given by

$$\frac{K'}{K_0}\equiv k(v')\,H_{33}(\lambda,v'/c)=\frac{k(v')}{2\cos(\lambda\pi/2)[1+\int_b^\infty f(t)\,\mathrm{d}t]}. \tag{44}$$

The function f must satisfy the integral equation (39), which can be simplified to (see Appendix A)

$$f(s)=A(s,b)+\int_b^\infty A(s,u)f(u)\,\mathrm{d}u,\quad s>b, \tag{45}$$

$$A(s,u)=\frac{1}{\pi}\frac{\cosh(s/2)}{\cosh(u/2)}\,\mathrm{Im}\left[\frac{\sinh(u-2\mathrm{i}\lambda\pi)}{\cosh(s)-\cosh(u-2\mathrm{i}\lambda\pi)}\right]. \tag{46}$$

Note that Eqs. (45) and (46) do not involve the real constant a. Therefore, the latter integral equation can be solved independently of the value of the constant a. Once the function f is determined, the stress intensity factor just after branching is computed *a posteriori*, by using Eq. (44).

A complete analytical solution of the integral equation (45) cannot be derived in the general case. However, for the special case $\lambda=1/2$, it is straightforward to show that $A(s,u)=0$. Therefore, the solution of Eq. (45) is readily given by $f(s)=0$, and Eq. (44) yields

$$H_{33}(1/2,v'/c)=\frac{1}{\sqrt{2}}. \tag{47}$$

For the general case, the numerical resolution of integral equation (45) can be done without difficulty. In Fig. 3, examples of solutions are shown for some values of λ and v'. In Fig. 4, the function $H_{33}(\lambda,v'/c)$ is plotted as a function of the branching angle and for some values of the speed of the crack branches. Note that in Fig. 4, the interval $1/2\leqslant\lambda\leqslant 1$ has not been considered, because it is not pertinent for the subsequent discussion.

4. Results and discussion

Using a method developed in Adda-Bedia and Arias (2003), the elastodynamic stress fields associated with the propagation of antiplane branched cracks have been determined. Within this approach, the dynamic stress intensity factor just after branching, as given by Eq. (5), is computed as a function of the stress intensity factor just before branching, the branching angle and the instantaneous velocity of the crack tip. The corresponding results are summarized in Fig. 4. First, it is shown that $H_{33}(0,v'/c)=1/\sqrt{2}$,

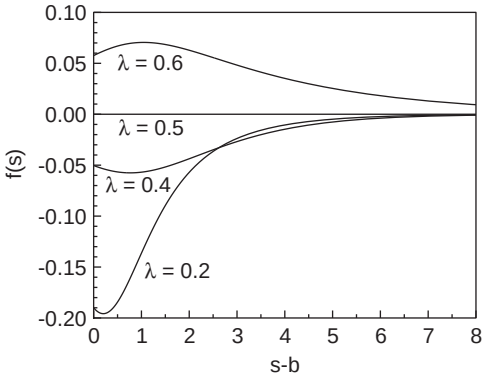

Fig. 3. Plot of the function $f(s)$, solution of Eq. (45), for some values of the branching angle and for $v'/c = 0.2$.

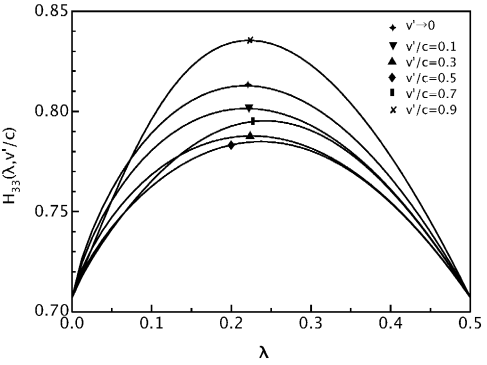

Fig. 4. Plot of the function H_{33} as a function of the branching angle and for some values of the crack tip speed just after branching. Note that $K'/K_0 = \sqrt{1 - v'/c}\, H_{33}(\lambda, v'/c)$, where K' is the dynamic stress intensity factor just after branching, and K_0 is the rest stress intensity factor just before branching. Note that for $\lambda \to 0$, H_{33} coincides exactly with the corresponding elastostatic result given by Eq. (48).

independently of v'. For a given branches velocity, H_{33} increases with λ, attains a maximum at a given branching angle that depends on v', and decreases again with λ, by satisfying $H_{33}(1/2, v'/c) = 1/\sqrt{2}$ and $H_{33}(1, v'/c) = 0$. However, the principal result of Fig. 4 concerns the dynamic stress intensity factor just after branching for a vanishingly small velocity. The latter quantity coincides exactly with the stress intensity factor just after branching computed by using an elastostatic approach (Smith, 1968),

$$H_{33}(\lambda, v' \to 0) = \frac{1}{\sqrt{2}} \left(\frac{1-\lambda}{\lambda} \right)^{\lambda/2}. \tag{48}$$

This result differs from the previous one dealing with the kinked crack configuration (Adda-Bedia and Arias, 2003), where the dynamic stress intensity factor just after kinking for a vanishingly small velocity was found to be slightly different from the

corresponding elastostatic solution. This difference may be due to numerical errors induced by the method used in Adda-Bedia and Arias (2003) for computing the dynamic stress intensity factor just after kinking. Indeed, the present approach, as given in Section 3 and in Appendix A, is more elaborated than in Adda-Bedia and Arias (2003). The representation of the function $F(\gamma)$, as given by Eqs. (40)–(42) allowed analytical computations without mapping the function $F(\gamma)$ into a complex half-plane. As a consequence, the resolution of the numerical problem, as given by Eqs. (45) and (46), has been straightforward. Applying the same approach for the kinked crack case would be necessary for validating the behavior of the dynamic stress intensity factor just after kinking, as a function of the kinking angle and of the velocity just after kinking. Unfortunately, an equivalent representation of the corresponding function $F(\gamma)$ for the kinked crack case is not available yet.

4.1. Dynamic branching instability

Eshelby (1970) posed the question how large must be the single crack speed so that there will be enough energy available to form two slow cracks instead of the single fast one. The simplest branched configuration that Eshelby analyzed is the limiting case where the branches subtend a vanishingly small angle and both prolong the original crack plane. In this case, Eshelby reported $v = 0.6c$ and $v' \to 0$ as the minimum speeds which could allow branching or surface roughening (Eshelby, 1970). However, since no solution was available for two branches with an arbitrary angle between them and propagating at arbitrary velocities, this result has been considered as a rough estimate.

The dynamic energy release rate is a quantity associated to a single moving crack tip. It is defined as the rate of mechanical energy flow out of the body and into the crack tip per unit crack advance. For the single moving crack before branching, it is given by (Freund, 1990)

$$G = \frac{K^2}{2\mu\sqrt{1 - v^2/c^2}} = \frac{1}{2\mu}\, g(v) K_0^2, \tag{49}$$

where K_0 is the rest stress intensity factor, and

$$g(v) = \sqrt{\frac{1 - v/c}{1 + v/c}}. \tag{50}$$

The function $g(v)$ does not depend on the details of the applied loading or the configuration of the body being analyzed. It depends on the local instantaneous speed of the crack tip and on the properties of the material only. Due to the symmetry of the branching configuration, the energy release rate just after branching G' of each crack tip is given by

$$G' = \frac{K'^2}{2\mu\sqrt{1 - v'^2/c^2}} = \frac{1}{2\mu}\, g(v') H_{33}^2(\lambda, v'/c) K_0^2. \tag{51}$$

In Fig. 5, the energy release rate just after branching G' is plotted as a function of the branching angle and for some values of the velocity just after branching. It is

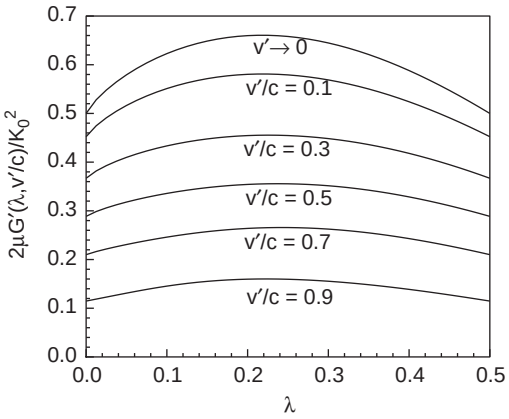

Fig. 5. Plot of the energy release rate just after branching G', scaled by $K_0^2/(2\mu)$, as a function of the branching angle and for some values of the crack tip speed just after branching.

shown that for a constant branching angle, G' is a decreasing function of v'. Therefore, the energy release rate just after branching is maximized when the branches start to propagate quasi-statically ($v' \to 0$). Moreover, G' always displays a maximum at a given branching angle that depends on the branches velocity v'.

According to the Generalized Griffith's criterion (Griffith, 1920), a crack must grow in such a way that its energy release rate is equal to the dynamic fracture energy of the material, Γ, which is assumed to be a property of the material and whose value may depend on the instantaneous crack tip speed. This growth criterion should be applied for each crack tip before and after branching. At the onset of branching, the conditions

$$G \equiv \Gamma(v) \quad \text{and} \quad G' \equiv \Gamma(v'), \tag{52}$$

should be satisfied. Therefore, the growth criterion introduces an intrinsic relationship between the energy release rates just before and just after branching, which reads

$$G' = \frac{\Gamma(v')}{\Gamma(v)}\, G. \tag{53}$$

Eq. (53) is a necessary condition for the existence of a branching configuration. Otherwise, the single crack tip propagation should be maintained. Moreover, condition (53) shows that if a branching instability occurs, it is universal in the sense that it does not depend either on the loading configuration or on the geometry of the body. The branching thresholds depend on the properties of the material only. In the case of a constant fracture energy, Eq. (53) reduces to

$$g(v) = g(v')H_{33}^2(\lambda, v'/c). \tag{54}$$

Eq. (50) shows that $g(v)$ is a decreasing function of the velocity, which satisfies $g(0) = 1$, and $g(c) = 0$. Moreover, Fig. 5 shows that the right-hand side of Eq. (54) displays a maximum, whose value is smaller than unity. Therefore, branched solutions exist only if the velocity v exceeds a critical velocity v_c. This threshold is given by the

least velocity v for which Eq. (54) admits a solution. This solution corresponds to a branched configuration with a speed $v_c' \to 0$, and a branching angle of 39.6° ($\lambda_c = 0.22$), given by the maximum of $H_{33}(\lambda, 0)$. Using Eq. (54), one finds that the corresponding critical speed of the single crack tip speed before branching is given by $v_c = 0.39c$.

The thresholds of the branching instability given by ($v_c' \to 0, \lambda_c = 0.22, v_c = 0.39c$) have to be compared to the ones reported by Eshelby (1970), ($v_c' \to 0, \lambda_c \to 0, v_c = 0.6c$). The assumptions of zero branching angle and vanishing branches velocity were necessary, as no solution was available for two branches with an arbitrary angle between them and propagating at an arbitrary speed. The present exact computations confirm that the resultant zero velocity after branching is the least velocity for which a branched configuration exists. Consequently, the critical branching angle, which is computed directly from the elastostatic solution, is given by the maximum of $H_{33}(\lambda, 0)$. Therefore, the resultant critical velocity of the initial single crack is smaller than the one computed from the zero branching angle assumption.

Finally, the critical speed for branching, $v_c = 0.39c$, agrees with the one deduced from numerical simulations using a phase field model of brittle fracture under antiplane loading (Lobkovsky and Karma, 2003). However, since dynamic fracture experiments are often performed under inplane situations, a theoretical study of this case is still lacking. Although the resolution of a branched configuration of a dynamical crack under inplane loading seems difficult to perform, the analogy with the mode III loading suggests that a quasistatic approach would be sufficient, or at least a good approximation, for the determination of the branching instability thresholds.

Acknowledgements

I wish to thank R. Arias, M. Ben Amar and J.R. Rice for enlightening discussions. Laboratoire de Physique Statistique de l'Ecole Normale Supérieure is associated with CNRS (UMR 8550) and with Universities Paris VI and Paris VII.

Appendix A

In the following, we focus on the transformation of the integral equation (39) into Eq. (45). Using the representations (41), (42), it is shown that

$$\mathrm{Im}[F(s + \mathrm{i}\lambda\pi)] = 2a \cosh(b/2) \left[I(s,b) + \int_b^\infty I(s,t) f(t)\, \mathrm{d}t \right], \tag{A.1}$$

$$I(s,t) = \mathrm{Re} \left[\frac{\sinh(s/2)}{\cosh(s) - \cosh(t)} + \frac{\sinh((s + 2\mathrm{i}\lambda\pi)/2)}{\cosh(s + 2\mathrm{i}\lambda\pi) - \cosh(t)} \right]. \tag{A.2}$$

Eq. (A.2) can be easily transformed into

$$I(s,t) = \frac{\sinh(s/2)}{\cosh(s) - \cosh(t)} + \frac{\sinh(s/2)}{\cosh(t/2)} \mathrm{Re} \left[\frac{\cosh((t - 2\mathrm{i}\lambda\pi)/2)}{\cosh(s) - \cosh(t - 2\mathrm{i}\lambda\pi)} \right]. \tag{A.3}$$

Using Eqs. (A.1) and (A.3), the integration over s' in Eq. (39) can be computed analytically. After some algebraic manipulation and using Eq. (43), an integral equation satisfied by the real function f is deduced. It is given by

$$\int_b^\infty \frac{\sqrt{\cosh(t)-\cosh(b)}}{\cosh(t)-\cosh(s)} f(t)\sinh(t/2)\,\mathrm{d}t = H(s,b) + \int_b^\infty H(s,t) f(t)\,\mathrm{d}t, \quad \text{(A.4)}$$

$$H(s,t) = \mathrm{Re}\left[\frac{\sinh(t-2\mathrm{i}\lambda\pi)}{2\cosh(t/2)} \frac{\sqrt{\cosh(t-2\mathrm{i}\lambda\pi)-\cosh(b)}}{\cosh(s)-\cosh(t-2\mathrm{i}\lambda\pi)}\right], \quad \text{(A.5)}$$

where the integral in the left-hand side of Eq. (A.4) must be taken in the sense of Cauchy principal value. One can write Eq. (A.4) differently by noticing that it is in the form of a Hilbert singular integral equation. Thus, one can invert it to obtain (Muskhelishvili, 1953)

$$f(s) = A(s,b) + \int_b^\infty A(s,u) f(u)\,\mathrm{d}u, \quad s > b, \quad \text{(A.6)}$$

$$A(s,u) = -2\cosh(s/2) \int_b^\infty \frac{H(t,u)\sinh(t)}{\sqrt{\cosh(t)-\cosh(b)}(\cosh(t)-\cosh(s))} \frac{\mathrm{d}t}{\pi^2}. \quad \text{(A.7)}$$

Using Eq. (A.5), one can compute analytically the integration over the variable t in Eq. (A.7). The result leads to Eq. (46).

References

Adda-Bedia, M., Arias, R., 2003. Brittle fracture dynamics with arbitrary paths-I. Dynamic crack kinking under general antiplane loading. J. Mech. Phys. Solids 51, 1287–1304.

Broberg, K.B., 1999. Cracks and Fracture. Academic Press, London.

Dempsey, J.P., Kuo, M.K., Achenbach, J.D., 1982. Mode III kinking under stress wave loading. Wave Motion 4, 181–190.

Eshelby, J.D., 1969. The elastic field of a crack extending nonuniformly under general antiplane loading. J. Mech. Phys. Solids 17, 177–199.

Eshelby, J.D., 1970. Energy relations and the energy-momentum tensor in continuum mechanics. In: Kanninen, M.F., Adler, W.F., Rosenfield, A.R., Jaffee, R.I. (Eds.), Inelastic Behaviour of Solids. McGraw-Hill, New York, pp. 77–115.

Freund, L.B., 1990. Dynamic Fracture Mechanics. Cambridge University Press, New York.

Griffith, A.A., 1920. The phenomenon of rupture and flow in solids. Philos. Trans. R. Soc. (London) A 221, 163–198.

Kostrov, B.V., 1966. Unsteady propagation of longitudinal shear cracks. Appl. Math. Mech. 30, 1241–1248.

Lobkovsky, A.E., Karma, A., 2003. Unsteady Crack Motion and Branching in a Phase-Field Model of Brittle Fracture, Preprint.

Miles, J.W., 1960. Homogeneous solutions in elastic wave propagation. Q. Appl. Math. 18, 37–59.

Muskhelishvili, N.I., 1953. Singular Integral Equations. Noordhoff, Groningen.

Rice, J.R., Ben-Zion, Y., Kim, K.S., 1994. Three-dimensional perturbation solution for a dynamic planar crack moving unsteadily in a model elastic solid. J. Mech. Phys. Solids 42, 813–843.

Smith, E., 1968. Crack bifurcation in brittle solids. J. Mech. Phys. Solids 16, 329–336.

Williams, M.L., 1952. Stress singularities resulting from various boundary conditions in angular corners of plates in extension. J. Appl. Mech. 19, 526–528.

ELSEVIER

Journal of the Mechanics and Physics of Solids
53 (2005) 227–248

JOURNAL OF THE
MECHANICS AND
PHYSICS OF SOLIDS

www.elsevier.com/locate/jmps

Brittle fracture dynamics with arbitrary paths III. The branching instability under general loading

M. Adda-Bedia*

Laboratoire de Physique Statistique de l'Ecole Normale Supérieure, 24 rue Lhomond, F–75231 Paris Cedex 05, France

Received 14 November 2003; received in revised form 14 May 2004

Abstract

The dynamic propagation of a bifurcated crack under arbitrary loading is studied. Under plane loading configurations, it is shown that the model problem of the determination of the dynamic stress intensity factors after branching is similar to the anti-plane crack branching problem. By analogy with the exact results of the mode III case, the energy release rate immediately after branching under plane situations is expected to be maximized when the branches start to propagate quasi-statically. Therefore, the branching of a single propagating crack under mode I loading should be energetically possible when its speed exceeds a threshold value. The critical velocity for branching of the initial single crack depends only weakly on the criterion applied for selecting the paths followed by the branches. However, the principle of local symmetry imposes a branching angle which is larger than the one given by the maximum energy release rate criterion. Finally, it is shown that an increasing fracture energy with the velocity results in a decrease in the critical velocity at which branching is energetically possible.

Keywords: A. Crack branching and bifurcation; Dynamic fracture; Stress intensity factors; B. Crack mechanics; C. Analytic functions

1. Introduction

The bifurcation of the crack tip into two or more branches is a well-known phenomenon in brittle crack propagation (Ravi-Chandar and Knauss, 1984; Fineberg et al., 1992; Gross et al., 1993; Sharon et al., 1995; Sharon and Fineberg, 1996,

* Fax: +33-1-44-32-34-33.
E-mail address: adda@lps.ens.fr (M. Adda-Bedia).

0022-5096/$ - see front matter © 2004 Elsevier Ltd. All rights reserved.
doi:10.1016/j.jmps.2004.06.001

1999; Boudet et al., 1996; Boudet and Ciliberto, 2000). Recent experiments on PMMA and glass samples (Sharon et al., 1995; Sharon and Fineberg, 1996, 1999) have established that the branching phenomenon results from the dynamic instability of a single propagating crack. The instability occurs when the crack speed exceeds a critical velocity v_c, which depends neither on the applied stress nor on the geometry of the plate. Above v_c, a single crack is no longer stable. Instead, a repetitive process of micro-branching occurs, which changes the crack dynamics. Simultaneously, the acoustic emission from the crack tip region increases (Gross et al., 1993; Boudet et al., 1996; Boudet and Ciliberto, 2000), the crack velocity develops strong oscillations. In addition a pattern which is correlated with the velocity oscillations, is created on the fracture surface (Fineberg et al., 1992). Crack branching has also been observed in simulations of dynamic crack propagation using molecular dynamics (Abraham et al., 1994), finite element calculations of constitutive equations on a lattice (Xu and Needleman, 1994), numerical simulations using a phase field model of brittle fracture (Lobkovsky and Karma, 2004; Henry and Levine, 2004), and by modeling the elastic medium as a two-dimensional lattice of coupled springs (Marder and Gross, 1995).

Yoffe (1951) observed that for crack speeds less than a critical velocity v_y, the transverse tensile stress in the vicinity of a crack tip reaches its maximum along the direction of crack growth. For crack speeds larger than v_y, this component of the stress develops a maximum along two other symmetric directions. Yoffe suggested that this modification of the local singular stress field could account for the observation that rapidly growing cracks in brittle materials bifurcate into branched cracks. Since then, the origin of the branching instability has been discussed elsewhere (Freund, 1990; Adda-Bedia et al., 1996). However, all the theoretical attempts to explain the branching predict critical speeds larger than the experimental ones. A possible cause for the failure of theory is that it was focused on the stress distributions around the tip of a single straight crack, prior to branching. These analyses indicate that the stress field around the crack tip is deformed at high velocities; however, this does not provide us with a crack growth or a branching criterion.

As in the single crack case, a growth criterion for a branched crack must be based on the equality between the energy flux into the two propagating tips and the surface energy which is added as a result of this propagation (Griffith, 1920). Eshelby proposed this approach (Eshelby, 1970; Rice et al., 1994), posing the question of how large the single crack speed must be so that there will be enough energy available to form two slow cracks instead of a single fast one. Since after branching twice as much surface area is created, the branches would not advance unless their velocity is lower than that of the single crack. The simplest branched configuration that Eshelby analyzed is the idealized limiting case where the branches subtend a vanishingly small angle and both prolong the original crack plane. In this case, the energy release rate of two branches propagating at velocity v', equals twice that of a single crack moving at velocity v, and it is maximal when the branches velocity is $v' \to 0$. For the mode III case, Eshelby reported $v = 0.6c_s$, where c_s is the shear wave speed, as the minimum speed which allows branching or surface roughening (Eshelby, 1970). This result remained a rough estimate, as no full dynamic solution was available for two branches with an arbitrary angle between them.

Recently, a method for determining the elastodynamic stress fields associated with the propagation of anti-plane kinked or branched cracks has been developed (Adda-Bedia and Arias, 2003; Adda-Bedia, 2004). Particularly, the dynamic propagation of a bifurcated crack under anti-plane loading was considered (Adda-Bedia, 2004). It was shown that the corresponding model problem admits a self-similar solution, which is a convolution integral of a known kernel and a harmonic function that satisfies a simple integral equation. The dependence of the stress intensity factor immediately after branching was determined as a function of the stress intensity factor immediately before branching, the branching angle and the instantaneous velocity of the crack tip. The jump in the dynamic energy release rate due to the branching process was also computed. When applying the Eshelby's growth criterion for a branched crack, it has been shown that the minimum speed of the initial single crack which allows branching is equal to $0.39c_s$. At the branching threshold, the corresponding bifurcated cracks start their propagation at a vanishing speed with a branching angle of approximately 40° (Adda-Bedia, 2004).

The present work is an attempt to generalize the approach of (Adda-Bedia and Arias, 2003; Adda-Bedia, 2004) to the dynamic propagation of a bifurcated crack under arbitrary loading. Especially, under plane loading configurations, the dynamic stress intensity factors immediately after branching are studied. It is shown that the formulation of the corresponding model problem is identical to the anti-plane case. The difficulty for solving the branching problem under plane loading configurations completely lies in the existence of two characteristic wave speeds and in the vectorial nature of the displacement field. However, this analogy allows for the reasonable hypothesis that under plane loading configurations, the jump in the energy release rate due to branching is maximized when the branches start to propagate quasi-statically. Using Eshelby's approach, the branching of a single propagating crack under mode I loading is found to be energetically possible when its speed exceeds a threshold value. The critical branching parameters depend of the criterion applied for the selection of the paths followed by the bifurcated cracks. For instance, the maximum energy release rate criterion (Erdogan and Sih, 1963) or the principle of local symmetry (Gol'dstein and Salganik, 1974). It is found that the critical velocity for branching of the initial single crack is weakly sensitive to the applied criterion. However, the principle of local symmetry gives a larger branching angle, which is more consistent with experimental observations. Finally, it is shown that an increasing fracture energy with the velocity results in a decrease in the critical velocity at which branching is energetically possible.

This paper is organized as follows. In Section 2, the results concerning the general elastostatic problem of a crack of finite length with two side-branches of infinitely small lengths are presented. Although the material of this section can be found elsewhere (Smith, 1968; Amestoy and Leblond, 1992), the results are recalled here for completeness, since they are used in the subsequent analysis of the dynamic crack branching problem. In Section 3, the model problem for the determination of the dynamic stress intensity factors after branching is presented. It is shown that the formulation of such a problem for both the plane and the anti-plane loading configurations are equivalent. The similarity between these two problems allows us to propose that even under plane loading configuration, the maximum of the energy release rate immediately after

branching is attained when the branches propagate quasi-statically. In Section 4, these results are combined with Eshelby's approach for determining a crack branching criterion, and computing the critical branching quantities. In the last Section, the results are compared with experimental data, and their relevance with respect to other models of dynamic crack branching is discussed.

2. The static branching problem

Let us start by giving the general solution of the elastostatic problem depicted in Fig. 1. An infinite sheet is stretched in the presence of a crack contour consisting of a main crack of length L and two symmetric side branches of equal lengths l emerging from a common origin. The angle between the two side-branches is denoted by $2\pi\lambda$, with $0 < \lambda < 1$. In particular, the case of a main crack with two side-branches of infinitely small lengths is studied. The complex stress function method is used and the stress intensity factors are derived. In the following, the resolution of the mode III loading is given in details, while the mixed mode I–II loading is briefly presented. Detailed analysis of a similar problem can be found in (Amestoy and Leblond, 1992).

2.1. Mapping function

The mapping of the exterior of the star shape crack in the z-plane, $z = x + \mathrm{i}y$, onto the exterior of the unit circle in the ζ-plane, $\zeta = \xi + \mathrm{i}\eta$, is considered. The conformal mapping of the contour depicted in Fig. 1 is given by the function (Smith, 1968)

$$z = \omega(\zeta) = A\,\zeta^{-1}(\zeta - 1)^{2\lambda}\left[(\zeta - \mathrm{e}^{-\mathrm{i}\alpha})(\zeta - \mathrm{e}^{\mathrm{i}\alpha})\right]^{(1-\lambda)}, \tag{1}$$

where A and α are real positive constants. As can be seen from Fig. 1, The points $\zeta_k = \mathrm{e}^{\mathrm{i}\beta_k}$, $(k = 1, 2, 3)$, corresponding to the tips B_k of the star shape crack in the z-plane,

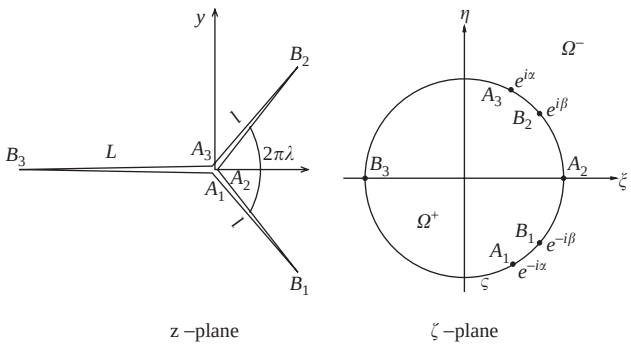

Fig. 1. Conformal mapping of a star shape crack in the z-plane onto the exterior of the unit circle in the ζ-plane. The x-axis is taken to be parallel to the main crack, and the argument of z is defined in the interval $[-\pi, \pi]$.

are the maxima of $\omega(\zeta)$. Their values are given by

$$\beta_3 = \pi; \quad \beta_2 = -\beta_1 = \beta \equiv 2\,\mathrm{Arcsin}\left(\sqrt{\lambda}\sin\frac{\alpha}{2}\right). \tag{2}$$

Then, the lengths of the cracks L and l can be expressed under the form

$$L = 4A\left(\cos\frac{\alpha}{2}\right)^{2(1-\lambda)}, \tag{3}$$

$$l = 4A\,\lambda^{\lambda}(1-\lambda)^{(1-\lambda)}\left(\sin\frac{\alpha}{2}\right)^2. \tag{4}$$

Eqs. (2)–(4) yield a unique solution of the conformal mapping parameters A, α and β as functions of l, L, and λ. In the vicinity of the tips B_k, the mapping function $z=\omega(\zeta)$ satisfies the following behavior

$$z - z_k \equiv \omega(\zeta) - \omega(\zeta_k) = \frac{1}{2}\,w''(\zeta_k)(\zeta-\zeta_k)^2, \tag{5}$$

$$\omega'(\zeta) = w''(\zeta_k)(\zeta-\zeta_k) = \sqrt{2w''(\zeta_k)(z-z_k)}. \tag{6}$$

In particular, at the point B_2 one has

$$\omega''(\zeta_2) = 4A\left(\frac{\lambda}{1-\lambda}\right)^{\lambda}\cos^2\left(\frac{\beta}{2}\right)(1+\cos^2\beta)\,\mathrm{e}^{\mathrm{i}(\lambda\pi-2\beta)}. \tag{7}$$

In the following, we will focus on the limiting case of a main crack of length L with two symmetric side branches of lengths l, with $l/L=\varepsilon\ll 1$. Consequently, to leading order in ε, Eqs. (2)–(4), (7) give

$$A = \frac{L}{4}, \tag{8}$$

$$\alpha = 2\,\lambda^{\lambda/2}(1-\lambda)^{(1-\lambda)/2}\sqrt{\varepsilon}, \tag{9}$$

$$\beta = 2\,\lambda^{(1+\lambda)/2}(1-\lambda)^{(1-\lambda)/2}\sqrt{\varepsilon}, \tag{10}$$

$$\omega''(\zeta_2) = 2L\left(\frac{\lambda}{1-\lambda}\right)^{\lambda}\mathrm{e}^{\mathrm{i}\lambda\pi}. \tag{11}$$

2.2. The mode III loading

For anti-plane strain deformation, the displacement $u_3(x,y)$ normal to the xy plane satisfies Laplace's equation

$$\Delta u_3 = 0. \tag{12}$$

A traction free boundary conditions are taken on crack surfaces, and the infinite elastic body is supposed to be loaded by an external shear stress σ_{23}^{∞}. These conditions are written

$$\vec{n}\cdot\vec{\nabla}u_3 = 0 \quad \text{on the crack surfaces,} \tag{13}$$

$$\sigma_{23} + \mathrm{i}\sigma_{13} = \sigma_{23}^{\infty} \quad \text{at infinity.} \tag{14}$$

The displacement and stress fields can be expressed by means of a complex function $\Phi(z)$, which is holomorphic outside the crack contour. In the z-plane, one has

$$u_3 = \frac{1}{2\mu}\left[\Phi(z) + \overline{\Phi(z)}\right], \tag{15}$$

$$\sigma_{13} - \mathrm{i}\sigma_{23} = \Phi'(z), \tag{16}$$

where μ is the Lamé shear coefficient and the bar indicates the complex conjugate. Note that $\overline{\Phi(z)}$ is a complex function which is holomorphic inside the crack contour. The problem can be easily solved in the ζ-plane. The boundary conditions (13), (14) read

$$\Phi(\zeta) - \overline{\Phi(\zeta)} = 0 \quad \text{as } |\zeta| \to 1^+, \tag{17}$$

$$\Phi'(\zeta) = -\mathrm{i}\sigma_{23}^{\infty} A \text{ as } \quad |\zeta| \to \infty. \tag{18}$$

The solution is readily obtained if $\Phi(\zeta)$ is given by (Smith, 1968)

$$\Phi(\zeta) = -\mathrm{i}\sigma_{23}^{\infty} A[\zeta - \zeta^{-1}]. \tag{19}$$

The stress intensity factor K_3' at the tip B_2 is defined by

$$K_3' = \lim_{z \to z_2} \sqrt{2\pi(z - z_2)}\,(\sigma_{23} + \mathrm{i}\sigma_{13})\mathrm{e}^{\mathrm{i}\lambda\pi}. \tag{20}$$

Using the behavior of $\Phi(\zeta)$ when $\zeta \to \zeta_2$, and relating it to the square root singularity of the stress field leads to:

$$K_3' = i\Phi'(\zeta_2)\sqrt{\frac{\pi \mathrm{e}^{\mathrm{i}\lambda\pi}}{w''(\zeta_2)}}. \tag{21}$$

One can easily verify that this quantity is real. For the limiting case where the two side-branches are of infinitely small lengths, it can be shown that

$$K_3' = F_{33}(\lambda) K_{03}, \tag{22}$$

where $K_{03} = \sigma_{23}^{\infty}\sqrt{\pi L/2}$ is the stress intensity factor of the main crack of length L in the absence of the side-branches. The function F_{33} is given by

$$F_{33}(\lambda) = \frac{1}{\sqrt{2}}\left[\frac{1-\lambda}{\lambda}\right]^{\lambda/2}. \tag{23}$$

The function $F_{33}(\lambda)$ as given by Eq. (23) is universal in the sense that it is independent of the applied loading. The discontinuity introduced by the vertices A_j is not intuitive, since the stress intensity factor dependence of λ is not given by a simple angular contribution. As shown in Fig. 2, the function $F_{33}(\lambda)$ displays a maximum at a branching angle corresponding to $\lambda = 0.22$.

2.3. The mixed mode I–II loading

In the following, the branching problem in plane situation is presented briefly. Effectively, the approach is analogous to the kinked crack problem which has been studied

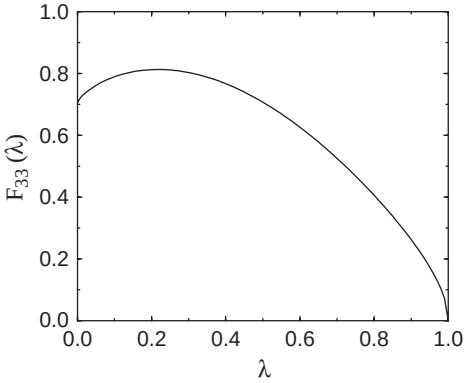

Fig. 2. Plot of the function $F_{33}(\lambda)$ as defined by Eq. (23).

previously (Amestoy and Leblond, 1992). More details of the analysis can be found in (Amestoy and Leblond, 1992) and references therein.

According to Muskhelishvili (1953), the stresses at a point $z=x+\mathrm{i}y=\omega(\zeta)$ can be expressed, in the ζ-plane, by the complex stress functions $\Phi(\zeta)$ and $\Psi(\zeta)$. For the case where traction free boundary conditions are taken on the crack surfaces and where the loading is given by external stresses σ_{11}^{∞}, σ_{22}^{∞} and σ_{12}^{∞}, the complex stress functions satisfy the following conditions

$$\Phi(\zeta)+\frac{\omega(\zeta)}{\overline{\omega'(\zeta)}}\overline{\Phi'(\zeta)}+\overline{\Psi(\zeta)}=Cte \quad \text{for } |\zeta|\to 1^{+}, \tag{24}$$

$$\Phi(\zeta)=\Gamma A \quad \text{for } |\zeta|\to\infty, \tag{25}$$

$$\Psi(\zeta)=\Gamma' A \quad \text{for } |\zeta|\to\infty, \tag{26}$$

where $\Gamma=(\sigma_{11}^{\infty}+\sigma_{22}^{\infty})/4$ and $\Gamma'=(\sigma_{22}^{\infty}-\sigma_{11}^{\infty})/2+\mathrm{i}\sigma_{12}^{\infty}$.

We focus on the asymptotic case where the two side-branches are of infinitely small lengths. Let us perform a second conformal mapping given by

$$\zeta=\exp \mathrm{i}\alpha Z, \tag{27}$$

which maps the region $|\zeta|>1$ onto the domain $\Im Z<0$ (see Fig. 3).

Following the same steps as in (Amestoy and Leblond, 1992), one finds that the problem reduces to resolving the integral equation

$$U(Z)=K_0+(1-\mathrm{e}^{-2\mathrm{i}\pi\lambda})\int_{-1}^{0} q(t)\,\frac{\overline{U(t)}}{(t-Z)^2}\,\frac{\mathrm{d}t}{4\mathrm{i}\pi} +(1-\mathrm{e}^{2\mathrm{i}\pi\lambda})\int_{0}^{1} q(t)\,\frac{\overline{U(t)}}{(t-Z)^2}\,\frac{\mathrm{d}t}{4\mathrm{i}\pi}, \tag{28}$$

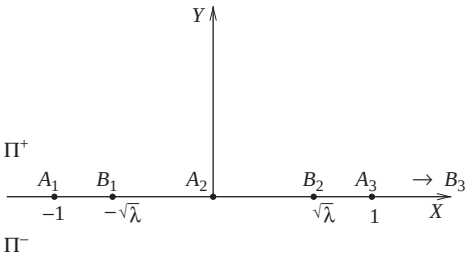

Fig. 3. The Z-plane corresponding to the conformal mapping $\zeta = \exp \mathrm{i}\alpha Z$.

where

$$U(Z) = \sqrt{\frac{8\pi}{L}}\Phi'(Z), \tag{29}$$

is a holomorphic function in the domain $\Im Z < 0$. The function $q(t)$ in Eq. (28) is given by

$$q(t) = \frac{t(t^2-1)}{(t+\sqrt{\lambda}+\mathrm{i}\varepsilon)(t-\sqrt{\lambda}+\mathrm{i}\varepsilon)}. \tag{30}$$

The term K_0 in Eq. (28) is the complex stress intensity factor of the main crack of length L in the absence of the side-branches. It is given by

$$K_0 = K_{01} - \mathrm{i}K_{02} = (\sigma_{22}^{\infty} - \mathrm{i}\sigma_{12}^{\infty})\sqrt{\frac{\pi L}{2}}. \tag{31}$$

On the other hand, it can be shown (Amestoy and Leblond, 1992) that the complex stress intensity factor K' at the crack tip B_2 is given by

$$K' = K_1' - \mathrm{i}K_2' = F_{33}(\lambda)\mathrm{e}^{-\mathrm{i}\lambda\pi}U(\sqrt{\lambda}), \tag{32}$$

which depends of the branching angle and linearly of the stress intensity factors K_{01} and K_{02}. This result is also universal in the sense that it is independent of the applied loading. Once the integral Eq. (28) is solved, the stress intensity factors K_1' and K_2' are uniquely determined. For this purpose, a useful decomposition of $U(Z)$ is given by

$$U(Z) = K_{01}U_1(Z) - \mathrm{i}K_{02}U_2(Z). \tag{33}$$

Eq. (28) is now decomposed into two independent equations

$$U_{1,2}(Z) = 1 \pm (1-\mathrm{e}^{-2\mathrm{i}\pi\lambda})\int_{-1}^{0} q(t)\,\frac{\overline{U_{1,2}(t)}}{(t-Z)^2}\,\frac{\mathrm{d}t}{4\mathrm{i}\pi}$$
$$\pm(1-\mathrm{e}^{2\mathrm{i}\pi\lambda})\int_{0}^{1} q(t)\,\frac{\overline{U_{1,2}(t)}}{(t-Z)^2}\,\frac{\mathrm{d}t}{4\mathrm{i}\pi}. \tag{34}$$

Eq. (34) can be easily computed numerically using an iterative method similar to the one used in determining the corresponding functions for the kinked crack problem. The computation of the functions $U_1(Z)$ and $U_2(Z)$ can be performed on any curve belonging to the lower half Z-plane, and that includes the points A_1, A_2 and A_3. The details of this method can be found in (Amestoy and Leblond, 1992).

Finally, the main results of this section can be summarized as follow. The stress intensity factors immediately after branching at the crack tip B_2 of the infinitely small side-branch are related to the stress intensity factors of the main crack of length L in the absence of the side-branches by the vectorial equation

$$\begin{pmatrix} K_1' \\ K_2' \\ K_3' \end{pmatrix} = \begin{pmatrix} F_{11}(\lambda) & F_{12}(\lambda) & 0 \\ F_{21}(\lambda) & F_{22}(\lambda) & 0 \\ 0 & 0 & F_{33}(\lambda) \end{pmatrix} \begin{pmatrix} K_{01} \\ K_{02} \\ K_{03} \end{pmatrix}. \tag{35}$$

The elements of the matrix F in Eq. (35) are given by

$$F_{11}(\lambda) = F_{33}(\lambda)\Re\left[e^{-i\pi\lambda}U_1(\sqrt{\lambda})\right], \tag{36}$$

$$F_{12}(\lambda) = F_{33(\lambda)}\Im\left[e^{-i\pi\lambda}U_2(\sqrt{\lambda})\right], \tag{37}$$

$$F_{21}(\lambda) = -F_{33}(\lambda)\Im\left[e^{-i\pi\lambda}U_1(\sqrt{\lambda})\right], \tag{38}$$

$$F_{22}(\lambda) = F_{33}(\lambda)\Re\left[e^{-i\pi\lambda}U_2(\sqrt{\lambda})\right] \tag{39}$$

and $F_{33}(\lambda)$ is given by Eq. (23). The remaining elements in Eq. (35) are computed once Eq. (34) are solved numerically. The corresponding results are summarized in Figs. 2 and 4.

3. The dynamic branching problem

The process of dynamic crack branching can be decomposed as follows. A semi-infinite straight crack that propagates at a speed $v(t)$ for $t < 0$ suddenly stops at $t = -\tau$, with $\tau \to 0^+$. At $t \to 0^+$, the crack branches locally with a branching angle equal to $\lambda\pi$ (see Fig. 5). For $t > 0$, the new branches propagate straightly at a velocity $v'(t)$, following the new directions $\pm\lambda\pi$. It is well established (Kostrov, 1975; Freund, 1990) that the dynamic stress intensity factors, $K_l(t)$, of the straight crack prior to branching are related to the rest stress intensity factors, $K_{0l}(t)$, of the same configuration by

$$K_l(t) = k_l(v)K_{0l}(t), \tag{40}$$

where $k_l(v)$, $l = 1, 2, 3$, are known universal functions of the instantaneous crack tip speed $v(t)$. Their explicit forms can be found in (Freund, 1990).

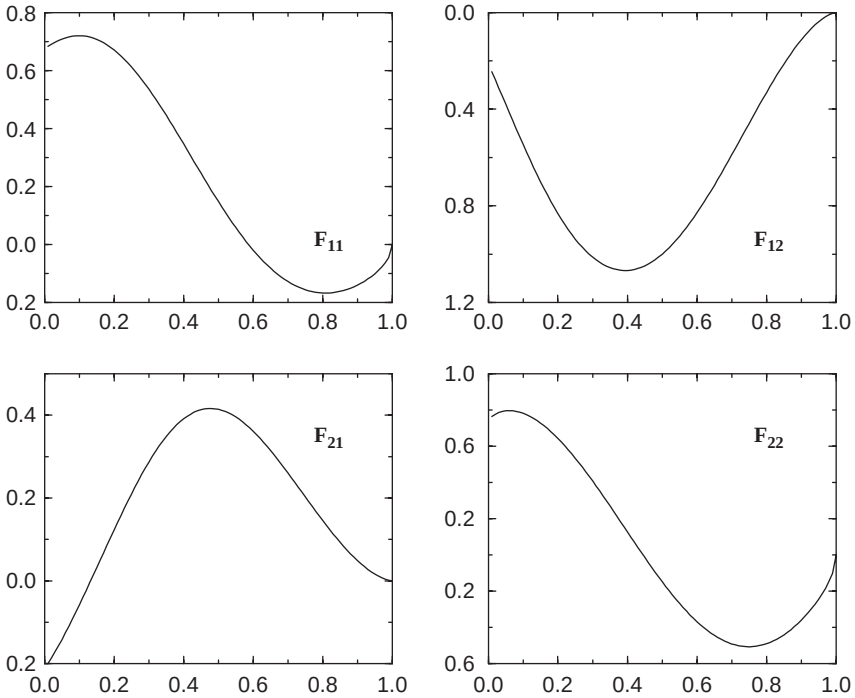

Fig. 4. Plot of the elements of the matrix $F_{lm}(\lambda)$ as defined by Eqs. (36)–(39).

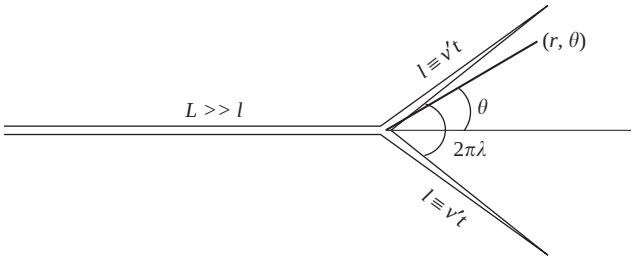

Fig. 5. Schematic representation of the dynamic branching problem.

Since there is no time scale, and consequently no length scale, against which the independent variables can be scaled, the dynamic stress intensity factors immediately after branching, K'_l for $t \to 0^+$, at each crack tip can always be written in the form of a universal function of the velocities and branching angle multiplying the rest stress intensity factors before branching, K_{0l} for $t \to 0^-$

$$K'_l = \sum_m k_l(v')H_{lm}(\lambda, v, v')K_{0m}. \tag{41}$$

As in the quasi-static case (Leblond, 1989), the matrix H is universal in the sense that it depends neither on loading configuration nor on the geometry of the body. Indeed in the limits $t \to 0^+$ and $\tau \to 0^+$ that are considered, the dynamic branching problem does not involve radiation effects, so it is always equivalent to a crack propagating in an unbounded body. Moreover, H should approach the elastostatic solution for a vanishingly small velocity of the side-branches

$$\lim_{v' \to 0} H_{lm}(\lambda, v, v') = F_{lm}(\lambda). \tag{42}$$

The present dynamic branching problem consists in determining the behavior of the matrix H as a function of the branching angle and of the instantaneous velocities immediately before and immediately after branching. In the following, the results of the anti-plane case are recalled (Adda-Bedia and Arias, 2003; Adda-Bedia, 2004), and the model problem for the determination of the plane dynamic stress intensity factors immediately after branching is presented.

3.1. The mode III loading

Under anti-plane loading conditions, it is known that when the initial crack stops, a static stress distribution is restored behind a wave front that propagates from the crack tip at the shear wave speed (Eshelby, 1969; Freund, 1990). Thus for $t > 0$, the propagation of the branches occurs within a stationary stress field induced by the arrest of the original single crack. Moreover, in the limit $t \to 0^+$, the lengths of the branched parts of the crack are vanishingly small, so that the breaking process after branching occurs in the region determined by the square root singular stress intensity factor field of the semi-infinite straight crack. Therefore, the dynamic branching problem consists of two symmetric branches reminiscent from a preexisting stationary straight crack, that start to propagate at time $t = 0$, in the directions $\pm\lambda\pi$, by negating a time-independent traction distribution on the newly broken surfaces given by (Williams, 1952)

$$\sigma_{23}^{(s)}(r < v't, \pm\lambda\pi) = \frac{K_{03}}{\sqrt{2\pi r}} \cos\frac{\lambda\pi}{2}, \tag{43}$$

where K_{03} is the rest stress intensity factor of the crack tip prior to branching. A direct consequence of Eq. (43) is that the matrix element H_{33} must be independent of the velocity prior to branching.

$$H_{33}(\lambda, v, v') \equiv H_{33}(\lambda, v'/c_s). \tag{44}$$

Using these arguments, a method for determining the elastodynamic stress fields associated with the propagation of branched cracks was developed in (Adda-Bedia, 2004). Particularly, it was shown that the corresponding model problem admits a self-similar solution, which is a convolution integral between a known kernel and a harmonic function that satisfies a simple integral equation. Once the integral equation is solved, the stress intensity factor immediately after branching is computed *a posteriori* using an additional condition. The function H_{33} can then be computed *exactly* as a function of the branching angle λ and of the instantaneous velocity v'.

3.2. The mixed mode I–II loading

Under plane loading situations, when the initial crack stops, the static stress distribution is restored in the crack plane only (Freund, 1990); ahead of the crack tip, this happens behind a wave front that propagates at the shear wave speed, c_s, and behind the crack tip, behind a wave front that propagates at the Rayleigh wave speed, c_R. These two properties are sufficient to determine the dynamics of a single crack moving straightly (Freund, 1990). However, for a dynamic crack of arbitrary path, one has to specify the whole angular distribution of the stress field in the vicinity of the crack tip induced by the crack arrest, which is given by (Kostrov, 1975; Madariaga, 1977)

$$\sigma_{ij}^{(d)}(r,\theta,t) = \frac{K_{01}(t+\tau)}{\sqrt{2\pi r}}\, f_{ij}^{(1)}(\chi,\theta) + \frac{K_{02}(t+\tau)}{\sqrt{2\pi r}}\, f_{ij}^{(2)}(\chi,\theta), \tag{45}$$

where c is a characteristic wave speed of the material, K_{01} and K_{02} are the rest stress intensity factors of the crack tip prior to branching, and

$$\chi \equiv \frac{r}{c(t+\tau)}. \tag{46}$$

Here, the time delay τ is present because of our decomposition of the branching process.

Therefore, contrary to the anti-plane case, the present branching problem should be expressed as follows. Two symmetric branches reminiscent from a preexisting stationary straight crack, start to propagate at time $t=0^+$, in the directions $\pm\lambda\pi$, with a velocity v', by negating a traction distribution on the newly created surfaces, $\sigma_{ij}^{(d)}$ $(r < v't, \pm\lambda\pi, t)$, given by Eq. (45). Due to the presence of both dilatational and shear elastic waves, there is no sharp limit between the dynamic and the static distributions of the stress fields in the neighborhood of the crack tip. Indeed, the stress distributions at any point off the crack plane relax continuously and reach the static distributions for $\chi \to 0$ only (Kostrov, 1975; Madariaga, 1977)

$$\lim_{\chi\to 0} f_{ij}^{(l)}(\chi,\theta) = \Sigma_{ij}^{(l)}(\theta), \tag{47}$$

where $\Sigma_{ij}^{(l)}$ are the well-known angular variations of the static square root singular stress intensity factor field (Williams, 1952).

Thus in general, the propagation of the branches does not occur within stationary stress fields. Moreover, the functions $f_{ij}^{(l)}$ depend explicitly on the crack tip velocity prior to the crack arrest (Madariaga, 1977). Therefore, contrary to the mode III case, the elements of the matrix H_{lm} corresponding to the inplane configuration can depend explicitly on the velocity before branching. However, the determination of the stress fields immediately after branching makes the problem simpler. Since the single straight crack stops at $t=-\tau$, with $\tau \to 0^+$, and the branches start to propagate at $t \to 0^+$, one always has

$$\chi \equiv \frac{r}{c(t+\tau)} < \frac{v't}{c(t+\tau)} \to 0. \tag{48}$$

We emphasize on the importance of the order in which the limits must be taken. The decomposition of the crack branching process as described above imposes that the limit $t \to 0^+$ must be taken before the limit $\tau \to 0^+$. Therefore, the stress intensity factor

field immediately after branching is determined by solving a branching problem where the traction distribution that has to be negated during the propagation of the branches is given by the static square root singular stress intensity factor field of the initial straight crack

$$\sigma_{ij}^{(s)}(r < v't, \pm\lambda\pi, t) = \frac{K_{01}}{\sqrt{2\pi r}}\Sigma_{ij}^{(1)}(\pm\lambda\pi) + \frac{K_{02}}{\sqrt{2\pi r}}\Sigma_{ij}^{(2)}(\pm\lambda\pi), \tag{49}$$

Therefore, the dependence of the velocity of the single crack tip before branching is suppressed from the stress distribution that has to be negated during the propagation of the branches. Consequently, the matrix elements H_{lm} related to plane loading situations should be also independent of the velocity prior to branching.

$$H_{lm}(\lambda, v, v') \equiv H_{lm}(\lambda, v'/c). \tag{50}$$

It is important to notice that the stress intensity factors immediately after branching involve the history of crack propagation before branching only through the rest stress intensity factors. More precisely, they do not have any explicit dependence of the velocity of the single crack tip. This important result is mainly due to the absence of intrinsic time or length scales in linear elasticity theory. Similarly to what happens in the anti-plane case, the property (49) implies that the resulting elastic fields should exhibit self-similar properties. However, the in-plane configuration is characterized by two displacement potentials that satisfy wave equations with two different wave speeds (Broberg, 1999; Freund, 1990). Thus, self-similar solutions of the displacement potentials are necessarily given in terms of two different self-similar "coordinates"; $(c_s t/r, \theta)$ and $(c_d t/r, \theta)$, where c_d (c_s) is the dilatational (shear) wave speed. The coupling between the dilatational and shear elastic waves makes the complete resolution of the resulting problem unapproachable. However, the similarity between the mode III and the in-plane problems suggests that the main features of the mode III results should be preserved.

4. Dynamic branching instability

A growth criterion for a branched crack must be based on the equality between the energy flux into each propagating tip and the surface energy which is added as a result of this propagation (Griffith, 1920). The dynamic energy release rate is defined as the rate of mechanical energy flow out of the body and into the crack tip per unit crack advance. It is well established that the energy release rate G for a single straight crack is given by (Kostrov, 1975; Freund, 1990)

$$G = \frac{1}{2\mu}\sum_{l=1}^{3} A_l(v)K_l^2 = \frac{1}{2\mu}\sum_{l=1}^{3} g_l(v)K_{0l}^2, \tag{51}$$

where μ is the Lamé shear coefficient, and

$$g_l(v) = A_l(v)k_l^2(v). \tag{52}$$

The functions $A_l(v)$ and $g_l(v)$ do not depend on the details of the applied loading or on the configuration of the body being analyzed. They only depend on the local

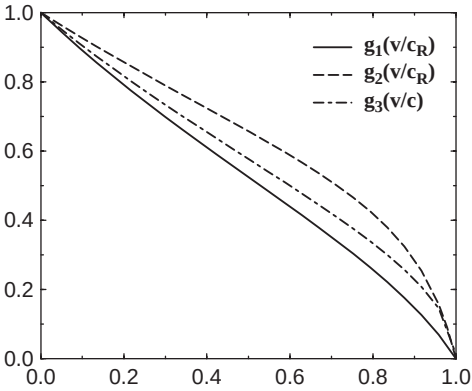

Fig. 6. Plot of the universal functions $g_1(v/c_R)$, $g_2(v/c_R)$ and $g_3(v/c_s)$ for $(c_d/c_s)^2 = 3$. Here, c_d (resp. c_s) denotes the dilatational (resp. shear) wave speed of the material.

instantaneous speed of the crack tip and on the properties of the material only. For completeness, the functions $g_I(v)$ are reproduced in Fig. 6.

The dynamic energy release rate is a quantity associated to a single moving crack tip. Thus, after branching one has to determine it for each crack tip. Due to the symmetry of the branching configuration, the energy release rate immediately after branching G' for each crack tip is given by

$$G' = \frac{1}{2\mu}\sum_{I=1}^{3} A_I(v') K'^2_I. \tag{53}$$

When the initial single crack is propagating under a mode III loading, Eq. (53) reduces to

$$G'_3 = \frac{1}{2\mu}\, g_3(v') H^2_{33}(\lambda, v'/c_s) K^2_{03}, \tag{54}$$

where K_{03} is the rest stress intensity factor immediately before branching. In (Adda-Bedia, 2004), it has been shown that for a constant branching angle, G'_3 is a decreasing function of v'. Therefore, the energy release rate immediately after branching is maximized when the branches start to propagate quasi-statically ($v' \to 0$), that is when $G'_3 \equiv G'^{(s)}_3$. Equivalently, if the loading configuration before branching is of mode I type, the energy release rate immediately after branching G'_1 at each crack tip is given by

$$G'_1 = \frac{1}{2\mu}\left[g_1(v') H^2_{11}(\lambda, v'/c_s) + g_2(v') H^2_{21}(\lambda, v'/c_s)\right] K^2_{01}, \tag{55}$$

where K_{01} is the rest stress intensity factor immediately before branching. At the present stage, the exact computation of the energy release rate immediately after branching under in-plane configurations is not possible. Nevertheless, the exact resolution of the mode III problem does give indications about the general behavior of G'_1. Indeed, in many physical aspects of crack propagation, the results corresponding to mode III and

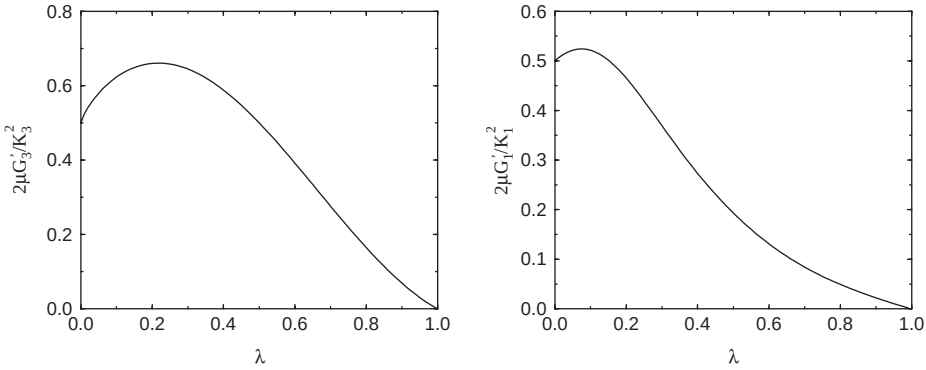

Fig. 7. Plot of the maximum energy release rate immediately after branching as a function of the branching angle, for the cases of a mode III loading (left) and a mode I loading (right).

to in-plane configurations are qualitatively similar (Broberg, 1999; Freund, 1990). As for the anti-plane case, the in-plane elastic fields immediately after branching exhibit self-similar properties, and the corresponding stress intensity factors do not depend explicitly of the velocity of the single crack tip before branching. These similar properties allow to predict the general behavior of the energy release rate immediately after branching.

The results of (Adda-Bedia, 2004) show that $H_{33}(\lambda, v'/c_s)$ depends only weakly on v'. Indeed, the ratio $H_{33}(\lambda, v'/c)/F_{33}(\lambda)$ is very close to unity (up to $\pm 5\%$) for all values of λ and v'/c_s. The similarity between the anti-plane and the in-plane branching problem suggests that this behavior should be maintained for all the matrix elements $H_{lm}(\lambda, v'/c)$. Therefore, one expects that the energy release rate immediately after branching for in-plane configurations is also maximized when the branches start to propagate quasi-statically ($v' \to 0$), that is when $G'_1 \equiv G'^{(s)}_1$. Let us emphasize that this property results from arguments deduced from the analogy with the anti-plane results. Even if this property does not hold exactly for in-plane configurations, the analogy with the anti-plane case suggests that it is a good approximation. Nevertheless, a complete resolution of the in-plane dynamic branching problem would be necessary to check this hypothesis. Fig. 7 displays the plots of $G'^{(s)}_3$ and $G'^{(s)}_1$ as functions of the branching angle. It is shown that their behavior are qualitatively equivalent. They are both equal to $1/2$ for "zero" branching angle and they both display a maximum at a given branching angle.

According to the generalized Griffith criterion (Griffith, 1920), the crack must grow in such a way that the energy release rate is always equal to the dynamic fracture energy of the material, $\Gamma(v)$, which is assumed to be a property of the material and whose value may depend on the instantaneous crack tip speed (Boudet et al., 1996; Sharon and Fineberg, 1999). This growth criterion, $G \equiv \Gamma(v)$, should be applied for the crack tips before and after branching. This insures that each crack tip is always propagating according to the Griffith criterion. Therefore, the growth criterion introduces an intrinsic

relation between the energy release rates immediately before and immediately after branching, which reads

$$G' = \frac{\Gamma(v')}{\Gamma(v)}\, G. \tag{56}$$

Eq. (56) is a necessary condition for the existence of a branching configuration. Otherwise, the single crack tip propagation should be maintained. This equation, however, is not a sufficient condition for determining the branching threshold parameters, which must be deduced from some other criteria. For instance, the maximum energy release rate criterion (Erdogan and Sih, 1963) or the principle of local symmetry (Gol'dstein and Salganik, 1974). These two criteria have been applied essentially to problems related to the selection of single quasi-static crack paths, and give almost similar numerical predictions. However, it has been shown that the principle of local symmetry is more coherent and it is now widely admitted as the second additional equation of motion (Leblond, 1989; Adda-Bedia et al., 1999). In the following, these two criteria will be used to predict the branching instability and will be compared with the experimental results.

4.1. The maximum energy release rate (MERR) criterion

Eshelby (1970) posed the question of how large must be the single crack velocity v, so that by decelerating, there is enough energy available to form two cracks propagating at a velocity v'. This approach can be interpreted as being equivalent to the maximum energy release rate criterion. Since the energy release rate after branching is always largest when $v' \to 0$, the maximum energy release rate after branching depends of the branching angle only.

Let us start by the case of constant fracture energy and focus on the in-plane crack propagation. Using Eq. (56), one deduces that the critical velocity before branching must be a solution of

$$g_1(v) = F_{11}^2(\lambda) + F_{21}^2(\lambda). \tag{57}$$

Fig. 6 shows that $g_1(v)$ is a decreasing function of the velocity that satisfies $g_1(0)=1$, and $g_1(c_R)=0$. On the other hand, the right-hand side of Eq. (57) displays a maximum, whose value is less than unity (see Fig. 7). Therefore, this equation is not always satisfied, and branched solutions exist when the velocity v exceeds a critical velocity v_c only. This threshold value is given by the least velocity v for which Eq. (57) admits a solution. It corresponds to a branched solution with a non-vanishing branching angle, $\lambda_c = 0.07$, given by the maximum of $F_{11}^2(\lambda)+F_{21}^2(\lambda)$, and a corresponding critical speed, $v_c \approx 0.5 c_R$, given by Eq. (57).

4.2. The principle of local symmetry (PLS)

While the MERR criterion states that the crack should follow a direction of maximum energy release rate, the principle of local symmetry states that the path taken by a crack in a brittle homogeneous isotropic material is the one for which the local stress field

Table 1
Branching thresholds v_c and λ_c for different branching criteria and loading modes. For the inplane case, the thresholds are given using a Poisson ratio such that $(c_d/c_s)^2 = 3$

	MERR, mode III	MERR, mode I	PLS, mode I
v_c	$0.392\ c_s$	$0.503\ c_R$	$0.518\ c_R$
λ_c	0.22	0.07	0.13

at the tip is of mode I type (Gol'dstein and Salganik, 1974). It is not obvious that the crack propagation still satisfies this criterion in the dynamic case. However, there is an argument in favor of this scenario (Adda-Bedia et al., 1999). The dynamic energy release rate can be seen as the component, F_1, of the configurational force along the direction of crack motion. The Griffith energy criterion can thus be reinterpreted as a material force balance between F_1 and a resistance force to crack advance per unit length of the crack front: $F_1 \equiv \Gamma$. However, this equation of motion is not sufficient to determine the trajectory of a crack if it is allowed to deviate from straight propagation. If one assumes that configurational forces balance holds at the crack tip, one should also impose that the component of the material force perpendicular to the direction of crack propagation must vanish (Adda-Bedia et al., 1999). Since this quantity is proportional to K_2, it results that the crack propagation occurs in such a way as to keep a purely opening mode at its tip.

In the case of PLS, at any stage of crack propagation two equations of motion must be fulfilled: the Griffith energy criterion and the pure opening condition at the crack tip. When a main crack subjected to a mode I loading branches into two symmetric cracks, these conditions are satisfied by the single crack tip prior to branching as long as the crack tip follows a straight path. On the other hand, immediately after branching, these two conditions must be written as

$$g_1(v) = F_{11}^2(\lambda), \tag{58}$$

$$F_{21}(\lambda) = 0. \tag{59}$$

Now, the branching angle, λ_c, is selected in a different way from the MERR criterion, while the arguments for determining the critical velocity, v_c, are the same. Thus, the result of application of these equations gives also a selected branching angle and a critical speed for branching. From Table 1, it is seen that the critical branching velocity $v_c \approx 0.52 c_R$ does not differ too much from the one deduced by using MERR criterion, while the critical branching angle is twice larger, $\lambda_c = 0.13$. Note that this value is approximately equal to the branching angle $\lambda_c = 0.15$ calculated by using an analysis of a branched crack based on the body force method combined with a perturbation procedure (Isida and Noguchi, 1992).

4.3. Effect of velocity dependent fracture energy

Eq. (56) obviously shows that a velocity dependent fracture energy affects the results of the latter calculations. As the two branching criteria are based to some level on

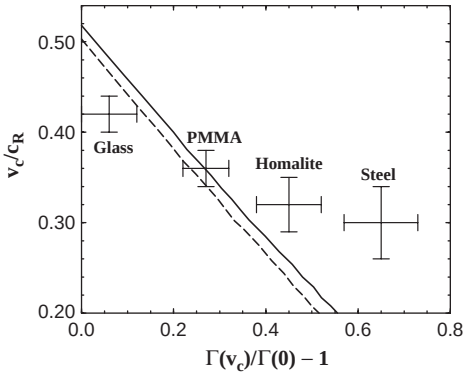

Fig. 8. Plot of the critical branching velocity for the case of velocity dependent fracture energy and for $(c_d/c_s)^2 = 3$. The solid line corresponds to the values deduced from PLS and the dashed line to those deduced from the MERR criterion. The experimental values reported are estimates taken from (Sharon and Fineberg, 1999) for Glass and PMMA, (Dally, 1979) for Homalite 100 and (Congleton, 1973; Anthony et al., 1970) for "Pitho" tool steel.

energy balance, their results should be modified by the behavior of $\Gamma(v)$. When taking into account this new degree of freedom, Eq. (57), related to MERR criterion, becomes

$$\frac{\Gamma(0)}{\Gamma(v)}\, g_1(v) = F_{11}^2(\lambda) + F_{21}^2(\lambda) \tag{60}$$

and in the case of PLS, Eq. (58) becomes

$$\frac{\Gamma(0)}{\Gamma(v)}\, g_1(v) = F_{11}^2(\lambda), \tag{61}$$

while Eq. (59) is not modified. In general, $\Gamma(v)$ is an increasing function of the velocity (Boudet et al., 1996; Sharon and Fineberg, 1999). Therefore, the left-hand side of Eqs. (60), (61) decreases faster than in the constant fracture energy case, and the energy balance can thus be achieved at lower velocity, while the critical branching angles remain the same. Although $\Gamma(v)$ can be a nonlinearly dependent function of the crack tip speed, it is only the amount of $\Gamma(v_c)/\Gamma(0)$ which is of importance in determining the critical crack tip velocity v_c. In Fig. 8, this quantity is plotted for different values of $\Gamma(v_c)/\Gamma(0)$, when either MERR criterion or PLS is applied.

5. Discussion

Under tensile mode loading, it is shown that the formulation of the problem for determining the dynamic stress intensity factors immediately after branching is identical to the anti-plane case. This analogy allows us to formulate the hypothesis that under plane loading configurations, the jump in the energy release rate due to branching is also maximized when the branches start to propagate quasi-statically. Therefore, the branching of a single propagating crack under mode I loading is found to be energetically possible when its speed exceeds a threshold value. The critical velocity v_c is only

weakly dependent on the Poisson ratio of the material, and is only slightly modified by changing the crack propagation criterion from the maximum energy release rate criterion to the principle of local symmetry (see Table 1 and Fig. 8). Still, the branching angle in the case of PLS is twice as large as the one that results from the application of MERR criterion; 23.4° instead of 12.6°. Finally, for a velocity dependent fracture energy, the critical velocity for branching v_c decreases with increasing $\Gamma(v_c)/\Gamma(0)$. The present work establishes the necessary conditions at which branching is energetically possible. It does not address the stability of the single straight propagating crack with respect to a branched configuration. In either experiments or numerical simulations, the selection mechanism might be due to the presence of noise which allows the system to visit all possible configurations.

Fig. 8 displays a comparison with estimates of critical speeds for branching taken from existing experimental data. It is shown that the predicted decrease of v_c with increasing $\Gamma(v_c)/\Gamma(0)$ is found in experiments as well. The present energy balance approach allows to obtain this result, which cannot be done in calculations based on analysis of the stress field around a single crack tip. Fig. 8 shows that except for the case of PMMA, for which there is a good agreement between the measured (Sharon and Fineberg, 1999) and the calculated critical velocity, the experimental data show a weaker dependence of v_c on $\Gamma(v_c)/\Gamma(0)$. However, the critical velocities for branching and the velocity dependence of the fracture energy for both Homalite and Steel should be taken as very rough estimates (Congleton, 1973; Anthony et al., 1970; Dally, 1979). More precise experiments on different materials are needed in order to establish the behavior of the critical speed for branching with the fracture energy dependence of the velocity. On the other hand, the critical velocity for branching is larger by 24% than the measured value for glass, a material which is commonly assumed to have a nearly constant fracture energy (Sharon and Fineberg, 1999). However, the calculated critical speed for branching, $v_c = 0.52c_R$, agrees with the one deduced from numerical simulations using a phase field model of brittle fracture under in-plane loading (Henry and Levine, 2004). In order to fit the experimental critical velocity of $0.42c_R$, a variation of fracture energy with velocity of approximately 15% is needed (see Fig. 8), which is slightly larger than the error bars of the experimental results reported in (Sharon and Fineberg, 1999).

Let us emphasize that the present work is based on exact results of the anti-plane branching problem (Adda-Bedia, 2004). Moreover, it is proven that similarly to the anti-plane case, the in-plane elastic fields exhibit self-similar properties immediately after branching, and the corresponding stress intensity factors do not explicitly depend on the velocity of the single crack tip before branching. These similar properties allow for the assumption that the main results of the mode III case should hold for in-plane configurations. Therefore, one expects that the energy release rate immediately after branching for in-plane configurations is also maximized when the branches start to propagate quasi-statically. Even if this property might not hold exactly for in-plane configurations, the analogy with the anti-plane case suggests that it must be a good approximation. One may wonder if the zero velocity immediately after branching is physically relevant, since it seems in contradiction with both experimental observations and numerical simulations. A possible explanation of this discrepancy is that the

branches start their propagation at vanishingly small speeds, but accelerate rapidly to velocities of the same order of the principal crack speed. This scenario is consistent with the results of single crack propagation in the framework of linear elastic fracture mechanics. Nevertheless, real materials are not ideally brittle and in numerical simulations one always introduces intrinsic small length scales (or time scales), which may explain the observed smooth variation of the crack speeds before and after branching. The velocity jump predicted using linear elastic fracture mechanics may be seen as an asymptotic result which is exactly valid for ideally brittle materials.

Fig. 7 shows that under mode I loading conditions, the angular variation of the energy release rate immediately after branching has a shallow maximum in the region $0 \leqslant \lambda \leqslant 0.2$. The flatness of G' at low branching angles explains the weak variation of v_c with the type of criterion applied, but is an indication in favor of the PLS versus the MERR criterion. Effectively, If the MERR criterion were the relevant one, there would not be a clear selection of the branching angle and one would expect branching for a wide range of angles. This contradicts experimental observations (Sharon et al., 1995), which show a clear selection of the branching angle. On the other hand, $F_{21}(\lambda)$ is steep around its zero value and thus, the PLS gives a well-defined selected branching angle which is equal to 23.4°, independently of the Poisson ratio of the material. Sharon et al. (1995) reported that the micro-branches which appear immediately after the onset of the branching instability are not straight. Instead, the "branching angle" increases as one approaches the branching point. Measuring the tangent to the profile of the branch at a distance of 5 μm from the branching point, the authors reported branching angles of 30° for glass and PMMA. These angles are of the same order of magnitude as the predictions of the present model based on PLS, but nearly three times larger than the predictions when using MERR. Therefore, these observations suggest that the relevant criterion for branching must be the PLS one.

Finally, previous attempts to predict the critical velocity for branching in the framework of linear elasticity were focused on the properties of the stress fields around the tip of a single fast crack (Yoffe, 1951; Freund, 1990; Adda-Bedia et al., 1996). These works indicated that above a critical velocity, a component of the singular stress field, which was regarded as the relevant one for path selection, attains a maximum off the original direction of propagation. It was suggested that in these conditions, the single straight crack solution becomes unstable. Still, none of these models dealt with the resultant state of the system, that of two branches. One must verify that the new branched state is energetically possible. The present work, which is based on Eshelby's approach, targets these points by applying growth criteria to the branched state. More recent works challenge the dynamic branching problem, using numerical simulations and calculations on the molecular scale (Abraham et al., 1994; Marder and Gross, 1995). One might argue that since the first stages of the branching process occur within the process zone, branching criteria based on continuum models are meaningless. It may be that the branching criterion must be based on processes at the molecular scale. Indeed, the present model does not target the question of when a tip of a crack will bifurcate, it determines the conditions which are necessary for the propagation of two branches. Calculations at molecular scales may show that even at lower velocities, the tip is unstable and the material tends to be opened off the original

direction. However, these flows may not be able to grow to the continuum scale. Instead, they might affect the fracture energy of the *single crack* and its fracture surface topology. As experimental data show (Sharon et al., 1995; Sharon and Fineberg, 1996), the change in the dynamics of the crack occurs simultaneously with the appearance of micro-branches of 10–100 μm length. This is certainly a continuum scale. Thus, deviations from straight crack which occur before the appearance of "continuum scale branches" do not drastically change the crack dynamics and can be included within the process zone.

Acknowledgements

I wish to thank R. Arias and J.R. Rice for enlightening discussions. I also thank E. Sharon for his comments on many experimental facts which are included in the discussion Section. Laboratoire de Physique Statistique de l'Ecole Normale Supérieure is associated with CNRS (UMR 8550) and with Universities Paris VI and Paris VII.

References

Abraham, F.F., Brodbeck, D., Rafey, R.A., Rudge, W.E., 1994. Instability dynamics of fracture, a computer simulation investigation. Phys. Rev. Lett. 73, 272–275.

Adda-Bedia, M., 2004. Brittle fracture dynamics with arbitrary paths—II. Dynamic crack branching under general antiplane loading. J. Mech. Phys. Solids 52, 1407–1420.

Adda-Bedia, M., Arias, R., 2003. Brittle fracture dynamics with arbitrary paths—I. Dynamic crack kinking under general antiplane loading. J. Mech. Phys. Solids 51, 1287–1304.

Adda-Bedia, M., Ben Amar, M., Pomeau, Y., 1996. Morphological instabilities of dynamic fracture in brittle solids. Phys. Rev. E 54, 5774–5779.

Adda-Bedia, M., Arias, R., Ben Amar, M., Lund, F., 1999. Generalized Griffith criterion for dynamic fracture and the stability of crack motion at high velocities. Phys. Rev. E 60, 2366–2376.

Amestoy, M., Leblond, J.B., 1992. Crack paths in plane situations–II. Detailed form of the expansion of the stress intensity factors. Int. J. Solids Struct. 29, 465–501.

Anthony, S.R., Chubb, J.P., Congleton, J., 1970. The crack-branching velocity. Philos. Mag. 22, 1201–1216.

Boudet, J.F., Ciliberto, S., 2000. Interaction of sound with fast crack propagation: an equation of motion for the crack tip. Physica D 142, 317–345.

Boudet, J.F., Ciliberto, S., Steinberg, V., 1996. Dynamics of crack propagation in brittle materials. J. Phys. II France 6, 1493–1516.

Broberg, K.B., 1999. Cracks and Fracture. Academic Press, London.

Congleton, J., 1973. Practical applications of crack-branching measurements, Proceedings of the International Conference on Dynamic Crack Propagation, Noordhoff International Publishing, Leiden, pp. 427–438.

Dally, J.W., 1979. Dynamic photoelastic studies of fracture. Exp. Mech. 19, 349–361.

Erdogan, G., Sih, G.C., 1963. On the crack extension in plates under plane loading and transverse shear. J. Basic Eng. 85, 519–527.

Eshelby, J.D., 1969. The elastic field of a crack extending nonuniformly under general anti-plane loading. J. Mech. Phys. Solids 17, 177–199.

Eshelby, J.D., 1970. Energy relations and the energy-momentum tensor in continuum mechanics. In: Kanninen, M.F., Adler, W.F., Rosenfield, A.R., Jaffee, R.I. (Eds.), Inelastic Behaviour of Solids. McGraw-Hill, New York, pp. 77–115.

Fineberg, J., Gross, S.P., Marder, M., Swinney, H.L., 1992. Instability in the propagation of fast cracks. Phys. Rev. B 45, 5146–5154.

Freund, L.B., 1990. Dynamic Fracture Mechanics. Cambridge University Press, New York.

Gol'dstein, R.V., Salganik, R.L., 1974. Brittle fracture of solids with arbitrary cracks. Int. J. Fract. 10, 507–523.

Griffith, A.A., 1920. The phenomenon of rupture and flow in solids. Philos. Trans. R. Soc. London A 221, 163–198.

Gross, S.P., Fineberg, J., Marder, M., McCormick, W.D., Swinney, H.L., 1993. Acoustic emission in dynamic fracture. Phys. Rev. Lett. 71, 3162–3165.

Henry, H., Levine, H., 2004. Dynamic instabilities of fracture under biaxial strain using a phase field model, cond-mat/0402563.

Isida, M., Noguchi, H., 1992. Stress intensity factors at tips of branched cracks under various loadings. Int. J. Fract. 54, 293–316.

Kostrov, B.V., 1975. On the crack propagation with variable velocity. Int. J. Fract. 11, 47–56.

Leblond, J.B., 1989. Crack paths in plane situations—I. General form of the expansion of the stress intensity factors. Int. J. Solids Struct. 25, 1311–1325.

Lobkovsky, A.E., Karma, A., 2004. Unsteady Crack Motion and Branching in a Phase-Field Model of Brittle Fracture. Phys. Rev. Lett. 92, 245510.

Madariaga, R., 1977. High-frequency radiation from crack (stress drop) models of earthquake faulting. Geophys. J. R. Atron. Soc. 51, 625–651.

Marder, M., Gross, S.P., 1995. Origin of crack tip instabilities. J. Mech. Phys. Solids 43, 1–48.

Muskhelishvili, N.I., 1953. Some basic problems of the mathematical theory of elasticity. Noordhoff, Groningen.

Ravi-Chandar, K., Knauss, W.G., 1984. An experimental investigation into dynamic fracture—III. On steady-state crack propagation and crack branching. Int. J. Fract. 26, 141–154.

Rice, J.R., Ben-Zion, Y., Kim, K.S., 1994. Three–dimensional perturbation solution for a dynamic planar crack moving unsteadily in a model elastic solid. J. Mech. Phys. Solids 42, 813–843.

Sharon, E., Fineberg, J., 1996. Microbranching instability and the dynamic fracture of brittle materials. Phys. Rev. B 54, 7128–7139.

Sharon, E., Fineberg, J., 1999. Confirming the continuum theory of dynamic brittle fracture for fast cracks. Nature 397, 333–335.

Sharon, E., Gross, S.P., Fineberg, J., 1995. Local branching as a mechanism in dynamic fracture. Phys. Rev. Lett. 74, 5096–5099.

Smith, E., 1968. Crack bifurcation in brittle solids. J. Mech. Phys. Solids 16, 329–336.

Williams, M.L., 1952. Stress singularities resulting from various boundary conditions in angular corners of plates in extension. J. Appl. Mech. 19, 526–528.

Xu, X.P., Needleman, A., 1994. Numerical simulations of fast crack growth in brittle solids. J. Mech. Phys. Solids 42, 1397–1434.

Yoffe, E.H., 1951. The moving Griffith crack. Philos. Mag. 42, 739–750.

Path Prediction of Kinked and Branched Cracks in Plane Situations

M. Adda–Bedia

*Laboratoire de Physique Statistique de l'Ecole Normale Supérieure, 24 Rue Lhomond, 75231 Paris Cedex 05, France**

(Received 10 July 2004; published 28 October 2004)

Using the asymptotic expansion of the stress field ahead a curved extension of a straight crack, some general results on the paths selected by kinked and branched cracks are derived. When dealing with the dynamic branching instability of a single propagation crack, the experimentally observed shape of the branches is recovered without introducing any adjustable parameter. It is shown that the length scale introduced by the curved extension of the branches is given by the geometrical length scale of the experiment. The theoretical results agree quantitatively with the experimental findings.

DOI: 10.1103/PhysRevLett.93.185502 PACS numbers: 62.20.Mk, 46.50.+a, 81.40.Np, 83.60.Uv

The field of fracture mechanics is concerned with the quantitative description of the mechanical state of a deformable body containing a crack or cracks. The continuum theory of fracture mechanics studies the nucleation of cracks, the conditions for which they propagate and their dynamics [1,2]. In the framework of continuum theory of brittle fracture, the relationship between internal stress and deformation and the pertinent balance laws of physics dealing with mechanical quantities do not include the possibility of material separation. Indeed, the "equation of motion" of the crack tip is based on additional statements for crack growth. The most popular criterion for crack propagation in a two dimensional elastic body consists of two parts; the Griffith hypothesis and the principle of local symmetry.

The Griffith energy criterion [1,2] states the intensity of the loading necessary to promote propagation through $\mathcal{G} = \Gamma$, where $\mathcal{G}$ is the energy release rate, which is defined as the rate of mechanical energy flow into the crack tip per unit crack advance, and Γ is the fracture energy of the material. The principle of local symmetry states that the crack advances such that the in-plane shear stress in the vicinity of the crack tip vanishes. This rule was first proposed for quasistatic cracks [3], and generalized to rapidly moving cracks [4]. Moreover, it was shown that the two criteria rise from the same physical origin [4]. The energy release rate is the component, F_1, of the driving force along the direction of crack motion. The Griffith energy criterion can thus be reinterpreted as a material force balance between F_1 and a resistance force to crack advance per unit length of the crack front; $F_1 = \Gamma$. However, this equation of motion is not sufficient to determine the trajectory of a crack. If one assumes that material force balance holds at the crack tip, one should impose that the component of the material force perpendicular to the direction of crack propagation vanishes. This condition is identically satisfied if the loading in the vicinity of the crack tip is purely tensile.

The Griffith criterion and the principle of local symmetry predict adequately the path and the stability of slowly propagating cracks [5]. Controlled experiments on quasistatic cracks confirm the theoretical results [6]. In the case of fast crack propagation, the experiments on PMMA (poly-methyl-methacrylate) and glass samples [7–9] have identified a dynamic instability of a propagating crack which is related to a transition from a single crack to a branched crack configuration. Some aspects of this dynamic instability were described within the theory of brittle fracture mechanics [10]. However, the subsequent shape of the branches has not been explained yet.

The main purpose of the present study deals with this aspect of the branching instability. Following the analysis of [11,12], the asymptotic expansion of the static stress field ahead of a curved extension of a crack tip is presented. Using these exact results, some features of the paths selected by kinked and branched cracks are derived. As a main result, the experimentally observed shape of the branches is recovered without introducing any additional parameter. Moreover, in the case of the experiments in [7–9], the length scale introduced by the curved extension of the branches is found to be the width of the sample. The present study shows that both the branching instability threshold, the branching angle and the subsequent paths of the branches are predicted within the continuum theory of brittle fracture mechanics.

Stress field ahead of a curved extension of a crack.— Consider an elastic body containing a straight crack with a kinked curved extension of length s and a kink angle $\lambda\pi$ (see Fig. 1). Let xOy denote the coordinate system

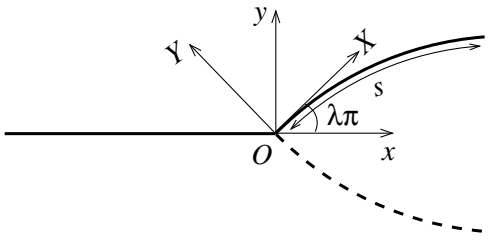

FIG. 1. Schematic representation of a straight crack with a kinked (or symmetrically branched) curved extension.

with the Ox axis directed along the initial straight crack, and let XOY denote the coordinate system with the OX axis directed along the tangent to the extension at the point O. These two coordinate systems are related by

$$X = x\cos\lambda\pi + y\sin\lambda\pi, \tag{1}$$

$$Y = y\cos\lambda\pi - x\sin\lambda\pi. \tag{2}$$

Using minimal assumptions, it was shown in [11] that the asymptotic shape of the crack extension is necessarily given by

$$Y = aX^{3/2} + O(X^2), \tag{3}$$

where a is a curvature parameter whose dimension is $(\text{length})^{-1/2}$. Moreover, the expansion of the static stress intensity factors $K_l'(s)$ $(l = 1, 2)$ at the crack tip in powers of s obeys the general form

$$K_l'(s) = \sum_{m=1,2} F_{lm}(\lambda)K_m + \sum_{m=1,2}[G_m(\lambda)T\delta_{lm} + aH_{lm}(\lambda)K_m]\sqrt{s} + O(s). \tag{4}$$

In this expansion, K_l and T are the static stress intensity factors and the nonsingular stress in the universal expansion of the stress field at the original crack tip O without the kinked extension, which is given by

$$\sigma_{ij}(r,\theta) = \sum_{l=1,2}\frac{K_l}{\sqrt{2\pi r}}\Sigma_{ij}^{(l)}(\theta) + T\delta_{ix}\delta_{jx} + O(\sqrt{r}), \tag{5}$$

where (r, θ) are the polar coordinates with $r = 0$ located at the point O, and $\Sigma_{ij}^{(l)}$ are known functions describing the angular variations of the stress field components [2]. The functions F_{lm}, G_l, and H_{lm} are universal in the sense that they depend neither on the geometry of the body nor on the applied loading. They depend on the kink angle only and their computation was performed in [12].

The asymptotic expansions as given by (3) and (4) must necessarily be considered if the extension of the crack is obtained by actual propagation of the crack and not simply by arbitrary machining of the body [11]. Because of the linearity of the problem, the expressions (3) and (4) can be predicted from dimensional arguments. Since the K_l's scale as stress $\times \sqrt{\text{length}}$ and T scales as stress, the first order expansion of the stress intensity factors in (4) must involve an additional parameter whose dimension is $1/\sqrt{\text{length}}$. This parameter is provided by the asymptotic expansion (3) of the kinked extension.

It is straightforward to extend these results to quasistatic branched cracks. The crack tip of each branch extension must obey similar asymptotic expansions, with different universal functions F_{lm}, G_l, and H_{lm}. The functions F_{lm} for a symmetrically branched configuration have been computed in [10], while the computation of G_l and H_{lm} can be carried out using the same approach as for the kinked crack problem [12].

The detailed expansion of the stress intensity factors being available, it remains to combine it with a propagation criterion for crack path prediction. The Griffith energy criterion [1,2] and the principle of local symmetry [3] impose that the advance of the crack tip is controlled by the following equations

$$\mathcal{G}_1'(s) \equiv \frac{1}{2\mu}K_1'^2(s) = \Gamma, \tag{6}$$

$$K_2'(s) = 0, \tag{7}$$

where μ is the Lamé shear coefficient of the material. Note that Eq. (7) imposes the symmetry of the stress field in the vicinity of the crack tip which in turn restricts the crack direction of propagation. Therefore, the crack path is mainly selected by the principle of local symmetry, while Eq. (6) controls the intensity of the loading necessary to the crack propagation. In the following, the stability of a tensile crack and the path selection of branched cracks will be discussed in the light of these general results.

Response of a tensile crack to a shear perturbation.— Cotterell and Rice [13] analyzed the stability of an initially straight crack under tensile loading in the presence of a small shear perturbation. They found that the nonsingular stress T governs the stability mechanism. The so called T-criterion states that when $T > 0$, the straight crack propagation is unstable and the crack path grows exponentially. While when $T < 0$, the straight crack propagation is stable and the crack path behaves as $y(x) \sim \sqrt{x}$.

Equation (7) states that each coefficient in the expansion (4) of $K_2'(s)$ in terms of s must vanish. Therefore, in the presence of a small shear loading ($|K_2| \ll K_1$) the extension of the initial straight crack must satisfy

$$\lambda \approx -\frac{2}{\pi}\frac{K_2}{K_1}, \tag{8}$$

$$a \approx \frac{8}{3}\sqrt{2\pi}\lambda\frac{T}{K_1}, \tag{9}$$

where the expansions of the functions F_{lm}, G_l, and H_{lm} in terms of $\lambda \ll 1$ have been used [12]. Equation (8) fixes the kink angle that develops due to the presence of the shear loading, while Eq. (9) determines the subsequent curvature of the crack path. Moreover, Eqs. (8) and (9) show that the signs of λ and (a/λ) are governed by the signs of K_2 and T, respectively ($K_1 > 0$). Therefore, when $T > 0$ the perturbation induced by the shear loading is amplified and the departure from straight crack propagation increases. On the contrary, when $T < 0$ the instability of the crack path induced by the kinking process is decreased and tends to stabilize the straight crack advance (see Fig. 2). These results are consistent with the T criterion [13]. However, the subsequent paths followed

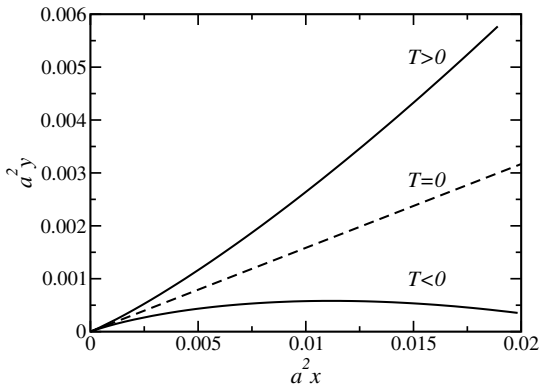

FIG. 2. Subsequent paths of an initially straight crack subjected to a small shear perturbation such that $\lambda = 0.05$.

by the cracks in either the stable or unstable case clearly differ from those predicted in [13]. This discrepancy results from the fact that the perturbation method developed in [13] is inadequate for cracks that are not smooth [12].

The condition $T < 0$ insures the stability of a straight crack propagation but it is not a necessary condition. Effectively, the straight crack might be stable even when $T > 0$, because of the presence of other stabilizing effects. A popular case study that confirms the limitations of the T criterion concerns the stability of a straight crack in a heated strip [6]. The analysis of a smooth wavy perturbation around a straight crack has shown that the crack path stability is governed by the competition between a stabilizing effect; the finite width of the strip, and a destabilizing effect; the heterogeneous thermal field [5]. The threshold of instability was found to be larger than the one predicted from the T criterion.

Shape of branched cracks.—Experiments in glass and PMMA [8,9] have established that the bifurcation of a crack tip into two branches results from the dynamic instability of a single propagating crack. When the crack speed exceeds a critical velocity v_c, a single moving crack is no longer stable and a repetitive process of microbranching occurs, which changes the crack dynamics. Although the lengths of the microbranches are broadly distributed, their functional form is well defined [9]. Once formed, the branch follows a trajectory of the form $y(x) \cong 0.2x^{0.7}$. Furthermore, this scaling behavior does not hold at distances below 5 μm from the branching point, where branching angles of approximately 30° have been reported [9].

The problem for determining the in-plane dynamic stress intensity factors immediately after branching was formulated in [10]. It was shown that the in-plane elastic fields immediately after branching exhibit self-similar properties, and the corresponding stress intensity factors do not explicitly depend of the velocity of the single crack tip before branching. These properties are similar to the antiplane crack branching problem, which was solved exactly in [14]. This analogy allowed for the conclusion that under plane loading configurations, the jump in the energy release rate due to branching is maximized when the branches start to propagate quasistatically. Consequently, the branching of a single propagating crack under tensile loading is found to be energetically possible when its speed exceeds a threshold value [10]. Moreover, for a velocity dependent fracture energy, the critical velocity for branching, v_c, decreases with increasing $\Gamma(v_c)/\Gamma(0)$. The theoretical results for the critical velocity and the branching angle agree fairly with both experimental [8,9] and numerical results [15].

Since the branches start their propagation at vanishingly small speed [10], a quasistatic approximation is suitable for the determination of the subsequent paths followed by the branches. At a first approach, the influence of the crack tip velocity may be discarded. Consider a straight crack subjected to a tensile loading ($K_2 = 0$), that bifurcates into two symmetric branches. The two new branches propagate by satisfying the principle of local symmetry. Therefore at each crack tip, each coefficient in the expansion (4) of $K_2'(s)$ in terms of s must vanish, which gives

$$F_{21}(\lambda) = 0, \tag{10}$$

$$a = -\frac{G_2(\lambda)}{H_{21}(\lambda)}\frac{T}{K_1}. \tag{11}$$

Equation (10) imposes $\lambda = 0.13$, corresponding to a branching angle of 24° [10], which is close to the experimental one estimated in [8,9]. Equation (10) determines the departure from a straight propagation of the branches. The functions G_l and H_{lm} are not available. However, we will assume that for $\lambda = 0.13$, the quantity $G_2(\lambda)/H_{21}(\lambda)$ is positive and of order unity. Ultimately, the computation of these functions will be a crucial step to confirm the following results.

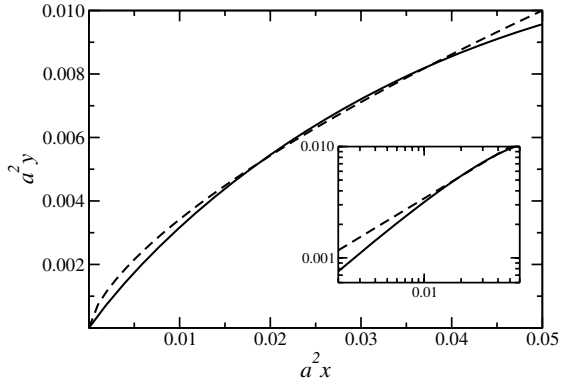

FIG. 3. Subsequent path of a crack after branching. The dashed curve corresponds to the function $y(x) = 0.074(x/|a|)^{2/3}$. The inset shows the same plots in Logarithmic scales.

Figure 3 shows the path followed by the branch as given by Eqs. (10) and (11), with the assumption that $a < 0$. The shape of the branch is very close to a power law form given by $y(x) = 0.074(x/|a|)^{2/3}$, which would correspond to a branched configuration with a branching angle of 90°. In order to compare with the experimental results, it is convenient to replace the power law behavior obtained in [9] by a more "realistic" function given by $y(x) = \alpha x^{2/3}$, with $\alpha \simeq 0.15$–0.25 mm$^{1/3}$. Therefore, the experimental and theoretical shape of the branch coincide if one takes $|a| \simeq (0.074/\alpha)^{3/2} \simeq 0.16$–$0.35$ mm$^{-1/2}$.

Furthermore, the curvature parameter a can be determined from the loading conditions and the geometry of the experiment. Effectively, it can be easily shown that the boundary conditions and the strip geometry of the experiments in [7–9] impose

$$\frac{T}{K_1} = \frac{\kappa - 2}{\sqrt{2(\kappa - 1)}} \frac{1}{\sqrt{W}}, \tag{12}$$

where $\kappa = (c_d/c_s)^2 \simeq 3$ is a material constant and W is the width of the strip. Here, c_d (c_s) is the dilatational (shear) wave speed of the material. Equations (11) and (12), show that the curvature parameter a scales as $1/\sqrt{W}$. The widths of plates used in experiments [8,9] were between 50 and 200 mm, so that $(T/K_1) \simeq 0.04$–0.07 mm$^{-1/2}$. If one takes $G_2(\lambda)/H_{21}(\lambda) \simeq 4$, the estimate of parameter a from the loading conditions is very close to the one evaluated directly from the comparison between the theoretical and the experimental shape of the branch. This result confirms that the length scale which governs the curvature of the branches is the geometrical length scale of the experiment. The introduction of a length scale which is related to some nonlinear process in the vicinity of the crack tip is not needed for describing the shape of the branches.

Conclusion.—In this Letter, some general results of the paths selected by kinked and branched cracks were derived. In the case of the response of a tensile crack to a small shear perturbation, it is shown that the T criterion is directly recovered from the asymptotic expansion of the stress field ahead a curved extension of a straight crack. However, the subsequent path followed by the kinked crack in either the stable or unstable case differs from those predicted in [13]. Concerning the dynamic branching instability, the shape of the microbranches was recovered and the length scale introduced by the curved extension of the branches was determined. The quantitative comparison with the experimental data of [8,9] was performed successfully. Although most of the present analysis was confined within a quasistatic approximation, the results should persist for dynamic cracks. A discussion on the relevance of the zero velocity immediately after branching can be found in [10]. The present results are in favor of the continuum theory of fracture mechanics combined with both the Griffith criterion and the principle of local symmetry. This framework provides the minimal ingredients for the prediction of the branching instability threshold, the branching angle and the subsequent path of the branches.

I thank V. Hakim, H. Henry and A. Karma for fruitful discussions.

*Associated with CNRS (UMR 8550) and with Universities Paris VI and Paris VII.

[1] L. B. Freund, *Dynamic Fracture Mechanics* (Cambridge University Press, New York, 1990).
[2] K. B. Broberg, *Cracks and Fracture* (Academic Press, London, 1999).
[3] R.V. Gol'dstein and R. L. Salganik, Int. J. Fract. **10**, 507 (1974).
[4] M. Adda–Bedia, R. Arias, M. Ben Amar, and F. Lund, Phys. Rev. E **60**, 2366 (1999).
[5] M. Adda–Bedia and Y. Pomeau, Phys. Rev. E **52**, 4105 (1995); M. Adda–Bedia and M. Ben Amar, Phys. Rev. Lett. **76**, 1497 (1996).
[6] A. Yuse and M. Sano, Nature (London) **362**, 329 (1993); O. Ronsin, F. Heslot, and B. Perrin, Phys. Rev. Lett. **75**, 2352 (1995).
[7] J. Fineberg, S. P. Gross, M. Marder, and H. L. Swinney, Phys. Rev. B **45**, 5146 (1992).
[8] E. Sharon, S. P. Gross, and J. Fineberg, Phys. Rev. Lett. **74**, 5096 (1995).
[9] E. Sharon and J. Fineberg, Phys. Rev. B **54**, 7128 (1996).
[10] M. Adda–Bedia, J. Mech. Phys. Solids (to be published).
[11] J. B. Leblond, Int. J. Solids Struct. **25**, 1311 (1989).
[12] M. Amestoy and J. B. Leblond, Int. J. Solids Struct. **29**, 465 (1992).
[13] B. Cotterell and J. R. Rice, Int. J. Fract. **16**, 155 (1980).
[14] M. Adda–Bedia, J. Mech. Phys. Solids **52**, 1407 (2004).
[15] A. Karma and A. E. Lobkovsky, Phys. Rev. Lett. **92**, 245510 (2004); H. Henry and H. Levine, Phys. Rev. Lett. **93**, 105504 (2004).

PHYSICAL REVIEW E **73**, 035106(R) (2006)

Second-order variation in elastic fields of a tensile planar crack with a curved front

M. Adda-Bedia and E. Katzav
Laboratoire de Physique Statistique de l'Ecole Normale Supérieure, 24 rue Lhomond, F-75231 Paris Cedex 05, France

D. Vandembroucq
Surface du Verre et Interfaces, Unité Mixte de Recherche CNRS/Saint-Gobain, 39 Quai Lucien Lefranc, 93303 Aubervilliers Cedex, France

(Received 23 December 2005; published 30 March 2006)

We derive the second-order variation in the local static stress intensity factor of a tensile crack with a curved front. We then discuss the relevance of this result to the stability analysis of such fronts, and propose an equation of motion of planar crack fronts in heterogeneous media that contains two main ingredients—irreversibility of the propagation of the crack front and nonlinear effects.

DOI: 10.1103/PhysRevE.73.035106 PACS number(s): 62.20.Mk, 64.60.Ht, 81.40.Np

The propagation of a crack front in a brittle material is the playground of a number of physical phenomena, which range from dynamic instabilities of fast moving cracks [1] to quasistatic instabilities of crack paths [2,3], or of crack fronts [4–8]. Although the actual theory of brittle fracture mechanics succeeded to explain a number of instabilities, the experimentally observed self-affine roughness of a crack front propagating through a heterogeneous medium remains the subject of theoretical debate [5–7]. This phenomenon is of fundamental importance, because it may be regarded as an archetype of self-affine patterns induced by advancing fronts. Wetting of a disordered substrate being another example of systems with a similar structure [9,10].

In the framework of linear elastic fracture mechanics, an important step was performed by Rice [11] following a work of Meade and Keer [12]. He gave a general formula for the first-order variation in elastic fields of a planar curved crack front and subsequent analysis was mainly based on this work [5,6,13–16]. However, aspects related to crack-front roughness and stability could not be derived within this first-order perturbation solution. A possible explanation, which has been suggested in the context of the wetting problem [10], is that higher order variations might be necessary for the study of the stability and roughening properties of these fronts.

This paper aims at the determination of the second-order variation in elastic fields of a tensile crack front. The present approach is different from [11] and can be generalized to higher orders. It uses a methodology introduced in [8] for the study of the peeling-induced crack-front instability in a confined elastic film. Since the present study is performed in the framework of linear elastic fracture mechanics, our perturbation analysis is expected to hold as long as the radius of the curvature of the crack front remains larger than the size of the process zone where the plastic effects become dominant.

This solution is intended to be used for understanding the roughening of interfaces whose front dynamics does not belong to the Kardar-Parisi-Zhang (KPZ) [17] universality class. For this purpose, we propose a generalized equation of motion of the planar crack fronts in heterogeneous media that includes both the irreversibility of crack-front propagation and the nonlinear effects.

The problem of a half-plane crack located in the plane $y=0$ with a curved front (see Fig. 1) can be solved by using the linear equations of elasticity. It has been shown [12] that these equations are satisfied for a tensile loading that is symmetric to the crack plane if displacement components (u_y, u_x, u_z) are written as

$$Eu_y = -2(1-\nu^2)\Phi + (1+\nu)y\,\partial\Phi/\partial y, \tag{1}$$

$$Eu_x = (1+\nu)\,\partial(F + y\Phi)/\partial x, \tag{2}$$

$$Eu_z = (1+\nu)y\,\partial(F + y\Phi)/\partial z, \tag{3}$$

where $F(x,y,z)$ and $\Phi(x,y,z)$ are harmonic functions related by $\partial F/\partial y = (1-2\nu)\Phi$. E is the Young modulus and ν is the Poisson ratio. Consequently, the stress components that enter the crack-surface boundary conditions are given by

$$\sigma_{yy} = -\partial\Phi/\partial y + y\partial^2\Phi/\partial y^2, \tag{4}$$

$$\sigma_{yx} = y\partial^2\Phi/\partial y\,\partial x, \tag{5}$$

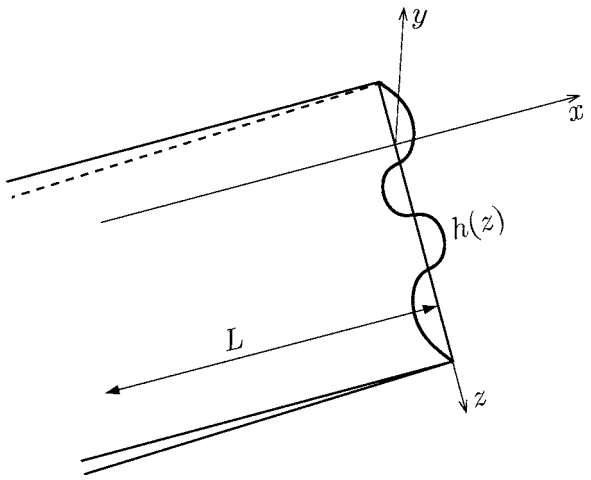

FIG. 1. Schematic of the problem of a half-plane crack on $y=0$ in an infinite body. The average penetration of the crack front in the x direction is L. The straight reference front in the z direction and the perturbation $h(z)$ around it are also shown.

$$\sigma_{yz} = y\partial^2\Phi/\partial y\,\partial z, \tag{6}$$

which satisfy the shear traction free boundary conditions on the crack plane. Thus, the problem of loading on the crack faces is one of finding a function Φ satisfying

$$\triangle\Phi(x,y,z) = 0, \tag{7}$$

having vanishing derivatives at infinity, and generating stress σ and opening gap Δu on $y=0$ given by

$$\sigma = -\partial\Phi/\partial y\big|_{y=0}, \quad \Delta u = -[4(1-\nu^2)/E]\Phi\big|_{y=0^+}, \tag{8}$$

respectively. Defining $h(z)$ as the position of the crack front, we may write the boundary conditions as

$$\Phi(x,0,z) = 0, \quad x > h(z), \tag{9}$$

$$\frac{\partial\Phi}{\partial y}(x,0,z) = p(x,z), \quad x < h(z), \tag{10}$$

$$\frac{\partial\Phi}{\partial x}(x,y,z), \frac{\partial\Phi}{\partial y}(x,y,z) \to 0, \quad (x^2+y^2) \to \infty, \tag{11}$$

where $p(x,z)$ is the normal pressure that loads the crack faces. The problem cannot be solved explicitly without specifying $p(x,z)$, but it is known from classical fracture mechanics analysis that solutions to it exhibit characteristic square-root stress singularities [16]. The harmonic function Φ generating such a singularity necessarily has the form given by

$$\Phi(x,0^+,z) \sim -\frac{2K(z)}{\sqrt{2\pi}}\sqrt{-X} - \frac{4A(z)}{3\sqrt{2\pi}}(-X)^{3/2}, \tag{12}$$

where $X \equiv x - h(z) \to 0^-$. The function $K(z)$ is given by

$$K(z) = K_I(z)[1+h'^2(z)]^{1/4}, \tag{13}$$

where $K_I(z)$ is the local stress intensity factor, which is defined with respect to a coordinates system lying in the plane perpendicular to the crack front at the location $x=h(z)$ and extending into the y direction [16]. The second term in Eq. (12) corresponds to the next order in the expansion of the stress field in the vicinity of the crack front, which is proportional to $\sqrt{h(z)-x}$. The parameter $A(z)$ has the dimension of the stress intensity factor over length.

As a first step, we will consider that K does not depend on z through the position of the crack front with respect to the x direction, i.e. $K(z,h(z))=K(z)$. This condition (to be relaxed later) is of course restrictive, but it will help to construct the full perturbation analysis. This simplification consists explicitly in assuming that a straight crack front will have the same stress intensity factor—wherever it is on the x axis. The real stress intensity factor will be found by relaxing this constraint in a similar way as done in [11].

The piecewise boundary conditions (9), (10), (12) motivate a change into a coordinate system on the crack front, i.e., from (x,y,z) to $(X \equiv x-h(z), y, z)$ [8]. We may then write Eq. (7) as

$$(1+h'^2)\frac{\partial^2\Phi}{\partial X^2} - h''\frac{\partial\Phi}{\partial X} - 2h'\frac{\partial^2\Phi}{\partial z\,\partial X} + \frac{\partial^2\Phi}{\partial y^2} + \frac{\partial^2\Phi}{\partial z^2} = 0, \tag{14}$$

where the prime denotes the derivative with respect to z. Now, we construct an expansion in powers of h, which accounts for the perturbation of the crack front. Without the loss of generality, we write the expansion in the following way:

$$\Phi = \phi_0 + \left(\phi_1 + h\frac{\partial\phi_0}{\partial X}\right) + \left(\phi_2 + h\frac{\partial\phi_1}{\partial X} + \frac{h^2}{2}\frac{\partial^2\phi_0}{\partial X^2}\right), \tag{15}$$

$$K(z) = K_0(z) + K_1(z) + K_2(z), \tag{16}$$

where the subscripts indicate the order of the perturbation expansion. The advantage of this way of writing the perturbation expansion is that it simplifies the equations for the zeroth-, first-, and second-order problem. A direct substitution of the expansion (15) into the equilibrium equation (14) yields

$$\frac{\partial^2\phi_i}{\partial X^2} + \frac{\partial^2\phi_i}{\partial y^2} + \frac{\partial^2\phi_i}{\partial z^2} = 0, \tag{17}$$

with $i=0,1,2$. To complete the formulation of the problem, we need to specify the boundary conditions of each order of the expansion. These are given by

$$\phi_i = 0, \quad y = 0, \quad X > 0, \tag{18}$$

$$\frac{\partial\phi_0}{\partial y} = p(X,z), \quad \frac{\partial\phi_1}{\partial y} = \frac{\partial\phi_2}{\partial y} = 0, \quad y = 0,\ X < 0, \tag{19}$$

$$\frac{\partial\phi_i}{\partial X}(X,y,z), \frac{\partial\phi_i}{\partial y}(X,y,z) \to 0, \quad (X^2+y^2) \to \infty. \tag{20}$$

The expansion of Eq. (12) to the second order in h yields

$$\phi_0(X,0^+,z) \sim -\frac{2K_0(z)}{\sqrt{2\pi}}\sqrt{-X} - \frac{4A_0(z)}{3\sqrt{2\pi}}(-X)^{3/2}, \tag{21}$$

$$\phi_1(X,0^+,z) \sim -\frac{K_0(z)h(z)}{\sqrt{-2\pi X}} - \frac{2K_1(z)}{\sqrt{2\pi}}\sqrt{-X} - \frac{4A_1(z)}{3\sqrt{2\pi}}(-X)^{3/2}, \tag{22}$$

$$\phi_2(X,0^+,z) \sim -\frac{K_0(z)h^2(z)}{4\sqrt{2\pi}(-X)^{3/2}} - \frac{K_1(z)h(z)}{\sqrt{-2\pi X}} - \frac{2[K_2(z)+A_1(z)h(z)]}{\sqrt{2\pi}}\sqrt{-X} \tag{23}$$

for $X \to 0^-$. It is assumed that the perturbation terms induced by $A_0(z)$ as given in Eq. (21) are negligible compared to those induced by $K_0(z)$. Indeed, dimensional analysis shows that $A_0(z) \sim K_0(z)/L$, where L is the geometrical length scale induced by the tractions $p(x,z)$ or by the average length of the crack plane in the x direction (see Fig. 1). This length scale is large compared to the characteristic scale of the per-

turbation $h(z)$. Therefore, we will neglect the corresponding contributions in the following. However, the contribution proportional to $(-X)^{3/2}$ of the first order as shown in Eq. (22) should be taken into account, because it depends on $K_0(z)$ and, thus, contributes to the stress intensity factor term of the second-order problem.

The zeroth-order problem cannot be solved without specifying the loading $p(x;z)$. However, this is not needed for solving the first- and second-order problems, which will depend on the stress intensity factor $K_0(z)$ only. However, if one takes into account, in the perturbation analysis, the contributions of the parameter $A_0(z)$, the resolution of the zeroth-order problem becomes necessary [8]. Let us decompose $\phi_i(X,y,z)$ into Fourier modes in the z axis,

$$\phi_i(X,y,z) = \frac{1}{2\pi}\int_{-\infty}^{\infty} \hat{\phi}_i(x,y,p)e^{ipz}dp, \tag{24}$$

and use polar coordinates (r,θ) in the (X,y) plane. The solutions for $\hat{\phi}_1$ and $\hat{\phi}_2$ are readily given by

$$\hat{\phi}_1(r,\theta,p) = -\frac{\hat{H}_1(p)}{\sqrt{2\pi r}}e^{-|p|r}\sin(\theta/2), \tag{25}$$

$$\hat{\phi}_2(r,\theta,p) = \frac{\hat{L}_2(p)}{4\sqrt{2\pi}r^{3/2}}(1+|p|r)e^{-|p|r}\sin(3\theta/2) - \frac{\hat{H}_2(p)}{\sqrt{2\pi r}}e^{-|p|r}\sin(\theta/2). \tag{26}$$

These forms satisfy the bulk equations (17) and the boundary conditions (18)–(20). The conditions (22) and (23) are then satisfied if the functions $\hat{H}_1(p)$, $\hat{H}_2(p)$, and $\hat{L}_2(p)$ are given by

$$\hat{H}_1(p) = \int_{-\infty}^{\infty} K_0(z)h(z)e^{-ipz}dz, \tag{27}$$

$$\hat{H}_2(p) = \int_{-\infty}^{\infty} \hat{K}_1(p')\hat{h}(p-p')\frac{dp'}{2\pi}, \tag{28}$$

$$\hat{L}_2(p) = \int_{-\infty}^{\infty} \hat{H}_1(p')\hat{h}(p-p')\frac{dp'}{2\pi}. \tag{29}$$

Identifying the stress intensity factors at each order as given by Eqs. (22) and (23) one finds

$$\hat{K}_1(p) = -\frac{1}{2}|p|\hat{H}_1(p), \tag{30}$$

$$\hat{K}_2(p) = -\frac{1}{16}\int_{-\infty}^{\infty}(6p'^2+p^2-4|p|\,|p'|)\hat{H}_1(p')\hat{h}(p-p')\frac{dp'}{2\pi}. \tag{31}$$

Before performing the inverse Fourier transform of these quantities, let us generalize these results to the case where the stress intensity factor depends on the location of the crack front in the x direction.

Until now, we have supposed that the stress intensity factor does not depend on the mean location of the crack front. This is not true in general for quasistatic cracks, which should be at equilibrium, and for which the condition $dK/dL<0$ must be satisfied. The decomposition of the perturbation follows from Rice's approach [11,16]. First, we locate the straight crack front on which the perturbation is performed at the position $[L+h(z)]$. The stress intensity factor at the leading order is then given by $K_0[z,L+h(z)]$ and the location of any point of the curved front is taken with reference to this position. It is clear that the perturbation expansion of the stress intensity factor will include contributions of the form $hh''K_0$, hdK_0/dL, and $h^2d^2K_0/dL^2$. However, one should neglect them because the terms induced by $A_0(z)$, which introduce contributions of the same order, were already neglected. Therefore, the perturbation expansion with respect to (h/L) will be at the leading order. Let us focus on the stress intensity factor $K_I[z,L+h(z)]$ as given by Eq. (13), and write

$$K_I(z) = K_{I0}(z) + K_{I1}(z) + K_{I2}(z) + O\left(h^3,\frac{h}{L}\right), \tag{32}$$

where the L dependence has been omitted. Therefore, using Eqs. (13), (30), and (31) and performing inverse Fourier transforms, we find that $K_{I0}(z)=K_0(z)$, and

$$K_{I1}(z) = PV\int_{-\infty}^{\infty} K_0(z')\frac{h(z')-h(z)}{(z'-z)^2}\frac{dz'}{2\pi}, \tag{33}$$

$$K_{I2}(z) = -\frac{1}{8}K_0(z)h'^2(z) + PV\int_{-\infty}^{\infty}\int_{-\infty}^{\infty} K_0(z') \times \frac{[h(z')-h(z)][h(z'')-h(z)]}{(z'-z)^2(z''-z')^2}\frac{dz''}{2\pi}\frac{dz'}{2\pi}, \tag{34}$$

Finally, when $K_0(z)$ is independent of z, the expansion to the second order in h and to the leading order in (h/L) of the mode I stress intensity factor is simplified into

$$\frac{K_I(z)}{K_0} = 1 - \frac{1}{8}h'^2(z) + PV\int_{-\infty}^{\infty}\frac{h'(z')}{z'-z}\left[1+PV\int_{-\infty}^{\infty}\frac{h'(z'')}{z''-z'}\frac{dz''}{2\pi}\right]\frac{dz'}{2\pi}, \tag{35}$$

$$\frac{\hat{K}_I(p)}{K_0} = 2\pi\delta(p) - \frac{1}{2}|p|\hat{h}(p) + \frac{1}{8}\int_{-\infty}^{\infty}[2|p|\,|p'| + p'(p-p')]\hat{h}(p')\hat{h}(p-p')\frac{dp'}{2\pi}. \tag{36}$$

Let us emphasize again that for the study of the crack-front stability, this perturbation expansion is incomplete, because the (h/L) contributions have been omitted. This statement is true even for a linear stability analysis. An example

of the importance of such contributions is given by the linear stability analysis of the peeling-induced crack front in a confined elastic film [8], where the (h/L) terms do rule the stability of the crack front. From a conceptual point of view, these terms are important to keep contact with the experiments [4], because a quasistatic moving crack front will always stop $(dK/dL<0)$, unless the applied force is increased. Indeed, the experimental realizations for the study of crack-front roughness use the large length scale L in order to make the interface moving, by applying an increasing opening in a cantilever beam configuration. We believe that such effects are also present in the wetting experiments, where the contact line is displaced by pulling off the substrate. In such conditions, the roughening of the interface results from a competition between the microscopic pinning effects and the destabilizing effects of the macroscopic driving.

We now propose an equation for the motion of a planar crack in a heterogeneous material. The present approach is very similar to the one introduced by Gao and Rice [13–15]. We write the equation of motion for the moving crack front as a stochastic partial differential equation by using two main ingredients—the irreversibility of the crack-front propagation and the nonlinear effects. We refer to $h(z)$ as the fluctuating part of the interface, so that by definition, the real location of the interface is given by $L+h(z)$, and L is its average. First, we expect a contribution of the form $[K_I(h) - K_c(z,h)]$, where the perturbative calculations to second order for $K_I(h)$ are given above, and $K_c(z,h)$ is some random toughness describing the heterogeneity of the material. Then, the irreversibility of the fracture process implies that the crack-front motion is possible only at locations of $h(z)$ where the stress intensity factor is larger than the local toughness $K_I(h)>K_c(z,h)$. This results in a term like $\Theta[K_I(h) - K_c(z,h)]$ where $\Theta(\cdot)$ is the Heaviside function. Finally, since the crack propagation is locally normal to the interface [16], one should include a KPZ-like term of the form $\sqrt{1+h'^2(z)}$. So a possible form, where the velocity is taken to be proportional to the difference (K_I-K_c) is given by

$$\frac{\partial h}{\partial t} \propto \sqrt{1+h'^2}(K_I(h) - K_c(z,h))\Theta(K_I - K_c). \qquad (37)$$

This is a highly nonlinear stochastic partial differential equation, even if just second-order terms are taken. Clearly, the presence of the Heaviside function complicates the treatment. In this equation, properties of the noise term need to be specified, and should be generically described by short-range correlations.

To summarize, we derived the second-order variation in the stress intensity factor of a tensile crack with a curved front propagating in a brittle material. We pointed out that for linear stability analysis one has to take into account the contributions coming from the large scales, and so the complete resolution of a given problem must be fully performed for that purpose. Finally, we proposed an equation of motion of the planar crack fronts in heterogeneous media that contains both the irreversibility of the propagation of the crack front and the nonlinear effects. We suggest that the proposed equation can be useful in studying the roughening of propagating crack fronts. In particular, we expect that the nonlocal character of the nonlinear term (in contrast to the local KPZ nonlinearity) is likely to change the universality class of the original equation obtained at first order. Finally, the perturbation method introduced in this study can be generalized without major difficulties to higher orders.

This work was supported by the EEC PatForm Marie Curie action (E.K.). We thank A. Boudaoud for fruitful discussions. Laboratoire de Physique Statistique de l'Ecole Normale Supérieure is associated with the CNRS (Contract No. UMR 8550) and Universities Paris VI and Paris VII.

[1] J. Fineberg and M. Marder, Phys. Rep. **313**, 2 (1999); M. Adda-Bedia, J. Mech. Phys. Solids **3**, 227 (2005).
[2] B. Cotterell and J. R. Rice, Int. J. Fract. **16**, 155 (1980).
[3] M. Adda-Bedia and Y. Pomeau, Phys. Rev. E **52**, 4105 (1995).
[4] J. Schmittbuhl and K. J. Måløy, Phys. Rev. Lett. **78**, 3888 (1997); A. Delaplace, J. Schmittbuhl, and K. J. Måløy, Phys. Rev. E **60**, 1337 (1999).
[5] D. S. Fisher, Phys. Rep. **301**, 113 (1998).
[6] E. Bouchaud *et al.*, J. Mech. Phys. Solids **50**, 1703 (2002).
[7] J. Schmittbuhl, A. Hansen, and G. G. Batrouni, Phys. Rev. Lett. **90**, 045505 (2003); J. Schmittbuhl, A. Hansen, and G. G. Batrouni, *ibid.* **92**, 049602 (2004); M. J. Alava and S. Zapperi, *ibid.* **92**, 049601 (2004).
[8] M. Adda-Bedia and L. Mahadevan Proc. R. Soc. London (to be published).
[9] A. Prevost, E. Rolley, and C. Guthmann, Phys. Rev. B **65**, 064517 (2002); S. Moulinet, C. Guthmann, and E. Rolley, Eur. Phys. J. E **8**, 437 (2002).
[10] R. Golestanian and E. Raphaël, Phys. Rev. E **67**, 031603 (2003); P. Le Doussal, K. J. Wiese, E. Raphaël, and R. Golestanian, Phys. Rev. Lett. **96**, 015702 (2006).
[11] J. R. Rice, J. Appl. Mech. **54**, 571 (1985).
[12] K. P. Meade and L. M. Keer, J. Elast. **14**, 79 (1984).
[13] H. Gao and J. R. Rice, J. Appl. Mech. **56**, 828 (1989).
[14] S. Ramanathan and D. S. Fisher, Phys. Rev. B **58**, 6026 (1998).
[15] S. Roux, D. Vandembroucq, and F. Hild, Eur. J. Mech. A/Solids **22**, 743 (2003); Y. Charles *et al.*, J. Mech. Phys. Solids **52**, 1651 (2004).
[16] J. B. Leblond, *Mécanique de la Rupture Fragile et Ductile* (Hermes Science, Paris, 2003).
[17] M. Kardar, G. Parisi, and Y. C. Zhang, Phys. Rev. Lett. **56**, 889 (1986).

Résumé :

Ce manuscrit décrit mes activités de recherche effectuées au Laboratoire de Physique Statistique de l'Ecole Normale Supérieure. Le principal sujet de recherche que j'ai étudié concerne dynamique de la propagation des fissures. L'approche suivie tourne autour de la formation de motifs dans des systèmes en présence d'une ou de plusieurs fissures. Une fois qu'une fissure est formée et qu'elle commence à se propager quelle trajectoire va-t-elle suivre ? quelle sera sa dynamique ? les instabilités dynamiques et morphologiques observées expérimentalement sont-elles corrélées ? lorsque plusieurs fissures sont présentes, comment interagissent-elles et quelle est la morphologie résultante ? peut-on contrôler le motif final en contrôlant seulement les conditions d'application des contraintes ou la géométrie globale ?

Récemment, j'ai commencé à aborder de nouveaux problèmes tournant autour de la morphogénèse induite par la mécanique. Le principal objectif de ces études est d'apporter une meilleure compréhension du comportement mécanique de certaines structures biologiques et physiques, et de leur morphogenèse.

Abstract :

This manuscript describes my research activities at Laboratoire de Physique Statistique de l'Ecole Normale Supérieure. The central subject deals with the dynamics of crack propagation as a pattern formation mechanism in systems in presence of one or many cracks. When a crack is formed and starts propagating, which path will it follow ? what will be its dynamics ? are the observed dynamical and morphological instabilities correlated ? what is the resulting pattern in the case of multiple crack propagation ? Can we control the final pattern by only controlling the applied loading and geometry of experiment ?

Recently, I started working on new problems dealing with pattern formation induced by mechanical constraints. The principal goal of these studies is to bring insights on the mechanical behaviour of some biological and physical structures, and their morphogenesis.